TriDurLE

National Center for Transportation Infrastructure Durability & Life-Extension

Project ID: 2020-SDSU-01

Post-Earthquake Serviceability Assessment of RC Bridge Columns Using Computer Vision

Final Report

by

Mostafa Tazarv[a], Kwanghee Won[b], Youjeong Jang[b], Kallan Hart[a], Evan Greeneway[a], and Aditya Harshvardhan[b]

Departments of Civil and Environmental Engineering[a] and Computer Science[b]
South Dakota State University
Brookings, South Dakota

for

December 30, 2021

ACKNOWLEDGEMENTS

DISCLAIMER

The contents of this report reflect the views of the authors, who are responsible for the facts and the accuracy of the information presented. This document is disseminated under the sponsorship of the Department of Transportation, University Transportation Centers Program, in the interest of information exchange. The U.S. Government assumes no liability for the contents or use thereof.

ABSTRACT

Modern seismic design codes ensure a large displacement capacity and prevent total collapse for bridges. However, this performance objective is usually attained at the cost of damage to target ductile members. For reinforced concrete (RC) bridges, the columns are usually the main source of ductility during an earthquake in which concrete cover, core, and reinforcement may damage, and the column may experience a large permanent lateral deformation. A significant number of the US bridges will experience large earthquakes in the next 50 years that may result in the bridge closure due to excessive damage. A quick assessment of bridges immediately after severe events is needed to maximize serviceability and access to the affected sites, and to minimize casualties and costs.

The main goal of this project was to accelerate post-earthquake RC bridge column assessment using "computer vision". When sending trained personnel to the affect sites is limited or will take time, local personnel equipped with an assessment software (on various platforms such as mobile applications, cloud-based tools, or built-in with drones) can be deployed to evaluate the bridge condition. The project in this phase was focused on the damage assessment of modern RC bridge columns after earthquakes. Substandard columns, other bridge components, and other hazards were not included.

To achieve the project goal, several tasks were completed. First, the literature was reviewed to collect information on the visual assessment of RC bridge columns, to identify existing RC bridge column test databases, and to synthesize the latest developments on computer vision. Second, a new definition was proposed to categorize RC bridge column damage types and condition states that are suitable for computer programing. Third, the most comprehensive database of modern RC bridge column experimental performance including more than 290 columns each with 30 parameters was developed. The database was then used to relate bridge damage states to displacement demands. Subsequently, an artificial intelligence (AI) enabled software was developed based on a photograph database of RC bridge columns to quickly detect cracking, spalling, and reinforcement, to comment on the RC column damage state, and to tag (green, yellow, or red) the column/bridge based on the extent of the damage. The software performs both preliminary damage assessment (PDA) and detailed damage assessment (DDA) using a few column parameters and provides a quick and safe assessment.

The main products of the present project are: (1) a comprehensive RC bridge column performance database, (2) an open-source computer program that performs post-earthquake PDA and DDA for RC bridge columns, and (3) cloud-based tools with graphical user interface (GUI) to better utilize the software. The column database and software source codes are available to public at no cost.

TABLE OF CONTENTS

ABBREVIATIONS

AASHTO	American Association of State Highway and Transportation Officials
AI	Artificial Intelligence
ASTM	American Society of Testing and Materials
ACI	American Concrete Institute
CNN	Convolutional Neural Network
CVT	Computer Vision Tool
EERI	Earthquake Engineering Research Institute
EI	Extended Investigation
FEMA	Federal Emergency Management Agency
FHWA	Federal Highway Administration
FR	Fast Reconnaissance
DDA	Detailed Damage Assessment
DI	Damage Index
DOT	Department of Transportation
DCNN	Deep Convolutional Neural Network
DNN	Deep Neural Network
DS	Damage State
ft	Feet
GUI	Graphical User Interface
in.	Inch
kip	1000 pounds
ksi	kip per square inch
PDA	Preliminary Damage Assessment
R-CNN	Region-Based Convolutional Neural Networks
SDSU	South Dakota State University
StEER	Structural Extreme Events Reconnaissance
USGS	United States Geological Survey

LIST OF TABLES

LIST OF FIGURES

EXECUTIVE SUMMARY

ES.1 Introduction

Even though bridges are designed for the "collapse prevention" performance level, they may damage under large earthquakes. For reinforced concrete (RC) bridges, the columns are usually the main source of ductility during an earthquake in which concrete cover, core, and reinforcement may damage, and the column may experience a large permanent lateral deformation.

Post-event bridge assessment is currently performed by sending trained inspectors to each site for a preliminary evaluation, data collection, and tagging the bridge (to remain open, to be closed, or to have limited access). Several inspectors might be needed per event, and the process is generally time consuming (a few hours per visit). An alternative and quick damage assessment of bridges immediately after severe events is needed to maximize serviceability and access to the affected sites, and to minimize casualties and costs. This is especially critical after earthquakes since the first few hours after ground shaking are the most critical time window for rescue operations.

ES.2 Objectives

The main goal of this project was to accelerate post-earthquake serviceability assessment of RC bridge columns using "computer vision". When sending trained personnel to the affect sites is limited or will take time, local personnel equipped with an assessment software (on various platforms such as mobile applications, cloud-based tools, or built-in with drones) can be deployed to evaluate the bridge condition. The project was focused on the damage assessment of modern RC bridge columns after earthquakes. Substandard columns, other bridge components, and other hazards were not included.

To achieve the project goal, several tasks were completed: (1) literature review, (2) new damage state definitions for RC bridge columns suited for computer programing, (3) development of a new experimental database specific to modern RC bridge columns, (4) development of empirical damage-displacement relationships, (5) development of an artificial intelligence (AI) software to detect RC column damages and to tag the column/bridge, and (6) development of a methodology to carry out preliminary damage assessment (PDA) and detailed damage assessment (DDA) of RC bridge columns after earthquakes. A summary of each task is presented herein, and the detailed discussion for each task is presented in the following chapters of the report.

ES.3 Literature Review

The literature was reviewed to collect information on the earthquake response of bridges, on how to perform post-earthquake inspection and performance assessment, and on emerging techniques such as computer vision that might expedite post-event structural inspection and/or assessment.

Various damage types have been reported for substandard RC bridges under earthquakes. A "substandard column" is the one that has not been designed and detailed per seismic requirements, and may have insufficient transverse reinforcement, lap splicing at the column ends or insufficient development length, and/or a relatively short length. Several studies have shown that substandard columns exhibit minimal ductilities usually resulting in the bridge failure (e.g., Chung et al., 1996; Moehle & Eberhard, 2000; ACI 314.4R, 2016).

The US seismic codes have significantly been enhanced after the 1994 Northridge earthquake. Per current code requirements, the damage of standard columns at the design level earthquakes should be limited and repairable. However, the literature lacks a systematic reconnaissance database for bridges especially those with standard columns after earthquakes. **Figure ES.1** shows earthquake damage of standard RC bridge columns collected in the present project.

(a) Llacolen Bridge Damage in the 2010 Maule EQ, Built in 2000 (Yen et al., 2011)

(b) Okirihata Oh-hashi Bridge Damage in the 2016 Kumamoto EQ., Built in 2001 (Istrati, 2016)

(c) Mianyang Airport Viaduct, Short Column Damage in the 2008 Wenchuan EQ, Built in 2001 (Yen et al., 2011)

(d) Bridge 2401 Damage at Bent Top in the Jan-March 2020 Puerto Rico EQs, Built in 1996 (Photo by Dr. Manuel Coll)

Figure ES.1 – Damage of Standard RC Bridge Columns

(e) Bridge 2401 Damage at Column Top in the Jan. 2020 Puerto Rico EQ, Built in 1996 (Photo by Dr. Manuel Coll)

(f) Bridge 2401 Damage at Column Top in the March 2020 Puerto Rico EQ, Built in 1996 (Photo by Dr. Manuel Coll)

(g) Bridge 2401 Damage at Column Top in the Jan. 2020 Puerto Rico EQ, Built in 1996 (Photo by Dr. Manuel Coll)

(h) Bridge 2401 Damage at Column Top in the March 2020 Puerto Rico EQ Built in 1996 (Photo by Dr. Manuel Coll)

Figure ES.1 – Damage of Standard RC Bridge Columns, Continued

Olsen et al. (2016; as NCHRP 833) reviewed the state Department of Transportations' (DOTs) policies and guidelines regarding post-event field operations for transportation infrastructure. NCHRP 833 proposed a four-stage post-event assessment for transportation infrastructure:

- Fast Reconnaissance (FR),
- Preliminary Damage Assessment (PDA),
- Detailed Damage Assessment (DDA), and
- Extended Investigation (EI).

Furthermore, the report marks and tags each affected structure using three levels:

- Inspected: Green tagged, meaning no damage was observed,
- Limited Use: Yellow tagged, limiting the access to light traffics and first responders, and
- Unsafe: Red tagged, closed to all traffics.

Figure ES.2 graphically shows the assessment stages and coding after an event based on NCHRP 833. When the structure is not obviously collapsed as determined in the Fast Reconnaissance (FR), onsite assessment is needed by trained emergency responders and engineers to tag the affected structures. Such assessment may require closure of the structures for hours and days after an event, which are the most critical hours for rescue operations.

UNSAFE = The structure requires further evaluation in the next assessment stage prior to being open to traffic.
LIMITED USE = Potentially dangerous conditions are believed to be present and usage is restricted to ensure public safety.
INSPECTED = The structure appears to be in the same condition as it was prior to the event.
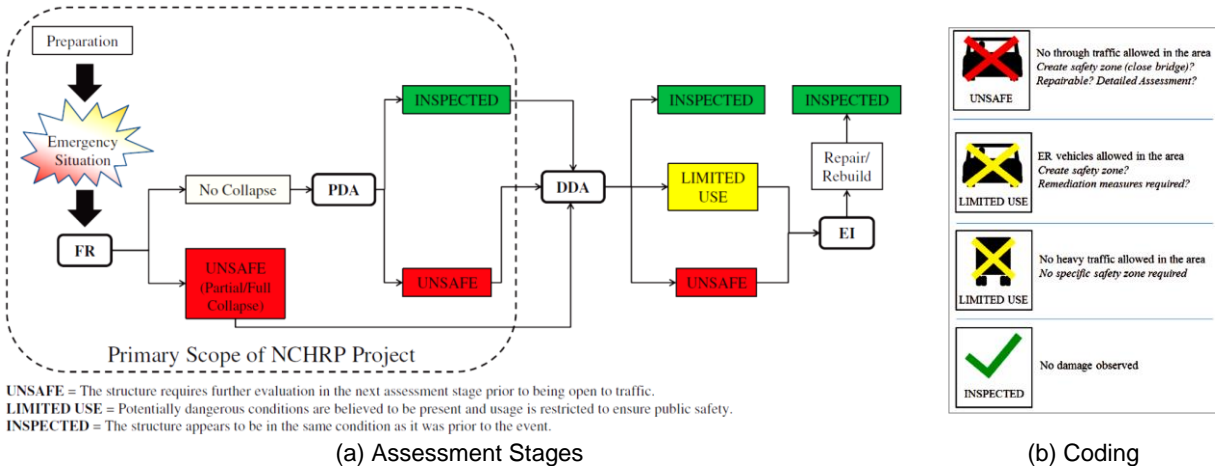
(a) Assessment Stages   (b) Coding
Figure ES.2 – Transportation Infrastructure Assessment Stages and Coding (NCHRP 833)

A survey of state DOTs revealed that "visual inspection" is the most common method of damage detection for bridges after a severe event (Alipour, 2016; as NCHRP 469), and other technologies such as nondestructive testing, sonar surveys, and photogrammetry were ranked lower. NCHRP 469 concluded that the visual inspection is the preferred method by state DOTs since it is quick, low cost, and requires minimal preparation. State DOT field operation manuals usually include descriptive text, illustrations, and inspection forms to help with a quick identification of event-caused bridge damages.

A few studies have defined damage-based performance levels for RC bridge columns. Ramirez et al. (2000) proposed a damage classification and a three-color tagging system (green, yellow, and red) for RC and steel bridge columns. Hose (2001) proposed a five-level performance classification for bridges, offered qualitative and quantitative performance descriptions for each level to quickly assess post-earthquake bridge performance, and graphically identified each damage level for brittle, strength-degrading, and ductile structures. Veletzos et al. (2008) adopted the five-level damage state and the three performance curves proposed by Hose (2001) and developed a post-earthquake inspection manual for Caltrans. They also proposed a flowchart to facilitate the determination of an RC column performance curve after an earthquake. Berry and Eberhard (2008) developed equations to estimate RC bridge column drift ratios, plastic rotations, and longitudinal bar strains at concrete cover spalling, longitudinal bar buckling, and longitudinal bar fracture (or a three-level damage state). Vosooghi and Saiidi (2010) proposed a six-level damage state for RC bridge columns, which was in general similar to the work by Hose (2001), and developed a relationship between the damage state and the maximum drift ratio demand, the residual drift ratio, and four other parameters for four column types: standard low shear under far-field motions, standard high shear under far-field motions, standard low shear under near-field motions, and sub-standard columns. Marsh et al. (2014) presented a four-stage plastic hinge mechanism for RC bridge columns and provided a curvature-based limit states for various failure modes. NCHRP 833 (Olsen et al., 2016) proposed a four-level damage state for bridge columns and bents. Recently, NCHRP 949 (Murphy et al., 2020) proposed a three-level performance assessment for RC bridge columns using steel bar and/or concrete strain limits.

Computer vision is an artificial intelligence (AI) technique that extracts information from digital images, videos, and other media. The use of computer vision has been emphasized in various civil engineering applications such as detecting structural elements, damages, and reporting. For example, Zhu et al. (2010) used image stitching techniques to detect bridge columns to expedite inspection. Narazaki et al. (2020) used semantic segmentation algorithms, a convolutional neural network (CNN), to recognize bridge components from images. Zhu et al. (2011) used a percolation-based method to detect cracks in RC columns. German et al. (2012) used an image segmentation, template-matching, and morphological filtering to detect concrete spalling and rebars. Jahanshahi and Marsi (2012) proposed crack detection method using a 3D scene reconstruction, segmentation, and feature extraction. Torok et al. (2014) used a similar method and successfully detected cracks longer than 0.5 cm. Valença et al. (2017) combined image processing and point cloud data obtained from a terrestrial laser scanner to detect concrete cracks. Li and Zhao (2019) trained a deep CNN using 60,000 images to detect concrete cracks and developed a mobile application. Other recent studies (e.g., Dung and Ann, 2019; and Liu et al. 2019) used either deep CNN or U-net (a CNN used for biomedical image segmentation) to detect concrete cracks and reported more than 90% precision. Furthermore, computer vision may be incorporated to expedite post-event structural inspection and document damages automatically. German et al. (2013) and later Paal et al. (2015) developed a framework to automatically detect RC building columns and their earthquake-caused damages, and to estimate the column damage state then the corresponding drift demand. Hoskere et al. (2017) utilized a pixel-wise deep CNN to detect concrete cracks, concrete spalling, exposed rebars, steel corrosion, steel fracture, steel fatigue cracks, and asphalt cracks. A 1695-image database cut from 339 photographs of 250 different structures was developed to label and train the network. The network was able to detect different types of damages, and the classification accuracy was more than 80%. Later, Hoskere et al. (2018) proposed a framework to generate vision-based condition-aware models to automate building inspection by detecting building, windows/doors, debris, sky, greenery, cracks, spalling, and exposed rebar. **Figure ES.3** shows sample results using the proposed network. More than 80% detection accuracy was reported.
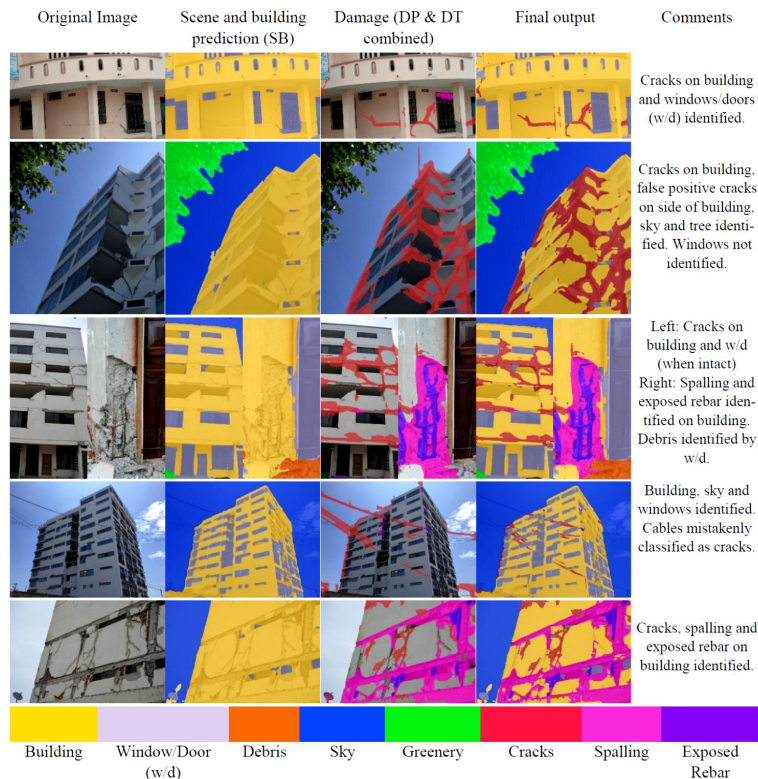
Figure ES.3 – Automated RC Building Component and Damage Detection (Hoskere et al., 2018)

Liang (2019) proposed a three-level image-based post-event inspection approach in which bridge failure, bridge columns, and column damages (cracking, spalling, and exposed rebar) can automatically be detected (**Fig. ES.4**). An image database including 1,154 photographs was formed, of which 80% was used for the labeling and network training and 20% was used for testing (evaluation). Bayesian optimization was used to enhance training with low number of images. The accuracy of the proposed method for the bridge failure detection was 98%, for the column detection was more than 80%, and for the column damage detection was 93%.
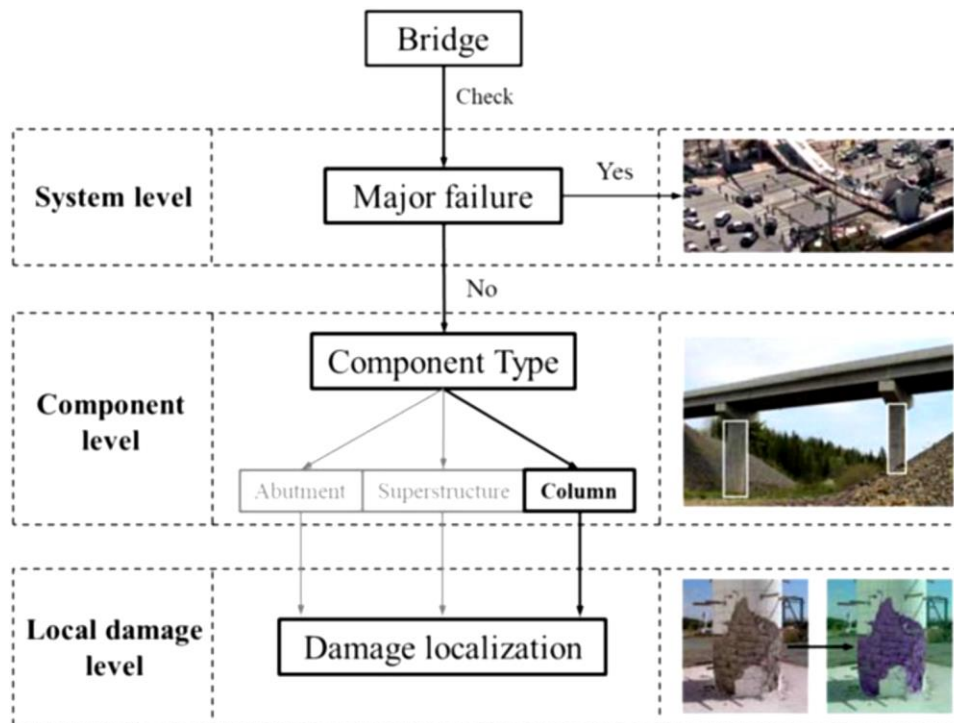
Figure ES.4 – Automated Image-Based Bridge Inspection Method (Liang, 2019)

Lattanzi et al. (2015) combined image segmentation and feature extraction with nonlinear regression analysis to relate RC columns damages to displacements. Photographs of four RC bridge columns at known displacements (during testing) were segmented to develop a set of numeric descriptors for cracking and spalling. Subsequently, nonlinear regression analysis was used to relate those numeric descriptors with the known displacements. Data of three columns was used for the network training, and data for the fourth column was used for the method evaluation. A strong correlation between cracking/spalling and displacement was observed. However, the model failed to predict the behavior of the fourth column since it was not a conventional RC bridge column.

ES.4 RC Bridge Column Damage States

Apparent (visible) damages of RC bridge columns include horizontal cracking, shear (vertical) cracking, spalling, exposure of transverse bar(s), exposure of longitudinal bar(s), buckling of longitudinal bar(s), crushing of core concrete, fracture of transverse bar(s), fracture of longitudinal bar(s), and complete collapse (significant out-of-plumbness or a flattened column). Note that bar yielding, which is a key design parameter, cannot visually be detected. Each of these damage types may further be classified with different levels. For example, one may use the area of the spalled region to differentiate insignificant from significant spalling because each corresponds to a different level of demand (seismic demand refers

to the column lateral displacement demand). Therefore, any damage definition and/or classification is somewhat subjective.

Table ES.1 presents a summary of RC bridge column damage levels (or states) defined in the past studies. Different studies used the abovementioned damage types to classify the progress of the damage from "none" to "the column collapse" in three to six levels (or states). Some provided only general and qualitative definitions, and some used more quantitative language. A few studies also provided equations to relate their proposed damage states to design parameters such as drifts and strains.

Table ES.1 – Summary of Past Studies on RC Bridge Column Damage State Definitions

References	Damage Definitions	Remarks
Ramirez et al. (2000)	Green Tag: Horizontal cracks. Yellow Tag: Diagonal cracks, loss of concrete cover. Red Tag: Bar buckling.	No quantitative measures were proposed.
Hose (2001) and Veletzos et al. (2008)	Level I: Onset of hairline cracks. Level II: Theoretical first yielding of longitudinal bars. Level III: Initiation of inelastic deformation, onset of concrete spalling, development of diagonal cracks. Level IV: Wide crack widths/spalling over full local mechanism region. Level V: Buckling of main reinforcement, rupture of transverse reinforcement, crushing of core concrete.	Quantitative measures were proposed for Levels II to V. For example, Level III is when "*residual cracks have a width of 1-2 mm; the length of spalled region is greater than 1/10 of the column cross-section depth*."
Berry and Eberhard (2008)	Equations were developed to estimate either drift ratios, plastic hinge rotations, or rebar strains at cover spalling, bar buckling, and bar fracture.	A statistical analysis was carried out on an RC bridge column database including more than 30 columns.
Vosooghi and Saiidi (2010) and later Saini and Saiidi, (2014)	Damage State 1: Flexural cracks. Damage State 2: First spalling and shear cracks. Damage State 3: Extensive cracks and spalling. Damage State 4: Visible lateral and longitudinal bars. Damage State 5: Imminent failure. Damage State 6: failure.	No quantitative measures were proposed. Equations were developed based on a statistical analysis on a database including more than 30 RC bridge columns to relate "damage states" to "drift demands" and "damage indexes" for four column type.
AASHTO MBEI (2013)	General descriptions of different RC column defects at four levels: Condition States 1 to 4.	The four-level "condition state" is suitable for regular inspections not after a severe event.
Marsh et al. (2014)	Stage 1: No damage, zero force. Stage 2: Just prior to yielding. Stage 3: Just following formation of plastic hinge. Stage 4: No definition, but seems to be within plastic deformation range.	Analytical equations were proposed to relate column damages (including cover failure, core failure, bar buckling, low-cycle fatigue, and bar fracture) to plastic curvatures.
Olsen et al. (2016)	None: No damage. Minor Damage: Fine shear cracks, horizontal cracks, small transverse cracks at column ends. Moderate Damage: Localized crushing of concrete, slight cover spalling, slightly exposed transverse or longitudinal bars. Severe Damage: Crushing of concrete cover, major spalling of concrete cover, exposed transverse or longitudinal bars, fracture transverse ties.	No quantitative measures were proposed.
Murphy et al. (2020)	Performance Level 1: Life Safety. Performance Level 2: Operational. Performance Level 3: Fully Operational.	Equations were proposed to relate the three performance levels to reinforcement tensile strains and concrete compressive strains.
FEMA HAZUS (2020)	None: No bridge damage. Slight Damage: Minor spalling. Moderate Damage: Shear cracks and spalling. Extensive Damage: Degrading without collapse, shear failure. Complete Damage: Collapse.	A drift-based limit was proposed per damage state.

To successfully assess the post-earthquake damage of an RC bridge column using a computer program, a quantitative definition of damage is needed. Based on the review of past studies on RC bridge column damage definitions (**Table ES.1**) and the available RC column test data, new quantitative damage state definitions but consistent with past studies (Veletzos et al., 2008; Vosooghi and Saiidi, 2010) were proposed for RC bridge columns to be used in computer programing. **Table ES.2** presents the new definitions and **Fig. ES.5** show sample photographs per proposed damage state. Included in the table, is a tagging guide that might be used for a preliminary damage assessment (PDA).

Table ES.2 – Proposed Computer Vision Damage States for RC Bridge Columns

Damage State	Qualitative Damage Description	Quantitative Damage Description for Computer Vision
1	Hairline cracks	Horizontal cracks each with an angle of $|\theta| > 80°$ (**Fig. ES.1a**)
2	Theoretical first yielding of longitudinal bars	At least three diagonal cracks each with an angle of $|\theta| < 70°$ (**Fig. ES.1b**)
3	Extensive cracks and spalling	Length of spalled region in any direction at any column face is greater than $0.1D_c$ but smaller than $0.3D_c$ (**Fig. ES.1c**)
4	Visible transverse and/or longitudinal reinforcement	Length of spalled region in any direction at any column face is greater than $0.5D_c$ and detect one transverse bar and/or one longitudinal bar (**Fig. ES.1d**)
5	First buckling and/or rupture of longitudinal bar(s), crushing of core concrete	Detect the first buckling and/or rupture of longitudinal bar(s), and/or detect at least two longitudinal bars and three transverse bars (**Fig. ES.1e**)
6	Total collapse in which the permanent drift ratio exceeds 10%	The angular change of the line connecting the column ends with respect to the column initial position exceeds 10° ($|\alpha| > 10°$) (**Fig. ES.1f**)

Notes:

α = The angle between the column axial direction before and after the deformation (see the figure below)

θ = The angle between the crack and the undeformed column axial direction (see the figure below)

D_c = The undamaged column diameter or the largest side dimension

███ = Inspected   ███ = Limited Use   ███ = Unsafe

xxi
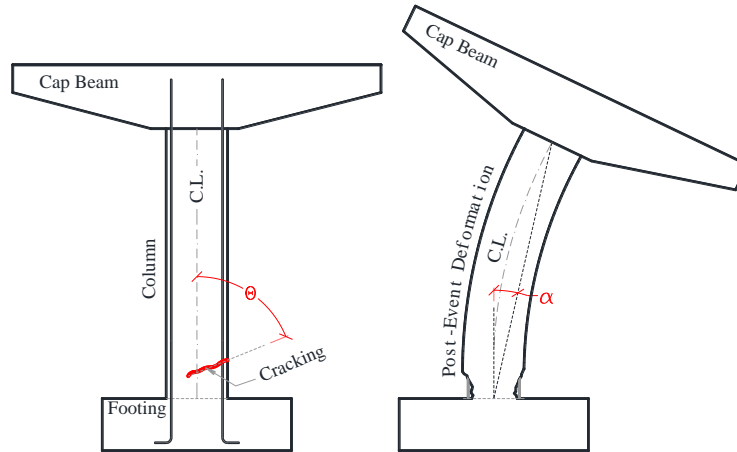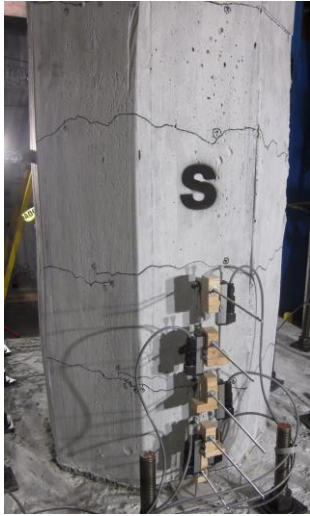
(a) Damage State 1 (DS1)
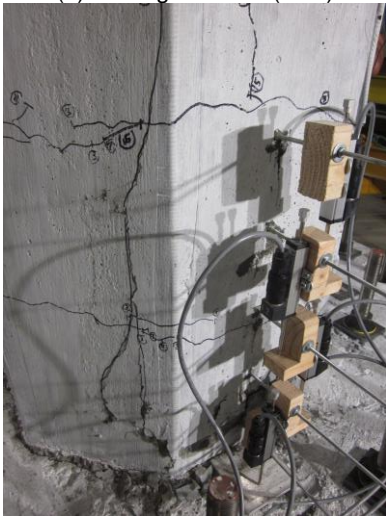
(b) Damage State 2 (DS2)
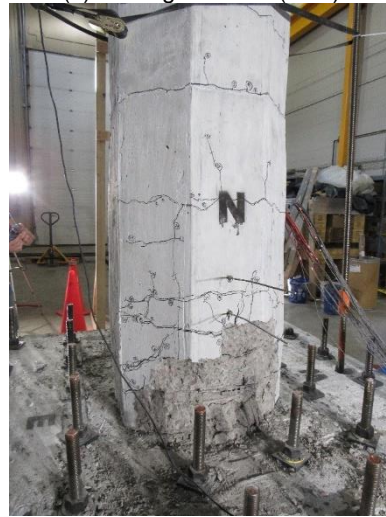
(c) Damage State 3 (DS3)

(d) Damage State 4 (DS4)

(e) Damage State 5 (DS5)

(f) Damage State 6 (DS6)

Figure ES.5 – Samples of RC Bridge Column Damage States

ES.5 RC Bridge Column Test Database

Table ES.3 summarizes the key information of RC column test databases available in the literature. The most comprehensive works are those by Berry and Eberhard (2008) and Ghannoum et al. (2015), which include a mix of standard and substandard, and building and bridge columns. Furthermore, the most recent database by Zheng at el. (2020) does not include several of experimental data that has been published in the past few years. Overall, the literature is missing a comprehensive and unified test database specific to modern RC bridge columns, those that are detailed to resist seismic loads.

Table ES.3 – Summary of Past Studies on RC Column Database

References	Type of Data Included	Remarks
Hose and Seible (1999)	A PDF document presenting experimental data and photographs of 12 RC bridge columns, three RC bridge sub-assemblies, and three RC column-bent systems. Column detailing, reinforcement, mechanical properties, and force-displacement hysteresis were included.	A mix of different shapes and reinforcement distribution, not in spreadsheet.
Berry and Eberhard (2008)	Two spreadsheets presenting experimental data for 160 circular columns and 247 rectangular columns. More than 20 parameters related to the column detailing, reinforcement, and mechanical properties were included. A digitized force-displacement hysteresis was included for all specimens.	A mix of standard and substandard columns, mix of building and bridge columns, displacements at different damage states was included, when data was available.
Veletzos et al. (2008)	A PDF document presenting the force-displacement hysteresis and photographs of more than 100 RC bridge columns.	A mix of standard and substandard columns, a mix of different shapes and reinforcement distribution, not in spreadsheet.
Rodriguez and Padilla (2009)	A spreadsheet presenting experimental data for 76 RC columns. A few parameters related to the column section and mechanical properties were included.	Several references were the same as those in Berry and Eberhard (2008).
Vosooghi and Saiidi (2010); updated by Saini and Saiidi, (2014)	A PDF document presenting experimental data of 38 RC bridge columns tested on shake table. A few column parameters and drifts at different damage states were included.	Not in spreadsheet.
Perus et al. (2013)	A spreadsheet presenting experimental data for 477 circular and rectangular columns. More than 45 parameters related to the column detailing, reinforcement, and mechanical properties were included. A digitized force-displacement hysteresis was included for all specimens.	The database was built upon the work by Berry and Eberhard (2008).
Ghannoum et al. (2015)	Two spreadsheets presenting experimental data for 172 circular columns and 326 rectangular columns. More than 50 parameters related to the column detailing, reinforcement, and mechanical properties were included. Key forces and displacements were included.	The database was built upon the work by Berry and Eberhard (2008), a mix of standard and substandard columns, mix of building and bridge columns.
Azadi-Kakavand et al. (2019)	Added the yield drift ratio and the displacement ductility to the database developed by Ghannoum et al. (2015).	Mainly the same as the database by Ghannoum et al. (2015).
Azadi-Kakavand and Allahvirdizadeh (2019)	A PDF document presenting experimental data of 196 RC columns. A few column parameters and drifts at two damage states were included.	Not in spreadsheet.
Zheng at el. (2020)	A spreadsheet presenting experimental data for 199 circular and rectangular columns. More than 50 parameters related to the column detailing, reinforcement, and mechanical properties were included. Drifts at different damage states were included.	Half of the columns were the same as those in Berry and Eberhard (2008).

As was discussed above, current test databases include a mix of bridge and building, standard and substandard columns, and report parameters that are not consistent with current codes or are not required for a bridge design. To achieve the present project goals, it was necessary to collect test data specific to modern RC bridge columns. A new performance database has been developed in the present work that includes all the key geometrical, material, and force-displacement properties of RC bridge columns designed with modern codes (especially those following seismic detailing). All parameters were collected following the current AASHTO SGS (2011) definitions. Furthermore, displacements (drifts) at six different damage states as defined in the previous section (**Table ES.2**) were included when the data was available. The new database is built upon the work by Ghannoum et al. (2015), which included test data published up to 2008. Nevertheless, all substandard and/or building columns were removed, the definitions were updated to be consistent with current AASHTO SGS, and new parameters were added

suited for seismic/bridge design. Furthermore, more than 100 new circular and 30 rectangular columns were added. The refined and updated RC bridge column database currently includes 222 circular and 68 rectangular columns. Two spreadsheets, one for circular and one for rectangular RC bridge columns, were developed each including more than 30 parameters per test specimen. The database is publicly available (Hart et al., 2021; https://doi.org/10.17603/ds2-1p5e-1v55). Furthermore, **Appendix A** includes the damage photographs of the columns included in the database at different damage states.

ES.6 RC Column Displacement Estimation

A detailed assessment of a bridge performance, especially the columns, under an earthquake, requires an accurate estimation of <u>demand</u> and <u>capacity</u>. Current methods to estimate a bridge column displacement demand and capacity were reviewed and new empirical equations were developed. Drift ratio (δ), which is the ratio of the column lateral displacement (Δ) to the column length (L) as defined in AASHTO SGS (2011), was utilized in lieu of displacement.

AASHTO SGS (2011) specifies three demand analysis methods: (1) equivalent static, (2), elastic dynamic analysis, and (3) nonlinear time history. Even though these procedures are used in the design step, they may be utilized after an earthquake to perform the bridge assessment. Further, the code-specified design spectrum for the affected sites, the spectrum for the current earthquake (the one that the bridge is affected with), or the current earthquake ground motions may be utilized in the linear and/or nonlinear analyses. For example, processed ground motions are available shortly after an earthquake in the US through different agencies. It is feasible to develop a software (e.g., cloud-based for a quick access and analysis) that utilizes the actual ground motions as the input for the dynamic analysis. Open-source structural software such as OpenSees (2016) can be used for this analysis. **Figure ES.6** illustrates the architecture of a cloud-based tool. Generic bent models can be pre-defined with the key modeling parameters to be provided by the user. The national bridge inventory (NBI) might also be accessed to populate some of the bent information. Overall, a dynamic analysis can be performed using the event ground motions to obtain the bent displacement and other demands.

Event Ground Motion (e.g., from CESMD)

Generic Bent Models
• Single Column
• Multi-Column
• Modeling parameters

Dynamic Analysis
• Linear
• Nonlinear

Report Displacement Demands

OpenSees
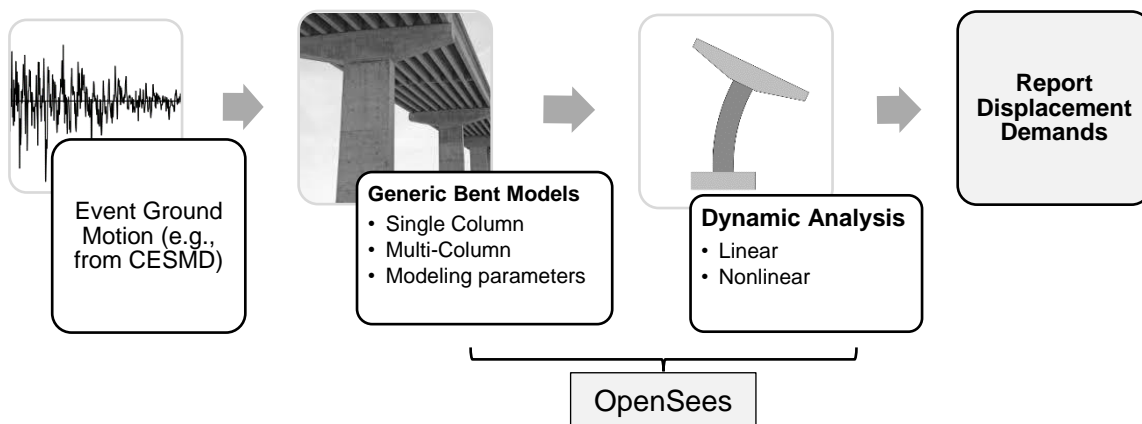
Figure ES.6 – Proposed Architecture for Cloud-Based Bridge Bent Dynamic Analysis

Nevertheless, an alternative approach to obtain seismic demands might be feasible if the post-earthquake conditions of the columns are related to the demands. Summaries of the past studies on how to relate observed damage of an RC column to seismic demands are presented in **Table ES.4**. Of which, the drift-damage equation by Berry and Eberhard (2008) is more convenient since it does not require additional structural analysis and the column drift demand can directly be estimated at different damage levels.

Table ES.4 – Summary of Past Studies on Relating RC Bridge Column Observed Damages to Demands

Damage	Drift Ratio, δ (%)	Plastic Rotation, θ_p (%)	Plastic Curvature, $\emptyset_p$ (rad/in)	Strain (in/in)	Reference
Cover Spalling	$1.6(1 - \frac{P_c}{A_g f_c'})(1 + \frac{L}{10.D_c})$	1.20	N.A.	0.008; compressive strain of the cover concrete	Berry and Eberhard (2008)
	N.A.	N.A.	$\frac{0.005}{c} - \emptyset_y$	N.A.	Marsh et al. (2014)
Core Crushing	N.A.	N.A.	$\frac{0.005 + 1.4 \frac{\rho_s f_{yh} \varepsilon_{suh}}{f_{cc}'}}{c - d''} - \emptyset_y$	N.A.	Marsh et al. (2014)
	N.A.	N.A.	N.A.	$1.4(0.004 + 1.4 \frac{\rho_s f_{yh} \varepsilon_{su}}{f_{cc}'})$ compressive strain of the core concrete	Murphy et al. (2020)
Long. Bar Buckling	$3.25(1 + \frac{150 \rho_s f_{yh} d_{bl}}{D_c f_c'})(1 - \frac{P}{A_g f_c'})(1 + \frac{L}{10.D_c})$	0.846δ	N.A.	$0.045 + 0.25 \frac{\rho_s f_{yh}}{f_c'} \leq 0.15$ tensile strain of long. steel bar	Berry and Eberhard (2008)
	N.A.	N.A.	$\frac{2 f_y / E_s}{c - d'} - \emptyset_y$	N.A.	Marsh et al. (2014)
	N.A.	N.A.	N.A.	$0.032 + 790 \frac{\rho_s f_{yh}}{E_s} - 0.14 \frac{P_c}{A_g f_c'}$ tensile strain of long. steel bar	Murphy et al. (2020)
Long. Bar Fracture	$3.5(1 + \frac{150 \rho_s f_{yh} d_{bl}}{D_c f_c'})(1 - \frac{P_c}{A_g f_c'})(1 + \frac{L}{10.D_c})$	0.857δ	N.A.	$0.045 + 0.30 \frac{\rho_s f_{yh}}{f_c'} \leq 0.15$ tensile strain of long. steel bar	Berry and Eberhard (2008)
	N.A.	N.A.	$\frac{\varepsilon_{sul}}{d - c} - \emptyset_y$	N.A.	Marsh et al. (2014)

Note: A_g is the column cross-sectional area; c is the depth from the extreme compression fiber of the cover concrete to the neutral axis; D_c is the column diameter (in.); d is the depth to the outer layer of tension steel from the extreme compression fiber; d' is the distance from the extreme compression fiber to the center of the nearest compression reinforcing bars, d'' is the distance from the extreme compression fiber of the cover concrete to the centerline of the perimeter hoop (thus, $c - d''$ is the depth of confined concrete under compression); d_{bl} is the nominal diameter of the column longitudinal reinforcing steel bars (in.); E_s is the steel bar modulus of elasticity (29000 ksi); f_{yh} is the yield stress of the column transverse reinforcing steel bars (ksi); f_c' is the concrete compressive strength (ksi); P_c is the column axial force (kips); L is the length of column from point of maximum moment to the point of moment contraflexure (in.); ε_{su} is the bar ultimate strain (ε_{suh} is for the transverse bar in "Core Crushing", ε_{sul} is for the longitudinal bar in "Long. Bar Fracture"), $\emptyset_y$ is the yield curvature (rad/in); ρ_s is the volumetric ratio of transverse reinforcement.

The new RC bridge column database compiled in the presented study was statistically analyzed to derive new empirical equations to estimate column drift ratios at the six damage states proposed in this study. **Table ES.5** presents a summary of the proposed equations and **Table ES.6** includes a summary of the statistical analyses. **Figure ES.7** schematically maps the drifts corresponding to these six damage states on an idealized pushover curve. Some of the statistical results were also included in the figure for completeness. It can be inferred that the proposed damage states cover the full range of the pushover curve all way from the linear-elastic region to the failure point. The first two damage states are within the column linear-elastic range. Furthermore, the drifts associated with the first three damage states (DS1 to DS3) are no more than 30% of the column failure drift thus one may assume this range (DS1 to DS3) as a safe domain for post-earthquake assessment. In other words, if the damage of an RC bridge column after an earthquake falls within DS1 through DS3, the column has approximately 70% reserved capacity thus may be assumed safe for post-earthquake serviceability and can be tagged "green" to be open to all traffics. DS4 has 50% reserved capacity thus may be tagged "yellow" to be open only to light traffics and first responders. Nevertheless, DS5 and DS6 have marginal to no safety thus the bridge must be tagged "red" and must be closed to all traffics. It is understood that the proposed serviceability limits are subjective. However, they are conservative and provide sufficient safety margin at the assigned rating levels. Note that the color coding of **Table ES.2** matches well with the drift limits discussed herein. This will allow performing post-earthquake assessments of RC bridge columns at different levels of PDA and DDA.

Table ES.5 – Summary of Proposed Damage State Based Drift Equations

Damage State	Proposed Equation
DS1	$\delta_{DS1} = 0.6\delta_{DS2}$
DS2	$\delta_{DS2} = \delta_y = L/4.5D_c$ for circular sections $\delta_{DS2} = \delta_y = L/5.12h_c$ for rectangular sections
DS3	$\delta_{DS3} = 0.3\delta_{DS6}$
DS4	$\delta_{DS4} = 0.5\delta_{DS6}$
DS5	$\delta_{DS5} = 0.8\delta_{DS6}$
DS6	$\delta_{DS6} = 1.3(1 + 150\rho_s)\left(1 - \frac{P_c}{A_g f'_c}\right)\left(1 + 0.3\frac{L}{D_c}\right)$ for circular sections $\delta_{DS6} = 2.2(1 + 25\rho_s)\left(1 - \frac{P_c}{A_g f'_c}\right)\left(1 + 0.3\frac{L}{h_c}\right)$ for rectangular sections

Notes: All drift ratios are in percentage (%), ρ_s is the volumetric ratio of transverse reinforcement according to AASHTO SGS [For a circular column, $\rho_s = 4A_{sp}/sD'_c$ where A_{sp} is the area of spiral or hoop reinforcing bar (in.² or mm²), s is the spacing of spiral or hoop (in. or mm), and D'_c is the core diameter of column measured from center of spiral or hoop (in. or mm). For a rectangular column, $\rho_s = A_v/sb'_c$ where A_v is the sum of area of the ties and cross ties running in the direction perpendicular to the axis of bending (in.² or mm²), s is the spacing of ties (in. or mm), and b'_c is the confined column cross-section dimension, measured out-to-out of ties, in the direction parallel to the axis of bending (in. or mm)], P_c is the column axial force (kips or kN), A_g is the column cross-sectional area (in² or mm²), f'_c is the concrete compressive strength (ksi or MPa), L is the length of column from point of maximum moment to the point of moment contraflexure (in. or mm), D_c is the column diameter (in. or mm), and h_c is the column side dimension in the testing (analysis) direction (in. or mm).

Table ES.6 – Summary of Statistical Analysis for Proposed Damage State Based Drift Equations

Section (Trans. Reinf.)	Damage State	No. of Columns	Average Error	Standard Deviation	Min Error	Max Error	Coefficient of Determination
Circular (Hoops or Spirals)	DS1	15	+9%	38%	-31.2%	+89.6%	0.89
	DS2	167	+1.4%	32.5%	-69.1	+82.2	0.90
	DS3	34	-5.5%	30.7%	-38.6	+79.7%	0.95
	DS4	40	-0.33%	29.4%	-35.2%	+74.8%	0.93
	DS5	38	+3.6%	21.5%	-19.9%	+55.9%	0.97
	DS6	173	+0.67%	29.6%	-53.5%	+77.7%	0.56
Rectangular (Ties)	DS1	6	+70.5%	140.5%	-28%	+284%	0.73
	DS2	56	+0.58%	35.7%	-59.7%	+89.6%	0.88
	DS3	10	-31.9%	18.9%	-54.5%	+5.4%	0.95
	DS4	13	+3.9%	35.4%	-44.9%	+65.9	0.94
	DS5	5	-9.7%	11.1%	-20%	+6.7%	0.99
	DS6	45	+2.1%	36.3%	-49.6%	+84.1%	0.0

Figure ES.7 – Damage State Drifts Mapped on Pushover Curves of RC Circular Bridge Columns

Estimation of displacement (or drift) capacity of an RC bridge column requires either a sectional (e.g., moment-curvature) or finite element analysis (e.g., pushover). Even though moment-curvature analysis is a convenient method to obtain column capacities, it does not include the bridge/bent overall geometry and geometric nonlinearities (such as P-Delta effects). More advanced and maybe accurate capacity estimation method for a bridge column is through a nonlinear static analysis, commonly referred to as a pushover analysis. The present study recommends performing pushover analysis for post-earthquake bridge column assessments. To facilitate this method, a cloud-based tool was developed, which can perform pushover analysis of any RC circular column using only eight parameters. A generic model was developed in OpenSees and is being utilized in the tool.

The accuracy of the proposed DS based drift demand equations was evaluated using a test data (Sjurseth, 2021) that was not included in the column database. The half-scale octagonal column was 96-in. (2438 mm) tall and had a diameter of 24 in. (610 mm). The column key properties and a summary of the drift demands at the six damage states are listed in **Table ES.7**. **Figure ES.8** schematically shows the calculated and measured responses. The proposed method estimates that this column will have a few flexural cracks at 0.53% drift, which agreed with the observed damage at this drift. The proposed method estimates that the column will yield at 0.89% drift. In fact, the column yielded in the testing during the first cycle of 0.75% drift. The drifts at DS3 and DS5 were overestimated, which is safe since the column will be assessed for larger demands. The estimated drifts at DS4 and DS6 were very close to those seen in the testing. The actual column failed by bar fracture during the first cycle of 10% drift. The proposed DS6 equation accurately estimated this drift level. Overall, a good agreement was observed when the drifts at critical points were estimated using the proposed empirical equations.

Table ES.7 – Validation of Proposed Drift Demand and Capacity Equations for a Half-Scale Octagonal Column

Key Inputs	Column Length, L = 96 in. (2438 mm); Column Diameter (Octagonal), D_c = 24 in. (610 mm); Number of Long. Bars = 10; Area of Each Long. Bar, A_{sl} = 0.76 in^2 (509 mm^2); Spacing b/w Transverse Bars, s = 2 in. (51 mm); Area of Each Transverse Bar, A_{sp} = 0.2 in^2 (129 mm^2); Concrete Strength, f'_c = 4.92 ksi (33.9 MPa); Column Axial Load, P_c = 155 kips (689.5 kN)
Intermediate Parameters	A_g (octagonal) = 476.9 in^2 (307676.8 mm^2); Clear cover = $0.045D_c = 0.045 \times 24 = 1.08\ in.\ (27.4\ mm)$, only 8% error compared with the actual cover of 1 in.; $\rho_s = \frac{4A_{sp}}{sD'_c} = \frac{4 \times 0.2}{2 \times (24 - 2 \times 1.08 - 0.5)} = 0.01874$; f_{yl} = 68 ksi (468.8 MPa) according to AASHTO SGS not test data; $\frac{P_c}{A_g f'_c} = \frac{155}{476.9 \times 4.92} = 0.066$;
Critical Points	**Proposed Equations**
DS6	$\delta_{DS6} = 1.3(1 + 150\rho_s)\left(1 - \frac{P_c}{A_g f'_c}\right)\left(1 + 0.3\frac{L}{D_c}\right) = 1.3(1 + 150 \times 0.01874)(1 - 0.066)(1 + 0.3 \times 4) = 10.18\%$
DS5	$\delta_{DS5} = 0.8\delta_{DS6} = 0.8 \times 10.18 = 8.14\%$
DS4	$\delta_{DS4} = 0.5\delta_{DS6} = 0.5 \times 10.18 = 5.09\%$
DS3	$\delta_{DS3} = 0.3\delta_{DS6} = 0.3 \times 10.18 = 3.05\%$
DS2	$\delta_{DS2} = \delta_y = \frac{L}{4.5D_c} = \frac{96}{4.5 \times 24} = 0.89\%$
DS1	$\delta_{DS1} = 0.6\delta_{DS2} = 0.6 \times 0.89 = 0.53\%$
Idealized Yield Drift	$\delta_{yi} = 1.2\delta_{DS2} = 1.07\%$
Plastic Shear Force	$V_p = 0.35 f_{yl}\frac{D_c^3}{L}\left(\frac{A_{sl}}{A_g}\right)\left(1 + \frac{P_c}{A_g f'_c}\right) = 0.35 \times 68 \times \frac{24^3}{96} \times \frac{10 \times 0.79}{476.9} \times (1 + 0.066) = 60.5$ kips (or 269 kN)

Figure ES.8 – Validation of Proposed Damage State Based Drift Equations for Octagonal Bridge Column Tested by Sjurseth (2021)
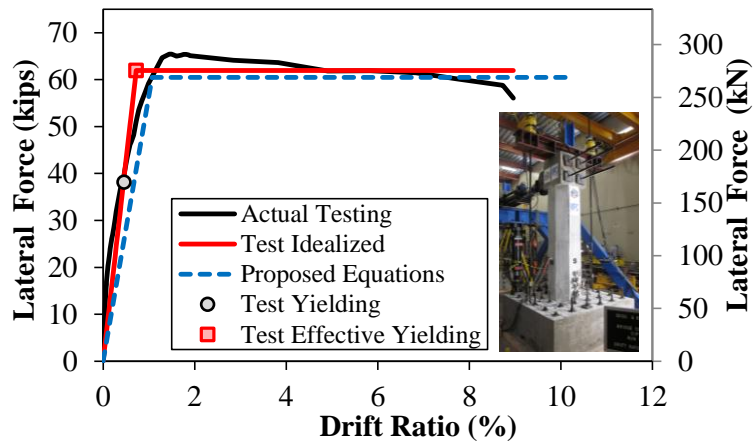
Figure ES.9 – Estimated vs Measured Idealized Pushover Curves for Octagonal Bridge Column Tested by Sjurseth (2021)

Figure ES.9 shows the measured and estimated idealized pushover curves for the half-scale octagonal RC bridge column. It can be seen that the proposed method results in an overall good agreement with the measured data, thus may be used for a quick assessment of RC bridge columns after an earthquake.

ES.7 RC Column Damage State Detection Software

In this project, a deep learning technique was used to detect damages and quantify their properties for the subsequent detailed damage assessment step. An instance segmentation technique (e.g., Mask R-CNN by He et al., 2017) was used to detect damages. The segmented regions were used to extract useful properties, such as length, orientation, and the number of instances within a specific region (Yein et al., 2018). A cascade approach was developed by using deep neural networks (DNNs) designed for classification (e.g., MobileNet by Sandler et al., 2018) and instance segmentation (e.g., Mask R-CNN) tasks. MobileNet V2, a CNN architecture for classification, was used for detecting cracks by classifying small image patches. Mask R-CNN was used to detect and segment the target column, spalling, and exposed vertical/horizontal bars in the image. The outputs of the DNNs were processed to extract the parameters used in defining the column damage state.
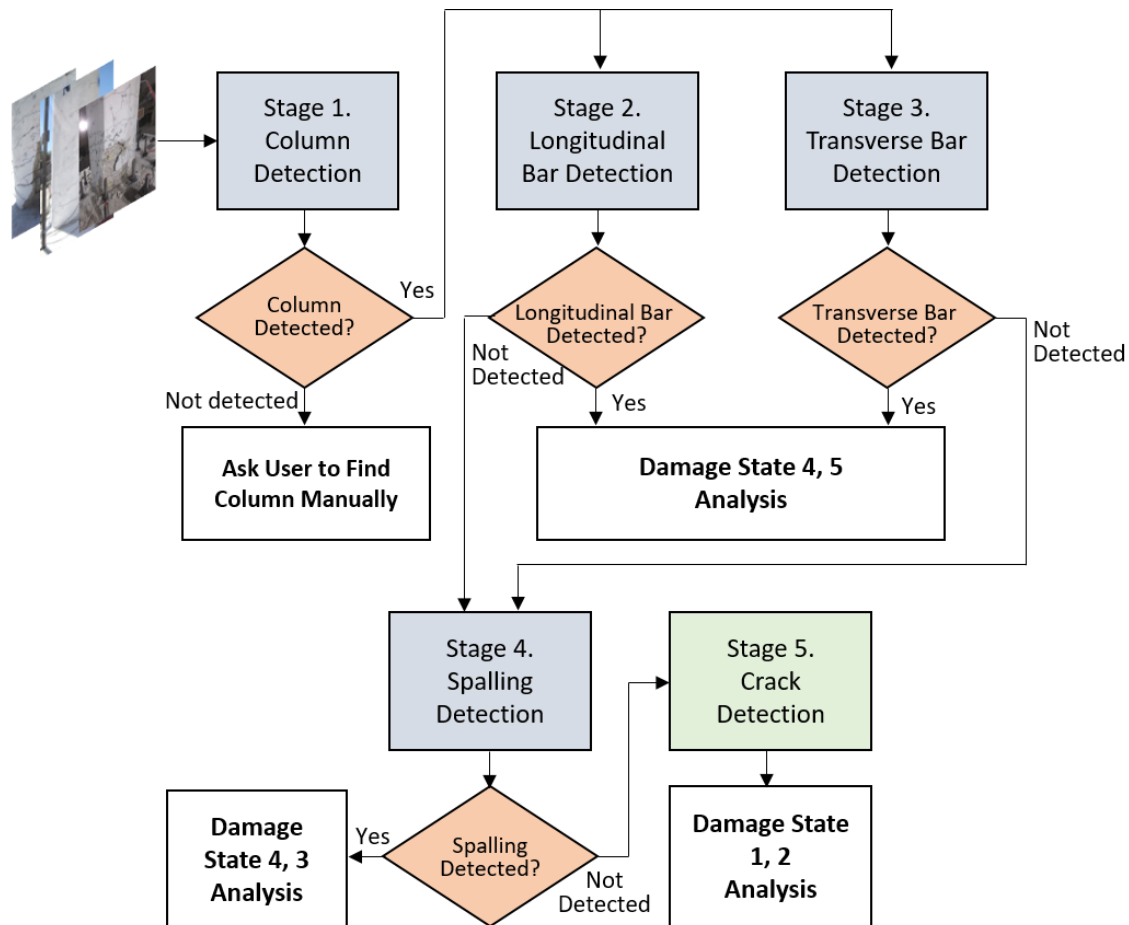
Figure ES.10 – AI-based Damage State Decision Flowchart

Figure ES.10 shows the flowchart of the cascade damage detection and damage state analysis. The proposed computer vision tool (CVT) starts the analysis first with the column detection, then looks for rebars. If no rebar is detected, it searches for spalling. If there is no spalling, the cracks are detected. This order of damage detection was selected because more server damages such as exposed rebar are more critical for damage assessment than cracking. For a successful damage state identification, cracking is evaluated with the number of horizontal and vertical cracks and their angles. For the spalling, the ratio of the longest width within the spalled region to the column width is estimated, and the number of vertical and horizontal exposed steel bars is counted. Based on these results, the proposed CVT determines the damage state following the proposed definition (**Table ES.2**).

The workflow was implemented using DNNs and additional computer codes that process the outcomes of DNNs and extract properties. For efficient computation, the DNN models for the detection tasks of Stages 1 to 4 were combined into a single DNN module, but the crack detection in Stage 5 was implemented as an independent module due to the different characteristics of the component. The flowchart contains potential interactions with users for the case that the DNNs fail to identify components in the image. Each of these modules is further discussed in the following sections.

Mask R-CNN (**Fig. ES.11**) was used for the initial detection of the damaged regions. ResNet101 (He et al., 2016) architecture was used as the backbone network, which is responsible for hierarchical spatial feature extraction. The Region Proposal Network (RPN) in the Mask R-CNN architecture generates anchors (rectangular areas of various scales and aspect ratios) over the image and scores the probability of the existence of objects at each location and bounding box. Bounding boxes with high probability were selected and downsized to a unit scale for the subsequent classification layers and mask generation layers. The classification subnetwork was fully connected layers with categorical output. The mask generation was done by predicting the binary value of each pixel in the mask. The size and location of the results of these subnetworks were recovered with respect to the input image. The backbone network is typically trained on a very large image dataset, such as ImageNet (Krizhevsky et al., 2012). However, the other components of Mask R-CNN must be retrained on the target problem and dataset.
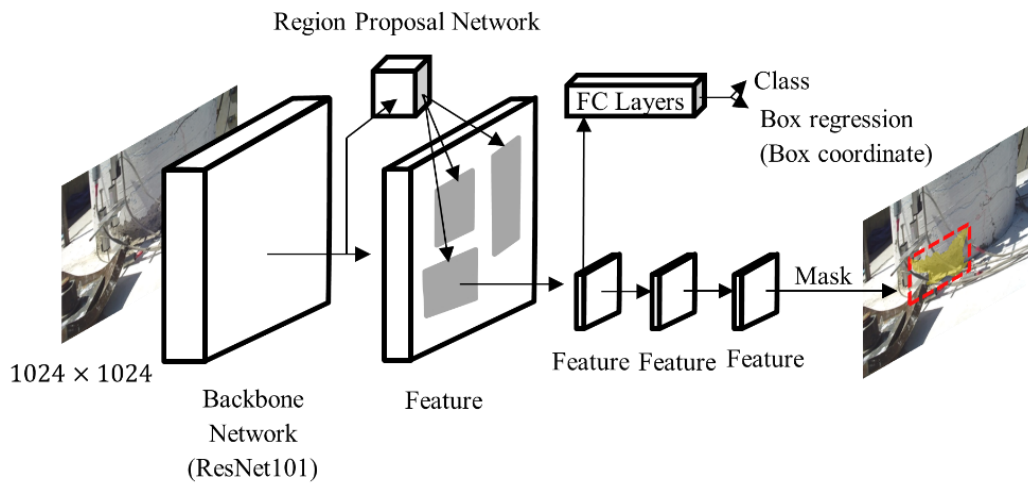
Figure ES.11 – Mask R-CNN Overall Network Architecture

For training the Mask R-CNN module, each image was labeled with four classes (column, spalling, transverse bar, and longitudinal bar) and one background class. The weight was initialized by pre-trained weight of the COCO dataset (Lin et al., 2014) with a batch size of 2 to fine-tune the network using the dataset collected in this study. The model was trained with NVIDIA GeForce GTX 1080 Ti, which is equipped with 12GB GPU RAM. The backbone architecture was ResNet101 and trained for 70 epochs with a learning rate of 0.02. During the training, Mask R-CNN weights were updated using a multi-task loss function. MobileNet V2 for crack detection was trained with the dataset collected in this study, and this module takes an input size of 224×224. MobileNet V2 rescaled the crack patches, and the same GPU was used with a batch size of 96. Further, a batch normalization was used between layers, and the ReLU activation function was used. The loss function of this network was a categorical cross-entropy loss, and the learning rate was empirically chosen as 0.0001. In the testing step, three shapes of RC columns (circular, octagonal, and rectangular) were used. **Figure ES.12** shows the detected damages for different damage states and **Table ES.8** presents the results of a sample analysis for the column shown in **Fig. ES.12e**. Each detected object was color-coded (red for columns, green for spalled region, blue for transverse bars, purple for longitudinal bars) for the ease of identification.
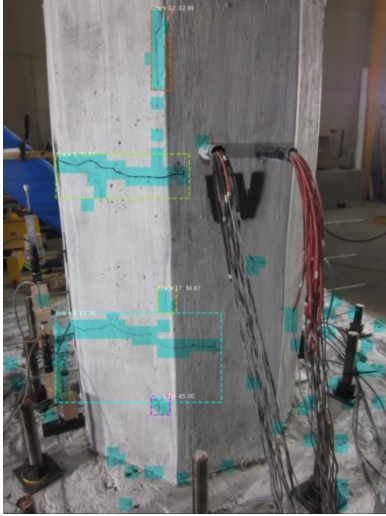
(a) Damage State 1 (DS1)

(b) Damage State 2 (DS2)

(c) Damage State 3 (DS3)

(d) Damage State 4 (DS4)
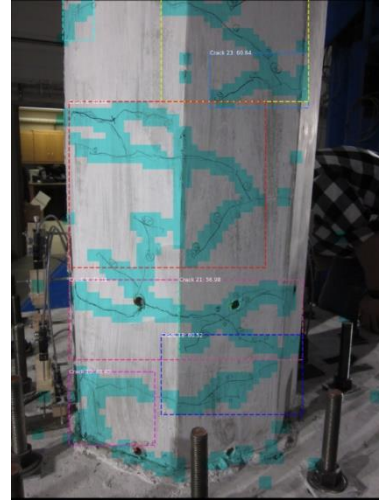
Column Photo Courtecy: Dr. Haber
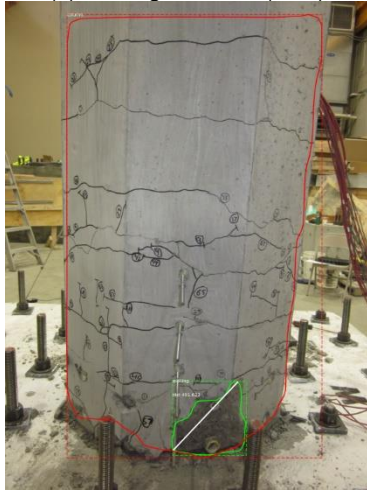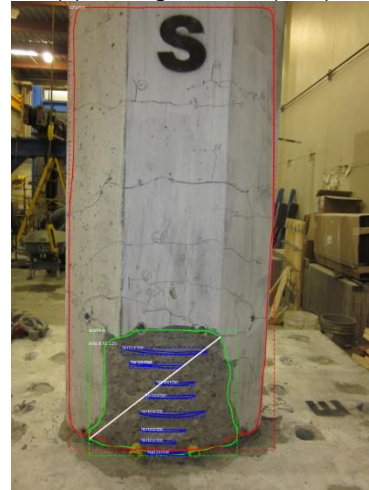
Column Photo Courtecy: Prof. Sideris
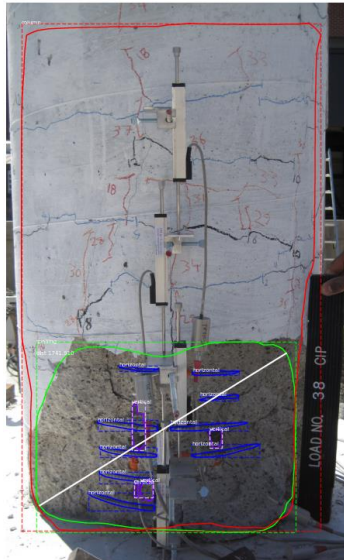
(e) Damage State 5 (DS5) for Circular Column
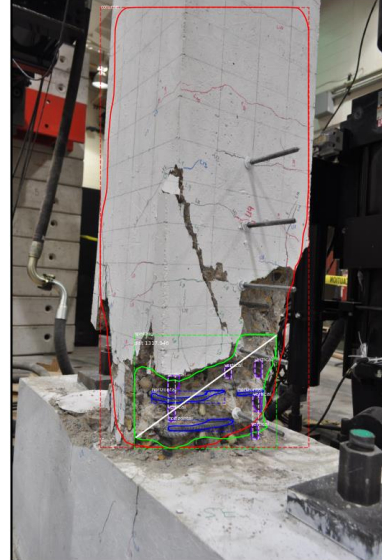
(f) Damage State 5 (DS5) for Rectangular Column

Figure ES.12 – Samples of Damage Assessment by AI Computer Vision Software

Table ES.8 – Sample of AI Computer Vision Analysis Results for Fig. ES.12e

Analysis Component	Computer Vision Analysis Results	Ground Truth (Actual)
Number of Horizontal Cracks	N/A	N/A
Number of Vertical Cracks	N/A	N/A
Maximum Length of Spalled Region (px)	1741.91	1904.2
Column Width (px)	N/A	1847 (24 in.)
Number of Transverse (Horizontal) Bars	6	6
Number of Longitudinal (Vertical) Bars	2	2
Damage State (DS)	5	5

The performance of the trained Mask R-CNN was evaluated in terms of "precision" and "recall", which are calculated by the instances of true positives (TPs), true negatives (TNs), false positives (FPs), and false negatives (FNs). The precision is the ratio of the true positives to the overall positive responses (TPs+FPs), and the recall is the ratio of the true positive to the sum of the true positives and false negatives. Each number is determined from the overlapping areas between resulted detection (masks) and the ground truth. The evaluation is performed on 20% of the dataset (equivalent to 46 images) which was set aside for testing. The performance of the trained Mask R-CNN module is measured in terms of the precision and recall of the localization and segmentation. The localization performance is measured based on the bounding boxes, and the segmentation performance is measured based on pixel-level detection results. **Table ES.9** presents the average precision and recall for each category (column, spalling, and exposed bars). The result shows that the performance of localization is above 90 percent and, the segmentation performance is over 88.9 percent.

Table ES.9 – Evaluation of Target Deficiency Detection for Each Component

Components	Number of Instances	Localization Precision (%)	Localization Recall (%)	Segmentation Precision (%)	Segmentation Recall (%)
Column	41	90.13	90.91	88.90	89.23
Spalled area	72	95.28	95.88	93.97	88.71
Transverse bar	56	95.27	95.82	92.71	93.14
Longitudinal bar	31	92.31	92.79	91.83	92.17
Average		93.24	93.85	91.10	90.81

Furthermore, the crack classification network was evaluated using the precision and recall. A total 4,842 images (2,320 images with cracks and 2,522 images without cracks) were tested, and the precision and recall scores were calculated for each class (cracked, uncracked, **Table ES.10**). Overall, the trained model showed more than 95% precision and recall. The classifier showed slightly better performance on uncracked images. On average, the model showed 97.4% and 96.1% precision and recall, respectively.

Table ES.10 – Evaluation of Target Deficiency Detection for Cracks

Component	Number of Images	Precision (%)	Recall (%)
Cracked	2,320	96.32	95.28
Uncracked	2,522	98.45	96.94
Average		97.38	96.11

ES.8 Proposed Post-Earthquake Bridge Column Evaluation Methodology

Due to a lack of national and unified specifications for bridges, the four-level assessment and the three-level coding proposed in the NCHRP 833 report were adopted in the present project to assess bridges after earthquakes. Of the four assessment levels, a relatively quick post-earthquake evaluation of RC bridge columns at the Preliminary Damage Assessment (PDA) and Detailed Damage Assessment (DDA) levels are feasible due to the incorporation of the computer vision. **Figure ES.13** shows a flowchart on how to carry out PDA and DDA using the tools and methods developed in the present project. PDA is done using photographs of columns and DDA requires the column details in addition to the photos.

In PDA, the user (who may not necessarily be a trained inspector or bridge engineer, but an authorized local personnel) will upload the bridge column damage photograph(s) to the computer vision tool (CVT). The photographs can be taken by a camera, cellphone, tablet, or drone. Per each photo of the column, this tool counts the exposed longitudinal and transverse bars, if any, measures the maximum spalled region length, if any, and counts the number of horizontal and vertical cracks. Subsequently, the column damage state (DS) is determined, and its serviceability is evaluated based on the proposed DS definitions (**Table ES.2**). For example, if DS4 is reported by CVT, the bridge is "yellow" tagged meaning that it should be open only to light traffics and first responders.
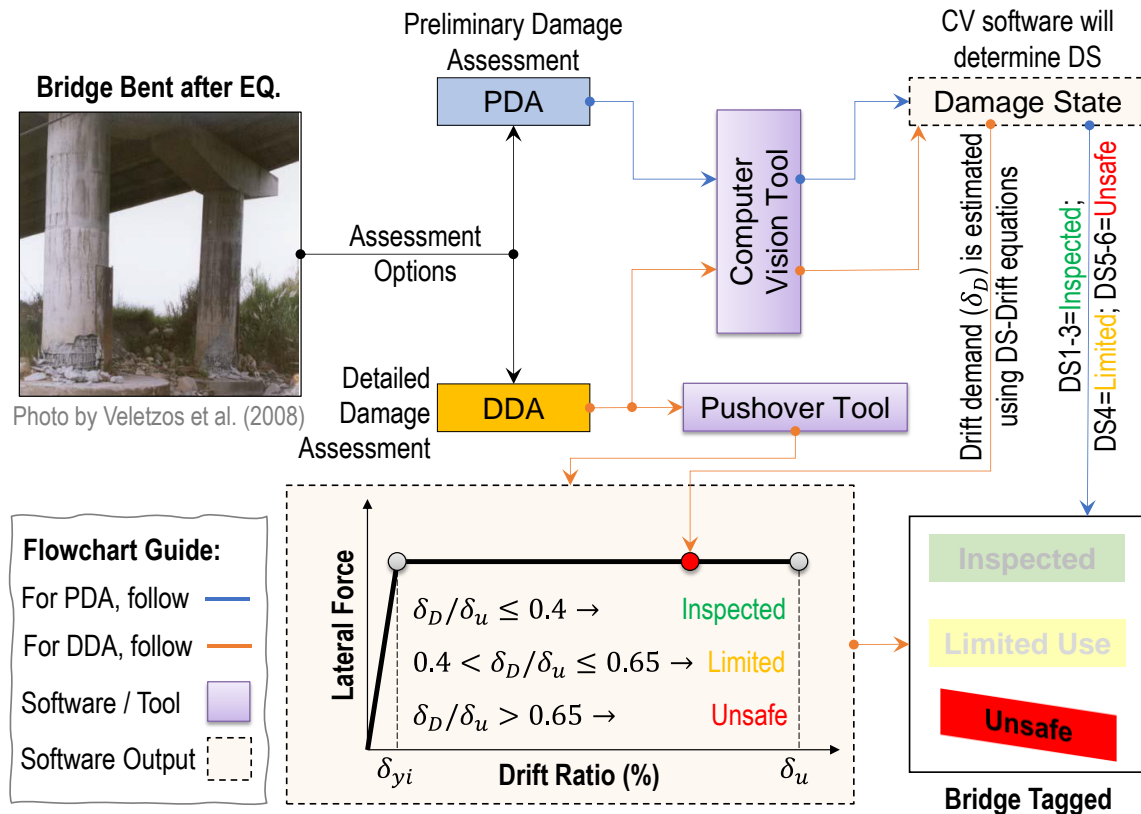
Figure ES.13 – Proposed Post-Earthquake RC Bridge Column Evaluation Using Computer Vision

In DDA, DS of the affected column should be determined, and the column pushover curve should be generated for a complete analysis. DS is determined using CVT. Subsequently, the column drift demand is determined using the proposed DS based drift equations (**Table ES.5**). OpenSees or any other structural analysis software may be used to carry out a pushover analysis. Then, the estimated drift demand should be mapped on the pushover curve. Based on the drift demand to the drift capacity ratio (δ_D/δ_u), the bridge column serviceability can be assessed (**Table ES.11**).

Table ES.11 – Drift Demand to Capacity Ratio in Detailed Damage Assessment (DDA) of RC Bridge Columns

Damage State	Drift Demand (δ_D)	Drift Capacity (δ_u)	Drift Demand to Capacity Ratio	Tag as
Determine DS1-6 using the computer vision tool	Estimate drift demand using the proposed damage state based drift equations	Obtain the drift capacity through a pushover analysis	$\delta_D/\delta_u \leq 0.4$	Inspected
			$0.4 < \delta_D/\delta_u \leq 0.65$	Limited Use
			$\delta_D/\delta_u > 0.65$	Unsafe

To facilitate the implementation of the proposed PDA and DDA, a website was developed to perform these analyses for RC bridge columns. When a damage photo of an RC bridge column is uploaded, the website runs the AI computer vision tool for PDA and DDA and also OpenSees for DDA on a server, and reports back to the user a summary result for PDA and DDA. Sample results for PDA and DDA using the cloud-based tools are shown in **Fig. ES.14-15**. **Appendix B** of the present report includes the details of the bridge assessment website.

Figure ES.14 – Sample Results of Cloud-Based Tools for Bridge Column Preliminary Damage Assessment

Figure ES.15 – Sample Results of Cloud-Based Tools for Bridge Column Detailed Damage Assessment

ES.9 Summary and Conclusions

To expedite post-earthquake inspection and assessment of RC bridge columns using computer vision, several tasks were completed. First, the literature was reviewed to collect information on visual assessment of RC bridge columns, to identify existing RC bridge column test database, and to synthesize the latest development on computer vision. Second, a new definition was proposed to categorize RC bridge column damage types and condition states that are suitable for computer programing. Third, the most comprehensive database of RC bridge column experimental performance including more than 30 parameters per test specimen was developed. The database was subsequently used to relate bridge column damage states to displacement demands. Furthermore, an artificial intelligence (AI) enabled software was developed based on a photograph database of damaged RC bridge columns to quickly detect cracking, spalling, and reinforcement, to comment on the RC column damage state, and to tag (green, yellow, or red) the column/bridge based on the extent of the damage. The software performs both Preliminary Damage Assessment (PDA) and Detailed Damage Assessment (DDA) using a few column parameters and provides a quick and safe assessment. The following conclusions can be drawn based on the analytical, statistical, and computer vision studies:

- The literature lacks a systematic reconnaissance database for bridges especially columns after earthquakes. The damage of only a few bridges after recent earthquakes has been documented/published.
- The proposed definitions for RC bridge column damage states are quantitative and may be used in computer programs for quick identification of various damage types and levels.
- The most comprehensive RC bridge column test database collected in the present project currently includes 222 circular and 68 rectangular columns, and can be accessed through a public domain.
- The empirical equations developed in the present project to estimate RC bridge column drift demands at the six damage states showed a reasonable accuracy for a large pool of test data. The equations were further validated using a half-scale octagonal bridge column that was not in the database.
- The drifts corresponding to the proposed six-level damage states cover the full range of the column pushover response, and are proposed as a baseline for serviceability assessments.
- With a reasonable accuracy, the generic OpenSees model performs a pushover analysis of any single-column RC bridge bent using only eight parameters. The tool was successfully incorporated in a website to confirm the feasibility of developing online tools for quick structural analysis of damaged bridges.
- For DDA, the serviceability of any RC bridge column after an earthquake can be evaluated using the drift demand to drift capacity ratio.
- The AI-based computer vision tool can detect RC bridge column cracks with a precision and recall of 97% and 96%, respectively. Furthermore, the precision and recall of this tool to detect concrete spalling was respectively more than 94% and 88%. The precision and recall for the rebar detection were more than 91%. Overall, the computer vision tool detects different damages of RC bridge columns relatively quick and with a reasonable accuracy.
- The angular histogram proposed in the present project can reveal the crack major angle with a reasonable accuracy.

A combined use of the computer vision tool, the generic pushover tool, and the empirical DS-based drift equations results in a package that can perform both PDA and DDA on RC bridge columns using a few parameters. The proposed flowchart was found feasible and was implemented in a website.

In summary, the findings of the present project can be utilized in a professional software, which can help transportation agencies with a quick, systematic, and safe serviceability assessment of RC bridge columns after earthquakes.

CHAPTER 1. INTRODUCTION

1.1 Introduction

Modern seismic design codes ensure a large displacement capacity and prevent total collapse for bridges. However, this performance objective is usually attained at the cost of damage to target ductile members. For reinforced concrete (RC) bridges, the columns are usually the main source of ductility during an earthquake in which concrete cover, core, and reinforcement may damage, and the column may experience a large permanent lateral deformation.

According to FHWA (2020), more than 618,000 bridges in the USA are in service (**Fig. 1.1**). Of which, 45% are in good conditions, 48% are in fair conditions, and 7% are in poor conditions. Furthermore, the latest national seismic hazard map (USGA, 2018) identifies 16 seismic prone states with a high risk of having a damaging earthquake in the next half century. Those states are Alaska, Arkansas, California, Hawaii, Idaho, Illinois, Kentucky, Missouri, Montana, Nevada, Oregon, South Carolina, Tennessee, Utah, Washington, and Wyoming (**Fig. 1.2**). These states have currently a total of 171,590 bridges in service. The exact number of bridges located in high-seismic regions yet to be determined; however, assuming a uniform seismicity per state, 28% of the national bridge inventory might experience a large earthquake that could cause a significant damage.

Each dot is a bridge
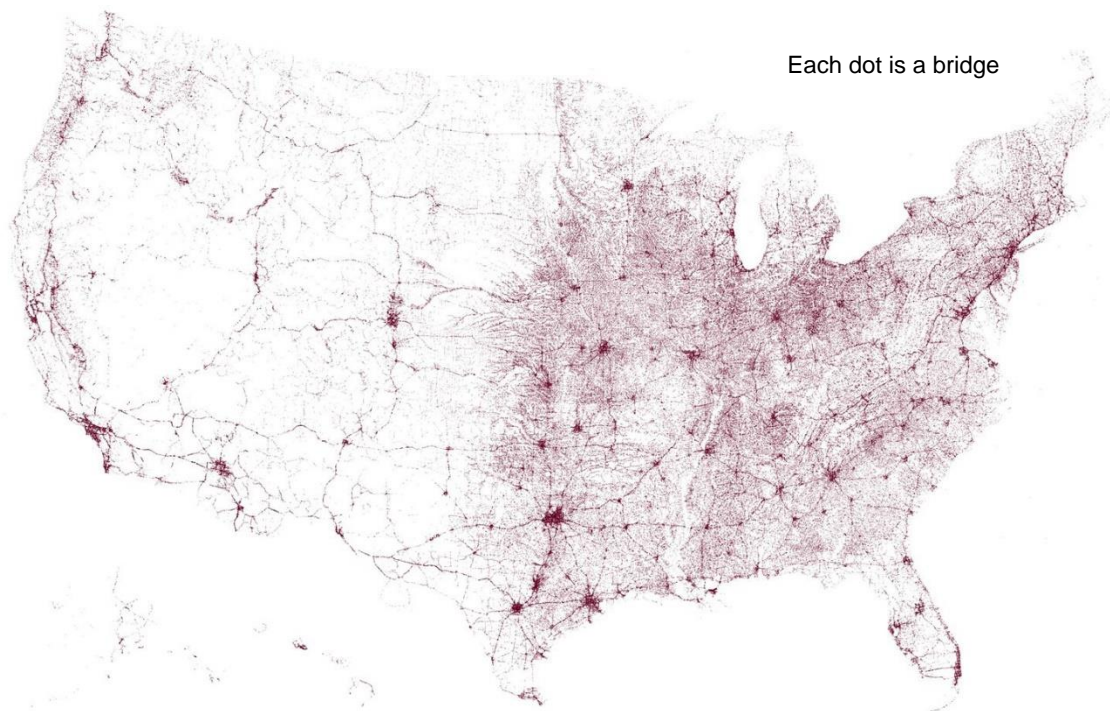
Figure 1.1 – Map of USA Bridges (Washington Post, 2015)
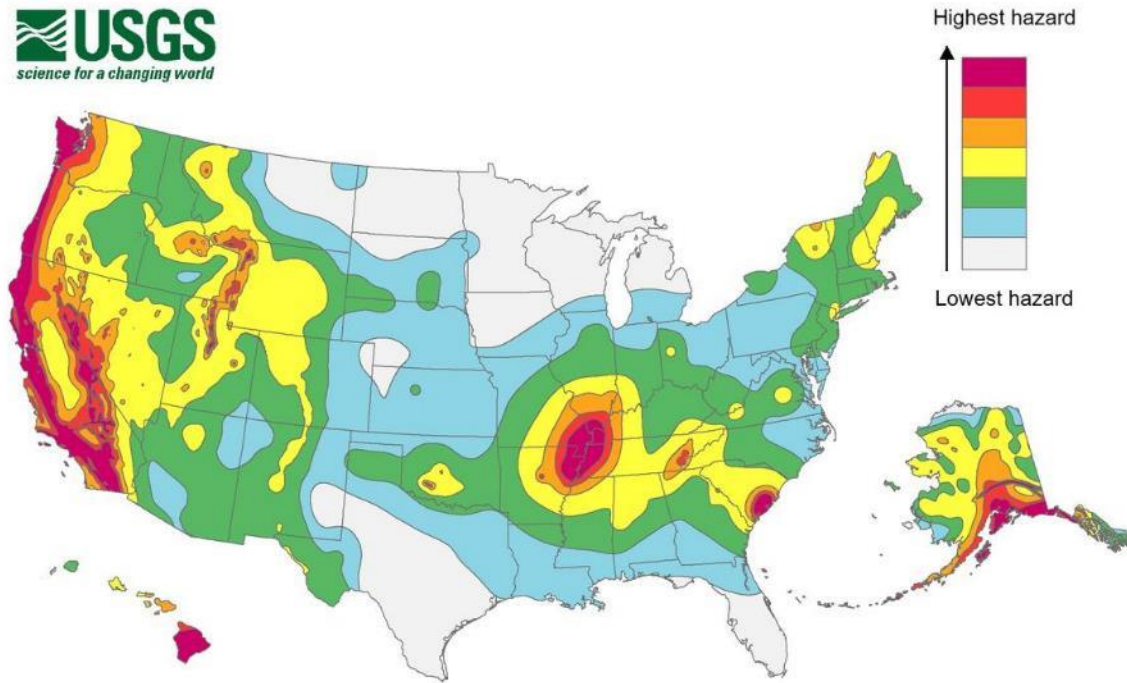
Figure 1.2 – USGS 2018 Seismic Hazard Map of USA (USGS, 2018)

Post-event bridge assessment is currently performed by sending trained inspectors to each site for a preliminary evaluation, data collection, and tagging the bridge (to remain open, to be closed, or to have limited access). Several inspectors might be needed per event, and the process is generally time consuming (a few hours per visit). An alternative and quick damage assessment of bridges immediately after severe events is needed to maximize serviceability and access to the affected sites, and to minimize casualties and costs. This is especially critical after earthquakes since the first few hours after ground shaking are the most critical time window for rescue operations.

1.2 Objectives and Scope

The main goal of this project was to accelerate post-earthquake serviceability assessment of RC bridge columns using "computer vision". When sending trained personnel to the affect sites is limited or will take time, local personnel equipped with an assessment software (on various platforms such as mobile applications, cloud-based tools, or built-in with drones) can be deployed to evaluate the bridge condition. The project was focused on the damage assessment of modern RC bridge columns after earthquakes. Substandard columns, other bridge components, and other hazards were not included.

To achieve the project goal, several tasks were completed. First, the literature was reviewed to collect information on visual assessment of RC bridge columns, to identify existing RC bridge column test database, and to synthesize the latest development on computer vision. Second, a new definition was proposed to categorize RC bridge column damage types and condition states that are suitable for computer vision. Third, the most comprehensive database of RC bridge column experimental performance including more than 30 parameters per column was developed. The database was subsequently used to relate bridge column damage states to displacement demands. Furthermore, an artificial intelligence (AI) enabled software was developed based on a photograph database of damaged RC bridge columns to quickly detect cracking, spalling, and reinforcement, to comment on the RC column damage state, and to tag (green, yellow, or red) the column based on the extent of the damage.

1.3 Expected Contributions

The main products in this phase of the project are: (1) a comprehensive RC bridge column performance database, (2) an open-source computer program that performs post-earthquake Preliminary Damage Assessment (PDA) and Detailed Damage Assessment (DDA) for RC bridge columns, and (3) cloud-based tools with graphical user interface (GUI) to better utilize the software. The RC bridge column database and the software source codes are available to public at no cost.

1.4 Document Outline

As part of cover materials, an executive summary was presented in a chapter with the same name. Chapter 1 presents an introduction of the study and the scope of the work. A literature review on visual bridge assessment, current RC column database, and computer vision is conducted, and a summary is presented in Chapter 2. Chapter 3 discusses the current methods of bridge column damage classification and provides a new definition for RC bridge column damage types and damage states suitable for computer programing. Chapter 4 provides a summary of the RC column bridge database development and findings. Chapter 5 presents methods to estimate the RC bridge column displacement demands and capacities using only a few column parameters. Development of the AI-enabled damage detection tools, their verifications, and sample results are presented in Chapter 6. Chapter 7 offers a flowchart on how to use all the tools developed in this project to perform PDA and DDA of RC bridge columns after earthquakes. Finally, the summary and conclusions of the study are presented in Chapter 8. Appendix A includes the photographs of columns appeared in the column experimental database (Ch. 4). Furthermore, Appendix B shows some features of the cloud-based tools developed in this project.

CHAPTER 2. LITERATURE REVIEW

2.1 Introduction

Inspection and assessment of civil infrastructure are usually performed after a localized or wide-spread event. However, national guidelines and specifications for post-event assessment of different structures under various hazards are currently in the development phase. For buildings, national documents exist to perform post-event assessments. Nevertheless, national guidelines and/or specifications to uniformly assess post-event performance of bridges are lacking.

This chapter is mainly focused on the post-earthquake assessment of bridges, state and national guidelines on how to perform such assessment, and presents a summary of emerging techniques such as computer vision that might expedite structural inspections after an event.

2.2 Post-Event Damage Assessment of Bridges

Bridges have been categorized based on their geometry (e.g., truss, arch, girder, cable-stayed, or suspension bridges), material types (concrete, steel, timber, or others), and/or seismic design (conventional or non-conventional). For example, AASHTO SGS (2011) only applies to conventional bridges, those that "*have slab, beam, box girder, and truss superstructures; and have pier-type or pile-bent substructures; and are founded on shallow- or piled-footings or shafts*." Bridges designed with current AASHTO SGS are expected to exhibit minimal damage under moderate earthquakes, and the collapse is prevented under rare earthquakes. Collapse prevention means that damages such as cracking, reinforcement yielding, major spalling, and local buckling of steel columns are allowed thus the affected bridge may be closed for repair, and partial or complete column/bridge replacement may be needed.

It is a common practice to detail conventional reinforced concrete (RC) bridges using "weak-column, strong-beam" design philosophy in which columns are the weak links in the system. Most of the column damage; therefore, is localized at the column ends (**Fig. 2.1**). Seismic isolations are also allowed but they are not very common. For example, Buckle et al. (2011) reported that approximately 200 bridges in the USA (less than 0.04% of the national inventory) have utilized a form of seismic isolation.
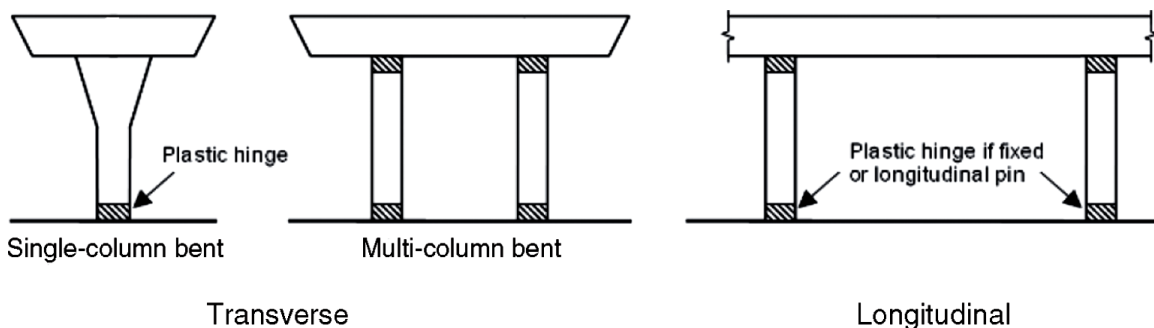
Figure 2.1 – Plastic Hinging in Modern Bridge Bents (ACI 314.4R, 2016)

Various damage types have been reported for conventional RC bridges under earthquakes. **Figure 2.2** shows post-earthquake condition of RC bridge columns designed per old codes, which are usually referred to as "substandard columns", those that are not designed and detailed per seismic requirements.

For example, substandard RC columns lack sufficient transverse reinforcement, have lap splicing at the column ends or insufficient development length, and may have relatively short lengths. The US seismic codes have significantly been enhanced and modernized after the 1994 Northridge earthquake (Moehle and Eberhard, 2000). In general, one may assume that bridges built in the USA before 1995 include substandard columns and those constructed afterwards usually incorporate standard columns. Moehle and Eberhard (2000) summarized the performance of bridges affected by the 1994 Northridge earthquake (**Table 2.1**). Bridge collapse and significant damage of RC columns were reported.

Table 2.1 – Summary of Bridge Damages under the 1994 Northridge Earthquake (Moehle and Eberhard, 2000)

Bridge Name	Route	Construction Year	Damage
La Cienega-Venice Undercrossing	I-10	1964	Collapse, Column Failures
Gavin Canyon Undercrossing	I-5	1967	Collapse, Unseating at Skewed Expansion
Route 14/5 Separation and Overhead	I-5/SR14	1971/1974	Collapse, Column Failures
North Connector	I-5/SR14	1975	Collapse, Column Failures
Mission-Gothic Undercrossing	SR118	1976	Collapse, Column Failures
Fairfax-Washington Undercrossing	I-10	1964	Column Failures
South Connector Overcrossing	I-5/SR14	1971/1972	Pounding at Expansion Hinges
Route 14/5 Separation and Overhead	I-5/SR14	1971/1974	Pounding at Expansion Hinges
Bull Creek Canyon Channel Bridge	SR118	1976	Column Failures

(a) Higashi-Nada Viaduct Collapse in the 1995 Hyogo-Ken Nanbu EQ (Chung et al., 1996)

(b) Bull Creek Canyon Channel Bridge Damage in the 1994 Northridge EQ. (Moehle & Eberhard, 2000)

(c) San Fernando Road Overhead Damage in the 1971 San Fernando EQ (Moehle & Eberhard, 2000)

(d) Juan Pablo II Bridge Damage in the 2010 Maule EQ, Built in 1974 (Yashinsky et al., 2010)

Figure 2.2 – Damage of Substandard RC Bridge Columns

(e) Shida Hashi Bridge Cracks at Column Base in the 2011 Tohoku EQ, Built in 1957 (EERI, 2011)

(f) Shida Hashi Bridge Cracks at Column Top in the 2011 Tohoku EQ, Built in 1957 (EERI, 2011)

(g) Fuji Bridge Damage with Insufficient Development in the 2011 Tohoku EQ, Built before 1990 (Kawashima and Buckle, 2013)

(h) Shear Failure of Pier Wall of the Wu-Shi Bridge in the Chi-Chi EQ (ACI 314.4R, 2016)

(i) Bridge 0729 Damage at Bent Top in the Feb. 2020 Puerto Rico EQ, Built in 1961 (Photo by Dr. Manuel Coll)

(j) Bridge 0729 Damage at Column Top in the Feb. 2020 Puerto Rico EQ, Built in 1961 (Photo by Dr. Manuel Coll)

Figure 2.2 – Damage of Substandard RC Bridge Columns, Continued

(k) Bridge PR-2 Mayagüez Damage at Bent Top in the Jan. 2020 Puerto Rico EQ, Built before 1980 (Miranda et al., 2020)

(l) Bridge PR-2 Mayagüez Damage at Column Top in the Jan. 2020 Puerto Rico EQ, Built before 1980 (Photo by Wallice J. de la Vega)

(m) Bridge 2417 Damage at Bent Top in the Jan. 2020 Puerto Rico EQ, Built in 1961 (Miranda et al., 2020)

(n) Bridge 2417 Damage at Column Top in the Jan. 2020 Puerto Rico EQ, Built in 1961 (Miranda et al., 2020)

Figure 2.2 – Damage of Substandard RC Bridge Columns, Continued

At the design level earthquakes, the damage of standard columns; however, should be limited and repairable. The literature lacks a systematic reconnaissance database for bridges especially columns after earthquakes. Earthquake Engineering Research Institute (EERI), Federal Highway Administration, (FHWA), and Structural Extreme Events Reconnaissance (StEER) have documented the damage of a few bridges after the recent earthquakes. **Figure 2.3** shows earthquake damage of standard RC bridge columns collected in the present project.

(a) Llacolen Bridge Damage in the 2010 Maule EQ, Built in 2000 (Yen et al., 2011)

(b) Mianyang Airport Viaduct, Short Column Damage in the 2008 Wenchuan EQ, Built in 2001 (Yen et al., 2011)

(c) Okirihata Oh-hashi Bridge Damage in the 2016 Kumamoto EQ., Built in 2001 (Istrati, 2016)

(d) Bridge 2401 Damage at Bent Top in the Jan-March 2020 Puerto Rico EQs, Built in 1996 (Photo by Dr. Manuel Coll)

(e) Bridge 2401 Damage at Column Top in the Jan. 2020 Puerto Rico EQ, Built in 1996 (Photo by Dr. Manuel Coll)

(f) Bridge 2401 Damage at Column Top in the March 2020 Puerto Rico EQ, Built in 1996 (Photo by Dr. Manuel Coll)

Figure 2.3 – Damage of Standard RC Bridge Columns

| (g) Bridge 2401 Damage at Column Top in the Jan. 2020 Puerto Rico EQ, Built in 1996 (Photo by Dr. Manuel Coll) | (h) Bridge 2401 Damage at Column Top in the March 2020 Puerto Rico EQ Built in 1996 (Photo by Dr. Manuel Coll) |

Figure 2.3 – Damage of Standard RC Bridge Columns, Continued

Modern design codes intend to maximize the serviceability of bridges after earthquakes by imposing seismic requirements. However, substandard and even standard bridges may damage under large earthquakes and their serviceability can be impacted. For example, in the 2011 M_w-9.0 Tohoku-Oki Japan earthquake, 885 bridges were damaged, 29 bridges were closed, and 433 bridges had limited access due to the extent of the damage (Kawashima and Buckle, 2013). A recent example is the damage of six bridges in the 2019-2020 Puerto Rico earthquakes. Three bridges were closed to the traffic due to the earthquake caused damages of RC columns (**Fig. 2.2i-n** for substandard column, and **Fig. 2.3d-h** for standard columns). After the 1989 Loma Prieta earthquake, the Mora Drive bridge was closed and opened to public several times due to a lack of consistent assessment method and a contradictory engineering judgment on the remaining capacity of the bridge (Veletzos et al., 2008). These examples indicate that the bridge serviceability should be quickly evaluated after an earthquake using a standard method and warning signs should be posted to inform the traffic.

Olsen et al. (2016; as NCHRP 833) reviewed the state Department of Transportations' (DOTs) policies and guidelines regarding post-event field operations for transportation infrastructure. **Table 2.2** presents a summary of their findings (all references and web links were updated herein). This NCHRP report proposed a four-stage post-event assessment for transportation infrastructure as summarized in **Table 2.3**:
- Fast Reconnaissance (FR),
- Preliminary Damage Assessment (PDA),
- Detailed Damage Assessment (DDA), and
- Extended Investigation (EI).

Furthermore, the report marks and tags each affected structure using three levels:
- Inspected: Green tagged, meaning no damage was observed,
- Limited Use: Yellow tagged, limiting the access to light traffics and first responders, and
- Unsafe: Red tagged, closed to all traffics.

Figure 2.4 graphically shows the assessment stages and coding after an event. When the structure is not obviously collapsed as determined in FR, onsite assessment is needed by trained emergency responders and engineers to tag the affected structures. Such assessment may require closure of the structures for hours and days after an event, which are the most critical hours for rescue operations.

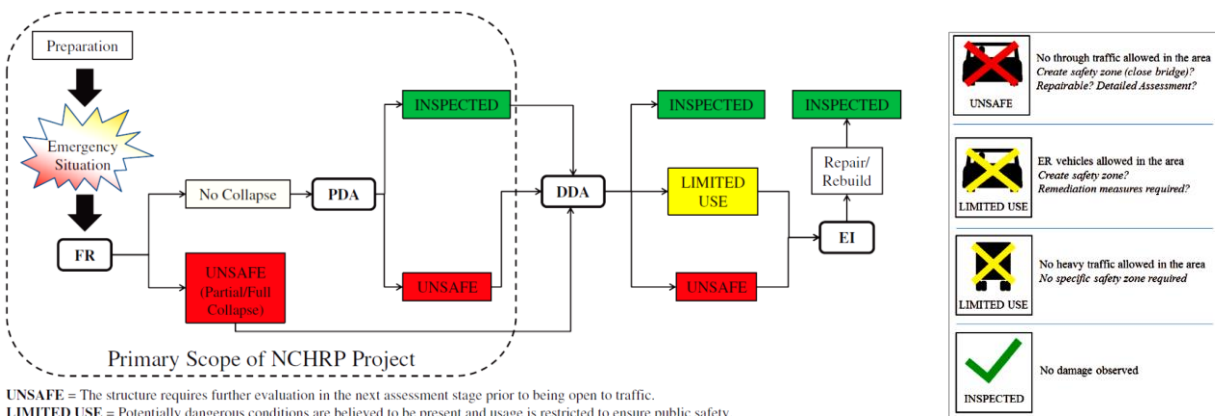**Table 2.2 – Summary of State DOTs Post-Event Procedures (NCHRP 833)**

Procedures	Bridges	Tunnels	Walls	Culverts	Embankments	Overhead Signs
Coding and/or Marking	Connecticut[A] Maryland New York[B] Ohio[C] Oregon[D]	Maryland New York[B] Ohio[C]	Maryland New York[B]	Maryland New York[B] Ohio[C] Oregon[D]	New York[B]	Colorado Connecticut[A]
General	FHWA[E] Connecticut[A] Illinois[F] Maryland Minnesota[G] Mississippi[H] New York[B] Ohio[I] Oregon[D] Pennsylvania[J] Utah[K] Washington[L] Wisconsin[M]	Oregon[D] Pennsylvania[J] Virginia Wisconsin[M]	Connecticut[A] Pennsylvania[J] Utah[K] Wisconsin[M]	Connecticut[A] Illinois[F] Maryland North Dakota Oregon[D] Pennsylvania[J] Utah[K] Virginia Wisconsin[M]	Oregon[D] Pennsylvania[J] Utah[K] Wisconsin[M]	Connecticut[A] Florida Hawaii North Dakota Pennsylvania[J] Utah[K] Wisconsin[M]
Earthquake	Arkansas California Illinois[N] Indiana[O] Iowa Kentucky[P] Mississippi[Q] New York[R] Washington[S] Oregon	None	None	Indiana[O] Kentucky[P] Mississippi[Q]	Indiana[O] Kentucky[P] Mississippi[Q]	Iowa
Tsunami	None	None	None	None	None	None
Tornado	None	None	None	None	None	None
High Winds	None	None	None	None	None	None
Hurricane and Storm Surge	None	None	None	None	None	None
Flooding	California Maryland Ohio[I]	None	None	None	None	None
Fire	California	None	None	None	None	None

A   Connecticut DOT—*Bridge Inspection Manual*: https://portal.ct.gov/DOT/Bridge-Safety-and-Evaluation/Bridge-Safety-and-Evaluation

B   New York State DOT (NYSDOT)—*Bridge Inventory Manual: https://www.dot.ny.gov/divisions/engineering/structures/manuals/bridge-inventory-manual*

C   Ohio DOT—*Bridge Inventory Coding Guide*: https://www.dot.state.oh.us/Divisions/Engineering/Structures/Documents/AWS_Ohio_Bridge_Inventory_Coding_Guide_2021-01.pdf

D   Oregon DOT—*Bridge Inspection Program Manual*: https://www.oregon.gov/odot/Bridge/Documents/Bridge_manuals/brinspecman2013.pdf

E   *Bridge Inspector's Reference Manual*: https://www.fhwa.dot.gov/bridge/nbis.cfm

F   Illinois DOT—*Bridge Element Inspection Manual*: https://idot.illinois.gov/Assets/uploads/files/Doing-Business/Manuals-Guides-&-Handbooks/Highways/Bridges/Inspection/BridgeElementInspectionManual.pdf

G   Minnesota DOT—Bridge Inspection: http://www.dot.state.mn.us/bridge/inspection.html

H   Mississippi DOT—*Bridge Safety Inspection Policy and Procedure Manual*: https://mdot.ms.gov/documents/Bridge%20Design/Manuals/Bridge%20Safety%20Inspection%20Policy%20and%20Procedures.pdf

I   Ohio DOT—Bridge Inspection and Maintenance: https://www.dot.state.oh.us/Divisions/Engineering/Structures/bridge%20operations%20and%20maintenance/Pages/default.aspx

J   Pennsylvania DOT (PennDOT)—*Bridge Safety Inspection Manual*: https://www.dot.state.pa.us/public/PubsForms/Publications/PUB%20238.pdf

K   Utah DOT—*Bridge Management Manual*, Chapter 5: Emergency Response Plan: https://www.udot.utah.gov/connect/about-us/project-development/structures-division/

L   Washington State DOT (WSDOT)—*Bridge Inspection Manual*: https://wsdot.wa.gov/Publications/Manuals/M36-64.htm

M   Wisconsin DOT—*Structures Inspection Manual*: https://wisconsindot.gov/Pages/doing-bus/eng-consultants/cnslt-rsrces/strct/inspection-manual.aspx

N   Illinois DOT—Earthquake Preparedness, Response and Recovery Plan: https://transops.s3.amazonaws.com/uploaded_files/Illinos-DOT-Earthquake-Preparedness-Response-and-Recovery-Plan.pdf

O   Indiana DOT—*Handbook for the Post-Earthquake Safety Evaluation of Bridges and Roads*: https://docs.lib.purdue.edu/jtrp/1567/

P   Kentucky Transportation Cabinet—*Post-Earthquake Investigation Field Manual for the State of Kentucky*: http://www.e-archives.ky.gov/pubs/transportation/TC_Rpt/KTC_06_30_SPR_234_01_1F.pdf

Q   Mississippi DOT—Annex E – Earthquake Response Plan

R   NYSDOT—*Post-Earthquake Bridge Inspection Guidelines*: https://www.dot.ny.gov/divisions/engineering/technical-services/trans-r-and-d-repository/C-06-14_Post-Eq%20Final%20Report_October%202010.pdf

S   WSDOT—*An Emergency Response Plan for Bridge Management*: https://www.wsdot.wa.gov/research/reports/fullreports/289.1.pdf

Table 2.3 – Damage Assessment Stages for Transportation Infrastructure (NCHRP 833)

	Fast Reconnaissance (FR)	Preliminary Damage Assessment (PDA)	Detailed Damage Assessment (DDA)	Extended Investigation (EI)
Objective	Global perspective	Rapid route reconnaissance	Detailed inspection	Special study to address a particular concern
Scope	All structures in affected area	All structures in affected area, starting with priority routes	Structure and site specific	Site specific, as needed
Inspection Method	Helicopter, small fixed-wing aircraft, UAVs, and other "fast" methods	Drive-through with quick stop at each structure	Inspection and special access equipment as needed, load rating and remaining strength analysis	Any special equipment that is needed
Personnel	Chief engineers or managing engineer in aircraft or vehicle; specialized technicians as needed; the public	PDARs-Trained emergency responders (maintenance & operations crews, design engineers)	Routine inspectors and specialists (e.g., structural, geotechnical, hydrological, mechanical, materials)	Specialists (e.g., structural, geotechnical, hydrological, mechanical, materials)
Time Frame	Immediate (within 4-6 hours)	Immediate (within 24 hours)	Start ASAP (usually within 8 hours) and continue as necessary	Subsequent to DDA
Outcome	Determine the geographic extent of damage, Identify impassible routes and traffic bottlenecks, Locate structures that have major damage or are obviously unsafe, Suggest priority for ground assessments	Determine the extent and type of damage, Identify/confirm impassible routes and traffic bottlenecks, Close unsafe structures, Code and mark, Recommend DDA for damaged or suspect structures, Preliminary damage level estimate	Code and mark as necessary, Close unsafe structures, Recommendations for restriction, repair, or further investigation, Preliminary cost estimates for agencies such as FEMA, Reopen structures deemed safe that were closed as a precautionary measure during PDA survey, Damage level estimate	Code and mark as necessary, Detailed damage analysis, Provide specific recommendations on necessary restrictions and/or repair, Approximate cost estimate for remedial work
Deliverable	Reconnaissance report with maps, geo-referenced photos, and/or video that defines the affected region	Digital PDA form/ database (one entry per structure) and physical marking on the structure	DDA report for each structure and daily summary report	Special engineering report
Coding Options	UNSAFE	UNSAFE, INSPECTED	UNSAFE, LIMITED USE, INSPECTED	UNSAFE, LIMITED USE, INSPECTED

UNSAFE = The structure requires further evaluation in the next assessment stage prior to being open to traffic.
LIMITED USE = Potentially dangerous conditions are believed to be present and usage is restricted to ensure public safety.
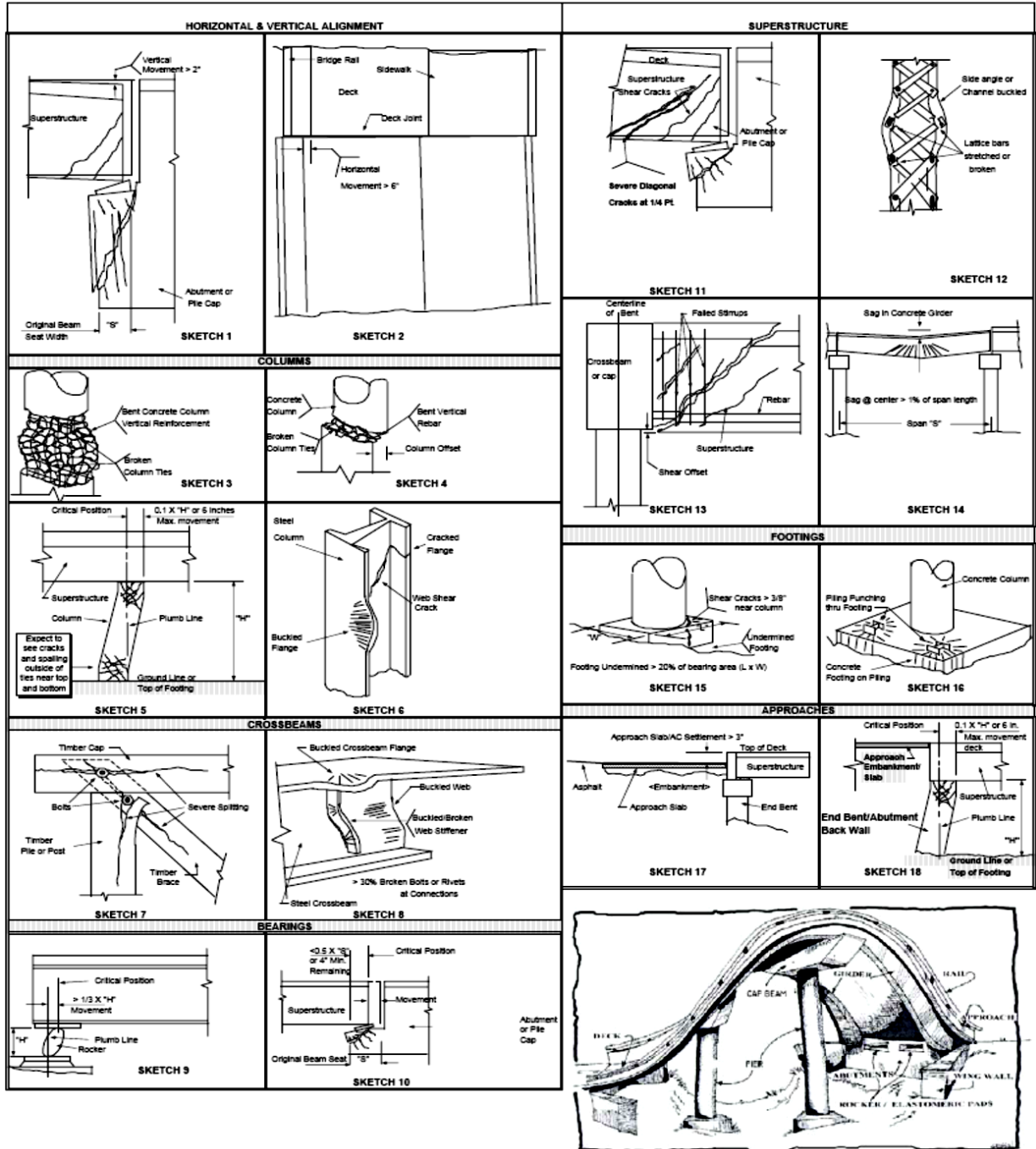**INSPECTED** = The structure appears to be in the same condition as it was prior to the event.

(a) Assessment Stages (b) Coding
Figure 2.4 – Transportation Infrastructure Assessment Stages and Coding (NCHRP 833)

A survey of state DOTs revealed that "visual inspection" is the most common method of damage detection for bridges after a severe event (Alipour, 2016, as NCHRP 469), and other technologies such as nondestructive testing, sonar surveys, and photogrammetry were ranked lower. NCHRP 469 concluded that the visual inspection is the preferred method by state DOTs since it is quick, low cost, and requires minimal preparation. State DOT field operation manuals usually include descriptive text (e.g., **Table 2.4**), illustrations (e.g., **Fig. 2.5**), and inspection forms (e.g., **Table 2.5**) to help with a quick identification of the event-caused bridge damages.

Table 2.4 – Post-Earthquake Bridge Damage Description (O'Connor, 2010)

Bridge Component / Damage	Possible Cause
Approach Slab or Pavement • Raised, lowered, cracked, or buckled	• Longitudinal forces • Lateral spread; Slope failure
Abutment and/or Foundation • Tipping or other displacement • Cracking • Movement of supporting soil	• Movement of soil behind abutment • Loads exceeding shear capacity, especially if superstructure smashes into the backwall, cheekwalls, or shear blocks • Liquefaction
Superstructure • Collapse of one or more spans • Span misalignment • Girder damage • Bowing, dips • Deck damage: spalling, exposed rebar	• Displacement beyond capacity of the bridge seat • Horizontal displacement • Abutment or pier damage or movement • Beam failure due to excessive shear or moment • Superstructures tend to move off a highly skewed seat
Bearings • Toppled • Unseating, misalignment • Sheared or bent anchor bolts	• Use of high, potentially unstable bearings • Frozen (non-functioning) bearings
Restrainers or other Seismic Retrofits • Damage to restrainers	• Insufficient capacity • Improper installation
Joints and Connections • Misalignment, spalling, cracking	• Inadequate development length of longitudinal reinforcement in adjacent member • Poor choice of connection details (insufficient translational restraint for pinned connection, etc.)
Pier (wall, stem, columns or capbeam) • Cracking from flexural or shear failure • Crushing or mushrooming • Longitudinal reinforcement tension failure • Buckling of longitudinal reinforcement • Torsional failure	• Uneven settlement of a footing • Insufficient confinement (number, size or spacing of bars) • Poor reinforcement details (hooks, laps, etc.)
Other • Damage to bridge railing	• Consequence of damage to other elements

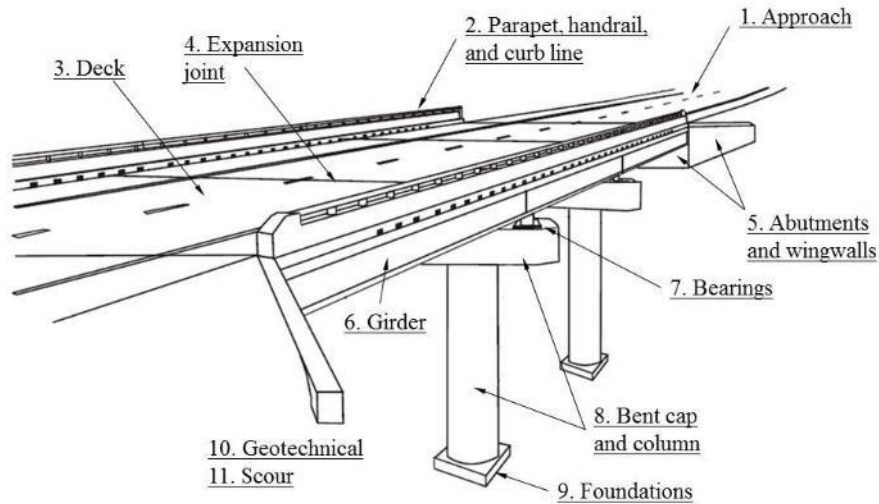**Figure 2.5 – Post-Event Bridge Damage Detection Guide (Alaska DOT, 2019)**

Table 2.5 – Preliminary Damage Assessment (PDA) Form for Bridges (NCHRP 833)

Inspector 1 Name/ID: _____	Structure ID: _____	**PDA Outcom**
Inspector 2 Name/ID: _____	Highway: _____	☐ INSPECTE
Agency: _____	Milepost: _____	(Green)
Date and time: _____	Route Carried on: _____	☐ UNSAFE
Latitude/Longitude: _____	Route Carried under: _____	(Red)
Structure material: ☐ Steel ☐ Concrete ☐ Other _____		

Damage Summary:	**Traffic Level:**	**Overall Comments:**
☐ 1 – None (0%)	☐ No traffic at all	_____
☐ 2 – Slight (0-1%)	☐ Traffic on all lanes	_____
☐ 3 – Light (1-10%)	☐ Traffic on some lanes	_____
☐ 4 – Moderate (10-30%)	**Scour:**	_____
☐ 5 – Heavy (30-60%)	☐ Unknown	_____
☐ 6 – Major (60-100%)	☐ Unlikely	_____
☐ 7 – Destroyed (100%)	☐ Likely, but cannot see	_____
	☐ Definitely	_____

Feature Description:					**Notes: (additional notes on back)**
1. Approach/ Embankments	☐ None	☐ Minor	☐ Moderate	☐ Severe	_____
2. Parapets, Handrail, and Curb Line	☐ None	☐ Minor	☐ Moderate	☐ Severe	_____
3. Deck	☐ None	☐ Minor	☐ Moderate	☐ Severe	_____
4. Expansion Joint	☐ None	☐ Minor	☐ Moderate	☐ Severe	_____
5. Abutments and Wingwalls	☐ None	☐ Minor	☐ Moderate	☐ Severe	_____
6. Girder	☐ None	☐ Minor	☐ Moderate	☐ Severe	_____
7. Bearings	☐ None	☐ Minor	☐ Moderate	☐ Severe	_____
8. Bent Cap and Column	☐ None	☐ Minor	☐ Moderate	☐ Severe	_____
9. Foundation	☐ None	☐ Minor	☐ Moderate	☐ Severe	_____
10. Geotechnical	☐ None	☐ Minor	☐ Moderate	☐ Severe	_____
Other_____	☐ None	☐ Minor	☐ Moderate	☐ Severe	_____

Recommendations: Choose a recommendation based on the evaluation and team judgment. DDA evaluations should only be recommended with an UNSAFE posting. Provide comments on the recommendations below.

☐ **None**   ☐ **DDA (Low Priority)**   ☐ **DDA (High Priority)**

Record any recommendations:_____
_____
_____
_____

(QR Code)

1. Approach
2. Parapet, handrail, and curb line
3. Deck
4. Expansion joint
5. Abutments and wingwalls
6. Girder
7. Bearings
8. Bent cap and column
9. Foundations
10. Geotechnical
11. Scour

United States Geological Survey (USGS) has developed two tools that help with a quick response after earthquakes: (1) ShakeMap, which provides near-real-time maps for an earthquake such as shaking intensity, and estimates losses (**Fig. 2.6**), and (2) ShakeCast, which is a cloud-based application (the latest version, V3.0) to deliver the ShakeMap information to critical users and facilities of the affected sites (**Fig. 2.7**). State DOTs such as Caltrans have been using ShakeCast to identify bridges with most probable damages (using predefined fragility curves), to prioritize bridges for inspection, and to inform local authorities for a quick response. It should be noted that these tools are for community level assessment, and they are not used for bridge system or component level structural analysis.

Fatalities: Green alert for shaking-related fatalities. There is a low likelihood of casualties
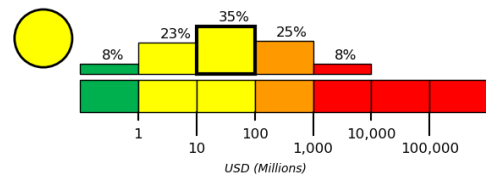
Costs: Yellow alert for economic losses. Some damage is possible and the impact should be relatively localized. Estimated economic losses are less than 1% of GDP of the United States. Past events with this alert level have required a local or regional level response.

(a) Intensity Map for the 2019 M$_w$-7.1 Ridgecrest Earthquake (California, USA)

(b) Loss Estimation for the 2019 M$_w$-7.1 Ridgecrest Earthquake (California, USA)

Figure 2.6 – USGS ShakeMap Sample Reports (ShakeMap, 2021)
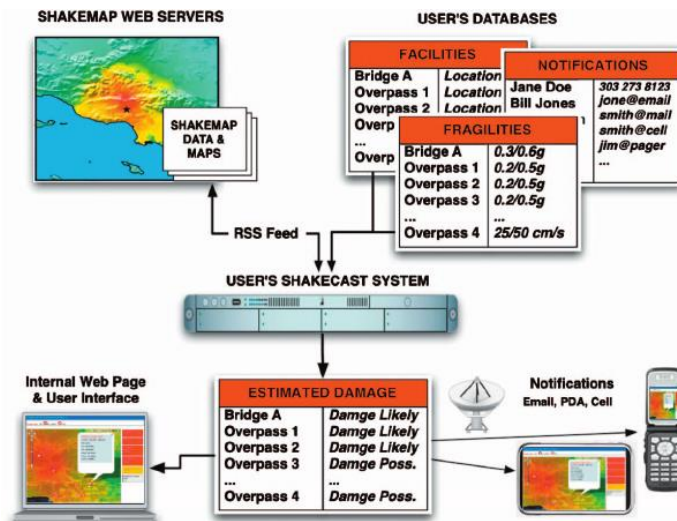
Figure 2.7 – USGS ShakeCast Flowchart (Lin et al., 2009)

Another community level hazard assessment tool is the Federal Emergency Management Agency (FEMA) HAZUS, which estimates risk information of different structures (e.g., residential and commercial buildings, bridges) under earthquakes, floods, tsunamis, and hurricanes. HAZUS is a pre-event assessment tool to determine high-risk areas for mitigation planning, and estimates physical, economic, and social impacts of the abovementioned natural hazards. Similar to ShakeCast, HAZUS uses the USGS ShakeMap data and fragility curves to estimate bridge damages under different earthquake scenarios.

Despite a lack of national and unified post-earthquake evaluation specifications for bridges, the building industry is equipped with nationwide and systematic post-earthquake assessment tools. For example, FEMA 154 (2015) offers a method for "Rapid Visual Screening of Buildings for Potential Seismic Hazards." Furthermore, FEMA has developed a free mobile application, ROVER: *Rapid Observation of Vulnerability and Estimation of Risk*, for pre- and post-earthquake inspection and evaluation of buildings.

The recommendations by NCHRP 833 may be used as a national guideline for post-earthquake bridge assessment. Furthermore, NCHRP 223 (Olsen et al., 2016) provides guidelines on the development of Smart Applications for bridge assessment, coding, and marking. Nevertheless, such tools yet to be developed for bridges.

2.3 Visual Methods of Bridge Column Assessment

It was discussed in the previous section that "visual inspection" is currently the preferred method for post-event assessment of bridges by many DOTs. For conventional bridges (as defined per AASHTO SGS, **Sec. 2.2**) located in seismic regions, columns are usually the main source of ductility to achieve the code-required collapse-prevention performance. From the literature, it could not be found what percentage of the US bridges has columns, and what are their constitutive materials. However, based on the current codes' language and feedback from DOTs and industry, it seems RC columns are more common in seismic areas than steel columns or those with other materials. Therefore, RC bridge column damage types and the level of each damage must be classified for a successful post-event visual assessment.

A few studies have defined damage-based performance levels for RC bridge columns. Ramirez et al. (2000) proposed a damage classification and a three-color tagging system (e.g., "Green Tag" indicating "Safe for Traffic", "Yellow Tag" indicating "Further Evaluation", and "Red Tag" indicating "Unsafe for Traffic") for RC and steel bridge columns (**Table 2.6**).

Table 2.6 – Damage Classification for Bridge Columns (Ramirez et al., 2000)

Member	Green Tag	Yellow Tag	Red Tag
RC Cap-Beams	Vertical cracks	Diagonal cracks	Bar buckling
RC Columns	Horizontal cracks	Diagonal cracks, loss of concrete cover	Bar buckling
Steel Beams and Columns	None	Any crack	Local buckling

Hose (2001) proposed a five-level performance classification for bridges (**Table 2.7**), offered qualitative and quantitative performance descriptions for each level to quickly assess post-earthquake bridge performance (**Table 2.8**), and graphically identified each damage level for brittle, strength-degrading, and ductile structures (**Fig. 2.8**). Subsequently, Hose (2001) reviewed the test data for 20 RC bridge columns, three RC sub-assemblies, and three RC column-bent systems and quantified the key points of each performance curve (e.g., the residual deformation index, *RDI = the ratio of the residual displacement to the idealized yield displacement*, in **Fig. 2.8**). After an earthquake, the damage level of an affected bridge column is visually determined using **Table 2.8**, the column performance curve is selected from **Fig. 2.8**, then the residual strength of the column is estimated using the critical values of the selected curve.

Table 2.7 – RC Bridge Column Damage-Based Performance Classification (Hose, 2001)

Level	Damage Classification	Damage Description	Repair Description	Socio-Economic Description
I	No	Barely visible cracks	No Repair	Fully Operational
II	Minor	Minor residual cracks	Possible Repair	Operational
III	Moderate	Open residual cracks, onset of spalling	Minimum Repair	Life Safety
IV	Major	Very wide cracks, extended concrete spalling	Repair	Near Collapse
V	Local Failure or Collapse	Visible permanent deformation, buckling/rupture of reinforcement	Replacement	Collapse

Table 2.8 – RC Bridge Column Damage-Based Performance Assessment (Hose, 2001)

Level	Performance Level	Qualitative Performance Description	Quantitative Performance Description
I	Cracking	Onset of hairline cracks	Barely visible residual and ultimate cracks
II	Yielding	Theoretical first yielding of long. bars	Residual crack width $\approx$ 0.2 mm; Ultimate crack width $\approx$ 0.5 mm
III	Initiation of Local Mechanism	Initiation of inelastic deformation, onset of concrete spalling, development of diagonal cracks	Residual crack width 1-2 mm; Length of spalled region > 1/10 cross-section depth
IV	Full Development of Local Mechanism	Wide crack widths/spalling over full local mechanism region	Residual crack width > 2 mm; Diagonal cracks extend over 2/3 of cross-section depth; Length of spalled region > 1/2 cross-section depth
V	Strength Degradation	Buckling of main reinforcement, rupture of transverse reinforcement, crushing of core concrete	Lateral capacity below 85% of maximum; Measurable dilation > 5% of original member dimension

(a) Brittle Behavior

(b) Strength-Degrading Behavior

(c) Ductile Behavior
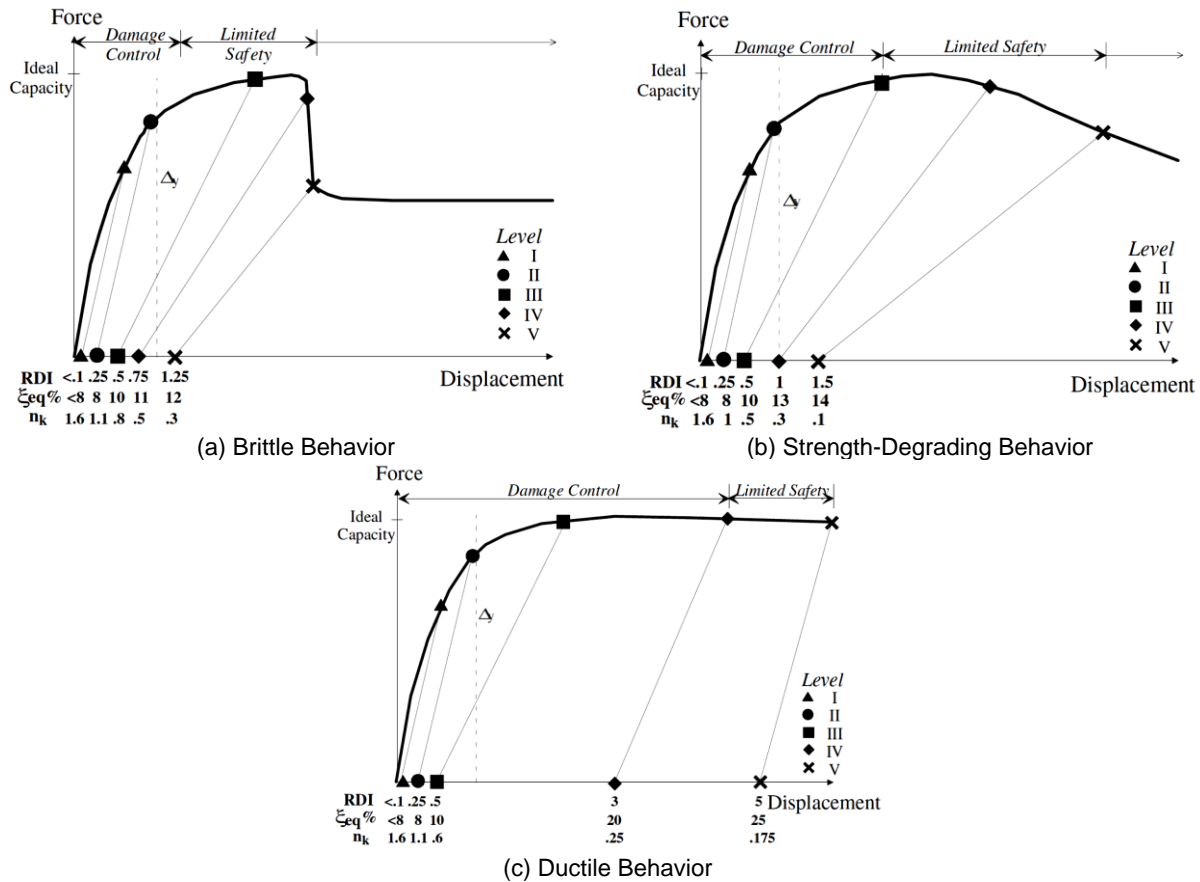
Figure 2.8 – RC Bridge Column Damage-Based Performance Curves (Hose, 2001)

17

Veletzos et al. (2008) complemented the work by Hose (2001) and expanded the RC column experimental database to include more than 100 specimens tested between 1990 to 2008 and bridges damaged under 14 major earthquakes between 1971 to 2008. This study adopted the five-level damage state and the three performance curves proposed by Hose (**Table 2.8**, **Fig. 2.8**) then classified the damage of each RC bridge column within their database. They used this information to develop post-earthquake inspection manual for Caltrans and to train inspectors and engineers. They also proposed a flowchart (**Fig. 2.9**) to facilitate the determination of an RC column performance curve after an earthquake. Similar to the Hose's proposed assessment method discussed above, the column performance is assessed by mapping the observed damage level (one of the five levels from **Table 2.8**) on the column selected performance curve (one of those in **Fig. 2.8** following the flowchart shown in **Fig. 2.9**) then commenting on the RC bridge column performance based on the remaining capacity. **Figure 2.10** shows an example of such assessment per performance curve. Note that this method is general and does not calculate displacements and forces (capacities or demands) in the process.
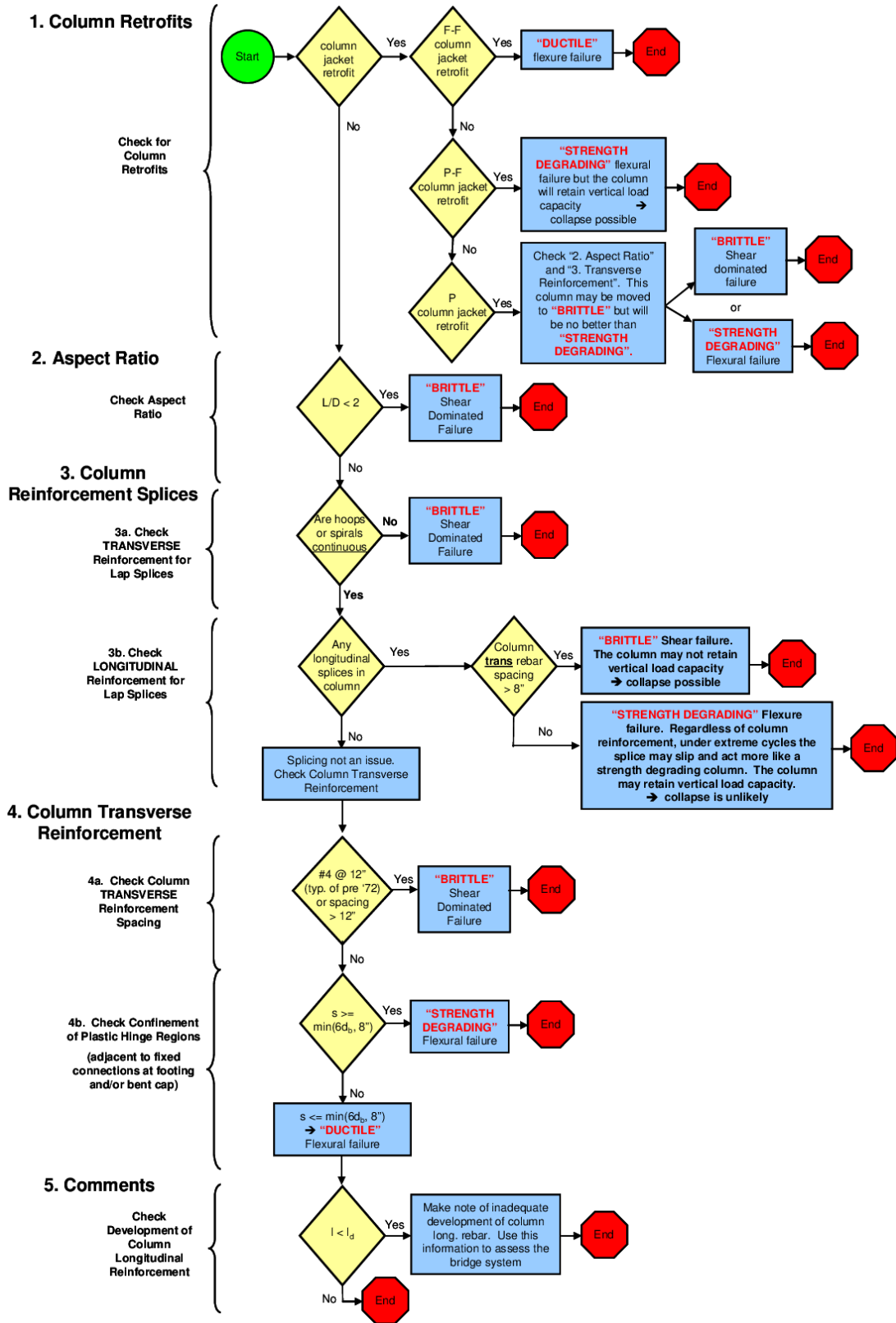
1. Column Retrofits

Check for Column Retrofits

Start

column jacket retrofit — Yes → F-F column jacket retrofit — Yes → **"DUCTILE"** flexure failure → End

No ↓ (F-F) No ↓

P-F column jacket retrofit — Yes → **"STRENGTH DEGRADING"** flexural failure but the column will retain vertical load capacity → collapse possible → End

No ↓

P column jacket retrofit — Yes → Check "2. Aspect Ratio" and "3. Transverse Reinforcement". This column may be moved to **"BRITTLE"** but will be no better than **"STRENGTH DEGRADING"**.

→ **"BRITTLE"** Shear dominated failure → End

or

→ **"STRENGTH DEGRADING"** Flexural failure → End

2. Aspect Ratio

Check Aspect Ratio

L/D < 2 — Yes → **"BRITTLE"** Shear Dominated Failure → End

No ↓

3. Column Reinforcement Splices

3a. Check TRANSVERSE Reinforcement for Lap Splices

Are hoops or spirals continuous — No → **"BRITTLE"** Shear Dominated Failure → End

Yes ↓

3b. Check LONGITUDINAL Reinforcement for Lap Splices

Any longitudinal splices in column — Yes → Column **trans** rebar spacing > 8" — Yes → **"BRITTLE"** Shear failure. The column may not retain vertical load capacity → collapse possible → End

No (trans) → **"STRENGTH DEGRADING"** Flexure failure. Regardless of column reinforcement, under extreme cycles the splice may slip and act more like a strength degrading column. The column may retain vertical load capacity. → collapse is unlikely → End

No ↓

Splicing not an issue. Check Column Transverse Reinforcement

4. Column Transverse Reinforcement

4a. Check Column TRANSVERSE Reinforcement Spacing

#4 @ 12" (typ. of pre '72) or spacing > 12" — Yes → **"BRITTLE"** Shear Dominated Failure → End

No ↓

4b. Check Confinement of Plastic Hinge Regions (adjacent to fixed connections at footing and/or bent cap)

s >= min(6d$_b$, 8") — Yes → **"STRENGTH DEGRADING"** Flexural failure → End

No ↓

s <= min(6d$_b$, 8") → **"DUCTILE"** Flexural failure

5. Comments

Check Development of Column Longitudinal Reinforcement

l < l$_d$ — Yes → Make note of inadequate development of column long. rebar. Use this information to assess the bridge system → End

No → End

Figure 2.9 – RC Bridge Column Performance Curve Decision Making Flowchart (Veletzos et al., 2008)
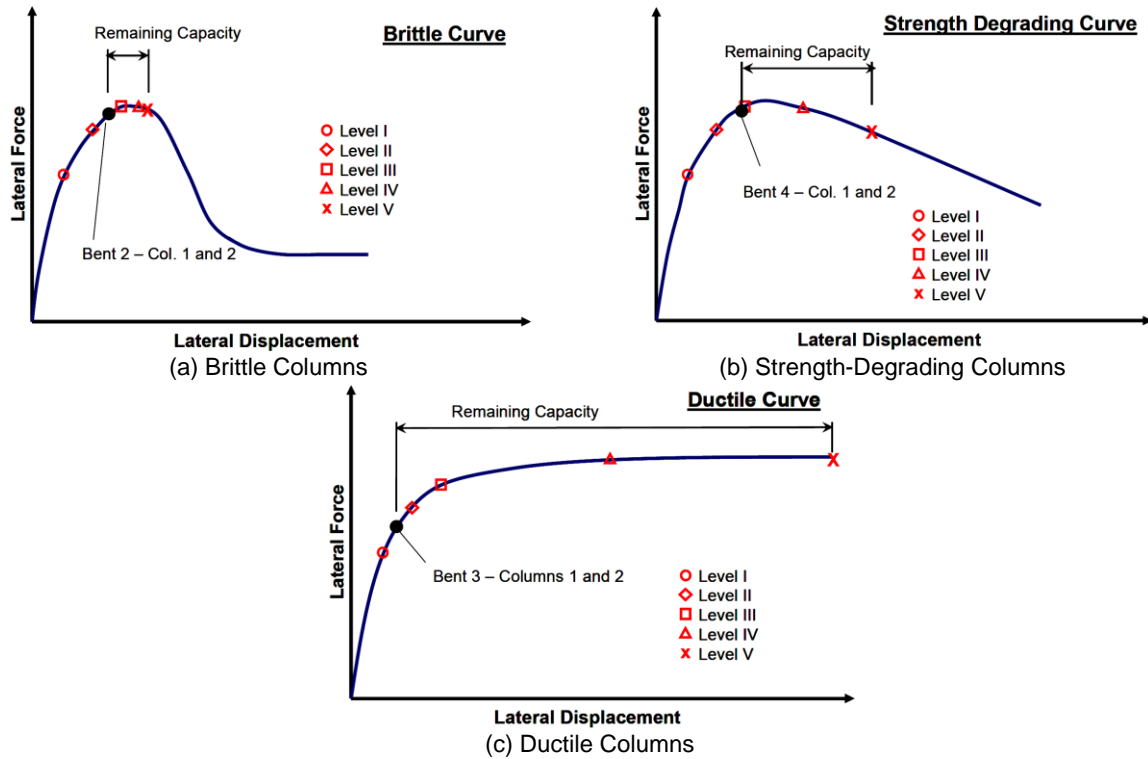
19

Figure 2.10 – Estimation of RC Bridge Column Post-Earthquake Reserved Capacity (Veletzos et al., 2008)

Berry and Eberhard (2008) developed equations to estimate RC bridge column drift ratios, plastic rotations, and longitudinal bar strains at concrete cover spalling, longitudinal bar buckling, and longitudinal bar fracture (or a three-level damage state). **Table 2.9** presents a summary of the equations, which were developed based on a statistical analysis of an RC bridge column database including more than 30 columns (a subset of the original database by Berry et al., 2004).

Table 2.9 – RC Column Response at Different Damage States (Berry and Eberhard, 2008)

| Damage State	E.D.P.	Equation	$\Delta_{dam}^{meas}/\Delta_{dam}^{calc}$ mean	cov (%)
Cover Spalling (29 columns)	Δ_{sp}^{calc}/L (%)	$1.6\ (1-P/A_g f_c')\ (1+L/10D)$	1.07	34.9
	$\theta_{p\_sp}^{calc}$ (%)	1.20	0.98	33.9
	ε_{sp}	0.008	0.99	34.7
Bar Buckling (33 columns)	Δ_{bb}^{calc}/L (%)	$3.25\ (1+150\rho_{eff}d_b/D)(1-P/A_g f_c')\ (1+L/10D)$	1.01	24.7
	$\theta_{p\_bb}^{calc}$ (%)	$0.0009\left(1+7.3\rho_{eff}\right)(1+1.3L/D+3f_y d_b/D)$	1.01	21.6
	$\theta_{p\_bb}^{calc}$ (%)	$2.75\ (1+150\rho_{eff}d_b/D)(1-P/A_g f_c')\ (1+L/10D)$	1.01	24.3
	ε_{bb}^{calc}	$0.045+0.25\rho_{eff}\leq 0.15$	1.00	23.6
Bar Fracture (20 columns)	Δ_{bf}^{calc}/L (%)	$3.5\ (1+150\rho_{eff}d_b/D)(1-P/A_g f_c')\ (1+L/10D)$	0.97	20.0
	$\theta_{p\_bf}^{calc}$ (%)	$0.0009\left(1+6.7\rho_{eff}\right)(1+2.4L/D+1.7f_y d_b/D)$	0.99	16.0
	$\theta_{p\_bf}^{calc}$ (%)	$3.0\ (1+150\rho_{eff}d_b/D)(1-P/A_g f_c')\ (1+L/10D)$	0.97	19.6
	ε_{bf}^{calc}	$0.045+0.30\rho_{eff}\leq 0.15$	0.96	20.5

Vosooghi and Saiidi (2010) proposed a six-level damage assessment for RC bridge columns (**Table 2.10**), which was in general similar to the work by Hose (2001) and Veletzos et al. (2008). **Figure 2.11** shows an example of each damage state for an RC bridge column tested on a shake table. Note that damage state (DS) 6, which is not included in the table, refers to the column failure. Vosooghi and Saiidi (2010) also developed a new RC bridge column performance database using data from more than 30 models tested on shake tables. Note that the column database in the previous studies was mainly on columns tested under cyclic loading. Furthermore, Vosooghi and Saiidi (2010) developed a relationship between the damage state and the maximum drift ratio demand, the residual drift ratio, and four other parameters for four column types: Standard Low Shear under Far-field motions (SLSF), Standard High Shear under Far-field motions (SHSF), Standard Low Shear under Near-field motions (SLSN), and Sub-Standard columns (SS). **Figure 2.12** shows the correlation between the maximum drift ratio demand (MDR) and the damage states. Such graphs can be used to estimate the RC bridge column displacement demand under an earthquake if the column type and the post-earthquake damage state are known. Furthermore, they proposed a method to generate a non-dimensional pushover curve for an RC bridge column using its post-earthquake damage state and the column category (e.g., SLSN). Subsequently, the column displacement demand is mapped on its pushover curve for complete assessment (e.g., **Fig. 2.13**).

Table 2.10 – RC Bridge Column Damage-Based Performance Assessment (Vosooghi and Saiidi, 2010)
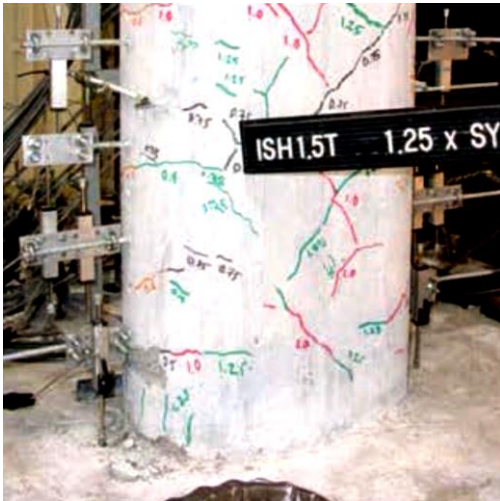
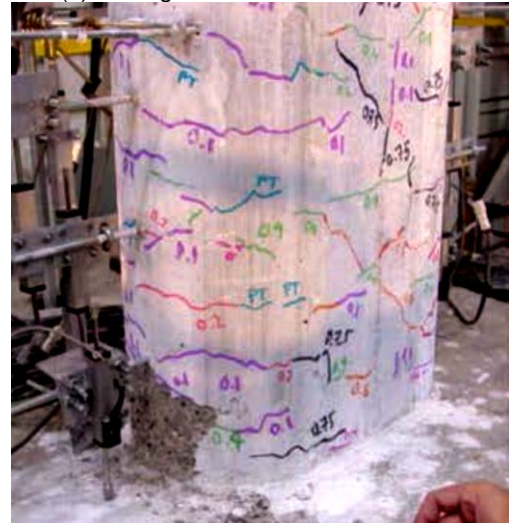| Damage State	Qualitative Performance Description	Quantitative Performance Description
1	Flexural cracks	
2	First spalling and shear cracks	
3	Extensive cracks and spalling	None
4	Visible lateral and longitudinal bars	
5	Imminent failure	
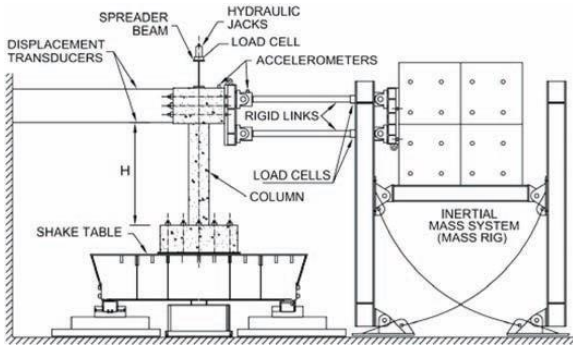
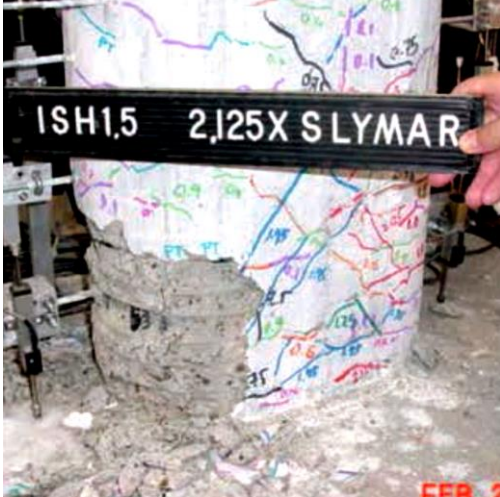(a) Sample Shake-Table Test Setup
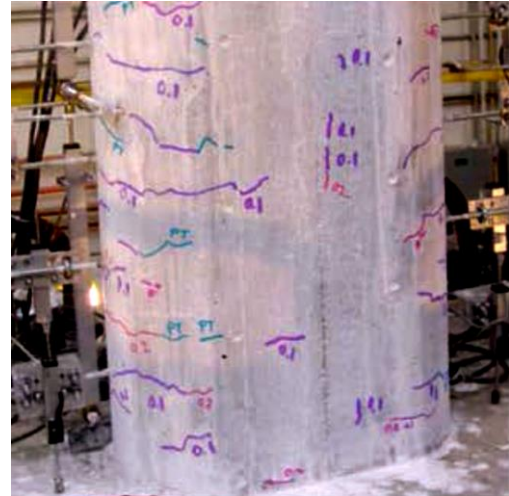
(b) Damage State 1 – Flexural Cracks

(c) Damage State 2 – First Spalling and Shear Cracks

(d) Damage State 3 – Extensive Cracks and Spalling

(e) Damage State 4 – Bar Exposure

(f) Damage State 5 – Imminent Failure

Figure 2.11 – RC Bridge Column Damage States by Vosooghi and Saiidi (2010)
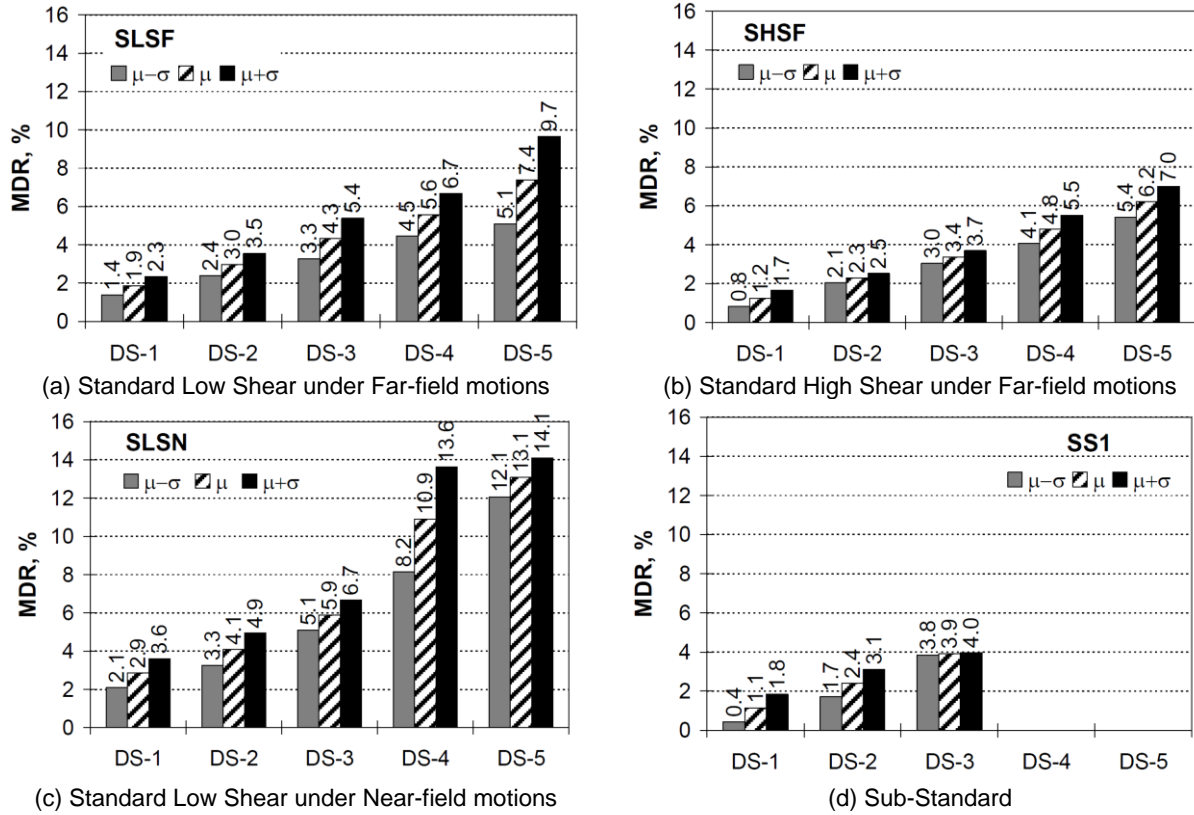
(a) Standard Low Shear under Far-field motions

(b) Standard High Shear under Far-field motions

(c) Standard Low Shear under Near-field motions

(d) Sub-Standard

Figure 2.12 – Maximum Drift Demand versus Damage State (Vosooghi and Saiidi, 2010)
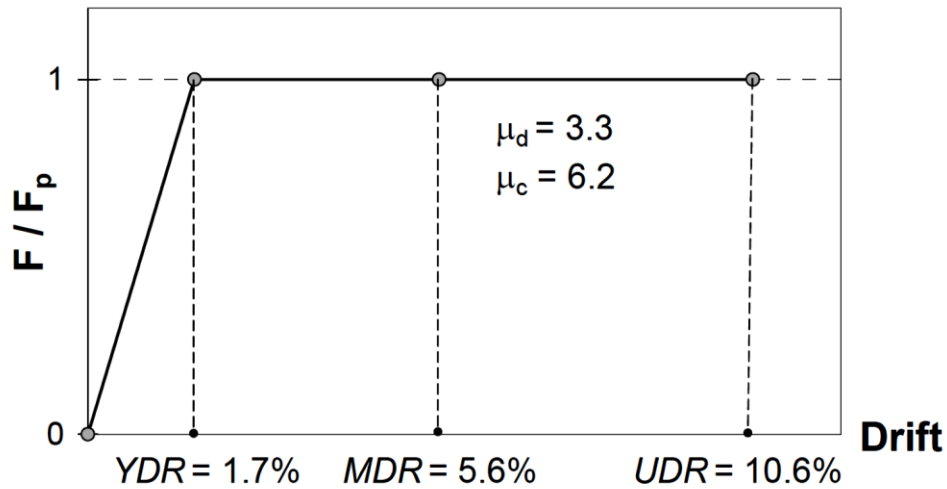
Figure 2.13 – Estimated Pushover Curve and Maximum Drift Demand (Vosooghi and Saiidi, 2010)

YDR: Yield Drift Ratio
MDR: Maximum Drift Ratio
UDR: Ultimate Drift Ratio
F/F_p: Normalize Baseshear

23

Chapter 6 in Marsh et al. (2014) presents a four-stage plastic hinge mechanism for RC bridge columns (**Fig. 2.14a-b**) and provides a curvature-based limit states for various failure modes (**Fig. 2.14c**). For example, if the column longitudinal bars buckle after an earthquake, the corresponding ultimate plastic curvature is estimated (from **Fig. 2.14c**) then the column displacement at the bar buckling can be calculated using AASHTO SGS equations (e.g., $\Delta_u = \Delta_{yi} + \emptyset_p L_p[L - 0.5L_p]$). Mapping this displacement on the pushover curve reveals the remaining capacity of the column and may be used to comment on the post-earthquake performance of the column.

(a) Plastic Hinge Mechanisms   (b) Plastic Hinge Stages
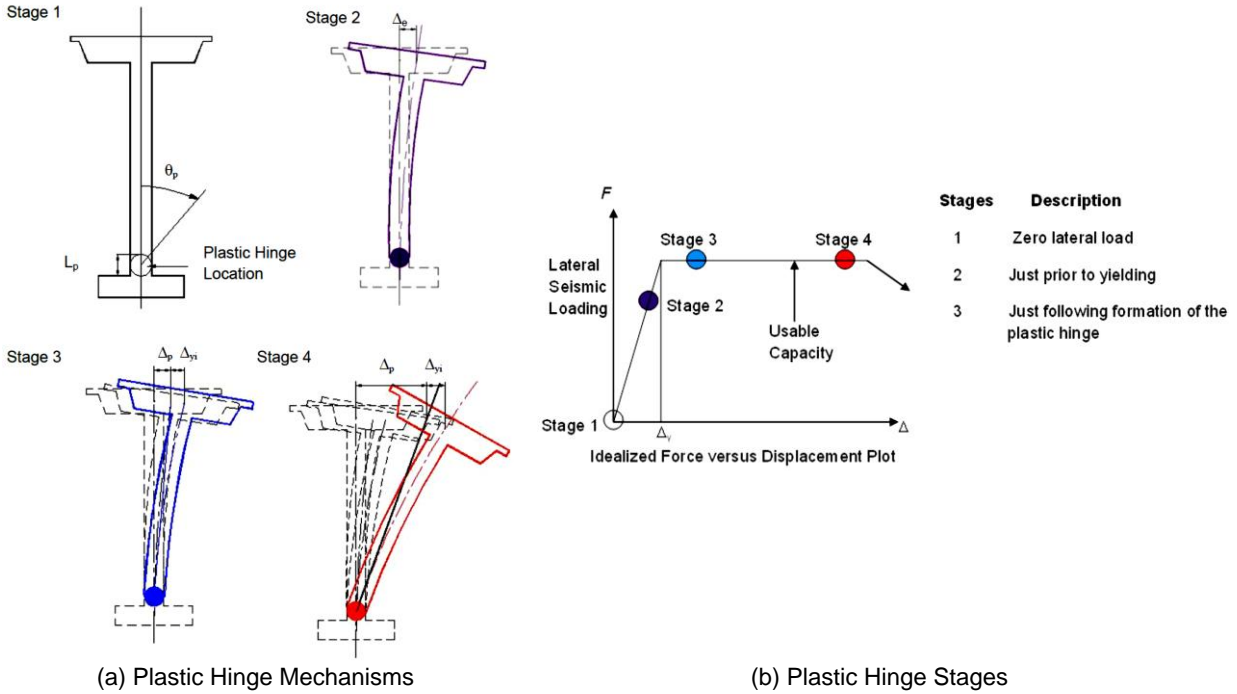
Column or Beam Limit State	Plastic Curvature, ϕ_p
Compression failure, unconfined Concrete	$\phi_p = \dfrac{\varepsilon_{cu}}{c} - \phi_y$
Compression failure, confined concrete	$\phi_p = \dfrac{\varepsilon_{cu}}{(c - d'')} - \phi_y$
Fracture of longitudinal reinforcement	$\phi_p = \dfrac{\varepsilon_{s\,max}}{(d - c)} - \phi_y$
Buckling of longitudinal bars	$\phi_p = \dfrac{\varepsilon_b}{(c - d')} - \phi_y$
Low-cycle fatigue of longitudinal reinforcement	$\phi_p = \dfrac{2\varepsilon_{ap}}{(d - d')} = \dfrac{2\varepsilon_{ap}}{D'}$

(c) Values of Plastic Curvature at Varrious Limit States

Figure 2.14 – RC Bridge Column Limit States (Marsh et al., 2014)

AASHTO Manual for Bridge Element Inspection (AASHTO MBEI, 2013) presents four-level condition states for the inspection of RC bridge columns as summarized in **Table 2.11**. Nevertheless, these definitions are general and not specific to earthquake damages.

Table 2.11 – AASHTO Damage Types and Condition States for RC Bridge Columns

Defect Types	Condition States			
	CS-1	CS-2	CS-3	CS-4
	Good	Fair	Poor	Severe
Delamination /Spall /Patched Area	None.	Delaminated. Spall 1 in. or less deep or 6 in. or less in diameter. Patched area that is sound.	Spall greater than 1 in. deep or greater than 6 in. diameter. Patched area that is unsound or showing distress. Does not warrant structural review.	The condition warrants a structural review to determine the effect on strength or serviceability of the element or bridge; OR a structural review has been completed and the defects and the defects impact strength or serviceability of the element or bridge.
Exposed Rebar	None.	Present without measurable section loss.	Present with measurable section loss, but does not warrant structural review.	
Efflorescence / Rust Staining	None.	Surface white without build-up or leaching without rust straining.	Heavy build-up with rust staining.	
Cracking (RC and others)	Width less than 0.012 in. or spacing greater than 3 ft.	Width 0.012–0.05 in. or spacing 1.0–3.0 ft.	Width greater than 0.05 in. or spacing less than 1 ft.	
Abrasion / Wear (PSC /RC)	No abrasion or wearing.	Abrasion or wearing has exposed coarse aggregate but the aggregate remains secure in the concrete.	Coarse aggregate is loose or has popped out of the concrete matrix due to abrasion or wear.	
Settlement	None.	Exists with tolerable limits or arrested with no observed structural distress.	Exceeds tolerable limits but does not warrant structural review.	
Scour	None.	Exists with tolerable limits or has been arrested with effective countermeasures.	Exceeds tolerable limits but is less than the critical limits determined by scour evaluation and does not warrant structural review.	
Damage	Not applicable.	The element has impact damage. The specific damage caused by the impact has been captured in condition state 2 under the appropriate material defect entry.	The element has impact damage. The specific damage caused by the impact has been captured in condition state 3 under the appropriate material defect entry.	The element has impact damage. The specific damage caused by the impact has been captured in condition state 4 under the appropriate material defect entry.

Built upon the work by Vosooghi and Saiidi (2010), Saini and Saiidi (2014) developed a probabilistic seismic design method for RC bridge columns. A unitless parameter named "Damage Index, *DI*" was used to relate each "damage state" to a point on the column pushover curve:

$$DI = \frac{\Delta_D - \Delta_{yi}}{\Delta_C - \Delta_{yi}} \qquad \text{(Eq. 2.1)}$$

where, Δ_D is the column displacement (or drift) demand, Δ_{yi} is the column idealized yield displacement (or drift), and Δ_C is the column displacement (or drift) capacity. The maximum value of *DI* is 1.0, which indicates that the column is failed under the earthquake. A *DI* of 0.0 or negative indicates that the column is in its linear-elastic range. A *DI* between 0.0 and 1.0 indicates that the column is within its post-yielding range. A similar index was used in previous studies (e.g., Vosooghi and Saiidi, 2010). Based on statical analysis of more than 30 RC bridge columns tested on shake tables and an analytical investigation, they proposed design *DI*s for different damage states. **Table 2.12** presents a summary of the work by Saini and Saiidi (2014) including the bridge serviceability at different damage state and the design damage index.

Table 2.12 – RC Bridge Column Serviceability Based on Damage State or Index (Saini and Saiidi, 2014)

Damage State DS	Service to Public	Service to Emergency	Emergency Repair	Design Damage Index DI	Earthquake Levels (Years)			
					O-ST	O-NST	Rec.	Imp.
DS-1	Yes	Yes	No	0	100	500	1000	1500
DS-2	Yes	Yes	Yes, only plastic hinge	0.15	500	1000	1500	2500
DS-3	No	Yes, 1 lane	Yes, entire column	0.35	1000	1500	2500	NA
DS-4	No	Yes, 1 lane	Yes, entire column	0.55	1500	2500	NA	NA
DS-5	No	No	Yes, entire column	0.8	2500	NA	NA	NA
DS-6	No	No	NA	1	NA	NA	NA	NA

O-ST = Ordinary Standard Bridge
O-NST = Ordinary Non Standard Bridge
Rec. = Recovery Bridge
Imp. = Important Bridge
NA = Not Applicable

NCHRP 833 (Olsen et al., 2016) proposed a four-level damage state for bridge columns and bents as summarized in **Table 2.13**. Note that the first level, which is "none" indicating that no damage was observed, was not included in the table. Similar four-level damage states were proposed for other bridge elements, which can be used after an event for the bridge "Preliminary Damage Assessment (PDA)".

Table 2.13 – Damage States for RC Bridge Columns and Bents (NCHRP 833)

Minor	Moderate	Severe
Fine shear cracks	Very visible shear cracks	Steep shear cracks
Vertical cracks in beams or horizontal cracks in columns and piers	Diagonal cracks in beams and/or loss of concrete cover	Bar buckling in beams, columns, and piers
Small transverse cracks at the column ends (without longitudinal cracks)	Localized crushing of concrete	Crushing of concrete cover
	Slight spalling of concrete cover	Major spalling of concrete cover
	Slightly exposed transverse and main bars	Exposed transverse and main bars
		Fractured transverse ties

NCHRP 949 (Murphy et al., 2020) recently proposed a three-level performance assessment for RC bridge columns using a pushover analysis based on steel bar and/or concrete strain limits (**Table 2.14**). **Figure 2.15** illustrates five points on a pushover curve that was used to impose limitations per performance level. It should be noted that the proposed strain-based assessment is best suited for a new design or in-depth analytical studies of damaged columns since structural analyses are needed to obtain the strain-displacement response of the column/bent.
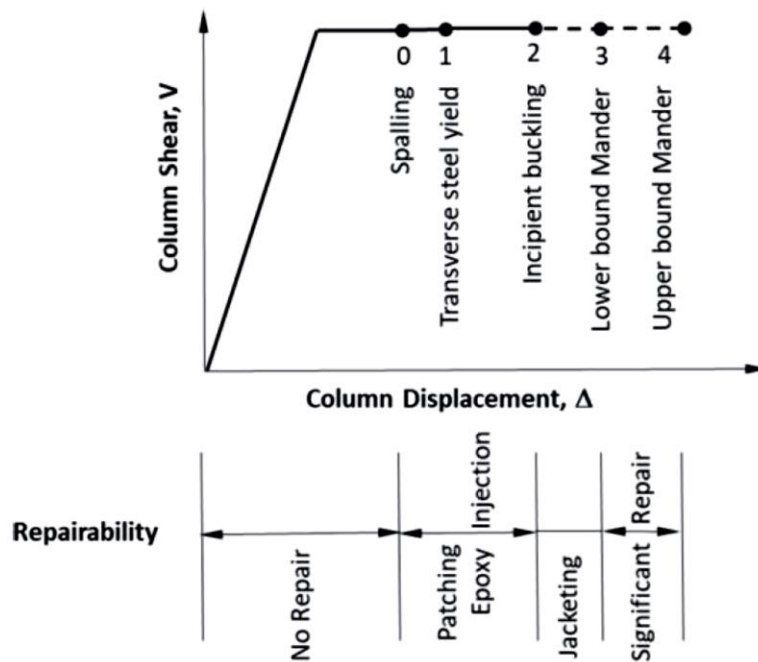
Figure 2.15 – Various Limit States for RC Bridge Columns (NCHRP 949)

27

Table 2.14 – Bridge Performance Levels and Potential Engineering Design Parameters (NCHRP 949)

Engineering Design Parameters	Performance Level		
	PL1: Life Safety	PL2: Operational	PL3: Fully Operational
Reinforcement tensile strain limit [a,b] (RC Column)	$\varepsilon_{s\ buckling}^{bar} = 0.032 + 790\rho_s \dfrac{f_{yhe}}{E_s} - 0.14 \dfrac{P}{f'_{ce}A_g}$	$\varepsilon_s = 0.8\,\varepsilon_{s\ buckling}^{bar}$	≤ 0.010
Concrete compressive strain limit (RC Column)	$\varepsilon_c = 1.4\left(0.004 + 1.4\dfrac{\rho_v f_{yh} \varepsilon_{su}}{f'_{cc}}\right)$	$\varepsilon_c = \left(0.004 + 1.4\dfrac{\rho_v f_{yh} \varepsilon_{su}}{f'_{cc}}\right)$	≤ 0.004
Steel tube tensile strain limit (RCFST)	≤ 0.025	$\varepsilon_s = 0.021 - \dfrac{D}{9100t} \geq \varepsilon_y$	$\leq \varepsilon_y$
Concrete compressive strain limit (RCFST)	NA	NA	NA
Superstructure-to-abutment vertical offset	No limit	$\leq 9"$	$\leq 1"$
Superstructure-to-abutment horizontal offset	No Limit	$\leq 6"$	$\leq 1"$
Approach fill settlement limit[c]	1/50	$\leq 1/100$	$\leq 1/250$
Lateral flow/spread limit due to liquefaction	Site Specific Evaluation Required	$\leq 12"$	$\leq 6"$

Note: This table provides recommended strain limits for common bridge element types. The table is not intended to be exhaustive with respect to bridge element types. For element EDPs not included in the table, the designer in concurrence with the owner and peer review may develop project-specific EDP criteria. See Article 6.1, "Strain Limits," of the AASHTO guidelines for further background on this table. NA = not applicable for RCFST.

[a] $\varepsilon_{s\ buckling}^{bar}$ is the tension strain in the reinforcing steel that will result in bar buckling in compression during the following cycle of seismic response. For definitions of the other variables in this table, refer to the *Seismic Guide Specifications*.

[b] Deterministic values are based on the median predictor for PL1. The reduced value for PL2 is based on a 20% probability of initial bar buckling from the median predictor to create a higher standard of performance.

[c] Approach fill settlement limits are defined in terms of vertical settlement versus horizontal distance of the approach slab (i.e., 1:50 is 0.5 feet settlement over a 25-foot approach slab length). For further discussion of approach fill settlement limits, see Article 6.3.3.1 of the AASHTO guidelines.

FEMA HAZUS (2020) defines the damage for <u>whole bridge</u> into five levels as presented in **Table 2.15**. The definition that are specific for columns are marked with underlines. FEMA uses a displacement-based limit by Basoz and Mander (1999) to quantify the damage levels. A displacement-based analysis (e.g., fragility curves) should be performed to relate the displacement to the column damage state. Furthermore, it is well documented that short RC columns exhibit smaller displacement capacities compared with tall columns thus the broad drift-based (Δ/L) classification presented in FEMA HAZUS may not be suitable for all columns.

Table 2.15 – Damage States for Bridge Components (FEMA HAZUS, 2020)

Damage State	Qualitative Performance Description	Quantitative (Column Drift)
None	No bridge damage	$\Delta/L < 0.01$
Slight	Minor cracking and spalling to the abutment, cracks in shear keys at abutments, minor spalling and cracks at hinges, **minor spalling at the column** (damage requires no more than cosmetic repair), or minor cracking to the deck	$0.01 < \Delta/L < 0.025$
Moderate	**Any column experiencing moderate (shear cracks) cracking and spalling** (column structurally still sound), moderate movement of the abutment (<2 inches), extensive cracking and spalling of shear keys, any connection having cracked shear keys or bent bolts, keeper bar failure without unseating, rocker bearing failure, or moderate settlement of the approach	$0.025 < \Delta/L < 0.05$
Extensive	**Any column degrading without collapse: shear failure** – (column structurally unsafe), significant residual movement at connections, major settlement approach, vertical offset of the abutment, differential settlement at connections, or shear key failure at abutments	$0.05 < \Delta/L < 0.075$
Complete	**Any column collapsing** and connection losing all bearing support, which may lead to imminent deck collapse, or tilting of substructure due to foundation failure	$\Delta/L > 0.075$

From: Δ is the column lateral displacement and *L* is the column length.

2.3.1 Visual Methods of Building Column Assessment

Studies on the RC bridge column damage states were reviewed in the previous section. A brief review of the past works carried out on buildings is also included herein for completeness.

For RC building columns, ATC-20 (1989) categorized the visual damage to (1) out-of-plumbness, (2) buckling, (3) cracking, (4) yielding, and (5) hazard of falling. Later, ATC-58 (as reported in Bearman, 2012) offered a six-level damage state to facilitate the visual inspection of RC building columns as summarized in **Table 2.16**. Based on a damage inspection database, Bearman (2012) proposed an eight-level damage state for visual inspection of RC building columns as summarized in **Tables 2.17** and **2.18**. Paal et al. (2015) modified the damage state definitions in Bearman (2012) (**Table 2.19**), and incorporated those in a computer program for a quick post-earthquake assessment of RC building columns.

Table 2.16 – Damage Types and Damage States for RC Building Columns (ATC 58)

Damage State	Frame Damage Description
C	**Damage to finishes:** Cosmetic finishes exhibit damage but residual concrete crack widths are too narrow to require repair. Hairline cracking of concrete. Longitudinal reinforcement yields.
0	**Concrete Cracking:** Residual crack widths that require epoxy injection. Residual concrete crack widths exceed 0.02 in. Yielding of longitudinal reinforcement.
1	**Moderate Concrete Cracking:** Residual crack widths that require epoxy injection. Residual concrete crack widths exceed 0.06 in.
2	**Concrete Spalling:** Spalling of cover concrete that exposes transverse but not longitudinal reinforcing steel.
3	**Concrete Crushing:** Spalling of cover concrete exposes longitudinal reinforcement. Strength loss initiates in laboratory.
4	**Steel yielding, buckling, and fracture:** Reinforcing steel experiences severe inelastic deformation and requires replacement. Longitudinal steel exhibits severe inelastic strain, buckling, or fracture.

Table 2.17 – Damage Types and States for Flexural RC Building Columns (Bearman, 2012)

Damage State	Flexure-Critical Damage Description (FC)
F1: Flexural Cracking	– Top and bottom 1/3 of column – Perpendicular to column axis – Span width of column – Uniformly spaced – Initially hairline cracks (<0.005 in.) – Prior to spalling ≈ 0.1 in. at peak displacement (HAL) – Prior to spalling ≈ 0.2 in. at peak displacement (LAL)
F2: Longitudinal Cracking	– Top and bottom 1/3 of column – Parallel to column axis – Prior to spalling ≈ 0.15 in. at peak displacement
F3: Shear Cracking	– Top and bottom 1/3 of column – At 35° to 65° angle from horizontal – Initially hairline cracks (<0.005 in.) – Prior to spalling ≈ 0.02 in. at peak displacement (HAL) – Prior to spalling ≈ 0.04 in. at peak displacement (LAL)
F4: Initial Concrete Spalling	– Initially occurs in top and bottom 1/4 of column faces – Complete spalling ≈ b from ends prior to failure
F5: Concrete Spalling Exposing Longitudinal Steel	– Initially exposed at ≈ $b/2$ from ends – Exposed length ≈ b
F6: Longitudinal Bar Buckling	– Initially occurs at ≈ $b/2$ from ends – Total buckling length prior to fracture ≈ $b/2$
F7: Crushing of Core Concrete	– Same location as bar buckling
F8: Longitudinal Bar Fracture	– Same location as bar buckling

b is the column width

Table 2.18 – Damage Types and States for Shear RC Building Columns (Bearman, 2012)

Damage State	Shear-Critical Damage Description (SC)
S1: Flexural Cracking and Longitudinal Cracking	– Same as FC HAL for F1 and F2 except as noted – Flexural cracks prior to S3 ≈ 0.05 in. – Longitudinal cracks prior to S3 ≈ 0.1 in.
S2: Shear Cracking	– Same as FC HAL for F3 except as noted – May occur at any height
S3.0: Widening and Localization of Shear Cracks	– May occur at any height – At 35° to 65° angle from horizontal – Prior to spalling ≈ 0.3 in. residual (HAL) – Prior to spalling ≈ 0.5 in. residual (LAL)
S3.1: Widening and Localization of Longitudinal Cracking on Side Faces	– May run the entire height of the column – Meet localized shear cracks near edge – Prior to spalling ≈ 0.5 in. residual

S3.2: Concrete Spalling on Side Faces	– Possible spall shapes
	  o Triangle where shear and longitudinal cracks meet
	  o Parallelogram encompassing primary shear cracks
	– Edges of spall are at 35° to 65° angle from horizontal
	– May occur at any height

S3.3: Longitudinal Bar Buckling	– May occur at any height
S3.4: Crushing of Core Concrete	– Typically occurs with Bar Buckling – May occur at any height

Table 2.19 – Damage Types and States for RC Building Columns (Paal et al., 2015)

Damage state	Damage description	Response mechanism	Drift (%)	
			LAL	HAL
D0	No damage	Unknown	0.0	0.0
D1	Flexural cracks Top and bottom 1/3 of column Span width of column Longitudinal cracks top and bottom 1/3 of column	Unknown	1.0	0.75
D2	Shear cracks top and bottom 1/3 of column	Unknown	2.0	1.75
S2	Shear cracks in middle 1/3 of column	Shear	0.5	0.5
S3.0	Widening and localization of shear cracks $W_c/b \geq 1/60$	Shear	1.5	1.25
S3.1	Longitudinal cracking on side faces	Shear	2.0	1.6
S3.2	Concrete spalling on side faces	Shear	2.0	1.6
S3.3	Longitudinal bar buckling/crushing of core concrete $L_T/b \geq 1$	Shear	2.0	1.6
F4	Concrete spalling Top and bottom 1/4 or 1/5 of respective faces	Flexure	1.5	0.75
F5	Concrete spalling exposing longitudinal Steel	Flexure	2.0	1.0
F6	Longitudinal bar buckling/crushing of core concrete $L_T/b \geq 1/2$	Flexure	6.0	3.5

2.4 RC Bridge Column Test Database

Earthquake-caused bridge damages have been documented in past studies (e.g., Housner and Thiel, 1994; Kawashima, 2000; Kawashima, 2001), and the most related publications were reviewed in **Sec. 2.2**. Furthermore, a handful studies reviewed past experimental works on RC columns, extracted key test parameters, and developed test databases. The major studies are briefly discussed herein.

Hose and Seible (1999) collected the experimental data and photographs of 12 RC bridge columns, three RC bridge sub-assemblies, and three RC column-bent systems. Subsequently, based on the five-level damage state discussed in the previous section (**Table 2.8**), they identified the key points of force-displacement curves and presented a photograph per damage level for each test specimen (**Fig. 2.16**).

Berry et al. (2004) developed a comprehensive database for RC columns including data for 160 circular columns and 247 rectangular columns. This database is commonly referred to as the Pacific Earthquake Engineering Research Center (PEER) column database and is currently available online at <https://nisee.berkeley.edu/spd/>. **Figure 2.17** shows a screenshot of one of the columns as a sample of what parameters were reported. This study also tried to determine the column displacement at following damage states: concrete crushing, significant concrete spalling, longitudinal bar buckling, longitudinal bar fracture, spiral fracture, and loss of axial load capacity. These displacements yet to be populated for several specimens within this database.

The database by Hose and Seible (1999) was further expanded by Veletzos et al. (2008) to include more than 100 RC column test data and RC bridges damaged under 14 earthquakes. **Figure 2.18** shows one sample of their work.

Rodriguez and Padilla (2009) summarized the experimental data for 76 RC columns, which were tested under different setups. **Table 2.20** presents the collected information for a few columns as a sample of the work. This database and that by Berry et al. (2004) shared the same references, thus several specimens are essentially the same in the two works. Rodriguez and Padilla (2009) used the 76-specimen database to develop a new analytical damage index for RC columns.

Vosooghi and Saiidi (2010) and later Saini and Saiidi (2014) developed a database of RC bridge columns tested on shake tables, which included 38 columns. **Table 2.21** presents the column specimens included in this database. These two studies also reported the drift at different damage states for the columns appeared in the database.

The Seismic Engineering Research Infrastructures for European Synergies (SERIES) developed three databases for RC columns, RC beams, and RC walls. Test data for rehabilitated and precast buildings is also reported. The database for RC columns (Perus et al., 2013), which was built upon the work by Berry et al. (2004), had a total of 477 circular and rectangular columns. The force-displacement hysteric response for all columns was digitized and is available in the database. The column database can be found online at <http://www.dap.series.upatras.gr/>.

Ghannoum et al. (2015) has expanded the work by Berry et al. (2004) and developed a new database for RC columns including 172 circular and 326 rectangular specimens. They tried to collect as many as 54 parameters per specimen including material properties, testing method, and critical forces and displacements. This database, also known as the ACI 369 column database, is available online at: <https://datacenterhub.org/resources/255>. Their work has recently been updated by Azadi-Kakavand et al. (2019) with two more parameters (the yield drift ratio and the displacement ductility), which can be found online at <https://www.designsafe-ci.org/>.
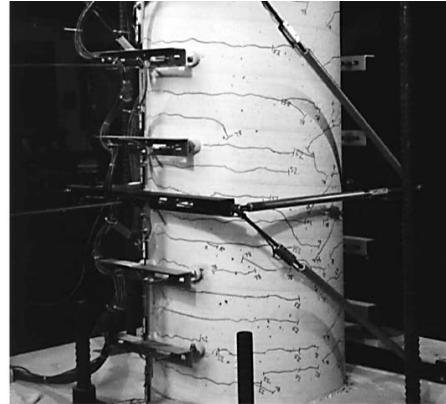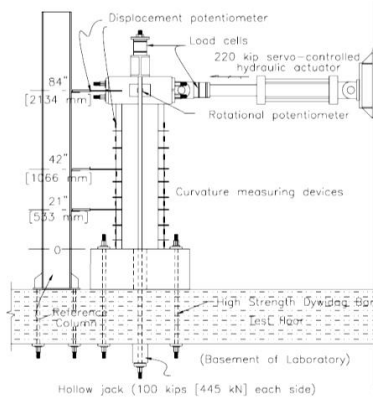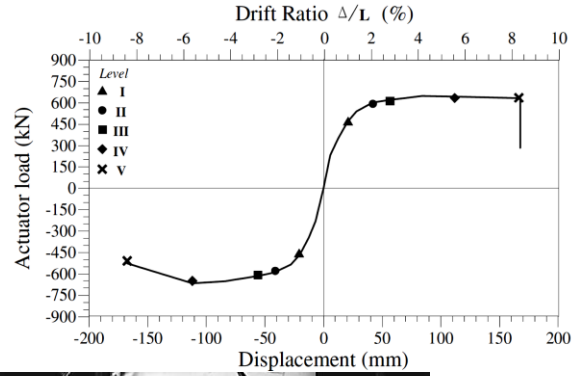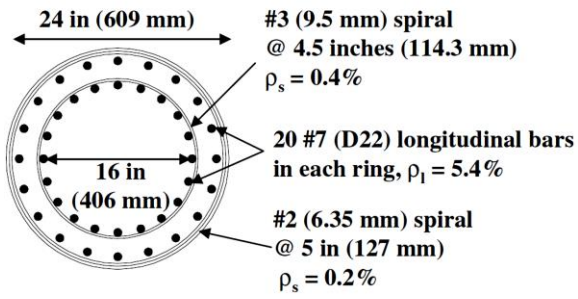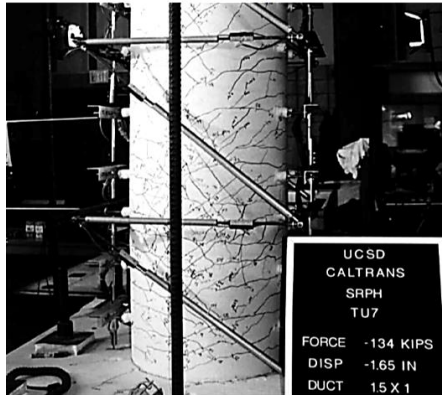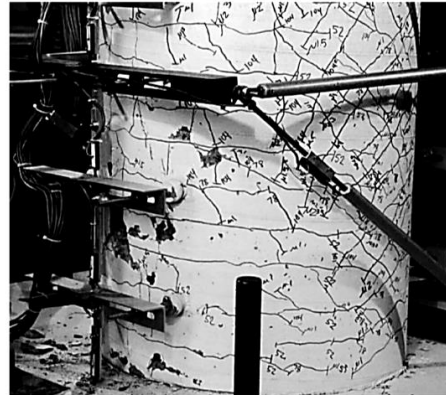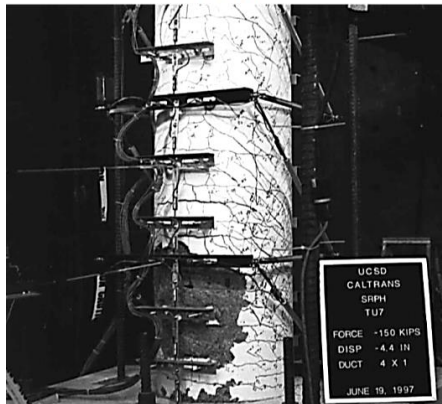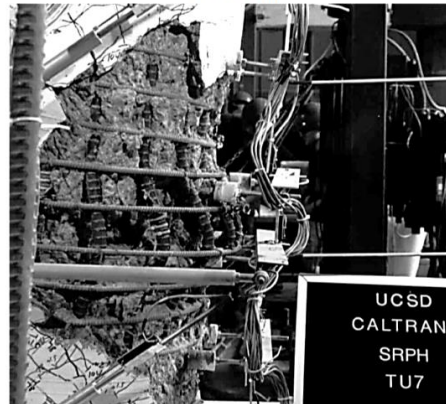
Figure 2.16 – Sample of Collected Column Test Data by Hose and Seible (1999)

Specimen Information

Name: Hamilton, 2002, UCI1
Type: Spiral
Comments: Cross-section D
Reference: Hamilton, C.H., Pardoen, G.C., Kazanjy, R.P., "Experimental Testing of Bridge Columns Subjected to Reversed-Cyclic and Pulse-type Loading Histories," Report 2001-03, Civil Engineering Technical Report Series, University of California, Irvine, 2002

Material Properties

Concrete Strength: 36.5 (MPa)
Transverse Steel: Yield Stress: 691.5 (MPa)
Longitudinal Steel: Yield Stress: 458.5 (MPa) Strength: 646 (MPa)

Geometry

Diameter: 406.4 (mm) Cross-Section: Circular
Length: L-Inflection: 1,854.2 (mm) L-Measured: 1,854.2 (mm)
Test Configuration: Cantilever

Loading

Axial Load: 0 (kN)
P-D: Feff provided
L-Bottom: 419.1

Longitudinal Reinforcement

Diameter: 12.7 (mm)
Number of Bars: 12
Reinforcement Ratio: 0.0117

Transverse Reinforcement

Diameter Spiral: 4.5 (mm)
Hoop Spacing, Sv: 31.8 (mm)
Cover to Center of Hoop Bar: 15 (mm)
Reinforcement Ratio: 0.53

Non-Dimensional Properties

Span-to-Depth Ratio: 4.56
Axial Load Ratio: 0

Test Results

Failure Type: Flexure
Damage Observation: Concrete Crushing: 0 (mm)
Significant Concrete Spalling: 0 (mm)
Long Bar Buckling: 0 (mm)
Long Bar Fracture: 0 (mm)
Spiral Fracture: 0 (mm)
Loss of Axial Load Capacity: 0 (mm)
Resources: Force Displacement Data (data)

Record Information

Version: 1 (April 8, 2003)

Closeup View

Diameter: 406.4 (mm) Cross-Section: Circular
Length: L-Inflection: 1,854.2 (mm) L-Measured: 1,854.2 (mm)
Test Configuration: Cantilever

Axial Load: 0 (kN)
P-D: Feff provided
L-Bottom: 419.1

Diameter: 12.7 (mm)
Number of Bars: 12
Reinforcement Ratio: 0.0117

Diameter Spiral: 4.5 (mm)
Hoop Spacing, Sv: 31.8 (mm)
Cover to Center of Hoop Bar: 15 (mm)
Reinforcement Ratio: 0.53

Span-to-Depth Ratio: 4.56
Axial Load Ratio: 0

Failure Type: Flexure
Damage Observation: Concrete Crushing: 0 (mm)
Significant Concrete Spalling: 0 (mm)
Long Bar Buckling: 0 (mm)
Long Bar Fracture: 0 (mm)
Spiral Fracture: 0 (mm)
Loss of Axial Load Capacity: 0 (mm)
Resources: Force Displacement Data (data)

Figure 2.17 – Sample of Column Data from PEER RC Column Database (Berry et al., 2004)
PEER RC Column Database can be found at: <https://nisee.berkeley.edu/spd/>
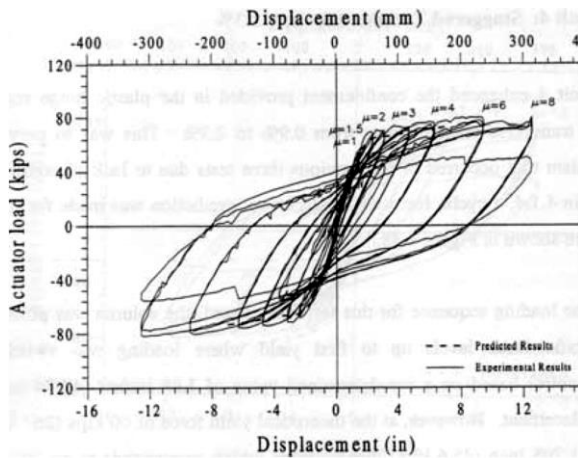
(a) Force-Displacement Graph
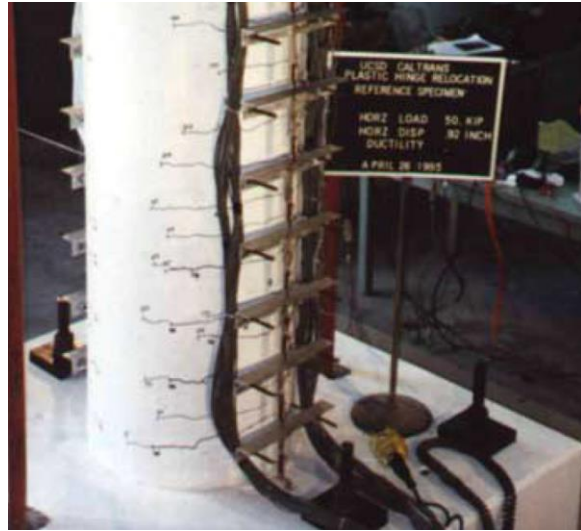
(b) Level I Damage
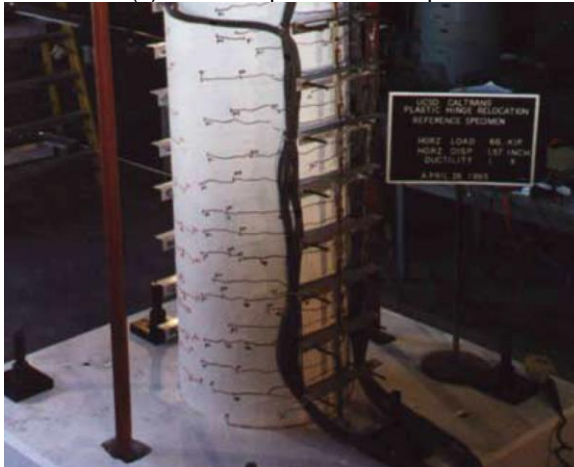
(c) Level II Damage

(d) Level III Damage

(e) Level IV Damage

(f) Level V Damage

Figure 2.18 – Sample of Collected Column Test Data by Veletzos et al. (2008)

Table 2.20 – RC Bridge Column Database by Rodriguez and Padilla (2009)

N° (1)	Designation (2)	Reference (3)	Section type (4)	f_c Mpa (5)	f_y Mpa (6)	f_{yt} Mpa (7)	P/A_g f'_c (8)	ρ_l (9)	ρ_t (10)	$\rho t/\rho ACI$ (11)	h mm (12)	M/VD (13)	K kN/mm (14)	θm (rad) (15)	E_H (m/sec)² (16)
1	AMCB60C	1	R	46.3	422.0	414.0	0.736	0.0275	0.0089	0.88	646	1.2	444.2	0.0046	3.60
2	ANG81U2	2	C	28.5	136.0	280.0	0.463	0.0243	0.0153	1.25	1600	4.0	21.6	0.0234	26.40
3	ANG81U3	1	R	23.6	156.0	320.0	0.380	0.0151	0.0283	4.27	1600	4.0	22.9	0.0318	49.38
4	ANG81U4	1	R	25.0	160.0	280.0	0.210	0.0151	0.0222	2.76	1600	4.0	16.3	0.0365	61.10
5	ANG85U12	2	C	28.6	330.4	328.0	0.078	0.0320	0.0102	0.97	600	1.5	53.5	0.0301	28.94
6	ANG85U3	2	C	36.0	84.2	328.0	0.000	0.0320	0.0051	0.39	1000	2.5	8.7	0.0403	28.15
7	ANG85U4	2	C	30.6	251.0	316.0	0.000	0.0320	0.0051	0.44	800	2.0	29.5	0.0225	15.78
8	ARA82102	1	R	20.6	145.0	323.0	0.333	0.0066	0.0118	2.06	750	1.5	80.6	0.0168	9.52
9	ARAK19	2	C	31.2	151.0	381.0	0.091	0.0381	0.0060	0.50	900	1.6	79.5	0.0137	4.38
10	ARAK9	2	C	30.5	201.0	368.0	0.093	0.0508	0.0070	0.58	600	1.1	174.8	0.0099	2.51
11	AT75N10	1	R	32.4	70.0	392.0	0.266	0.0167	0.0093	1.25	1676	5.5	5.6	0.0229	18.52
12	BETTONO11	1	R	29.9	177.0	414.0	0.104	0.0244	0.0026	0.40	914	1.5	77.0	0.0070	1.83
13	DAV75U1	2	C	33.2	155.0	312.0	0.046	0.0249	0.0043	0.34	2750	5.5	10.3	0.0221	57.25
14	GILL79S1	1	R	23.1	617.0	297.0	0.260	0.0179	0.0150	2.14	1200	2.2	120.5	0.0282	96.54
15	GILL79S4	1	R	23.5	642.0	294.0	0.600	0.0179	0.0250	3.48	1200	2.2	205.8	0.0129	56.20
16	IMAI86	1	R	27.1	381.0	336.0	0.072	0.0266	0.0036	0.50	1650	1.7	224.1	0.0105	8.15
17	J3WS21BS	2	C	26.5	163.7	334.0	0.194	0.0091	0.0393	1.18	500	1.0	104.3	0.0160	8.09
18	KANSTC1	1	R	27.9	68.0	506.0	0.088	0.0142	0.0038	0.77	1500	2.5	15.7	0.0230	25.05
19	KOWALSKIU1	2	C	34.2	137.9	414.0	0.032	0.0207	0.0093	0.94	2438	5.3	3.6	0.0615	226.73
20	KOWALSKIU2	2	C	34.2	133.4	414.0	0.032	0.0207	0.0093	0.94	2438	5.3	5.3	0.1080	336.91
21	KUN97A10	2	C	27.0	70.5	434.0	0.091	0.0200	0.0094	1.26	1372	4.6	5.4	0.0661	64.85
22	KUN97A11	2	C	27.0	65.8	434.0	0.091	0.0200	0.0094	1.26	1372	4.6	5.7	0.0548	56.69

Reference:

1) Reference: Taylor *et al.* NISTIR 5285 (1993).

2) Reference: Taylor *et al.* NISTIR 5984(1997).

3) Reference: Kawashima Earthquake Eng. Lab.(http://www.ce.washington.edu/~peera1/).

Table 2.21 – RC Bridge Column Database by Saini and Saiidi (2014)

Column model		Scale	Design code	Ground motion	Aspect ratio	Section dimensions, in	Long. steel ratio, %	Trans. steel ratio, %
328 [a]		0.5	BDS 1993	Quasi-static	3.0	24	2.8	0.9
828 [a]		0.5	ATC-32	Quasi-static	8.0	24	2.8	0.9
Bridge II [b]	B2E-II	0.25	NCHRP 12-49	Synthetic fault rupture	4.0	12	1.56	0.84
	B2W-II	0.25	NCHRP 12-49	Synthetic fault rupture	4.0	12	1.56	0.84
MN [b]		0.29	Caltrans 2004	Rinaldi	4.5	14	2.86	1.37
ETN [b]		0.29	Caltrans 2004	Rinaldi	7.75	14	2.86	1.54
SETN [b]		0.29	New spectrum	Rinaldi/RRS (Synthetic)	7.75	14	3.62	2.05
SVTN [b]		0.2	New spectrum	Rinaldi/RRS (Synthetic	8.21	12	3.0	1.82
ISH 1.0 [c]		0.2	Caltrans 2001	Sylmar Hospital	2.0	10 x 14.5	2.9	0.6
ISH 1.25 [c]		0.2	Caltrans 2001	Sylmar Hospital	2.0	10 x 15.62	2.8	0.9
ISH 1.50 [c]		0.2	Caltrans 2001	Sylmar Hospital	2.1	10 x 16.75	2.9	0.9
ISH 1.50T [c]		0.2	Caltrans 2001	Sylmar Hospital	2.1	10 x 16.75	2.9	0.9
ISL 1.0 [c]		0.25	Caltrans 2001	Sylmar Hospital	3.3	12 x 17.5	2.0	1.1
ISL 1.5 [c]		0.25	Caltrans 2001	Sylmar Hospital	3.6	12 x 20.25	2.0	1.1
Bridge-I [d]	N1E-I	0.25	NCHRP 12-49	CCN	3.0	12	1.56	0.84
	B1W-I	0.25	NCHRP 12-49	CCN	3.0	12	1.56	0.84
	B2E-I	0.25	NCHRP 12-49	CCN	4.0	12	1.56	0.84
	B2W-I	0.25	NCHRP 12-49	CCN	4.0	12	1.56	0.84
	B3E-I	0.25	NCHRP 12-49	CCN	2.5	12	1.56	0.84
	B3W-I	0.25	NCHRP 12-49	CCN	2.5	12	1.56	0.84
407 [e]		0.33	Caltrans 1991	Quasi-static	4.0	24	0.75	0.7
415 [e]		0.33	Caltrans 1991	Quasi-static	4.0	24	1.50	0.7
430 [e]		0.33	Caltrans 1991	Quasi-static	4.0	24	3.0	0.7
825 [e]		0.33	Caltrans 1991	Quasi-static	8.0	24	1.50	0.7
1015 [e]		0.33	Caltrans 1991	Quasi-static	10.0	24	1.50	0.7
NF-1 [f]		0.33	Caltrans 2004	Rinaldi	4.5	16	2.0	0.92
NF-2 [f]		0.33	AASHTO 2002	Rinaldi	4.5	16	2.2	1.10
RSC [g]		0.2	NCHRP 12-49	Quasi-static	4.5	10	2.04	0.74
SC-CAL [h]		0.25	Caltrans 1994	Artificial	4.5	12	2.83	0.66
SC-PBD [h]		0.25	PBD	Artificial	4.5	12	2.83	1.05
NHS1 [i]		0.33	Caltrans 2006	Sylmar Hospital	2.5	16	3.08	1.38
NHS2 [i]		0.33	Caltrans 2006	Sylmar Hospital	2.5	16	3.08	1.38
BENT 1 [j]	B1E	0.25	NCHRP 12-49	Northridge	5.0	12	1.56	0.86
	B1W	0.25	NCHRP 12-49	Northridge	5.0	12	1.56	0.86
BENT 2 [j]	B2E	0.25	NCHRP 12-49	Northridge	7.0	12	1.56	0.86
	B2W	0.25	NCHRP 12-49	Northridge	7.0	12	1.56	0.86
BENT 3 [j]	B3E	0.25	NCHRP 12-49	Northridge	6.0	12	1.56	0.86
	B3W	0.25	NCHRP 12-49	Northridge	6.0	12	1.56	0.86

[a] Calderone et al. (2001), [b] Choi et al. (2007, 2010), [c] Correal et al. (2006), [d] Johnson et al. (2008)
[e] Lehman and Moehle (2000), [f] Phan et al. (2007), [g] Saiidi et al. (2009), [h] Saiidi and Mortensen (2002)
[i] Vosooghi and Saiidi (2010), [j] Nelson et al. (2010)

Azadi-Kakavand and Allahvirdizadeh (2019) formed a database of 196 RC columns, performed statistical analysis on the database, and proposed data-driven equations to relate drift ratios (at flexural, flexural-shear, shear, and axial failures) to the column geometrical and design parameters.

Zheng at el. (2020) recently developed a new RC column database with 50% overlap with the PEER database. This 199-column database is grouped into "Era-3 Flexural Columns" (48 columns), "Era-2 Flexural Columns" (71 columns), "Era-1 Flexural Columns" (16 columns), "Era-1 Lap Spliced Flexural Columns" (7 columns), "Era-3 and Era-2 Shear Columns" (32 columns), "Era-1 Shear Columns" (22 columns), and "Era-1 Lap Spliced Shear Columns" (3 columns). Furthermore, displacement ductility at seven column damage state thresholds (CDSTs) was included. The database is available at: <https://www.designsafe-ci.org/data/browser/public/designsafe.storage.published/PRJ-2999>.

2.5 Computer Vision for Element and Damage Detection

Similar to what and how humans analyze their surroundings through the visual system, engineers have been trying to understand and automate such tasks using digital images and videos, which is usually referred to as "computer vision". Facial recognition, self-driving cars, and translation software are just a few daily life computer vision applications. Computer vision is gaining a substantial interest in structural engineering especially for structural element detection, damage detection, and health monitoring. A few sample studies are briefly discussed herein.

Computer vision can be used to detect structural components. For example, Zhu et al. (2010) used image stitching techniques to detect bridge columns to expedite inspection. They reported that this method was 89.7% accurate for a database of 114 RC bridge columns. **Figure 2.19** shows examples of successful and failed detections. Narazaki et al. (2020) used semantic segmentation algorithms, a convolutional neural network (CNN), to recognize bridge components from images. They reported 99% recognition accuracy for bridges and components (**Fig. 2.20**). However, the column detection precision was less than 65%.

(a) Successful Detection

(b) Failed Detection
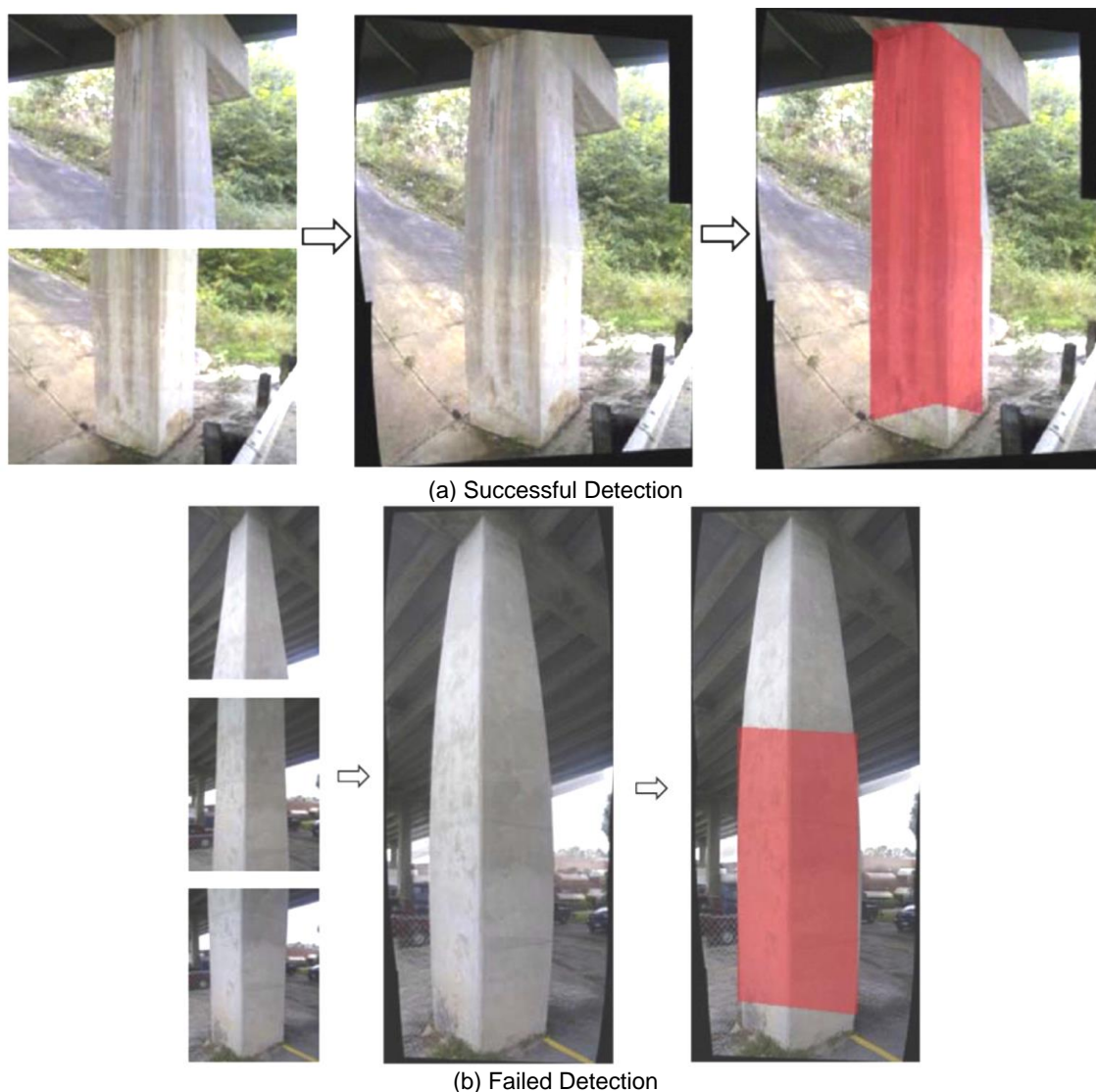
Figure 2.19 – RC Bridge Column Detection Using Image Stitching (Zhu et al., 2010)

MIoU:75.2,FWIoU:91.1 MIoU:74.7,FWIoU:90.8 MIoU:73.3,FWIoU:89.9

MIoU:49.3,FWIoU:79.0 MIoU:49.6,FWIoU:79.3 MIoU:60.1,FWIoU:77.3

MIoU:19.6,FWIoU:24.8 MIoU:19.0,FWIoU:24.2 MIoU:8.5,FWIoU:8.6

MIoU:62.9,FWIoU:82.3 MIoU:63.6,FWIoU:83.0 MIoU:68.9,FWIoU:72.8

MIoU:67.3,FWIoU:77.6 MIoU:67.1,FWIoU:77.3 MIoU:71.5,FWIoU:82.1

MIoU:24.9,FWIoU:47.9 MIoU:24.8,FWIoU:47.9 MIoU:26.5,FWIoU:52.6

MIoU:33.0,FWIoU:52.6 MIoU:32.8,FWIoU:51.9 MIoU:27.8,FWIoU:43.7

MIoU:24.4,FWIoU:97.6 MIoU:32.6,FWIoU:97.9 MIoU:100.0,FWIoU:100.

MIoU:22.5,FWIoU:89.8 MIoU:22.7,FWIoU:90.8 MIoU:100.0,FWIoU:100.

| Nonbridge | Columns | Beams&Slabs | Other Structural | Other Nonstructural |
| (a) | (b) | (c) | (d) | (e) |

(a) input, (b) groundtruth, (c) naïve configuration, (d) parallel configuration, and (e) sequential configuration

Figure 2.20 – Bridge Element Detection Using Convolutional Neural Networks (Narazaki et al., 2020)

Computer vision can also help to automatically detect structural damages such as cracks. Zhu et al. (2011) used a percolation-based method to detect cracks in RC columns. For 100 photographs, the average crack detection accuracy was 64% and the average recall was 92%. German et al. (2012) used an image segmentation, template-matching, and morphological filtering to detect concrete spalling and rebars (**Fig. 2.21**). The average precision and recall for 70 images were respectively 80% and 81% for a neighborhood size of 9 by 9.
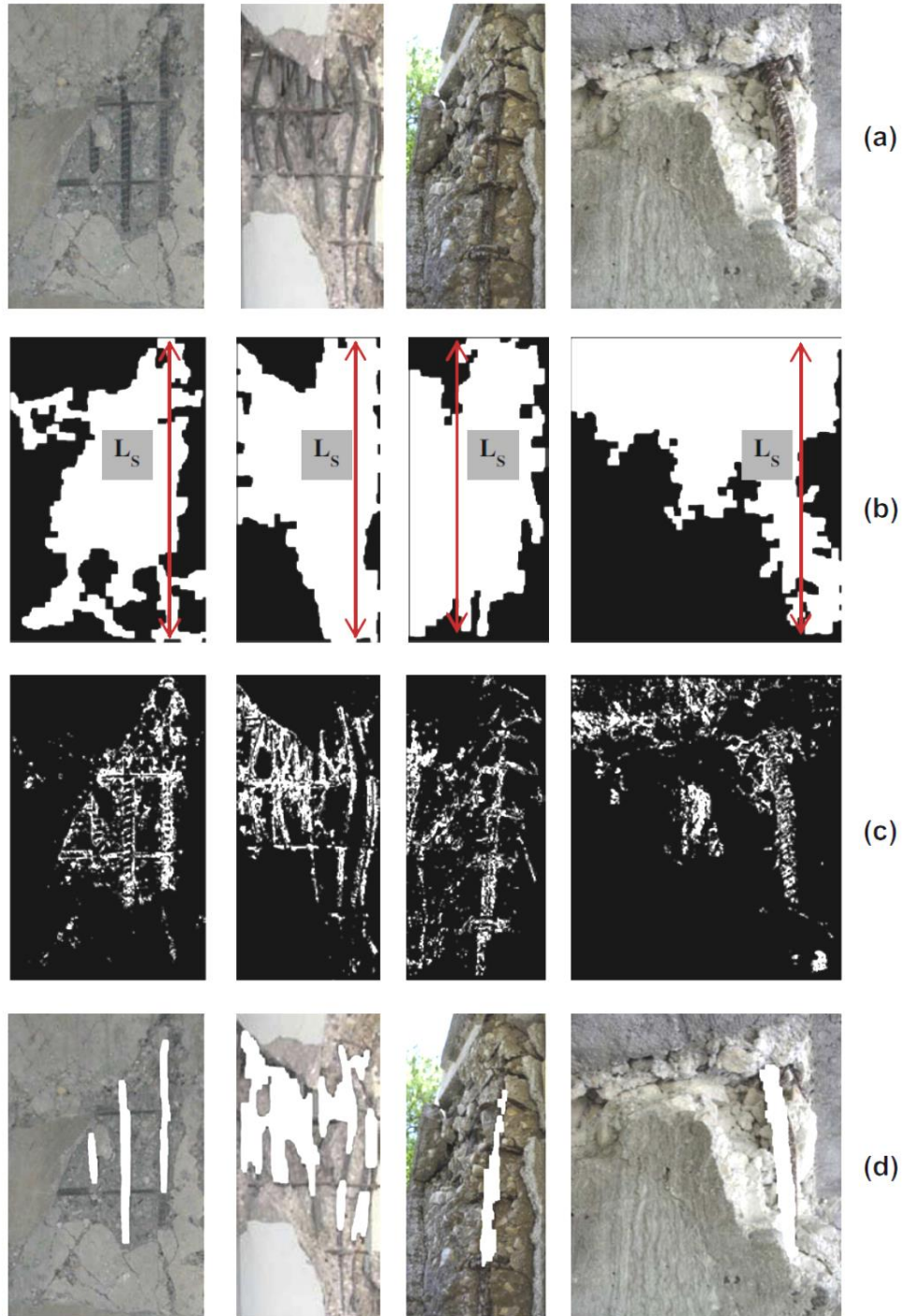
(a) original image; (b) labeled regions; (c) adaptively thresholded image; and (d) final matched and morphed reinforcement detection result

Figure 2.21 – RC Column Rebar Detection Using Image Segmentation (German et al., 2012)

Jahanshahi and Marsi (2012) proposed crack detection method using a 3D scene reconstruction, segmentation, and feature extraction. The novelty of the work was to detect cracks without knowing the distance between the camera and the object. For a database including 440 photos, the crack detection precision was 78%. Torok et al. (2014) used a similar method and successfully detected cracks longer than 0.5 cm. Valença et al. (2017) combined image processing and point cloud data obtained from a terrestrial laser scanner to detect concrete cracks (**Fig. 2.22**). Li and Zhao (2019) trained a deep CNN using 60,000 images to detect concrete cracks and developed a mobile application. The crack detection accuracy for 205 photographs was 99%. **Figure 2.23** shows one sample of the detected cracks using this CNN method. Other recent studies (e.g., Dung and Ann, 2019; and Liu et al. 2019) used either deep CNN or U-net (a CNN used for biomedical image segmentation) to detect concrete cracks and reported more than 90% precision.

(a) Detected Crack Patern   (b) Crack Measurement
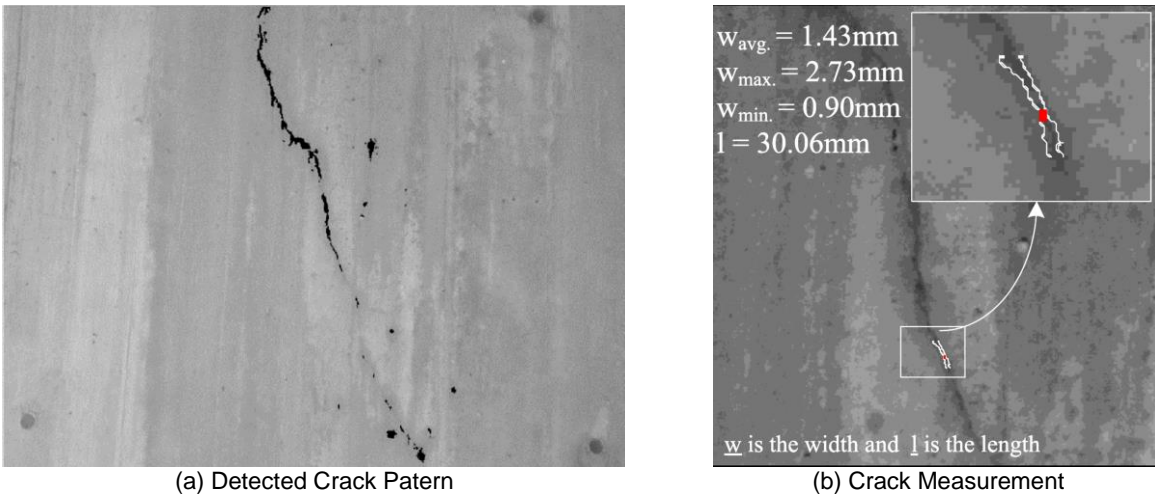
Figure 2.22 – Crack Detection Using Images and Point Cloud Data (Valença et al., 2017)
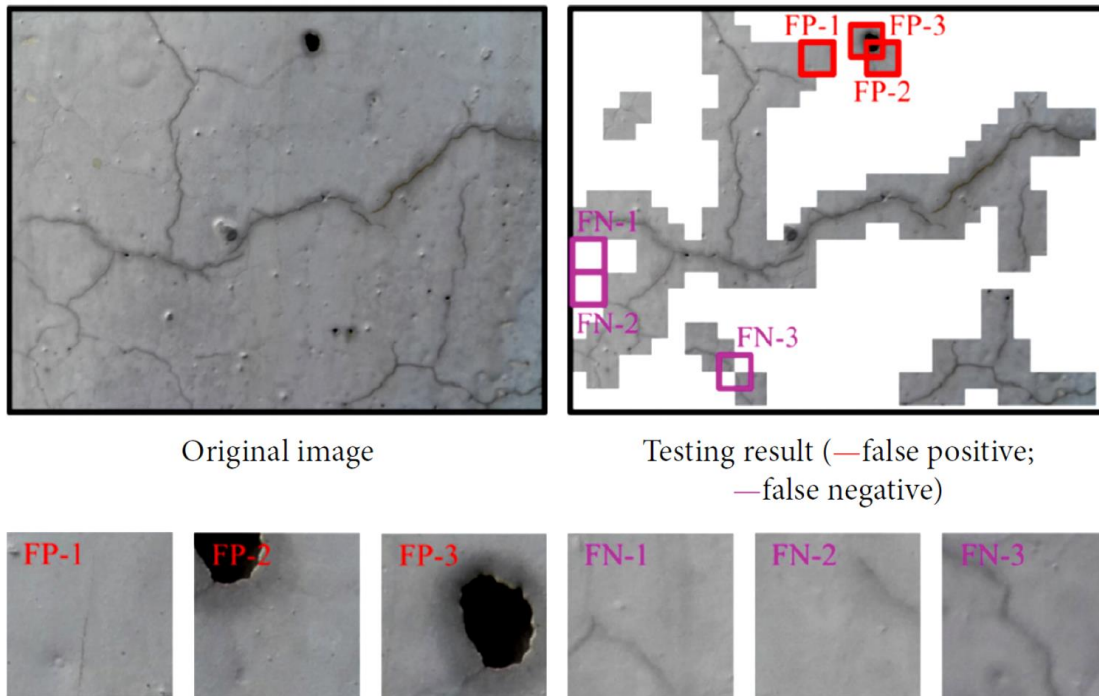
Figure 2.23 – Crack Detection Using Deep Convolutional Neural Network (Li and Zhao, 2019)

Computer vision may be incorporated to expedite post-event structural inspection and document damages automatically. German et al. (2013) and later Paal et al. (2015) developed a framework to automatically detect RC building columns and their earthquake-caused damages, and to estimate the column damage state then the corresponding drift demand. **Figure 2.24** shows a flowchart on how to determine the RC column damage state, which then will be used to estimate the drift demands using a statistical analysis of column test data (e.g., **Table 2.19**). For 50 column images, the overall accuracy for the damage state estimation was 88.5%. This might be the most advanced work that has been done in this topic on buildings. Such methods yet to be developed and implemented for bridges.
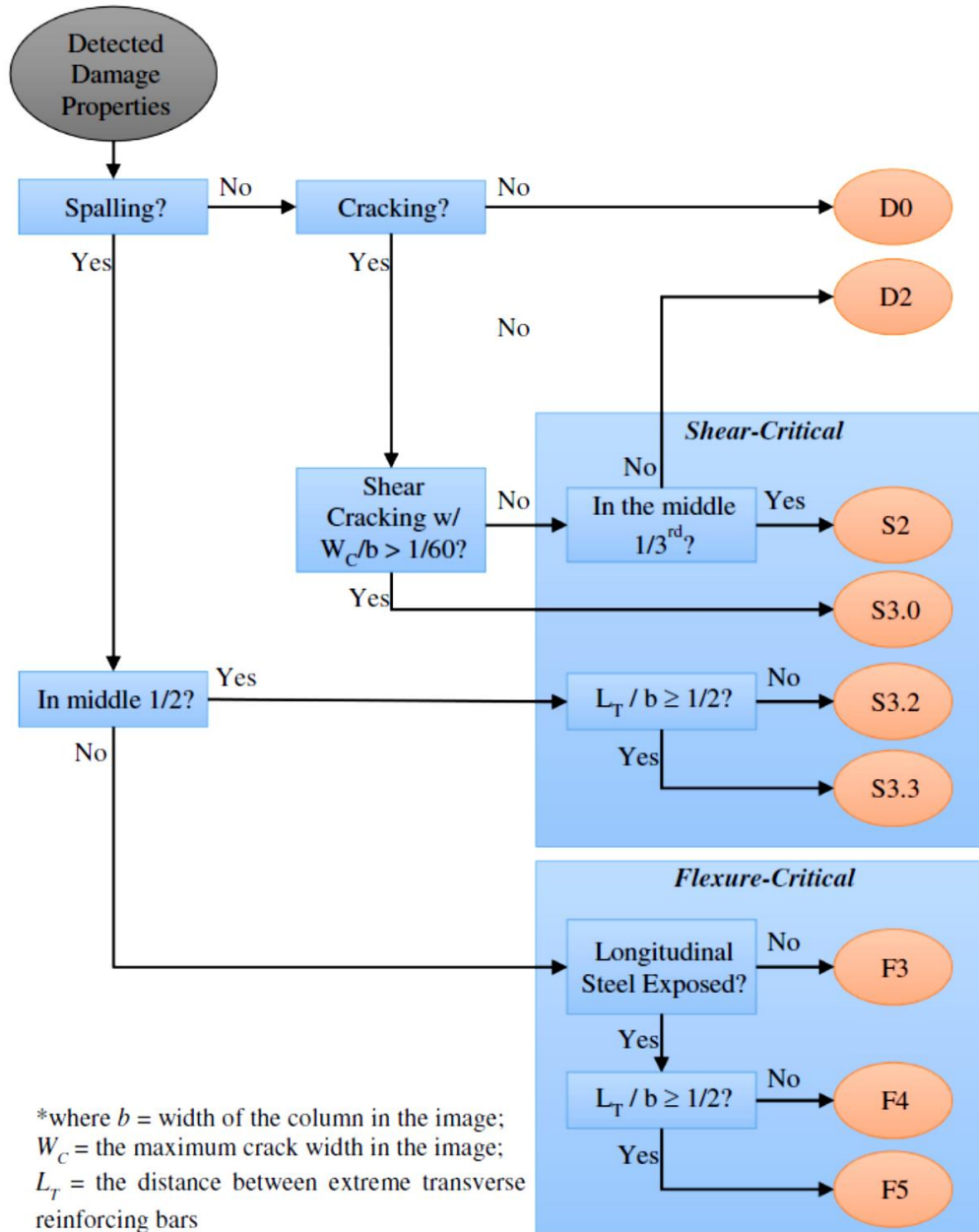
Figure 2.24 – Automated RC Building Column Damage State Estimation (Paal et al, 2015)

Hoskere et al. (2017) utilized a pixel-wise deep CNN to detect concrete cracks, concrete spalling, exposed rebars, steel corrosion, steel fracture, steel fatigue cracks, and asphalt cracks. A 1695-image database cut from 339 photographs of 250 different structures was developed to label and train the network. The

network was able to detect different types of damages and the classification accuracy was more than 80%. Later, Hoskere et al. (2018) proposed a framework to generate vision-based condition-aware models to automate building inspection by detecting building, windows/doors, debris, sky, greenery, cracks, spalling, and exposed rebar. **Figure 2.25** shows sample results using the proposed network. More than 80% detection accuracy was reported for each of the eight classes.
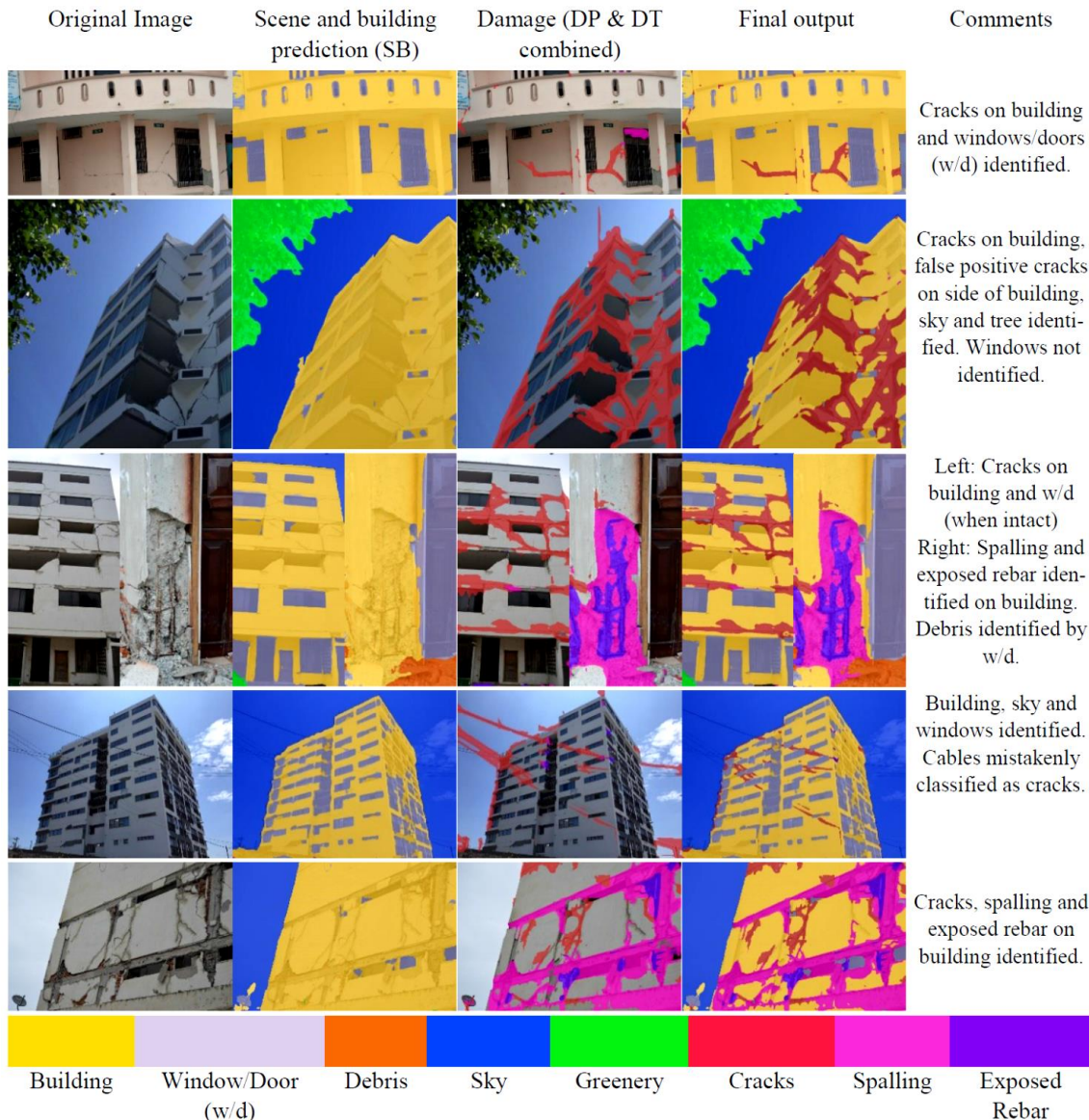
Figure 2.25 – Automated RC Building Component and Damage Detection (Hoskere et al., 2018)

Liang (2019) proposed a three-level image-based post-event inspection approach in which bridge failure, bridge columns, and column damages (cracking, spalling, and exposed rebar) are automatically detected (**Fig. 2.26**). An image database including 1,154 photographs was formed, of which 80% was used for labeling and network training, and 20% was used for testing (evaluating). Bayesian optimization was used to enhance training with low number of images (usually CNN needs thousands of images for a high-accuracy training). The accuracy for bridge failure detection was 98%, the column detection was more than 80%, and the column damage detection was 93%. **Figure 2.27** shows the damages detected for a few RC bridge columns.
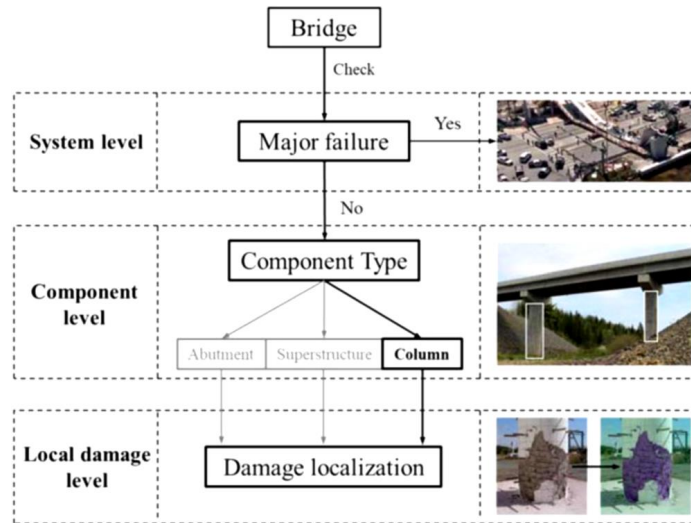
Figure 2.26 – Automated Image-Based Bridge Inspection Method (Liang, 2019)

a) Original images
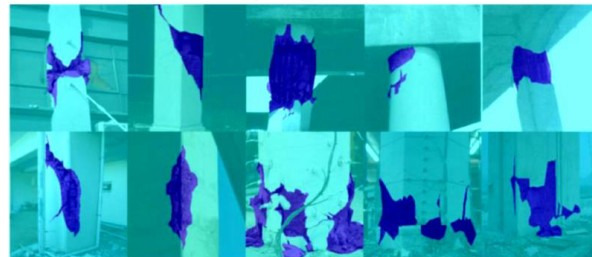
b) Ground-truth labels

c) Labeled images using Otsu's method
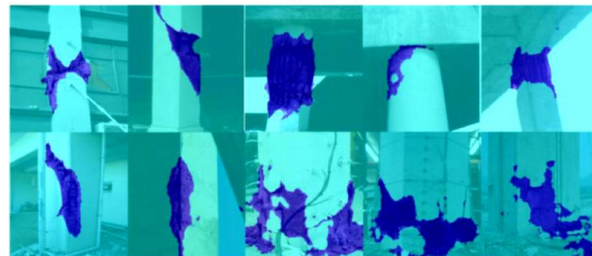
d) Labeled images using the proposed model

Figure 2.27 – Automated RC Bridge Column Damage Detection (Liang, 2019)

Yeum et al. (2019) used a CNN to automatically organize earthquake reconnaissance data of buildings and prepare a report for quick evaluation (**Fig. 2.28**). Photographs, GPS data, and drawings can be included in the report. They collected approximately 100,000 color images of structures after events and organized them per event (e.g., 90% of the database was for earthquake events). Overall, more than 80% classification recall and accuracy were reported for the building interior and exterior components.
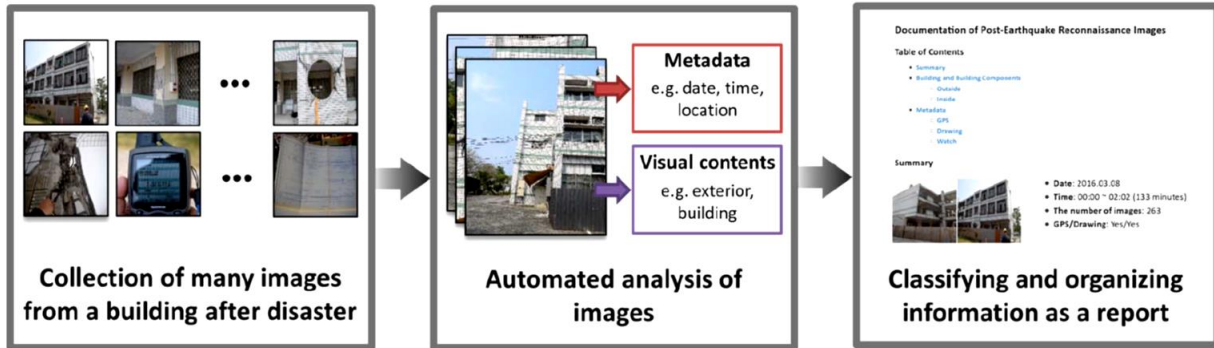
Figure 2.28 – Automated Organization of Reconnaissance Data (Yeum et al., 2019)

To unify bridge inspections, Hüthwohl et al. (2019) used a deep CNN to detect multiple bridge defects (e.g., cracking, delamination, efflorescence) per inspection image. They developed a database of 38,408 images then further refined it to include images with only one defect resulting in a 3,607-image database. Of which, 70% of the photos were used for network training and 30% was used for testing. The study reported 95% precision for crack detection and 86% precision for rebar detection. Other defects were also detected with high accuracies.

Computer vision can also be used to generate three-dimensional models of different structures (usually referred to as 3D reconstruction) before or after an event for detailed inspection. Several tools are available (**Fig. 2.29**). For detailed inspection, data from ground-based tools (e.g., drones) is needed for a successful 3D reconstruction. Yamazaki et al. (2015) used drone data combined with ground camera to reconstruct 3D models of damaged structures and district after the 2015 Gorkha earthquake in Nepal (**Fig. 2.30**). Such models may be further used for more detailed inspection and analysis.
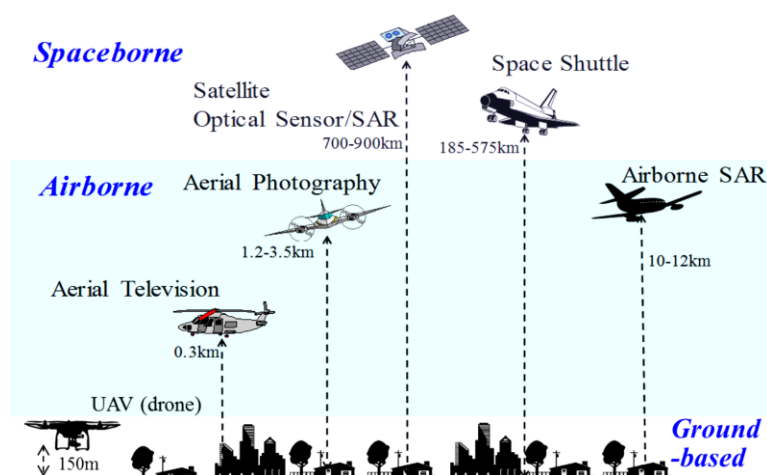
Figure 2.29 – Post-Event Remote Sensing Platforms (Yamazaki and Liu, 2016)

(a) Snapshot of Video Footage, (b) Estimated Camera Positions, (c) 3D model of the district
Figure 2.30 – 3D Reconstruction of a District in Sitapaila, Kathmandu, Nepal (Yamazaki et al., 2015)

The last study included herein is the only work that utilized computer vision to relate the apparent damages of RC bridge columns to the column displacements. Lattanzi et al. (2015) combined image segmentation and feature extraction with nonlinear regression analysis to relate RC columns damages to displacements. Photographs of four RC bridge columns at known displacements (during testing) were segmented to develop a set of numeric descriptors for cracking and spalling. Subsequently, nonlinear regression analysis was used to relate those numeric descriptors with the known displacements. Note that only cracking and spalling were included in the study. Data of three columns was used for the network training, and data for the fourth column was saved for the method evaluation. A strong correlation between cracking/spalling and displacement was observed. However, the model failed to predict the behavior of the fourth column since it was not a conventional RC bridge column (socket connection with post-tensioning tendons was used in the fourth column).

CHAPTER 3. RC BRIDGE COLUMN DAMAGE STATES

3.1 Introduction

A comprehensive literature review was presented in the previous chapter on post-event damage assessments. In this chapter, the findings of the literature review on RC bridge column damage types and damage states are synthesized. Subsequently, new damage state definitions are proposed for RC bridge columns, which are quantitative and better suited for computer programing.

3.2 Summary of RC Bridge Column Damage State Definitions

Apparent (visible) damages of RC bridge columns include horizontal cracking, shear (vertical) cracking, spalling, exposure of transverse bar(s), exposure of longitudinal bar(s), buckling of longitudinal bar(s), crushing of core concrete, fracture of transverse bar(s), fracture of longitudinal bar(s), and complete collapse (significant out-of-plumbness or a flattened column). Note that bar yielding, which is a key design parameter, cannot visually be detected. Each of these damage types may further be classified with different levels. For example, one may use the area of the spalled region to differentiate insignificant from significant spalling because each corresponds to a different level of seismic demand (seismic demand usually refers to the column lateral displacement demand). Therefore, any damage definition or classification is somewhat subjective.

Table 3.1 presents a summary of RC bridge column damage levels (or states) defined in the past studies. Detailed discussion of each study was presented in **Sec. 2.3** of this report. Different studies used the abovementioned damage types to classify the damage progress from "none" to the "column collapse" in three to six levels (or states). Some provided only general and qualitative definitions, and some used more quantitative language. A few studies also provided equations to relate their proposed damage states to design parameters such as drifts and strains. Overall, the literature provides information that might be used as the baseline in the present study to quantify RC bridge column damage.

Table 3.1 – Summary of Past Studies on RC Bridge Column Damage State Definitions

References	Damage Definitions	Remarks
Ramirez et al. (2000)	Green Tag: Horizontal cracks. Yellow Tag: Diagonal cracks, loss of concrete cover. Red Tag: Bar buckling.	No quantitative measures were proposed.
Hose (2001) and Veletzos et al. (2008)	Level I: Onset of hairline cracks. Level II: Theoretical first yielding of longitudinal bars. Level III: Initiation of inelastic deformation, onset of concrete spalling, development of diagonal cracks. Level IV: Wide crack widths/spalling over full local mechanism region. Level V: Buckling of main reinforcement, rupture of transverse reinforcement, crushing of core concrete.	Quantitative measures were proposed for Levels II to V. For example, Level III is when "*residual cracks have a width of 1-2 mm; the length of spalled region is greater than 1/10 of the column cross-section depth.*"
Berry and Eberhard (2008)	Equations were developed to estimate either drift ratios, plastic hinge rotations, or rebar strains at cover spalling, bar buckling, and bar fracture.	A statistical analysis was carried out on an RC bridge column database including more than 30 columns.
Vosooghi and Saiidi (2010) and later Saini and Saiidi, (2014)	Damage State 1: Flexural cracks. Damage State 2: First spalling and shear cracks. Damage State 3: Extensive cracks and spalling. Damage State 4: Visible lateral and longitudinal bars. Damage State 5: Imminent failure. Damage State 6: failure.	No quantitative measures were proposed. Equations were developed based on a statistical analysis on a database including more than 30 RC bridge columns to relate "damage states" to "drift demands" and "damage indexes" for four column type.
AASHTO MBEI (2013)	General descriptions of different RC column defects at four levels: Condition States 1 to 4.	The four-level "condition state" is suitable for regular inspections not after a severe event.
Marsh et al. (2014)	Stage 1: No damage, zero force. Stage 2: Just prior to yielding. Stage 3: Just following formation of plastic hinge. Stage 4: No definition, but seems to be within plastic deformation range.	Analytical equations were proposed to relate column damages (including cover failure, core failure, bar buckling, low-cycle fatigue, and bar fracture) to plastic curvatures.
Olsen et al. (2016)	None: No damage. Minor Damage: Fine shear cracks, horizontal cracks, small transverse cracks at column ends. Moderate Damage: Localized crushing of concrete, slight cover spalling, slightly exposed transverse or longitudinal bars. Severe Damage: Crushing of concrete cover, major spalling of concrete cover, exposed transverse or longitudinal bars, fracture transverse ties.	No quantitative measures were proposed.
Murphy et al. (2020)	Performance Level 1: Life Safety. Performance Level 2: Operational. Performance Level 3: Fully Operational.	Equations were proposed to relate the three performance levels to reinforcement tensile strains and concrete compressive strains.
FEMA HAZUS (2020)	None: No bridge damage. Slight Damage: Minor spalling. Moderate Damage: Shear cracks and spalling. Extensive Damage: Degrading without collapse, shear failure. Complete Damage: Collapse.	A drift-based limit was proposed per damage state.

3.3 Proposed Computer Vision Damage States for RC Bridge Columns

To successfully assess the post-earthquake damage of an RC bridge column using a computer program, a quantitative definition of damage is needed. Specific damage states (also referred to as "condition states", "damage indices", or "damage levels") combined with a comprehensive database of column performance will pave the way for the development of an artificially intelligence (AI) column assessment software.

Based on the review of past studies on RC bridge column damage definitions (**Table 3.1**) and the available RC column test data (see **Sec. 2.4**), new quantitative damage state definitions but consistent with the past studies (Veletzos et al., 2008; Vosooghi and Saiidi, 2010) are proposed for RC bridge columns to be used in computer vision. **Table 3.2** presents the new definitions and **Fig. 3.1-3.6** show sample photographs per proposed damage state. Included in the table, is a tagging guide that might be used for a Preliminary Damage Assessment (PDA). Furthermore, **Fig. 3.7** schematically shows where these damage states are located on a pushover curve. Further discussions are presented in Chapter 5.

Table 3.2 – Proposed Computer Vision Damage States for RC Bridge Columns

Damage State	Qualitative Damage Description	Quantitative Damage Description for Computer Vision
1	Hairline cracks	Horizontal cracks each with an angle of $|\theta| > 80°$ (**Fig. 3.1**)
2	Theoretical first yielding of longitudinal bars	At least three diagonal cracks each with an angle of $|\theta| < 70°$ (**Fig. 3.2**)
3	Extensive cracks and spalling	Length of spalled region in any direction at any column face is greater than $0.1D_c$ but smaller than $0.3D_c$ (**Fig. 3.3**)
4	Visible transverse and/or longitudinal reinforcement	Length of spalled region in any direction at any column face is greater than $0.5D_c$ and detect one transverse bar and/or one longitudinal bar (**Fig. 3.4**)
5	First buckling and/or rupture of longitudinal bar(s), crushing of core concrete	Detect the first buckling and/or rupture of longitudinal bar(s), and/or detect at least two longitudinal bars and three transverse bars (**Fig. 3.5**)
6	Total collapse in which the permanent drift ratio exceeds 10%	The angular change of the line connecting the column ends with respect to the column initial position exceeds 10° ($|\alpha| > 10°$) (**Fig. 3.6**)

Notes:
α = The angle between the column axial direction before and after the deformation (see the figure below)
θ = The angle between the crack and the undeformed column axial direction (see the figure below)
D_c = The undamaged column diameter or the largest side dimension

  ▇ = Inspected   ▇ = Limited Use   ▇ = Unsafe
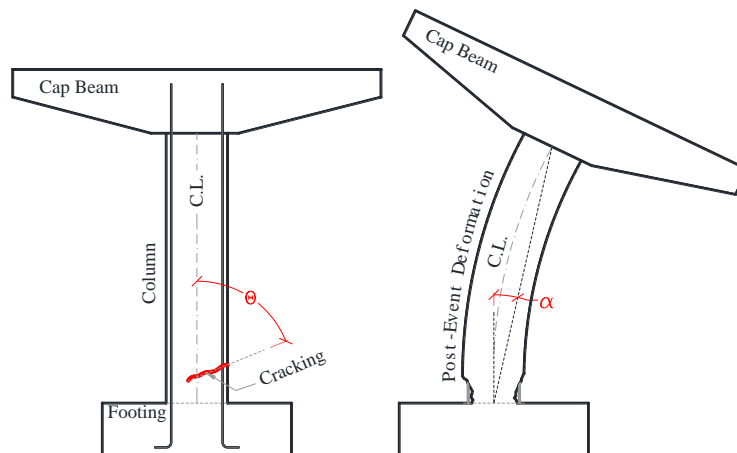
Cast-in-Place Column by Haber et al. (2013)
Photo at Drift Ratio: 0.5%
Column Height = 108 in.
Diameter = 24 in.
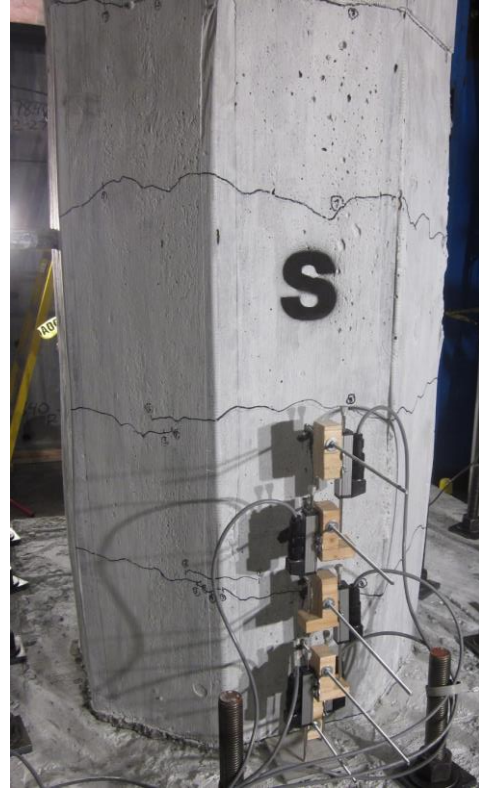
Cast-in-Place Column by Sjurseth (2021)
Photo at Drift Ratio: 0.5%
Column Height = 96 in.
Side Dimension = 24 in.

Full-Scale Column by Schoettler et al. (2015)
Photo at Drift Ratio: 0.85% (EQ1)
Column Height = 288 in. (324 with column head)
Diameter = 48 in.

R-5 Column from Hose and Seible (1999)
Photo at Drift Ratio: 0.125%
Column Height = 144 in.
Side Dimension = 28.7 in. by 19.25 in.

Figure 3.1 – Samples of RC Bridge Column Conditions at DS1

Cast-in-Place Column by Haber et al. (2013)
Photo at Drift Ratio: 0.75%
Column Height = 108 in.
Diameter = 24 in.
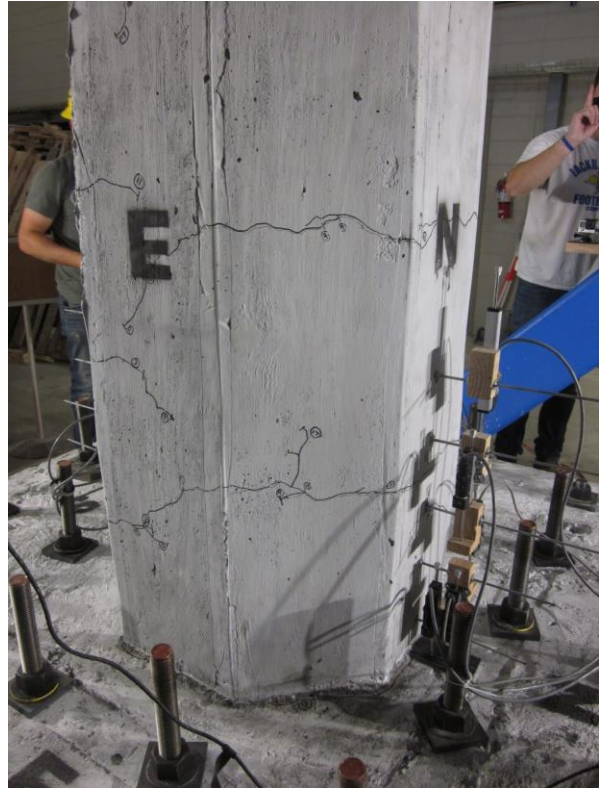
Cast-in-Place Column by Sjurseth (2021)
Photo at Drift Ratio: 0.75%
Column Height = 96 in.
Side Dimension = 24 in.
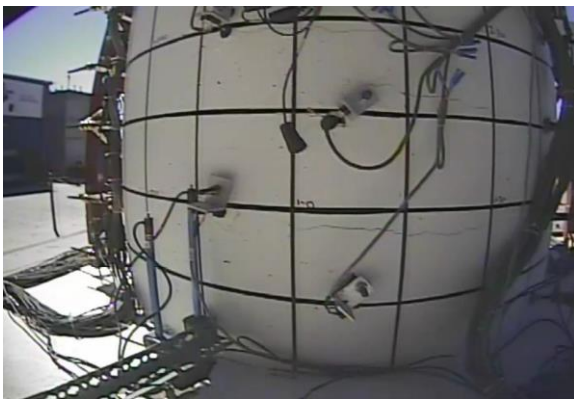
Full-Scale Column by Schoettler et al. (2015)
Photo at Drift Ratio: 1.82% (EQ2)
Column Height = 288 in. (324 with column head)
Diameter = 48 in.
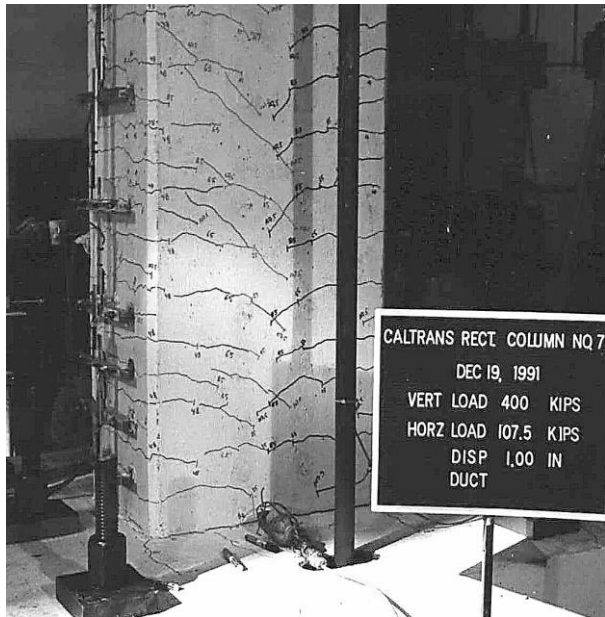
R-5 Column from Hose and Seible (1999)
Photo at Drift Ratio: 0.7%
Column Height = 144 in.
Side Dimension = 28.7 in. by 19.25 in.

Figure 3.2 – Samples of RC Bridge Column Conditions at DS2
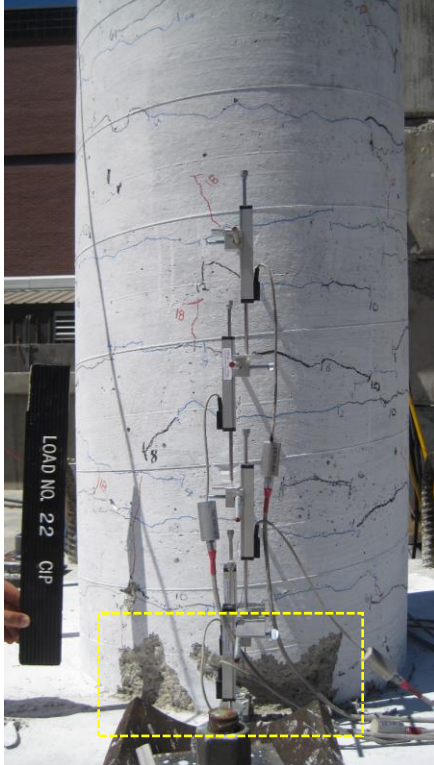
Cast-in-Place Column by Haber et al. (2013)
Photo at Drift Ratio: 3.0%
Column Height = 108 in.
Diameter = 24 in.
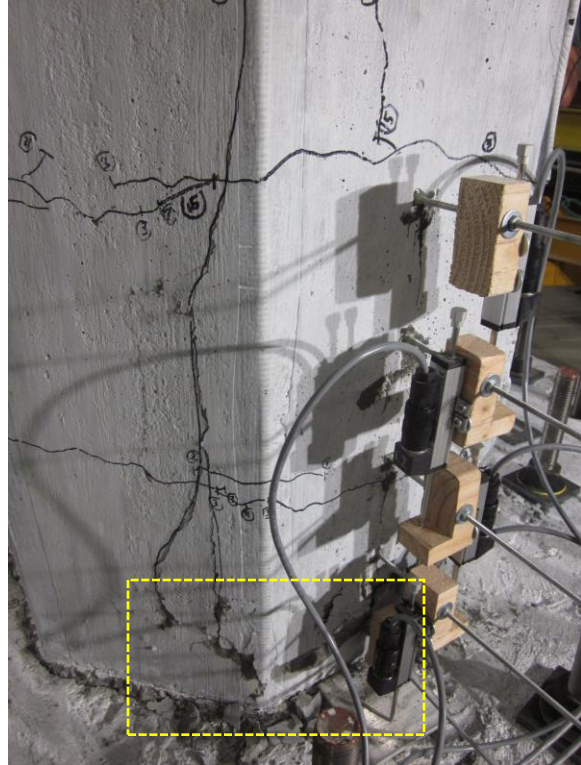
Cast-in-Place Column by Sjurseth (2021)
Photo at Drift Ratio: 2.0%
Column Height = 96 in.
Side Dimension = 24 in.

Full-Scale Column by Schoettler et al. (2015)
Photo at Drift Ratio: 4.93% (EQ3)
Column Height = 288 in. (324 with column head)
Diameter = 48 in.
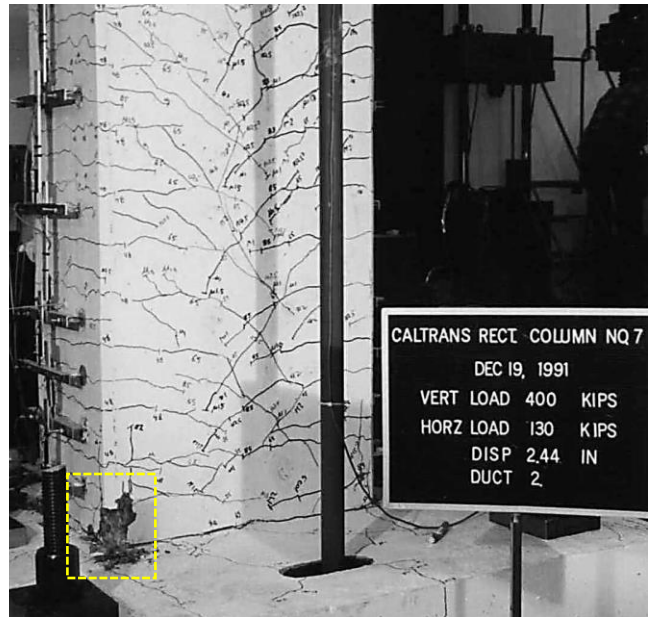
R-5 Column from Hose and Seible (1999)
Photo at Drift Ratio: 1.7%
Column Height = 144 in.
Side Dimension = 28.7 in. by 19.25 in.

Figure 3.3 – Samples of RC Bridge Column Conditions at DS3

Cast-in-Place Column by Haber et al. (2013)
Photo at Drift Ratio: 4.0%
Column Height = 108 in.
Diameter = 24 in.

Cast-in-Place Column by Sjurseth (2021)
Photo at Drift Ratio: 5.0%
Column Height = 96 in.
Side Dimension = 24 in.

Full-Scale Column by Schoettler et al. (2015)
Photo at Drift Ratio: 7.78% (or 8.60% in EQ5 including
residual displacements from EQ4)
Column Height = 288 in. (324 with column head)
Diameter = 48 in.
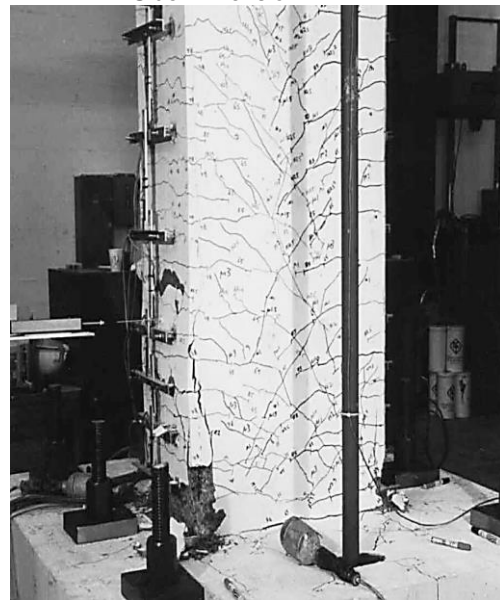
R-5 Column from Hose and Seible (1999)
Photo at Drift Ratio: 2.25%
Column Height = 144 in.
Side Dimension = 28.7 in. by 19.25 in.

Figure 3.4 – Samples of RC Bridge Column Conditions at DS4
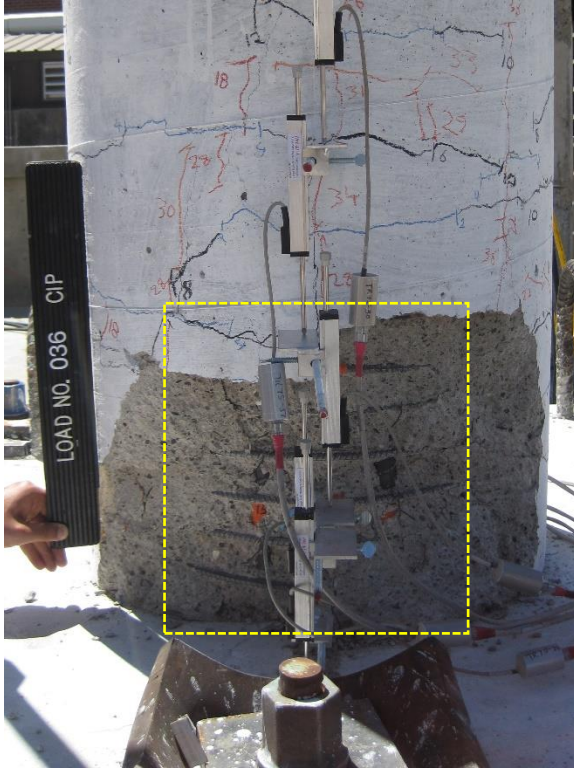
Cast-in-Place Column by Haber et al. (2013)
Photo at Drift: 6.0%; 6 Tran. & 2 Long. Bars Exposed
Column Height = 108 in.
Diameter = 24 in.
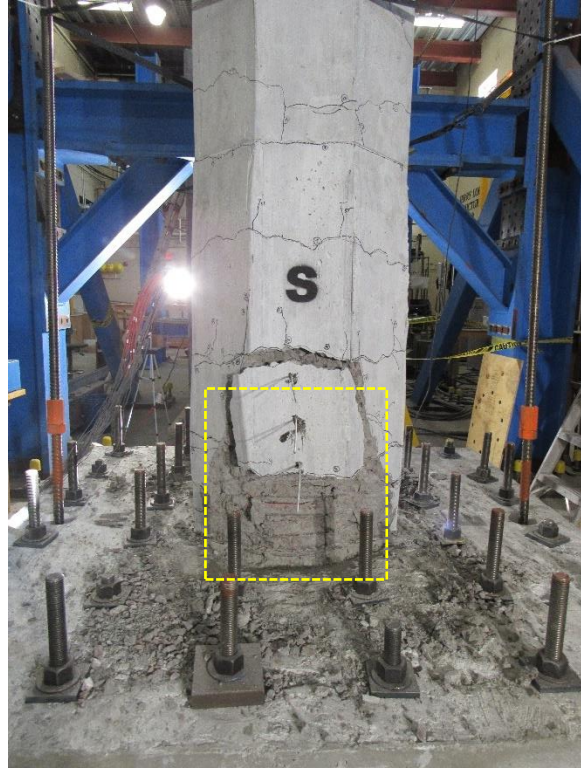
Cast-in-Place Column by Sjurseth (2021)
Photo at Drift: 7.0%; 3 Tran. & 2 Long. Bars Exposed
Column Height = 96 in.
Side Dimension = 24 in.

Not Available

Full-Scale Column by Schoettler et al. (2015)
Photo at Drift Ratio: N/A
Column Height = 288 in. (324 with column head)
Diameter = 48 in.

Not Available
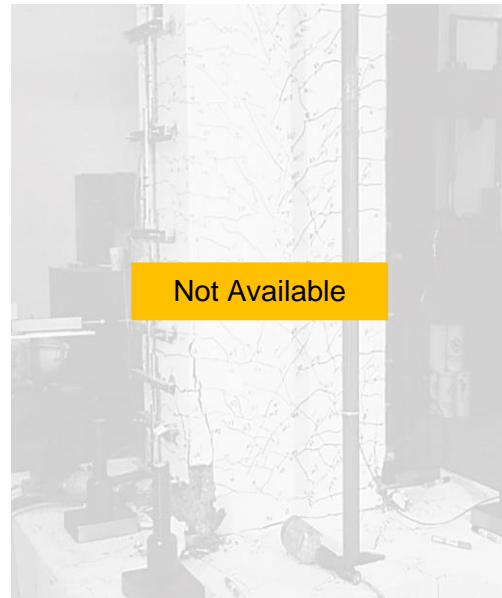
R-5 Column from Hose and Seible (1999)
Photo at Drift Ratio: N/A
Column Height = 144 in.
Side Dimension = 28.7 in. by 19.25 in.

Figure 3.5 – Samples of RC Bridge Column Conditions at DS5
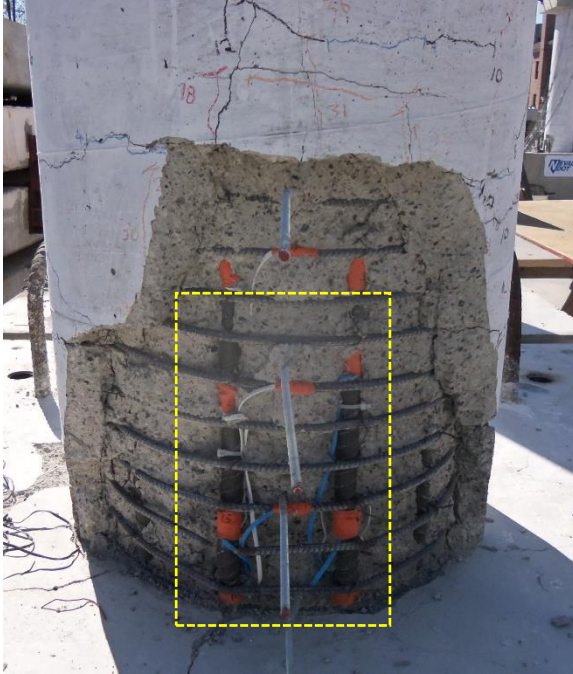
Cast-in-Place Column by Haber et al. (2013)
Photo at Drift Ratio: 10.0%; Bar Buckling & Fracture
Column Height = 108 in.
Diameter = 24 in.

Cast-in-Place Column by Sjurseth (2021)
Photo at Drift Ratio: 10.0%; Bar Fracture
Column Height = 96 in.
Side Dimension = 24 in.
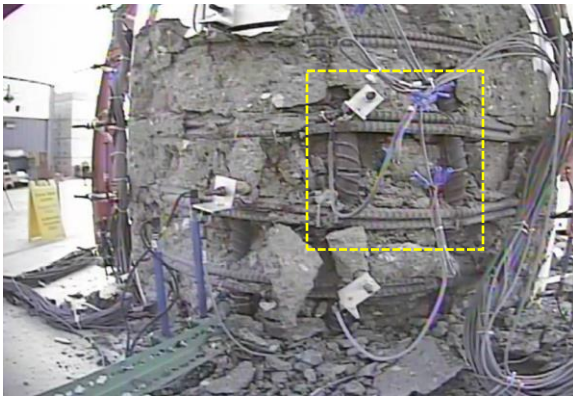
Full-Scale Column by Schoettler et al. (2015)
Photo at Drift Ratio: 8.2% (or 10.3% in EQ8 including
residual displacements from EQ7); Bar Fracture
Column Height = 288 in.
Diameter = 48 in.
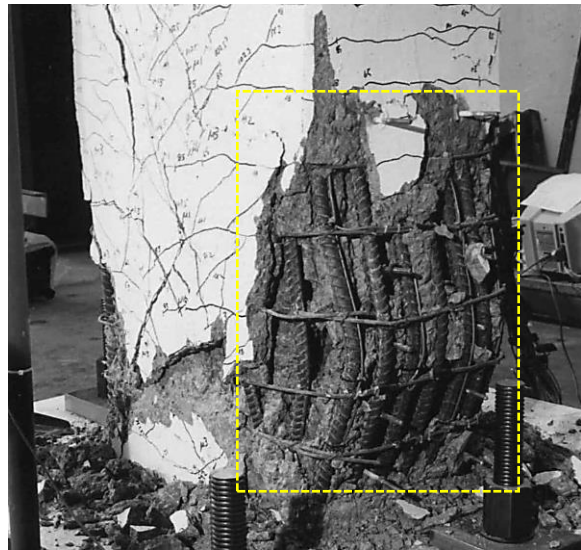
R-5 Column from Hose and Seible (1999)
Photo at Drift Ratio: 3.3%; Multiple Bar Buckling
Column Height = 144 in.
Side Dimension = 28.7 in. by 19.25 in.

Figure 3.6 – Samples of RC Bridge Column Conditions at DS6
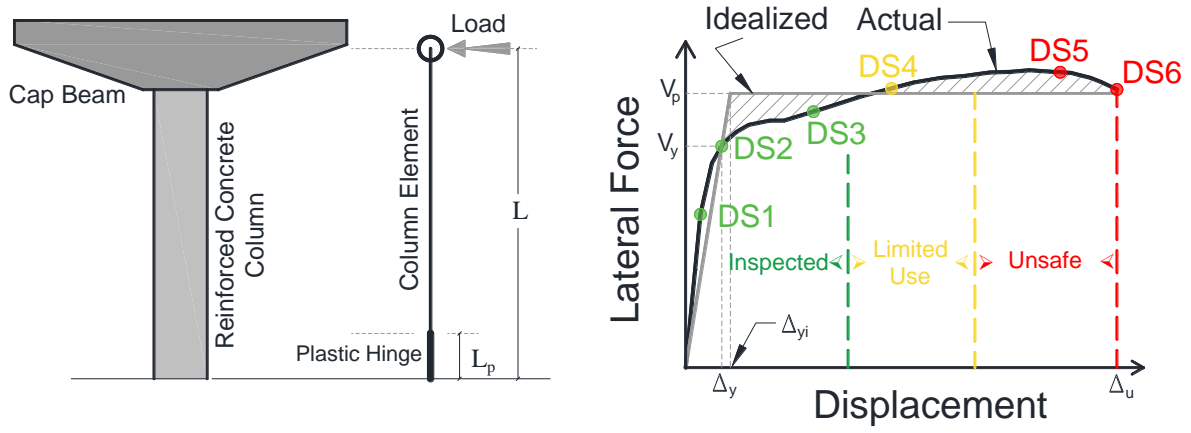
Figure 3.7 – Proposed Damage States Schematically Mapped on Pushover Curves

CHAPTER 4. MODERN RC BRIDGE COLUMN TEST DATABASE

4.1 Introduction

A few studies have developed experimental database for reinforced concrete (RC) columns. A review of the existing RC column databases was presented in **Sec. 2.4** of this report. This chapter discusses the new database that was developed in the present study.

4.2 Past RC Column Databases

Table 4.1 summarizes the key information of RC column test databases available in the literature. The most comprehensive works are those by Berry and Eberhard (2008) and Ghannoum et al. (2015), which include a mix of standard and substandard, and building and bridge columns. Furthermore, the most recent database by Zheng at el. (2020) does not include several of experimental data that has been published in the past few years. Overall, the literature is missing a comprehensive and unified test database specific to modern RC bridge columns, those that are detailed to resist seismic excitations.

Table 4.1 – Summary of Past Studies on RC Column Database

References	Type of Data Included	Remarks
Hose and Seible (1999)	A PDF document presenting experimental data and photographs of 12 RC bridge columns, three RC bridge sub-assemblies, and three RC column-bent systems. Column detailing, reinforcement, mechanical properties, and force-displacement hysteresis were included.	A mix of different shapes and reinforcement distribution, not in spreadsheet.
Berry and Eberhard (2008)	Two spreadsheets presenting experimental data for 160 circular columns and 247 rectangular columns. More than 20 parameters related to the column detailing, reinforcement, and mechanical properties were included. A digitized force-displacement hysteresis was included for all specimens.	A mix of standard and substandard columns, mix of building and bridge columns, displacements at different damage states was included, when data was available.
Veletzos et al. (2008)	A PDF document presenting the force-displacement hysteresis and photographs of more than 100 RC bridge columns.	A mix of standard and substandard columns, a mix of different shapes and reinforcement distribution, not in spreadsheet.
Rodriguez and Padilla (2009)	A spreadsheet presenting experimental data for 76 RC columns. A few parameters related to the column section and mechanical properties were included.	Several references were the same as those in Berry and Eberhard (2008).
Vosooghi and Saiidi (2010); updated by Saini and Saiidi, (2014)	A PDF document presenting experimental data of 38 RC bridge columns tested on shake table. A few column parameters and drifts at different damage states were included.	Not in spreadsheet.
Perus et al. (2013)	A spreadsheet presenting experimental data for 477 circular and rectangular columns. More than 45 parameters related to the column detailing, reinforcement, and mechanical properties were included. A digitized force-displacement hysteresis was included for all specimens.	The database was built upon the work by Berry and Eberhard (2008).
Ghannoum et al. (2015)	Two spreadsheets presenting experimental data for 172 circular columns and 326 rectangular columns. More than 50 parameters related to the column detailing, reinforcement, and mechanical properties were included. Key forces and displacements were included.	The database was built upon the work by Berry and Eberhard (2008), a mix of standard and substandard columns, mix of building and bridge columns.
Azadi-Kakavand et al. (2019)	Added the yield drift ratio and the displacement ductility to the database developed by Ghannoum et al. (2015).	Mainly the same as the database by Ghannoum et al. (2015).
Azadi-Kakavand and Allahvirdizadeh (2019)	A PDF document presenting experimental data of 196 RC columns. A few column parameters and drifts at two damage states were included.	Not in spreadsheet.
Zheng at el. (2020)	A spreadsheet presenting experimental data for 199 circular and rectangular columns. More than 50 parameters related to the column detailing, reinforcement, and mechanical properties were included. Drifts at different damage states were included.	Half of the columns were the same as those in Berry and Eberhard (2008).

4.3 New RC Bridge Column Database

As was discussed above, the current test databases include a mix of bridge and building, standard and substandard columns, and report parameters that might not be consistent with current bridge codes or are not require in a bridge design. To achieve the present project goals (**Sec. 1.2**), it is necessary to collect test data specific to standard RC bridge columns.

A new performance database has been developed in the present work that includes all the key geometrical, material, and force-displacement properties of RC bridge columns designed with modern codes (especially those following seismic detailing). All parameters were collected following the current AASHTO SGS definitions. Furthermore, displacements (drifts) at six different damage states as defined in **Sec. 3.3** were included when the data was available.

The new database is built upon the work by Ghannoum et al. (2015), which included test data published up to 2008. Nevertheless, all substandard and/or building columns were removed, the definitions were updated to be consistent with current AASHTO SGS (2011), and new parameters were added suited for seismic/bridge design. Furthermore, more than 100 new circular and 30 rectangular columns were added. The refined and updated RC bridge column database currently includes 222 circular and 68 rectangular columns. Two spreadsheets, one for circular and one for rectangular RC bridge columns, were developed each including more than 30 parameters per specimen. The database is publicly available (Hart et al., 2021; https://doi.org/10.17603/ds2-1p5e-1v55). Furthermore, **Appendix A** includes the damage photographs of the columns included in the database at different damage states.

4.4 Parameters Collected in RC Bridge Column Database

This section presents the parameters and definitions that were used in the new database. The left column below presents those terms that appeared in the database and the right column is the complete definition of each term.

Title:	The title of the study used in the database.
Author(s):	The author(s) of the study.
Year:	The publication year of the study. Note database was sorted by the publication year.
Column Name:	The specimen name/identification as presented in the original study.
Shape:	The column shape with non-circular section but with circular rebar distribution. Note this parameter is only for the circular database.
Column Diameter (D_c):	The circular column diameter (in.). Note this parameter is only for the circular column database.
Section Depth (h)	The rectangular column section depth parallel to loading (in.). Note this parameter is only for the column rectangular database.
Section Width (b)	The rectangular column section width perpendicular to loading (in.). Note this parameter is only for the rectangular column database.
Column Length (L):	The length of column from the point of maximum moment to the point of moment contraflexure (in.).
Clear Cover:	The clear distance between the column face and the transverse steel bar (in.).
No. of Bars:	The number of the column longitudinal reinforcing steel bars.
Bar Diameter (d_{bl}):	The nominal diameter of the column longitudinal reinforcing steel bars (in.).
Yield Stress of Longi. Reinf. (f_{yl}):	The yield stress of the column longitudinal reinforcing steel bars (psi).
Longi. Reinf. Ratio (ρ_l):	The ratio of the column longitudinal reinforcement area (A_{sl}) to the column cross-sectional area (A_g).
Trans. Reinf. Legs Perp. to Load:	The number of transverse reinforcements perpendicular to the loading. In circular database, "two" means one hoop.

Trans. Reinf. Legs Parallel to Load:	The number of transverse reinforcements parallel to the loading. In circular database, "two" means one hoop.
Trans. Bar Diameter (d_{bs}):	The nominal diameter of the column transverse reinforcing steel bars (in.).
Spacing of Trans. Reinf. (s):	The spacing of spiral, hoop, or tie reinforcement (in.).
Yield Stress of Trans. Reinf. (f_{yh}):	The yield stress of the column transverse reinforcing steel bars (psi).
Trans. Reinf. Volumetric Ratio (ρ_s):	The volumetric ratio of transverse reinforcement. For a circular column, $\rho_s = 4A_{sp}/sD'_c$ where A_{sp} is the area of spiral or hoop reinforcing bar (in.^{2}), s is the spacing of spiral or hoop (in.), and D'_c is the core diameter of column measured from center of spiral or hoop (in.). For a rectangular column, $\rho_s = A_v/sb'_c$ where A_v is the sum of area of the ties and cross ties running in the direction perpendicular to the axis of bending (in.^{2}), s is the spacing of ties (in.), and b'_c is the confined column cross-section dimension, measured out-to-out of ties, in the direction parallel to the axis of bending (in.).
Concrete Strength (f'_c):	The test-day concrete compressive strength (psi).
Axial Load (P_c):	The column axial force (kips).
Axial Load Ratio (ρ_{dl}):	The ratio of the column axial force (P_c) to the product of the concrete compressive strength (f'_c) and the column cross-sectional area (A_g); $\rho_{dl} = P_c / (f'_c . A_g)$.
Number of Loading Directions:	1 means uniaxial testing, 2 means biaxial testing.
Yield Force (V_y):	The lateral force corresponding to the first yielding of the column longitudinal bar(s) (kips).
Yield Drift Ratio (δ_y):	The drift ratio corresponding to the first yielding of the column longitudinal bar(s) (%). The drift ratio is the ratio of the column lateral displacement to the column length (L).
Maximum Lateral Force (V_{max})	The peak lateral load during the entire test (kips).
Drift Ratio at Maximum Lateral Force ($\delta_{F,max}$):	The drift ratio (%) corresponding to the peak lateral load (%).
Force at Failure ($0.85V_{max}$)	The lateral force (kips) at the column failure, which is defined at a point where the column force drops 15% compared with the peak lateral load (or $0.85V_{max}$).
Ultimate Drift Ratio (δ_u):	The drift ratio (%) corresponding to the column failure defined above.
Max Drift Ratio shown on Hysteresis/Backbone	The drift ratio (%) where the test was stopped.
DS1 Drift Ratio (δ_{DS1}):	The drift ratio (%) corresponding to Damage State 1 (as defined in **Table 3.2**).
DS2 Drift Ratio ($\delta_{DS2} = \delta_y$):	The drift ratio (%) corresponding to Damage State 2 (as defined in **Table 3.2**), which is equal to the drift ratio at the column yielding (δ_y).
DS3 Drift Ratio (δ_{DS3}):	The drift ratio (%) corresponding to Damage State 3 (as defined in **Table 3.2**).
DS4 Drift Ratio (δ_{DS4}):	The drift ratio (%) corresponding to Damage State 4 (as defined in **Table 3.2**).
DS5 Drift Ratio (δ_{DS5}):	The drift ratio (%) corresponding to Damage State 5 (as defined in **Table 3.2**).
DS6 Drift Ratio ($\delta_{DS6} = \delta_u$):	The drift ratio (%) corresponding to Damage State 6 (as defined in **Table 3.2**), which is equal to the drift ratio at the column failure (δ_u).
Idealized Yield Force (V_p)	The lateral force (kips) at the idealized yield point. Idealization follows the method discussed in **Section 8.5** of AASHTO SGS (2011).
Idealized Yield Drift (δ_{yi}):	The drift ratio (%) at the idealized yield point.

CHAPTER 5. RC BRIDGE COLUMN DISPLACEMENT ESTIMATION

5.1 Introduction

A detailed assessment of a bridge performance, especially its columns, under an earthquake, requires an accurate estimation of <u>capacity</u> and <u>demand</u>. In a force-based design, these two are presented with forces. However, modern design codes usually evaluate capacities and demands using displacements. In this chapter, the methods to estimate a bridge column displacement demand and capacity are presented. Drift ratio (δ), which is the ratio of the column lateral displacement (Δ) to the column length (L) as defined in AASHTO SGS (2011), is utilized in this chapter in lieu of displacement.

5.2 Displacement Demand Estimation

Based on the seismic design category (SDC A to D), the regularity of a bridge, and the number of bridge spans, AASHTO SGS (2011) allows three demand analysis methods: (1) equivalent static, (2), elastic dynamic analysis, and (3) nonlinear time history. Even though these procedures are usually used in the design step, they may be used after an earthquake to perform a Detailed Damage Assessment (DDA) of the bridge. Full description of each method and their requirements are presented in the AASHTO code. However, a short review is presented herein discussing how these methods may be incorporated in DDA tools after an earthquake for a quick assessment.

5.2.1 Displacement Demand Using Design Spectrum

For bridges in which the equivalent static analysis procedure is allowed by AASHTO SGS (2011), short-to medium-span bridges with a regular configuration, the AASHTO design spectrum specific to the affected site(s) can be used to quickly estimate the displacement demand of the columns. For example, if an earthquake happens in downtown Los Angeles, the design spectrum for this location (**Fig. 5.1**, the solid black curve) can be used to estimate the spectral (or design) acceleration (S_a) and/or the design displacement (S_d) of the bent using the bent natural (fundamental, or the first mode) period (T_m):

$$T_m = 2\pi \sqrt{\frac{W}{g.K}} \qquad \text{(Eq. 5.1)}$$

where, W is the seismic weight of the bent (kips), g is 386 in./s^2, and K is the effective lateral stiffness of the bent (kip/in).

$$S_d = \frac{S_a}{(\frac{2\pi}{T_m})^2} \qquad \text{(Eq. 5.2)}$$

Subsequently, the displacement demand of the event on the bent can be assumed to be the same as the spectral displacement. The advantage of this method is the simplicity and availability of design spectra for different locations of the U.S. Nevertheless, the actual earthquake might be stronger or weaker than the design spectrum.
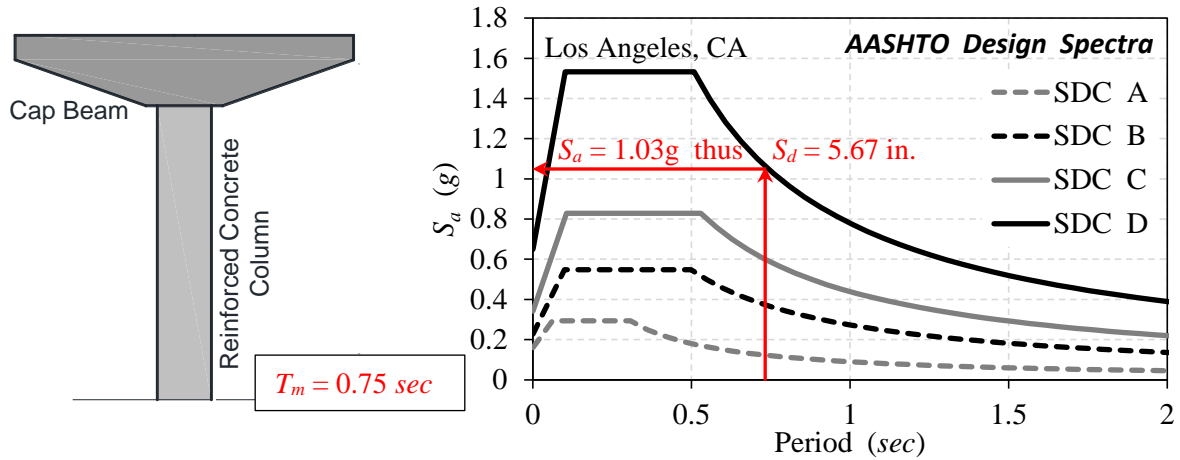
Figure 5.1 – Demand Estimation Using AASHTO Design Spectrum

5.2.2 Displacement Demand Using Event Spectrum

The U.S. has a dense array of seismometers, which record seismic events real-time or near-real-time. Several agencies and centers collect, process, and make the data publicly available shortly after an event. For example, USGS (https://earthquake.usgs.gov/) offers several tools mapping the latest or largest earthquakes and provides a detailed information. The Center for Engineering Strong Motion Data (CESMD, https://www.strongmotioncenter.org/) provides ground motion data. **Figure 5.2** shows a sample result obtained from this center for an earthquake happened on the same day of this writing. As soon as the ground motion data is available, the earthquake acceleration/displacement spectrum can be obtained (e.g., using the "Elastic Response Spectrum" tool by Tazarv, 2021) then the equivalent static analysis discussed in the previous section can be carried out using the event spectrum.
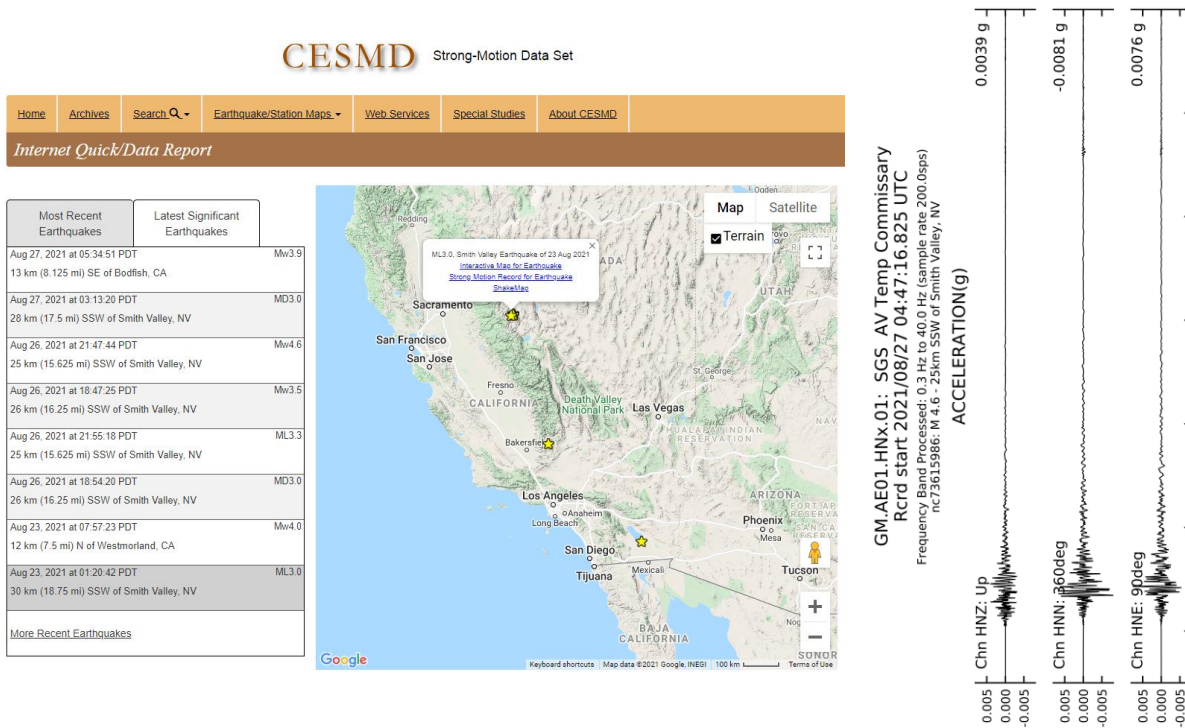
Figure 5.2 – Sample of Processed Ground Motion in Near-Real-Time by CESMD

61

5.2.3 Displacement Demand Using Event Ground Motion

As was discussed in the previous section, processed ground motions are available shortly after earthquakes in the U.S. through different agencies (such as CESMD). It is feasible to develop a software (e.g., cloud-based for a quick access and analysis) that utilizes the actual ground motions as the input for a linear or nonlinear dynamic analysis of the affected bridges/bents. Open-source structural software such as OpenSees (2016) can be used for this analysis. **Figure 5.3** illustrates the architecture of such cloud-based tool. Generic bent models can be pre-defined with the key modeling parameters to be provided by the user (e.g., the number of columns per bent, the column length, the column shape and size, reinforcement, concrete strength, etc.). The national bridge inventory (NBI) might also be accessed to populate some of the bent information. Overall, a dynamic analysis can be performed using the event ground motion to obtain the bent displacement demands.
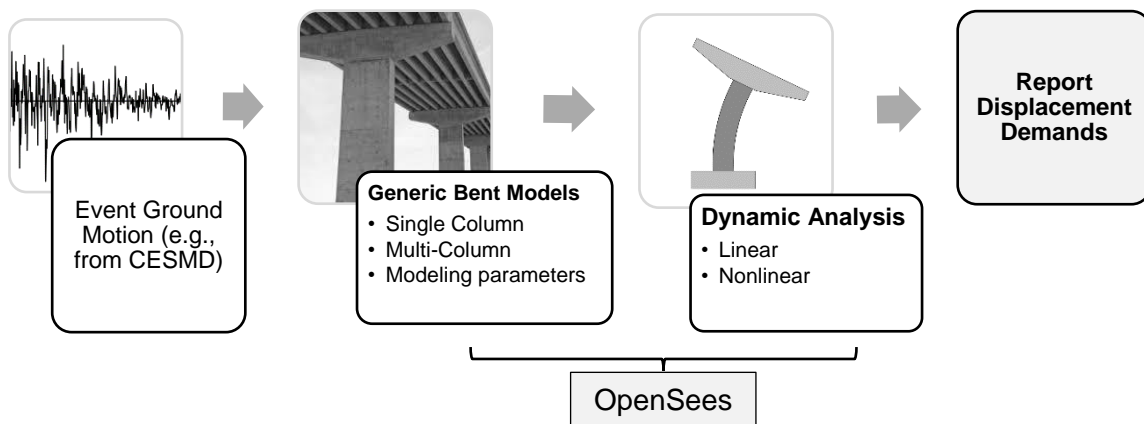
Figure 5.3 – Proposed Architecture for Cloud-Based Bridge Bent Dynamic Analysis

5.2.4 Displacement Demand Estimation Using Post-Earthquake Conditions

RC bridge columns may damage under large earthquakes. Post-earthquake conditions of a bridge column may be utilized to estimate the peak displacement demand during the shaking. In this section, methods to estimate bridge column displacement demands using post-event conditions are discussed.

5.2.4.1 Damage Based Seismic Demand Estimation

Past studies on how to relate observed damage of an RC column to its displacement, plastic rotation, plastic curvature, and/or strain demands were reviewed in **Sec. 2.3** of this report. **Table 5.1** summarizes the findings of the past studies. Note that the notations in these studies were unified herein following the AASHTO SGS definitions and some equations were expanded/simplified for the ease of use. A fiber-section analysis (e.g., moment-curvature, or pushover) should be performed to obtain the local response of a bridge column such as strains, plastic curvatures, or plastic rotations then the demand can be estimated based on the limits presented in **Table 5.1**. For example, if the observed damage of a bridge column after an earthquake is the buckling of its longitudinal bars, one may estimate the strain demands at this damage using the equation proposed by Berry and Eberhard (2008) or Murphy et al. (2020). The displacement corresponding to this strain demand is the displacement demand of the column caused by the earthquake. Overall, such analysis is feasible. Nevertheless, the proposed drift-damage equation by Berry and Eberhard (2008) is more convenient since it does not require additional structural analysis and the column drift demand can directly be estimated at different damage levels.

Table 5.1 – Summary of Past Studies to Relate RC Column Observed Damage to Seismic Demands

Damage	Drift Ratio, δ (%)	Plastic Rotation, θ_p (%)	Plastic Curvature, $\emptyset_p$ (rad/in)	Strain (in/in)	Reference
Cover Spalling (DS3)	$1.6(1-\frac{P_c}{A_g f_c'})(1+\frac{L}{10.D_c})$	1.20	N.A.	0.008; compressive strain of the cover concrete	Berry and Eberhard (2008)
	N.A.	N.A.	$\frac{0.005}{c}-\emptyset_y$	N.A.	Marsh et al. (2014)
Core Crushing (DS4 to DS5)	N.A.	N.A.	$\frac{0.005+1.4\frac{\rho_s f_{yh}\varepsilon_{suh}}{f_{cc}'}}{c-d''}-\emptyset_y$	N.A.	Marsh et al. (2014)
	N.A.	N.A.	N.A.	$1.4(0.004+1.4\frac{\rho_s f_{yh}\varepsilon_{su}}{f_{cc}'})$ compressive strain of the core concrete	Murphy et al. (2020)
Long. Bar Buckling (DS5)	$3.25(1+\frac{150\rho_s f_{yh}d_{bl}}{D_c f_c'})(1-\frac{P}{A_g f_c'})(1+\frac{L}{10.D_c})$	0.846δ	N.A.	$0.045+0.25\frac{\rho_s f_{yh}}{f_c'}\le0.15$ tensile strain of long. steel bar	Berry and Eberhard (2008)
	N.A.	N.A.	$\frac{2f_y/E_s}{c-d'}-\emptyset_y$	N.A.	Marsh et al. (2014)
	N.A.	N.A.	N.A.	$0.032+790\frac{\rho_s f_{yh}}{E_s}-0.14\frac{P_c}{A_g f_c'}$ tensile strain of long. steel bar	Murphy et al. (2020)
Long. Bar Fracture (DS6)	$3.5(1+\frac{150\rho_s f_{yh}d_{bl}}{D_c f_c'})(1-\frac{P_c}{A_g f_c'})(1+\frac{L}{10.D_c})$	0.857δ	N.A.	$0.045+0.30\frac{\rho_s f_{yh}}{f_c'}\le0.15$ tensile strain of long. steel bar	Berry and Eberhard (2008)
	N.A.	N.A.	$\frac{\varepsilon_{sul}}{d-c}-\emptyset_y$	N.A.	Marsh et al. (2014)

Note: A_g is the column cross-sectional area; c is the depth from the extreme compression fiber of the cover concrete to the neutral axis; D_c is the column diameter (in.); d is the depth to the outer layer of tension steel from the extreme compression fiber; d' is the distance from the extreme compression fiber to the center of the nearest compression reinforcing bars, d'' is the distance from the extreme compression fiber of the cover concrete to the centerline of the perimeter hoop (thus, $c - d''$ is the depth of confined concrete under compression); d_{bl} is the nominal diameter of the column longitudinal reinforcing steel bars (in.); E_s is the steel bar modulus of elasticity (29000 ksi); f_{yh} is the yield stress of the column transverse reinforcing steel bars (ksi); f_c' is the concrete compressive strength (ksi); P_c is the column axial force (kips); L is the length of column from the point of maximum moment to the point of moment contraflexure (in.); ε_{su} is the bar ultimate strain (ε_{suh} is for the transverse bar in "Core Crushing", ε_{sul} is for the longitudinal bar in "Long. Bar Fracture"), $\emptyset_y$ is the yield curvature (rad/in); ρ_s is the volumetric ratio of transverse reinforcement.

Note: For each type of damage, an equivalent damage state per the proposed definition (**Table 3.2**) was included for comparison. However, the past studies used different definitions or measures for damage states.

(a) Drifts at Cover Spalling (≈ Damage State 3)

(b) Drifts at Bar Buckling (≈ Damage State 5) for Circular Columns

(c) Drifts at Bar Fracture (≈ Damage State 6) for Circular Columns
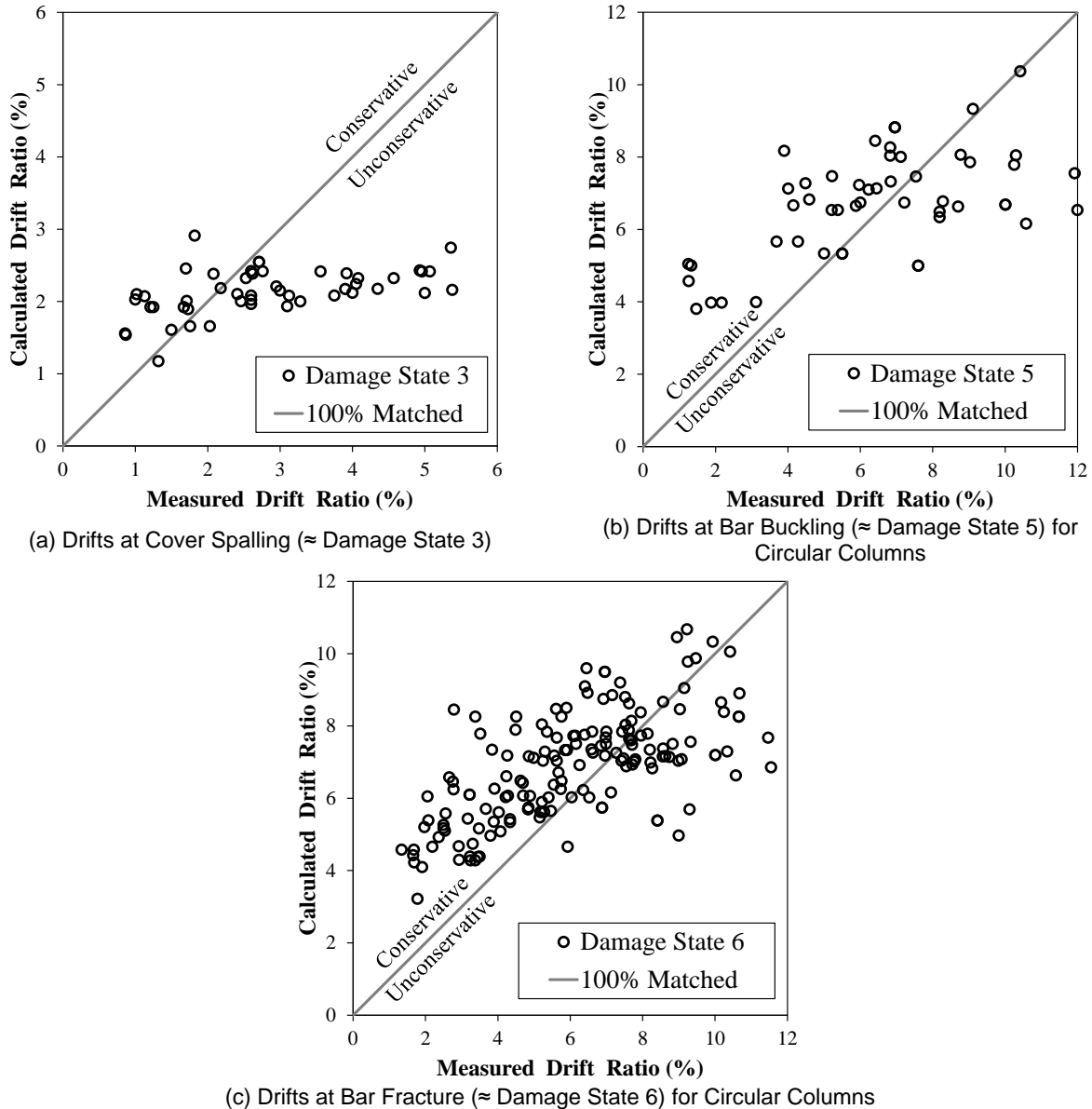
Figure 5.4 – Evaluation of Drift-Damage Relationship Proposed by Berry and Eberhard (2008)

For each type of damage listed in **Table 5.1**, an equivalent damage state per the proposed definition (**Table 3.2**) was included for comparison. Nevertheless, note that the past studies have used different definitions or measures for damage states thus they are not fully compatible.

A comprehensive database of bridge column experimental performance was collected in this project and was discussed in Chapter 4. In an attempt to validate the drift-damage relationship proposed by Berry and Eberhard (2008), the calculated drift ratio (%) at "Cover Spalling" (approximately equivalent to Damage State 3 of the present study) was compared with the measured (or observed) drift ratio (**Fig. 5.4a**). It can be seen that the proposed equation by Berry and Eberhard (2008) estimates the cover spalling drift ratio with a reasonable accuracy up to 3% drift. In other words, this equation saturates at 3% drift meaning that any RC column will lose its cover at 3% drift ratio or smaller. However, the cover of RC columns in some of the past experiments spalled at larger drifts. A similar validation was carried out at the damage levels of "Longitudinal Bar Buckling", approximately equivalent to Damage State 5, and "Longitudinal

Bar Fracture", which is close to Damage State 6. Note that Damage State 5 refers to the first bar buckling or rupture. However, the fracture of a single bar may not cause column failure. **Figures 5.4b** & **5.4c** show the observed versus estimated drift ratio for Damage State 5 and Damage State 6, respectively. It can be seen that the estimated drifts at the bar buckling generally follow the measured data, and the drift-damage equation at the bar fracture mostly reproduces a conservative drift ratio compared with the measured (observed) drift. Overall, the drift-damage equations proposed by Berry and Eberhard (2008) were found simple, and reasonably accurate to estimate RC bridge column displacement demands at cover spalling, bar buckling, and bar fracture using only a few parameters.

5.2.4.2 Peak Displacement Demand versus Residual Displacement

Under large earthquakes, RC bridge columns may not fully return to their initial (usually plumbed) position. This permanent lateral displacement is commonly referred to as "residual displacement". Residual drift ratio is defined as the ratio of the column residual displacement to the column height. Several parameters affect why an RC column may exhibit residual displacements, some key factors are the level of yielding (larger the post-yield displacement, larger the residual displacement), pulse-like motions, and column detailing. Overall, the estimation of residual displacements is difficult and needs nonlinear finite element analysis using special materials, elements, or procedures (Lee and Billington, 2010; Tazarv and Saiidi, 2013; Ardakani and Saiidi, 2018). Following the ATC 58 formulation for residual drifts specific to buildings, Ardakani and Saiidi (2018) proposed a simple equation to estimate the residual displacements of RC bridge columns as:

$$\beta = 0.04\mu^2 + 0.14\mu \qquad \text{(Eq. 5.3)}$$

where, β is the ratio of the residual displacement to the yield displacement, and μ is the displacement ductility (the ratio of the peak displacement to the yield displacement).

In the present project, **Eq. 5.3** was rewritten based on drifts in lieu of displacements, was rearranged, and was solved to obtain the peak drift ratio demand (δ_D) when the yield drift ratio (δ_y) and the residual drift ratio (δ_r) of an RC column are known:

$$\delta_D = \delta_y \left[-1.75 + \left(3.0 + 25\frac{\delta_r}{\delta_y} \right)^{0.5} \right] \qquad \text{(Eq. 5.4)}$$

After an earthquake, the residual displacement of RC bridge columns can be measured using surveying tools or mobile applications then **Eq. 5.4** can be used to estimate the peak drift demand of the column that happened during the earthquake. **Figure 5.5** shows the peak drift demands of three RC bridge columns (two from Ardakani's study, and one from a full-scale testing at UC San Diego shake table, Schoettler et al., 2015). Ardakani and Saiidi (2018) reported an R^2 (the coefficient of determination) of 0.82 when comparing the results of **Eq. 5.3** with the experimental data for six RC bridge columns tested on a shake table. Thus, **Eq. 5.4** has the same level of accuracy. Note that the yield drift ratio of the column should be known when using **Eq. 5.3** or **5.4**. In lieu of a detailed analysis, the yield drift ratio (%) of an RC bridge column may be estimated using the equation proposed by Priestley et al. (1996):

$$\delta_y = \frac{1}{3}\emptyset_y L^2 . \frac{100}{L} \cong \frac{100}{3}\left[\lambda \frac{\varepsilon_{yl}}{D_c} \right] L \qquad \text{(Eq. 5.5)}$$

where, λ is 2.45 for circular (transversely reinforced with spirals or hoops) RC columns and 2.14 for rectangular RC columns. For example, the estimated yield drift ratio using **Eq. 5.5** for the USCD full-scale column is 1.43% (100/3×2.45×(75.2ksi/29000ksi)×8.23m/1.219m), which is 16% higher than the measured yield drift ratio of 1.23%.
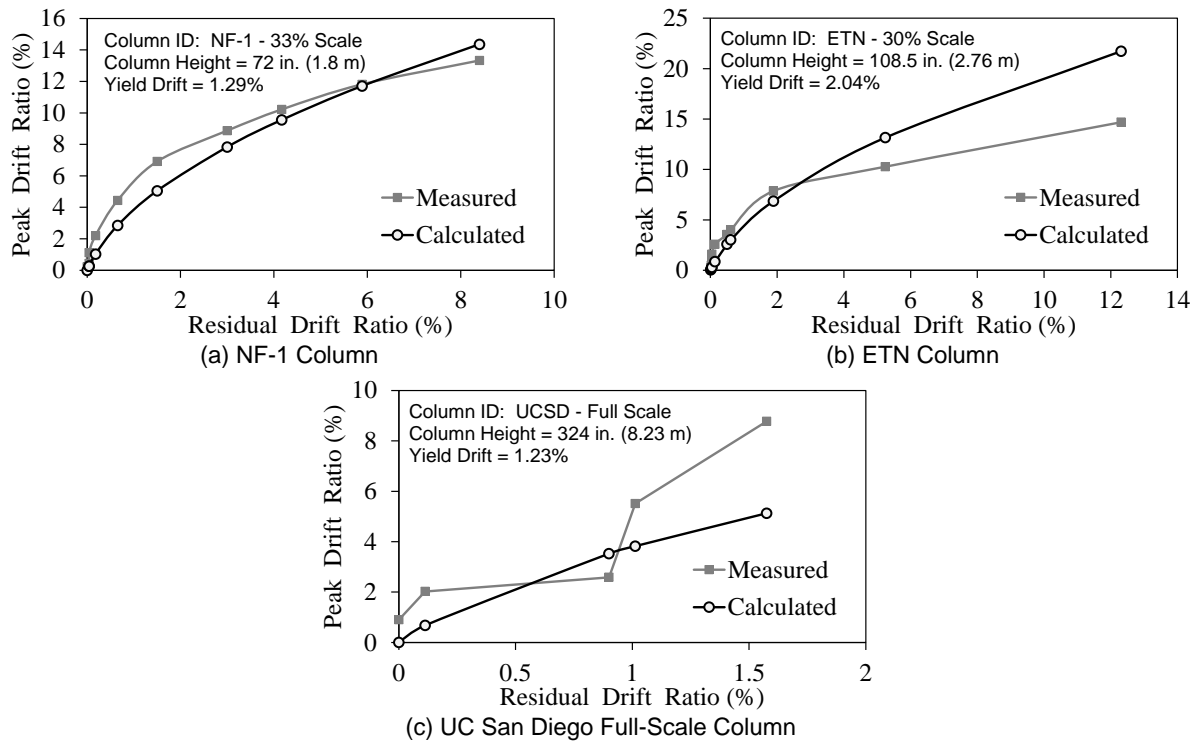
Figure 5.5 – Evaluation of Peak-Residual Drift Relationship Proposed by Ardakani and Saiidi (2018)

5.2.4.3 Proposed Damage State Based Drift Demand Estimation

As was discussed, the most comprehensive RC bridge column experimental database was collected in this study and a summary was presented in Chapter 4. Furthermore, Chapter 3 offered a new damage state definition for RC bridge columns suited for computer vision. The bridge column database was statistically analyzed to establish a relationship between the observed drifts and the corresponding damage states. This section presents the methodology and background that was used to derive empirical equations. Of six damage states (**Table 3.2**) data was richer for Damage State 6 (or DS6, which is the column failure based on the 15% drop in the baseshear) and Damage State 2 (or DS2, which is close to the yield point). The analysis is first presented for DS6 then DS5 to DS1.

5.2.4.3.1 Drift Demands at Damage State 6 (DS6)

Based on test data for 20 RC bridge columns, Berry and Eberhard (2008) developed an empirical equation to estimate the column drift ratio at the bar fracture (**Table 5.1**). One may assume that bar fracture is close to the failure point of a column thus this equation may be used to estimate drifts at DS6. **Figure 5.4c** shows the measured and calculated drift ratios (based on the equation by Berry and Eberhard, 2008) at DS6 but using the new dataset collected in the present project. Note that the new database includes 173 RC circular and 45 rectangular columns, those in which the data was available at DS6. For circular columns, the average error between the calculated (using the Berry's equation) and measured drifts at DS6 was +21.6% with a standard deviation of 49.9% and an R^2 (the coefficient of determination) of 0.47. R^2 has a range of 0.0 to 1.0, and an R^2 of unity means that the calculated drifts match perfectly with the measured drifts. This equation is relatively simple and generally follows the trend. The positive error indicates that the equation is mostly conservative by producing larger drifts at the bar fracture compared with the measured drifts. In other words, it is conservative since the estimated drift demands at this damage are larger than the drifts experienced by the column in the testing thus safer. In an attempt to reduce the error and to further simplify the equation by Berry and Eberhard (2008), new empirical

equations were developed for circular (**Eq. 5.6**) and rectangular (**Eq. 5.7**) columns. Note that circular refers to columns transversely reinforced with hoops or spirals, and rectangular refers to columns with ties. Also note that four parameters appeared in the first parentheses of the Berry's equation were removed for further simplification.

$$\delta_{DS6} = 1.3(1 + 150\rho_s)\left(1 - \frac{P_c}{A_g f_c'}\right)\left(1 + 0.3\frac{L}{D_c}\right)$$

<div align="right">(Eq. 5.6)
circular</div>

$$\delta_{DS6} = 2.2(1 + 25\rho_s)\left(1 - \frac{P_c}{A_g f_c'}\right)\left(1 + 0.3\frac{L}{h_c}\right)$$

<div align="right">(Eq. 5.7)
rectangular</div>

where, δ_{DS6} is the drift ratio (%) at DS6, ρ_s is the volumetric ratio of transverse reinforcement according to AASHTO SGS, P_c is the column axial force (kips or kN), A_g is the column cross-sectional area (in^2 or mm^2), f_c' is the concrete compressive strength (ksi or MPa), L is the length of column from the point of maximum moment to the point of moment contraflexure (in. or mm), D_c is the column diameter (in. or mm), and h_c is the column side dimension in the testing (analysis) direction (in. or mm).

Figure 5.6 compares the measured and calculated drift ratios at DS6 using the proposed equations. Drifts estimated using the equations by Berry and Eberhard (2008) were also included for completeness. The proposed equations resulted in a better match with the measured data. For example, the average error between the calculated and measured drifts at DS6 was reduced from +21.6% (in the Berry's equation) to +0.67% for the circular columns. Furthermore, the standard deviation of the error for the circular columns was reduced from 49.9% to 29.6%, and R^2 was increased from 0.47 to 0.56. Even though the database was carefully collected, scatter in the data is inevitable due to the nature of testing including methods and materials. Ony may develop a more complex empirical equation, which might have a better accuracy. Nevertheless, the proposed DS6 drift equations using only a few column parameters are relatively simple and predicts the column drift demands with a reasonable accuracy.

(a) Circular Columns   (b) Rectangular Columns
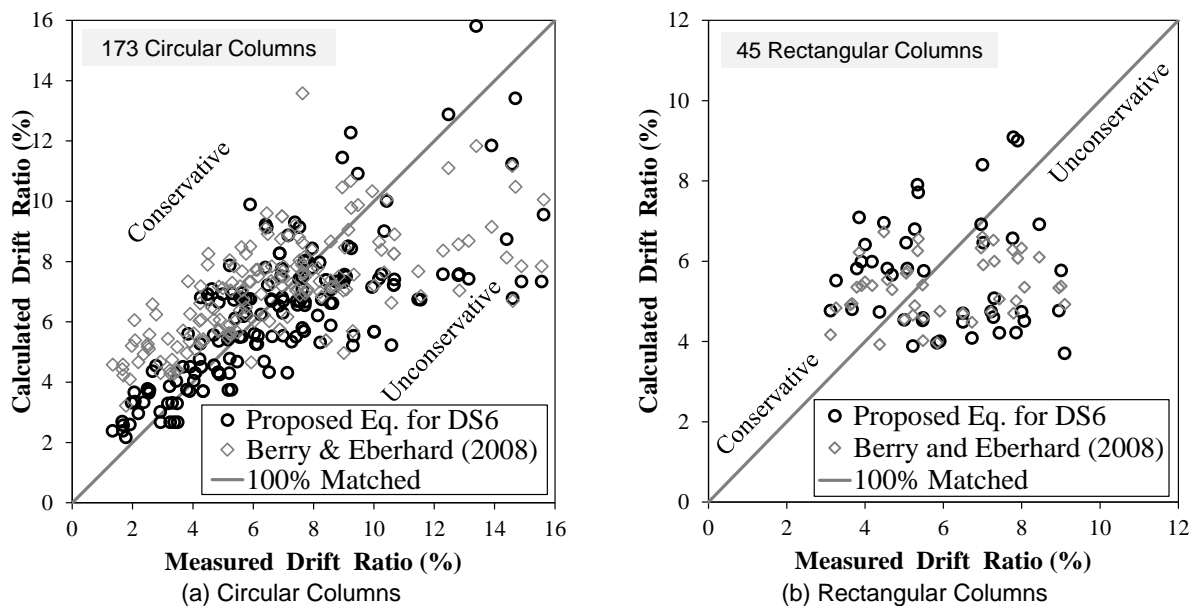
Figure 5.6 – Evaluation of Proposed Drift Equation at Damage State 6
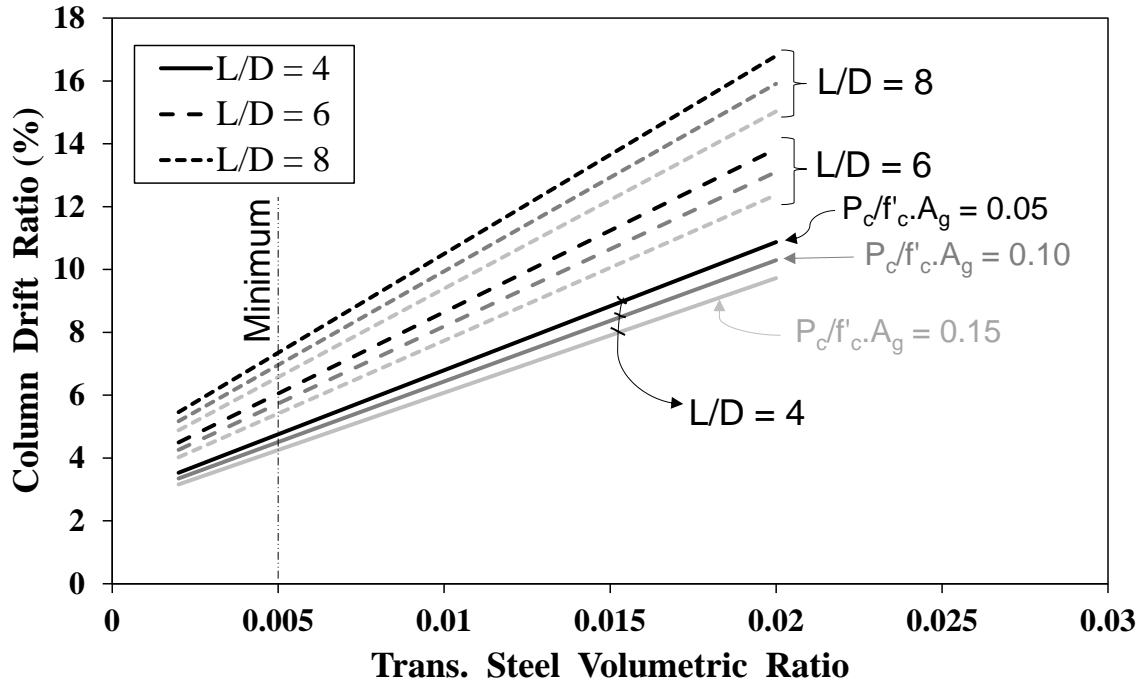
Figure 5.7 – Drift Ratios at Damage State 6 for Wide Range of RC Circular Bridge Columns

Figure 5.7 shows the estimated DS6 drift ratios (using **Eq. 5.6**) for a wide range of RC bridge columns, which may be used for a quick post-event assessment.

5.2.4.3.2 Drift Demands at Damage State 5 (DS5)

Since new definitions for damage states are used in this study, new equations should be developed to estimate RC bridge column drift ratios at these damage states. At DS5, data was available for 38 circular and 5 rectangular columns. It was found that the drift at DS5 is on average 20% less than that of DS6. Based on this observation, **Eq. 5.8** was proposed to estimate the DS5 drift ratios (δ_{DS5}) for both circular and rectangular columns.

$$\delta_{DS5} = 0.8\delta_{DS6} \qquad \qquad \text{(Eq. 5.8)}$$

Figure 5.8 shows a comparison of the measured and calculated drifts at this damage state. The average error was +3.6% and -9.7% for the circular and rectangular columns, respectively. An R^2 exceeding 0.96 was observed for both column datasets. Overall, the proposed equation is very simple, accurate, and includes the column properties based on the assumptions of DS6 equations.

(a) Circular Columns (b) Rectangular Columns
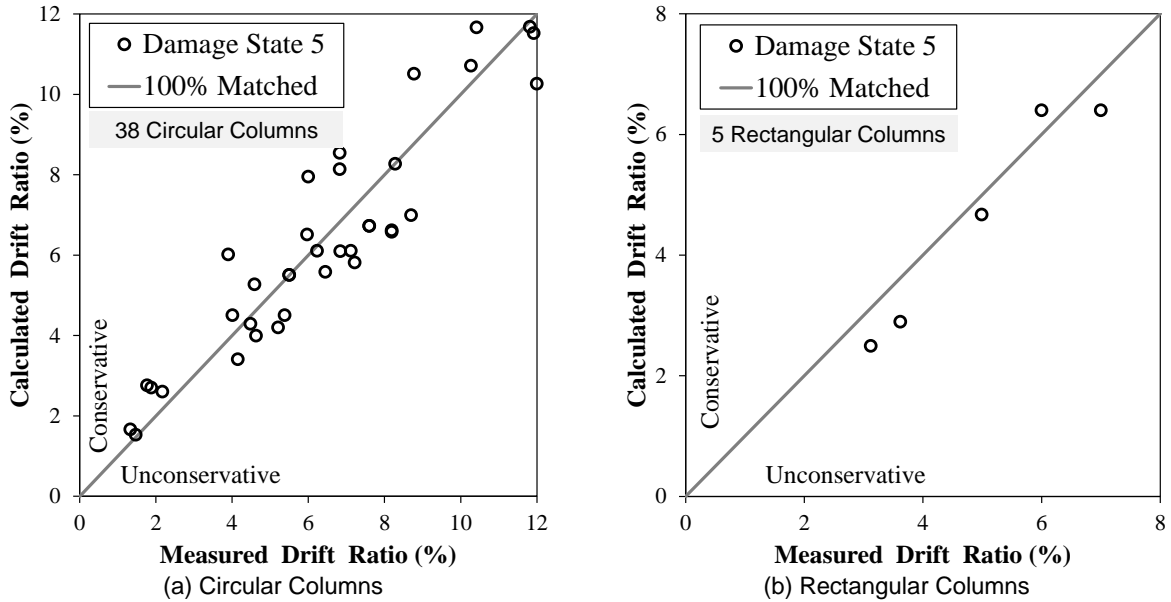
Figure 5.8 – Evaluation of Proposed Drift Equation at Damage State 5

5.2.4.3.3 Drift Demands at Damage State 4 (DS4)

For DS4, a similar analysis that was carried out for DS5 was repeated. It was found that drifts at DS4 are on average 48% smaller than DS6 drifts. **Equation 5.9** was developed based on this trend, which can be used for both circular and rectangular RC bridge columns. This equation has an average error of -0.33% for the circular columns and +3.9% for the rectangular columns. R^2 was more than 0.93 for both column datasets.

$$\delta_{DS4} = 0.5\delta_{DS6} \qquad\qquad \text{(Eq. 5.9)}$$

(a) Circular Columns (b) Rectangular Columns
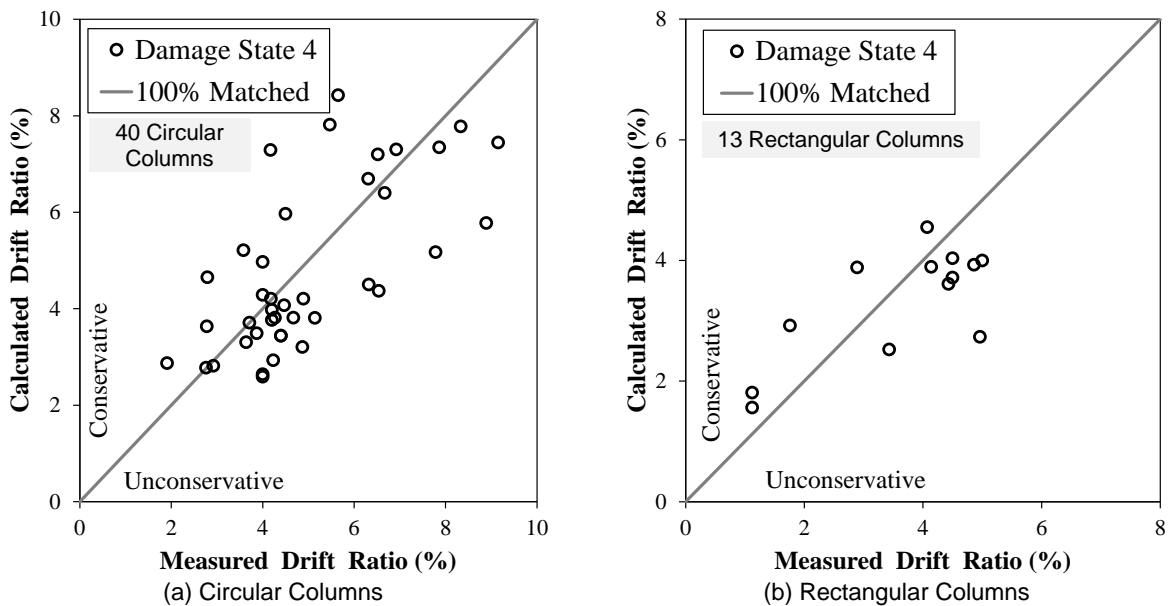
Figure 5.9 – Evaluation of Proposed Drift Equation at Damage State 4

69

5.2.4.3.4 Drift Demands at Damage State 3 (DS3)

Since Damage State 3 is representing drifts exceeding the yield point, DS3 drifts were also related linearly to DS6 drifts, similar to what was done for DS4 or DS5. On average, the DS3 drifts were 67% lower than DS6 drifts. **Equation 5.10** was developed based on this observation.

$$\delta_{DS3} = 0.3\delta_{DS6} \qquad \text{(Eq. 5.10)}$$

Figure 5.10 shows the measured and calculated DS3 drifts for circular and rectangular columns. The average error between the calculated and measured drifts was -5.5% and -31.9% for circular and rectangular columns, respectively. A larger error was observed for the rectangular columns since the analysis was performed on the circular dataset then the finding was expanded to the rectangular columns. The best fit for the rectangular columns resulted in a reduction factor of 0.45 (instead of 0.3 in **Eq. 5.10**). Nevertheless, **Eq. 5.10** is recommended for both column sections for simplicity.

(a) Circular Columns
(b) Rectangular Columns
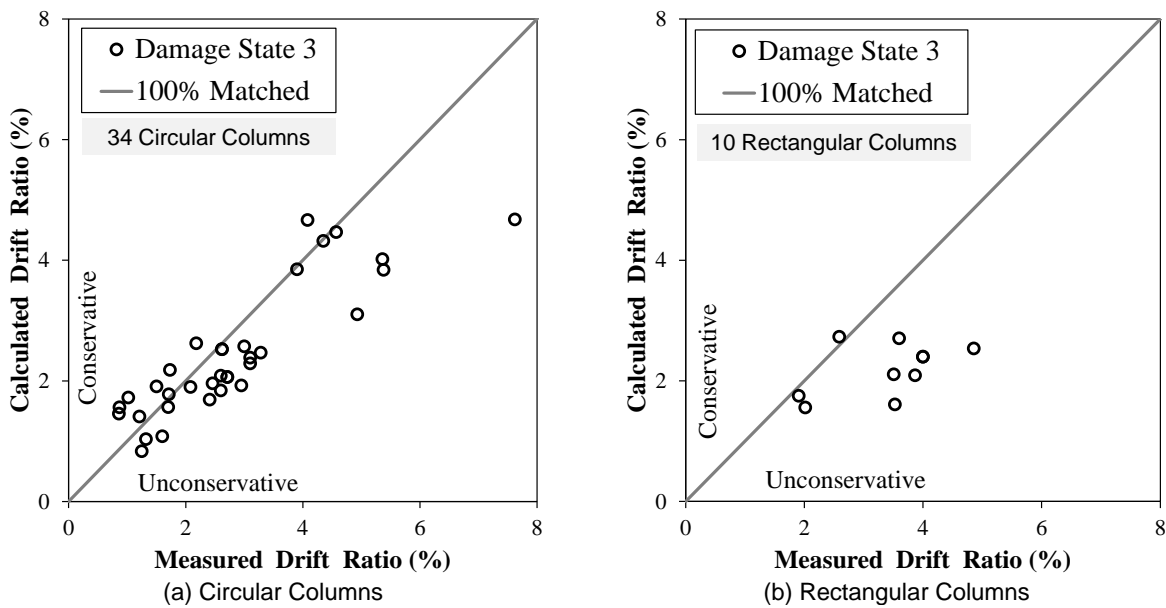
Figure 5.10 – Evaluation of Proposed Drift Equation at Damage State 3

5.2.4.3.5 Drift Demands at Damage State 2 (DS2)

DS2 was introduced mainly to capture the yield point of RC bridge columns through visual inspection. Column photographs at yielding were not available for all columns; however, the yield point was reported in several studies. Therefore, the yield point data was used to derive an equation for drifts at DS2. Priestley et al. (1996) proposed an equation to approximate the yield displacement of RC bridge columns, which was revised for drifts in the present study (**Eq. 5.5**). It is feasible to further simplify this equation for RC bridge columns assuming that the strain of longitudinal bars, ε_{yl}, is 0.00234 (= 68 ksi / 29000 ksi) according to the AASHTO SGS properties for reinforcing steel bars (ASTM A615 or ASTM A706). Furthermore, this equation can be recalibrated using the measured yield drifts of the columns in the new database. A statistical analysis of 167 circular and 56 rectangular RC bridge columns resulted in:

$$\delta_{DS2} = \delta_y \cong \frac{100}{3}\left[\lambda\frac{\varepsilon_{yl}}{D_c}\right]L = \frac{\lambda L}{12.8 D_c} \qquad \text{(Eq. 5.11)}$$

70

where, λ is 2.85 for circular and 2.50 for rectangular RC bridge columns. The simplified equation showed an average error of +1.4% and +0.58% for the circular and rectangular columns. An R^2 of 0.90 and 0.88 was also observed for the two column sections, respectively. Further, the accuracy of **Eq. 5.11** was better than that by Priestley et al. (1996) as shown in **Fig. 5.11** (e.g., the average error was improved from -14.2% to +1.4% for the circular columns, and from -15.2% to +0.58% for the rectangular columns). Overall, the proposed DS2 drift equation is relatively simple and reasonably accurate.
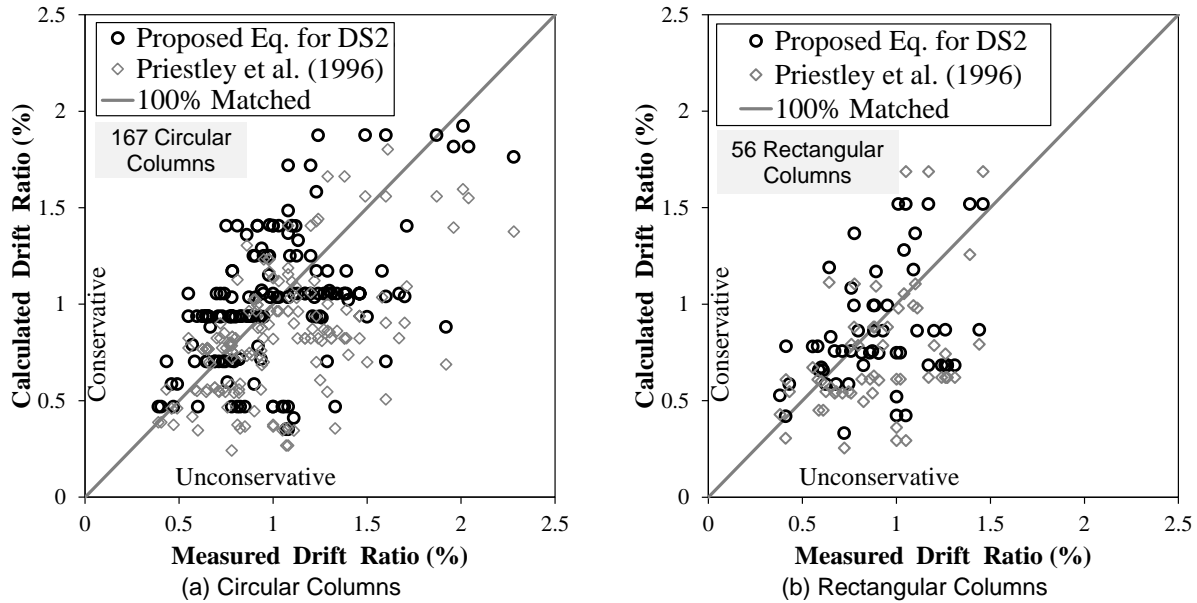
Figure 5.11 – Evaluation of Proposed Drift Equation at Damage State 2

It was important to make sure that the drifts at DS2 does not analytically exceed the DS3 drifts using the proposed equations. Both the circular and rectangular column databases were examined. Only two circular columns out of 223 columns (167 circular and 56 rectangular) had a δ_{DS2} that was larger than δ_{DS3} (no more than 20%). Both columns had excessively large axial load ratios and high aspect rations. For a practical range of RC bridge columns (e.g., axial load ratio of 15% or less), $\delta_{DS3} > \delta_{DS2}$ is met.

5.2.4.3.6 Drift Demands at Damage State 1 (DS1)

DS1 represents the RC bridge column behavior in the linear-elastic range. Therefore, a statistical analysis was performed to determine a relationship between the drifts at DS1 and DS2 (which is the yield drift). It was found that the DS1 drift is on average 61% of the DS2 drift, thus:

$$\delta_{DS1} = 0.6\delta_{DS2}$$

(Eq. 5.12)

Figure 5.12 shows the measured and calculated DS1 drifts for 15 circular and 6 rectangular RC bridge columns. The average error between the calculated and the measured drifts was +9% and +70.5% for the circular and rectangular columns. Note that the six datapoints available for the rectangular columns were not statistically sufficient to fully evaluate the proposed equation. Furthermore, since DS1 indicates small demands in the linear-elastic range, the large error for rectangular columns will not result in an unconservative post-earthquake assessment. DS2 through DS3 are other checkpoints for the "inspected" rating (**Table 3.2**). Overall, the proposed DS1 drift equation is simple and accurate at least for the circular columns. More data is needed for the rectangular columns to further validate/revise this equation.
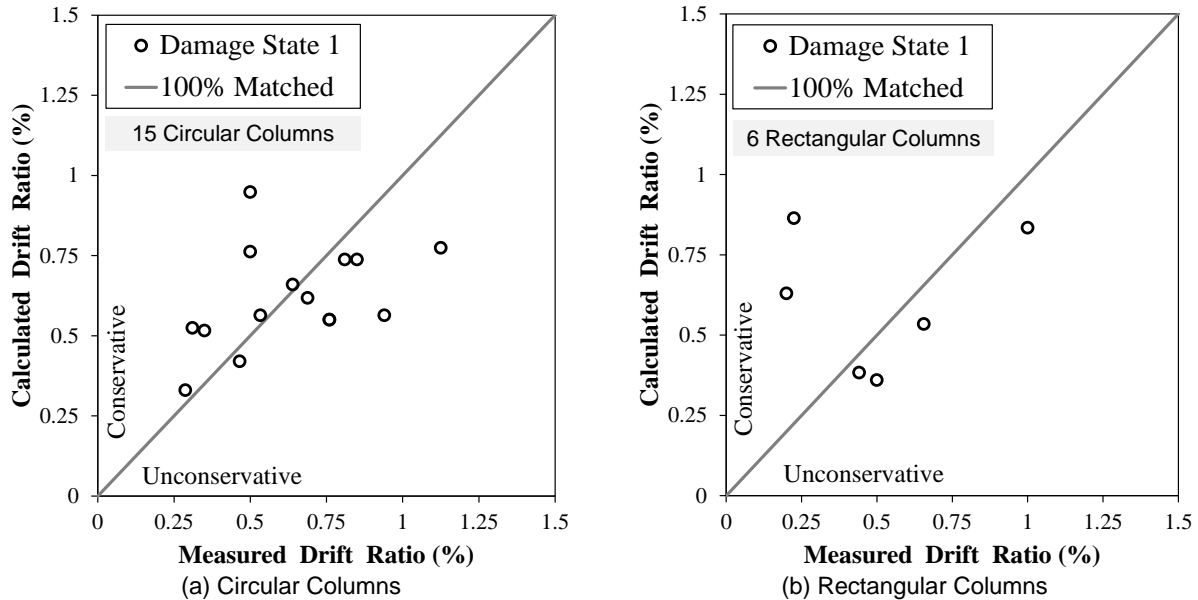
Figure 5.12 – Evaluation of Proposed Drift Equation at Damage State 1

5.2.5 Summary of Proposed Damage State Based Drift Equations

The new RC bridge column database collected in the present study was statistically analyzed to derive empirical equations to estimate column drift ratios at different damage states. **Table 5.2** presents a summary of the proposed equations and **Table 5.3** includes a summary of the statistical analyses. **Figure 5.13** schematically maps the drifts corresponding to these six damage states on an idealized pushover curve. Some of the statistical results were also included in the figure for completeness. It can be inferred that the proposed damage states cover the full range of the pushover curve all way from the linear-elastic region to the failure point.

The first two damage states are within the column linear-elastic range. A review of the RC bridge column database showed that the drifts at DS2 are on average 15% of DS6 drifts, and the DS1 drifts are only 9% of the DS6 drifts. Note, the proposed drifts for DS2 and DS1 are independent of DS6 drifts (**Table 5.2**). Those ratios presented above based on the DS6 drifts are provided only for comparison and should not be used for post-earthquake assessments. Furthermore, the drifts associated with the first three damage states (DS1 to DS3) are no more than 30% of the column failure drift thus one may assume this range (DS1 to DS3) as a safe domain for post-earthquake assessment. In other words, if the damage of an RC bridge column after an earthquake falls within DS1 through DS3, the column has approximately 70% reserved displacement capacity thus may be assumed safe for post-earthquake serviceability and can be tagged "green" to be open to all traffics.

DS4 has 50% reserved displacement capacity and can be tagged "yellow" to be open only to light traffics and first responders. Nevertheless, DS5 and DS6 have marginal to no safety thus the bridge must be tagged "red" and must be closed to all traffics. It is understood that the proposed serviceability limits are subjective. However, they are conservative and provide sufficient safety margin at the assigned rating levels. Note that the color coding of **Table 3.2** matches well with the drift limits discussed herein. This will allow performing post-earthquake assessments of RC bridge columns at different levels of PDA and DDA, which will be discussed later in Chapter 7.

Table 5.2 – Summary of Proposed Damage State Based Drift Equations

Damage State	Proposed Equation
DS1	$\delta_{DS1} = 0.6\delta_{DS2}$
DS2	$\delta_{DS2} = \delta_y = L/4.5D_c$ for circular sections $\delta_{DS2} = \delta_y = L/5.12h_c$ for rectangular sections
DS3	$\delta_{DS3} = 0.3\delta_{DS6}$
DS4	$\delta_{DS4} = 0.5\delta_{DS6}$
DS5	$\delta_{DS5} = 0.8\delta_{DS6}$
DS6	$\delta_{DS6} = 1.3(1 + 150\rho_s)\left(1 - \frac{P_c}{A_g f_c'}\right)\left(1 + 0.3\frac{L}{D_c}\right)$ for circular sections $\delta_{DS6} = 2.2(1 + 25\rho_s)\left(1 - \frac{P_c}{A_g f_c'}\right)\left(1 + 0.3\frac{L}{h_c}\right)$ for rectangular sections

Notes: All drift ratios are in percentage (%), ρ_s is the volumetric ratio of transverse reinforcement according to AASHTO SGS [For a circular column, $\rho_s = 4A_{sp}/sD'_c$ where A_{sp} is the area of spiral or hoop reinforcing bar (in.^{2} or mm^2), s is the spacing of spiral or hoop (in. or mm), and D'_c is the core diameter of column measured from center of spiral or hoop (in. or mm). For a rectangular column, $\rho_s = A_v/sb'_c$ where A_v is the sum of area of the ties and cross ties running in the direction perpendicular to the axis of bending (in.^{2} or mm^2), s is the spacing of ties (in. or mm), and b'_c is the confined column cross-section dimension, measured out-to-out of ties, in the direction parallel to the axis of bending (in. or mm)], P_c is the column axial force (kips or kN), A_g is the column cross-sectional area (in^2 or mm^2), f_c' is the concrete compressive strength (ksi or MPa), L is the length of column from the point of maximum moment to the point of moment contraflexure (in. or mm), D_c is the column diameter (in. or mm), and h_c is the column side dimension in the testing (analysis) direction (in. or mm).

Table 5.3 – Summary of Statistical Analysis for Proposed Damage State Based Drift Equations

Section (Trans. Reinf.)	Damage State	No. of Columns	Average Error	Standard Deviation	Min Error	Max Error	Coefficient of Determination
Circular (Hoops or Spirals)	DS1	15	+9%	38%	-31.2%	+89.6%	0.89
	DS2	167	+1.4%	32.5%	-69.1	+82.2	0.90
	DS3	34	-5.5%	30.7%	-38.6	+79.7%	0.95
	DS4	40	-0.33%	29.4%	-35.2%	+74.8%	0.93
	DS5	38	+3.6%	21.5%	-19.9%	+55.9%	0.97
	DS6	173	+0.67%	29.6%	-53.5%	+77.7%	0.56
Rectangular (Ties)	DS1	6	+70.5%	140.5%	-28%	+284%	0.73
	DS2	56	+0.58%	35.7%	-59.7%	+89.6%	0.88
	DS3	10	-31.9%	18.9%	-54.5%	+5.4%	0.95
	DS4	13	+3.9%	35.4%	-44.9%	+65.9	0.94
	DS5	5	-9.7%	11.1%	-20%	+6.7%	0.99
	DS6	45	+2.1%	36.3%	-49.6%	+84.1%	0.0

Figure 5.13 – Damage State Drifts Mapped on Pushover Curves of RC Circular Bridge Columns

5.3 Displacement Capacity Estimation

Estimation of displacement (or drift) capacity of an RC bridge column requires either a sectional (e.g., moment-curvature) or finite element analysis (e.g., pushover). Nevertheless, the estimation of the capacity is less challenging than that for the demand since the static capacity of a structure can safely be assumed the same as its dynamic capacity thus no dynamic analysis is required. Strain rate effects of steel and concrete are usually neglected for the capacity estimation.

Moment-curvature analysis is a sectional analysis to obtain a relationship between the moment and the curvature of the section. The curvatures at critical points (alternatively, the moment-curvature curve can be idealized using a bilinear model) are used to estimate the bridge column displacement capacity using the analytical plastic hinge length. Even though this is a convenient analysis, it does not include the bridge/bent overall geometry and geometric nonlinearities (such as P-Delta effects). More advanced and maybe accurate capacity estimation method for a bridge column is through a nonlinear static analysis, commonly referred to as a pushover analysis. A brief review of this topic is discussed first, then a generic cloud-based model is proposed to perform such analysis.

5.3.1 Pushover Analysis

AASHTO SGS (2011) allows a fiber-section lumped plasticity pushover analysis for RC bridge columns (**Fig. 5.14**), which is required for SDC D but might be used for other seismic regions. In this method, the reinforcing steel mechanical properties (ASTM A706 is required for SDC D, ASTM A615 can be used in other seismic regions or outside of the plastic hinges) are well established and quantified. The unconfined concrete (cover) has a peak stress at 0.002 strain and zero strength after spalling at 0.005 strain. The confined concrete (core) properties should be calculated based on the Manders's model. A computer software should be used to perform the pushover analysis following the abovementioned material models. P-Delta effects are usually included for a complete analysis.
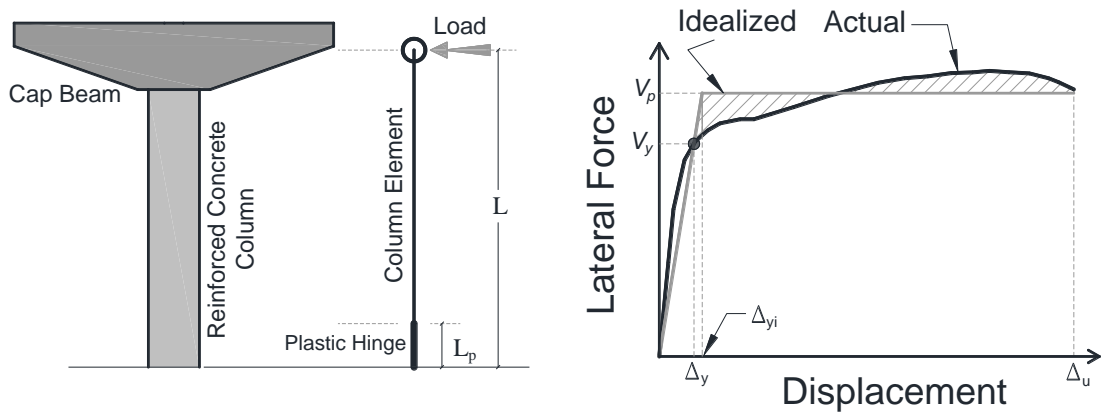
(a) Lump Plasticity Model
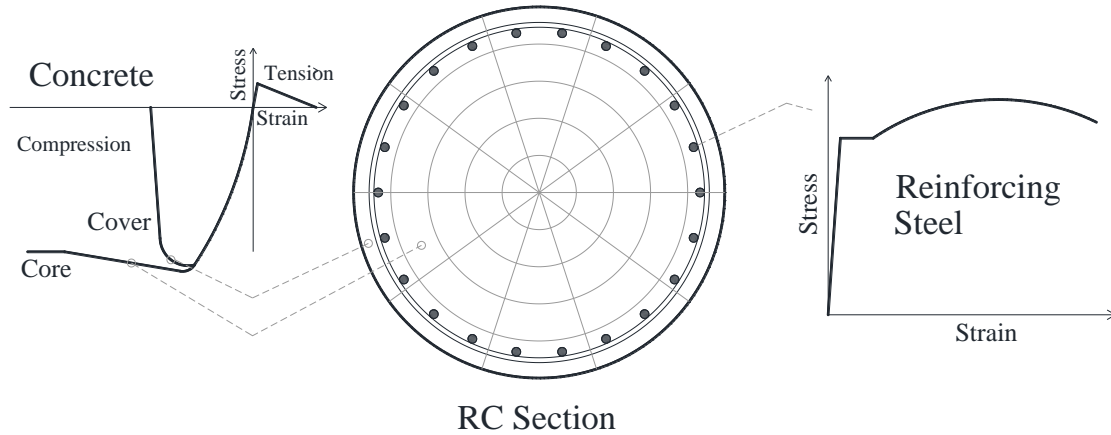
(b) Fiber Section and Material Models

Figure 5.14 – Pushover Analysis Based on AASHTO SGS Modeling Method

Similar to what was proposed for the dynamic analysis, it is feasible to develop a cloud-based software that can perform pushover analysis following the AASHTO SGS requirements. **Figure 5.15** shows the architecture of such software built with opensource tools such as OpenSees (2016). Generic bent models can be pre-defined with a few key modeling parameters to be provided by the user (e.g., the number of columns per bent, the column length, the column shape and size, reinforcement, concrete strength, etc.). The national bridge inventory (NBI) might also be accessed to populate some of the bent information.
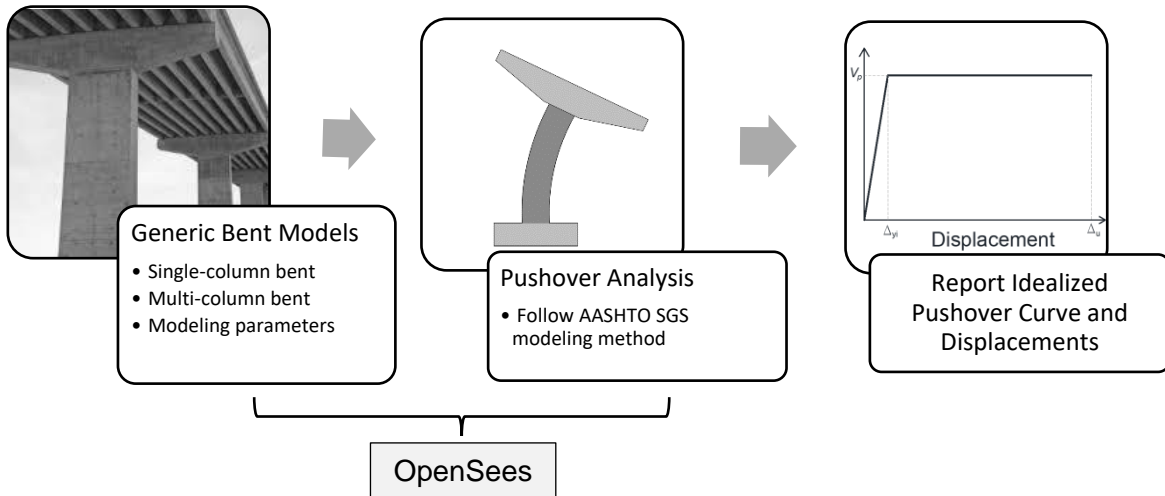
Figure 5.15 – Proposed Architecture for Cloud-Based Bridge Bent Pushover Analysis

5.3.1.1 Generic OpenSees Model for Pushover Analysis of any RC Bridge Columns

A generic model was developed in OpenSees to carry out pushover analysis of any RC bridge column using only a few parameters. The focus was on the circular single-column bents just to show the feasibility of developing a generic model. As minimum, the following parameters should be provided by the user:

1. The column length,
2. The column diameter,
3. The number of longitudinal reinforcing steel bars,
4. The area of each longitudinal reinforcing steel bar,
5. The spacing between the transverse reinforcement,
6. The area of each transverse reinforcement,
7. The concrete strength, and
8. The column axial load.

The generic model includes all the requirements by AASHTO SGS including stress-strain behavior for cover, core, and reinforcements. The reinforcement properties are based on those for ASTM A706 and are automatically adjusted for different bar sizes. The reduced expected strain and the expected strength are used. The Mander's model is followed to obtain the confinement properties. "Concrete01" and "ReinforcingSteel" material models were used for the concrete and steel fibers. The section is discretized into 30 circumferential by 10 radial fibers for the core and 10 by 10 for the unconfined concrete. Reinforcements are radially and evenly distributed (e.g., **Fig. 5.14b**). The AASHTO analytical plastic hinge length is calculated using the column length, the diameter of the longitudinal bars, and their expected yield strength. A "beamWithHinges", which is a force-based element, is used for the column element. P-Delta effects are included. However, the bond-slip effect was not directly included in the model since the analytical plastic hinge includes deformations caused by the bond-slip effect.

In the analysis, the column is pushed to 20% drift ratio, which is relatively high. Subsequently, a MATLAB function (developed by Tazarv; also available in Python for online applications developed by Won) is used to post-process the OpenSees output and to determine the column failure point, which is the minimum displacement at which the core concrete crushes, the reinforcement fractures, or the lateral load carrying capacity of the column drops by 15% compared with the peak baseshear. **Figure 5.16** shows one sample result for a 4-ft diameter, 16-ft tall RC bridge column using the generic OpenSees model and the MATLAB post-processing output. Additional analysis results including the failure point and the mode of failure are printed out for the ease of use (**Fig. 5.16c**).

(a) Post-Processing and Idealization   (b) Material Models
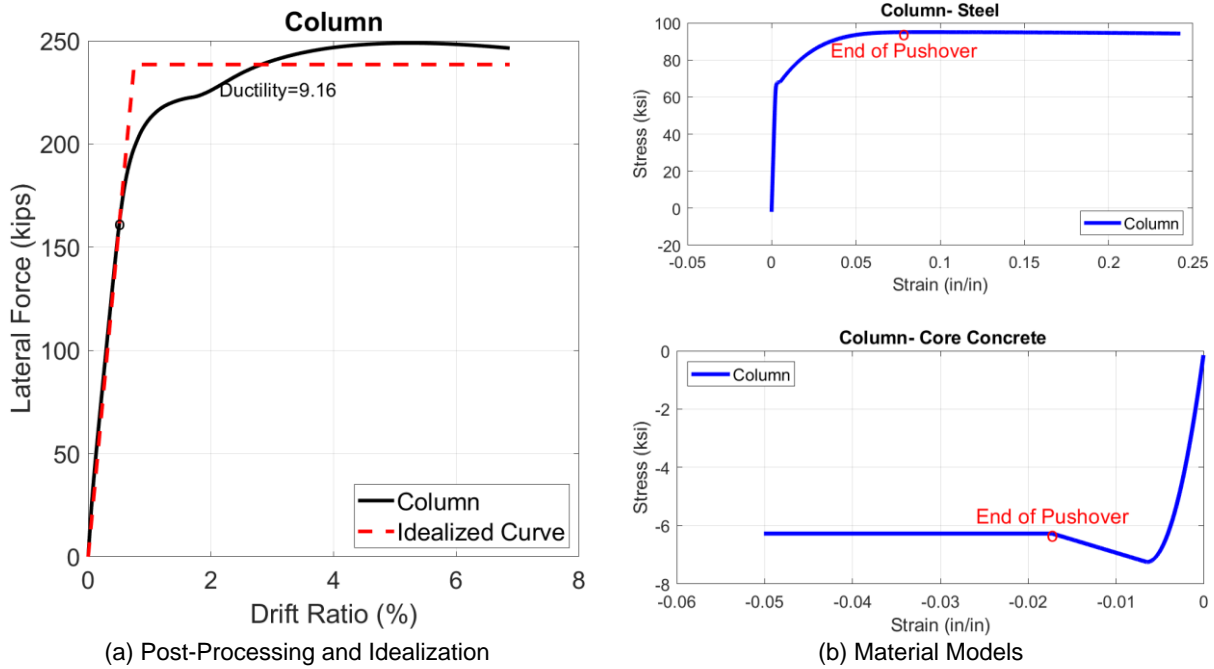
```
--------------------------ANALYSIS OUTPUT----------------------
'Column Length (in)'                 192
'Yield Drift (%)'                    0.51
'Effective Yield Drift (%)'          0.75
'Effective Yield Force (kips)'       238.52
'Ultimate Drift (%)'                 6.87
'Displacement Ductility'             9.16
'Mode of Failure'                    'Concrete Core Crushing'
----------------------------------------------------------------
```

Figure 5.16 – Sample of Pushover Analysis Using Generic Model for any Circular RC Bridge Columns Based on AASHTO SGS Modeling Methods

It is worth mentioning that the cracked stiffness was used for the column sections outside of the plastic hinge length. AASHTO requires a moment-curvature analysis to estimate the cracked stiffness of an RC column. Alternatively, a simple chart (e.g., **Fig. 5.17a**) can be used. To estimate the cracked stiffness, moment-curvature analyses were performed on 80 RC bridge columns covering a wide range of parameters. Polynomial curves were fitted, which showed a perfect match with those from the moment-curvature analyses (**Fig. 5.17b**). Based on this observation, an equation was developed to approximate the RC bridge effective stiffness as:

77

$$EI_{eff} = a(\frac{P_c}{A_g f_c'})^2 + b\left(\frac{P_c}{A_g f_c'}\right) + c$$

$$a = 25.213\frac{A_{sl}}{A_g} - 2.1765$$

$$b = -19.503\frac{A_{sl}}{A_g} + 1.4883$$ (Eq. 5.13)

$$c = 16.384\frac{A_{sl}}{A_g} + 0.0857$$

where, $\frac{P_c}{A_g f_c'}$ is the axial load ratio, and $\frac{A_{sl}}{A_g} = \rho_l$ is the column longitudinal reinforcement ratio. The average error between the approximated EI_{eff} and the code-specified ones was less than 1%.

(a) Moment-Curvature Results for 80 Bridge Columns (b) Fitted Curves shown with Dashed Red Lines
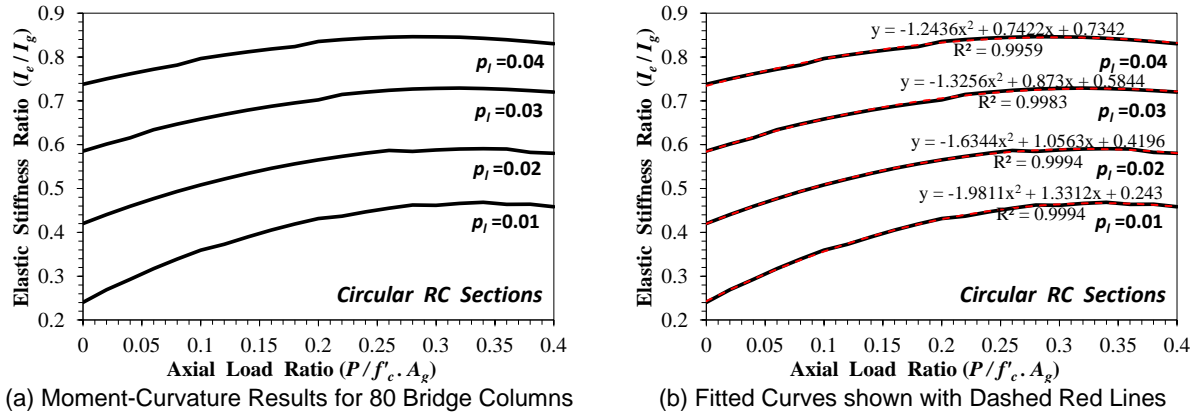
Figure 5.17 – Approximation of Cracked Stiffness for RC Bridge Columns

Furthermore, the clear cover is also needed, which is an environmentally controlled parameter, for the analysis. Ony may require this as one of the inputs from the user as the ninth parameter. However, the RC bridge column experimental data was reviewed to find an approximate value for the cover. It was found that the clear cover is on average 4.5% of the column diameter. When the information about the concrete cover is missing, one may use the following equation to estimate the clear cover:

Clear Cover = 0.045[Column Diameter or Side Dimension] (Eq. 5.14)

The proposed equation has an average error of -14.2% compared with the concrete covers from the experimental data and has a standard deviation of 37.7% with an R^2 of 0.78.

To validate the generic OpenSees model for any RC bridge columns, four circular columns tested between 2012 through 2021 were selected and analyzed. The columns had a wide range of force and displacement capacities. The concrete strength used in the model was that measured in the testing and the steel bar properties were from the AASHTO SGS but not the measured properties. **Fig. 5.19** shows the calculated and measured pushover curves. Overall, the generic OpenSees model, which was based on the AASHTO SGS requirements, reproduced the test data with a reasonable accuracy. Note that the approximation of the effective stiffness and the concrete cover discussed above had minimal effects on the column overall performance thus the level of the accuracy seen in the graphs are those inherent in the AASHTO SGS modeling methods.

In summary, it is feasible to develop a software that estimates the RC bridge column capacities incorporating only eight parameters with a reasonable accuracy. As part of this project and to showcase the feasibility of such analysis, a cloud-based pushover tool was developed (see **Appendix B**). The

website runs OpenSees behind the scenes using the proposed generic model and presents the post-processed results for a quick assessment.
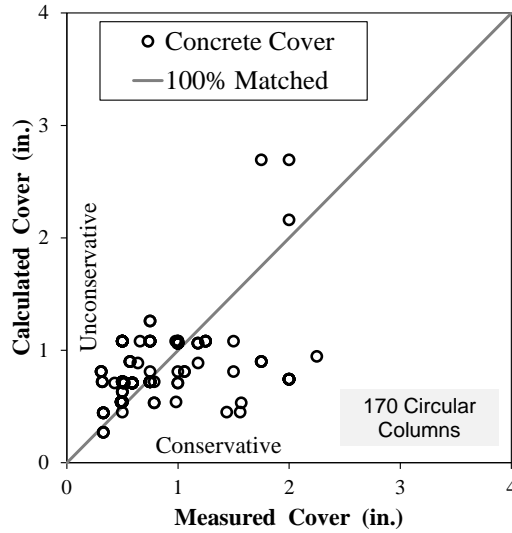
Figure 5.18 – Approximation of Clear Cover for RC Bridge Columns
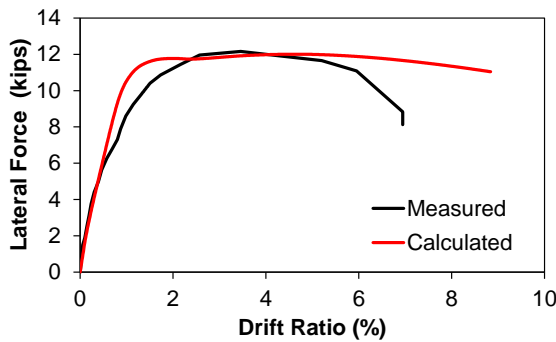
(a) Specimen 0%RCS Tested by AL-Hawarneh and
Alam (2021)
L = 68.11 in., Aspect Ratio = 5.67,
Axial Load Ratio = 0.092, ρ_s = 0.0124
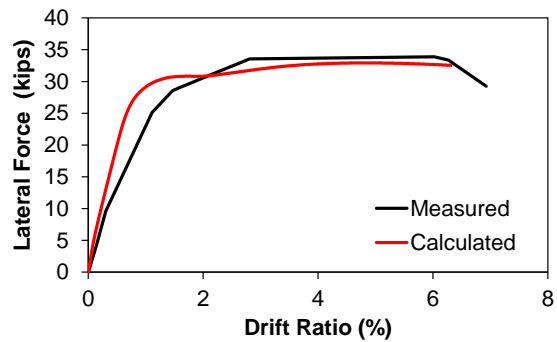
(b) Specimen LD-J1 Tested on Shake Table by
Mohammed et al. (2017)
L = 72 in., Aspect Ratio = 4.5,
Axial Load Ratio = 0.074, ρ_s = 0.011
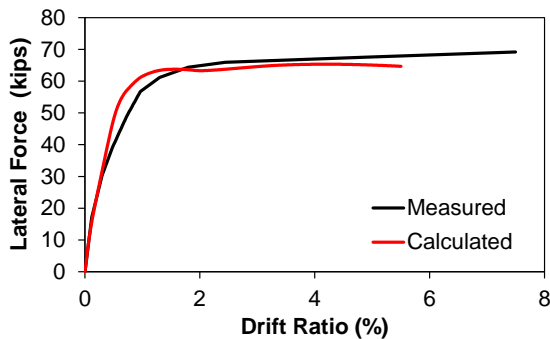
(c) Specimen T8 Tested by Goodnight et al (2013)
L=96 in., Aspect Ratio = 4,
Axial Load Ratio = 0.054, ρ_s = 0.00976
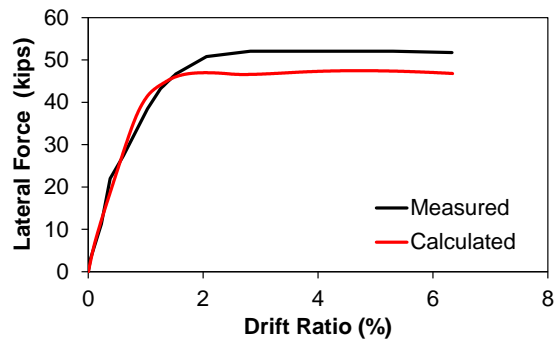
(d) Specimen H/D(6)- T/M(0) Tested by Prakash et al (2012)
L=144 in., Aspect Ratio = 6,
Axial Load Ratio = 0.07, ρ_s = 0.00606

Figure 5.19 – Pushover Analyses Results Using Proposed Generic OpenSees Model

5.3.2 Approximation of Idealized Pushover Curve

Critical points of a pushover curve might be estimated using the damage state based drift equations discussed in **Sec. 5.2** (**Table 5.2**). As shown in **Fig. 5.14**, to convert an actual pushover curve to its corresponding idealized curve, the idealized yield drift and the plastic force should be calculated by equating the area under the actual and idealized curves after the yield point (according to AASHTO SGS).

The RC bridge column database was analyzed to derive an empirical equation for the idealized point. The idealized response was not readily available for columns in the database. Therefore, 27 circular RC bridge columns tested between 2010 and 2021 were randomly selected, their measured force-displacement backbone was extracted, and then the response was idealized following the AASHTO SGS requirements. It was found that the idealized yield drift is on average 20% higher than the yield drift per column. Based on this observation, the following equation was developed to relate the idealized yield drift ratio (δ_{yi} in %) to the yield drift ratio, which is the same as the drift at DS2 (δ_{DS2} also in %):

$$\delta_{yi} = 1.2\delta_{DS2}$$

(Eq. 5.15)

Figure 5.20a shows the measured and calculated idealized yield drifts for the 27 circular RC bridge columns. The average error was -4.3% and the standard deviation was 16.5% with an R^2 of 0.97. A similar analysis was performed on 20 rectangular RC bridge columns tested between 2000 and 2014 (**Fig. 5.20b**). The average error was +12.4% and the standard deviation was 19.5% with an R^2 of 0.98. Overall, a good accuracy was observed. Therefore, in lieu of a finite element pushover analysis, **Eq. 5.15** may be used to estimate the idealized yield drift of an RC bridge column.
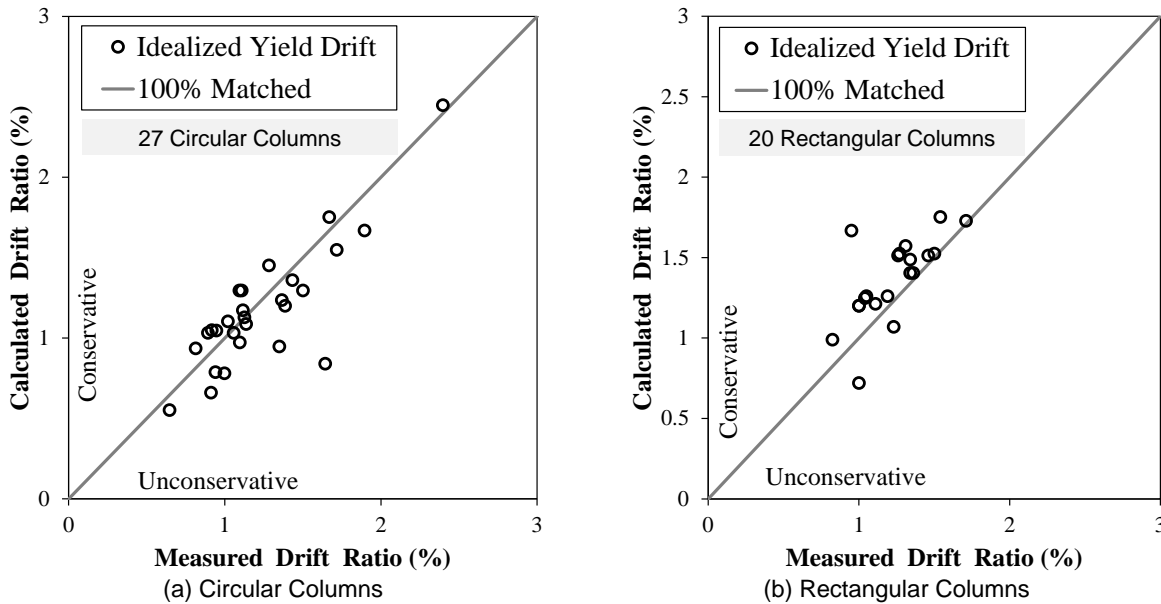
Figure 5.20 – Evaluation of Proposed Idealized Yield Drift Equation

The plastic (idealized) force for RC bridge columns was also estimated using the columns discussed above. From the reinforced concrete design for a single-layer rectangular section, it is known that the moment capacity of the section is related to the yield strength of the longitudinal bars (f_{yl}), the area of the longitudinal bars (A_{sl}), and a moment arm, which is a portion of the column side dimension (D_c). Furthermore, the plastic lateral force of a column (V_p) is the ratio of the column moment capacity to the

80

column length (L). It is also well established that the moment capacity of a column varies when the column axial load (P_c) changes. The axial load may be normalized to the product of the column area (A_g) and the concrete strength (f'_c). One may relate the plastic force of an RC bridge column to these key parameters as:

$$V_p = \frac{M_p}{L} \propto A_{sl} f_{yl} \frac{D_c}{L} \left(1 + \frac{P_c}{A_g f'_c}\right)$$

(Eq. 5.16)

This equation can be further simplified by multiplying it to A_g/A_g as:

$$V_p \propto A_{sl} f_{yl} \frac{D_c}{L} \left(1 + \frac{P_c}{A_g f'_c}\right) \frac{A_g}{A_g} \propto f_{yl} \cdot D_c^2 \cdot \frac{A_{sl}}{A_g} \cdot \left(\frac{L}{D_c}\right)^{-1} \cdot \left(1 + \frac{P_c}{A_g f'_c}\right)$$

(Eq. 5.17)

This equation indicates that when the axial load of the column increases, the plastic force also increases. Further, when the column aspect ratio (L/D_c) increases, the plastic forces deceases. It is obvious that when a larger section is used or when more longitudinal bars or stronger ones are used, the moment capacity thus the plastic shear force will be increased.

The column database was statistically analyzed to derive an empirical equation for the plastic shear forces:

$$V_p = 0.35 f_{yl} \frac{D_c^3}{L} \left(\frac{A_{sl}}{A_g}\right) \left(1 + \frac{P_c}{A_g f'_c}\right) \qquad \text{for circular columns}$$

(Eq. 5.18)

$$V_p = 0.45 f_{yl} \frac{h_c^3}{L} \left(\frac{A_{sl}}{A_g}\right) \left(1 + \frac{P_c}{A_g f'_c}\right) \quad \text{for rectangular columns}$$

where f_{yl} is the expected yield strength of the column longitudinal bars (ksi or MPa), D_c is the circular column diameter (in. or mm), h_c is the rectangular column side dimension in the testing (analysis) direction (in. or mm), $\frac{A_{sl}}{A_g}$ is the column longitudinal reinforcement ratio, and $\frac{P_c}{A_g f'_c}$ is the column axial load ratio. Note one may assume that f_{yl} is 68 ksi (or 468.8 MPa) according to AASHTO SGS.

Figure 5.21 shows the measured and calculated plastic shear forces (based on **Eq. 5.18**) for 27 circular and 20 rectangular RC bridge columns. For the circular columns, the average error between the calculated and the measured plastic forces was -1.5% with a standard deviation of 15% and an R^2 of 0.93. For the rectangular columns, the error was -8.5% with a standard deviation of 17.4% and an R^2 of 0.94. Approximately the same level of accuracy was observed when f_{yl} was assumed to be 68 ksi (or 468.8 MPa). Overall, the plastic shear force of an RC bridge column can be estimated using **Eq. 5.18** with a good accuracy.

To obtain a full pushover curve, the column failure point is also needed. Since DS6 is to represent the column behavior at or close to the failure, the empirical equation for DS6 drift (δ_{DS6} in **Table 5.2**) may be used as the end point of the pushover curve.
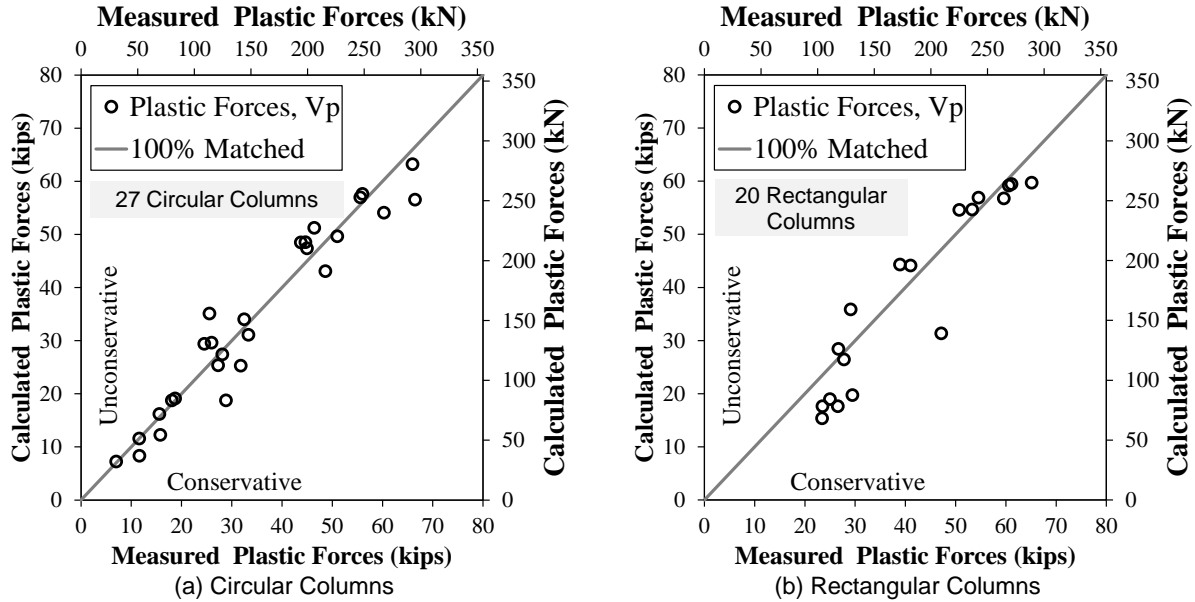
Figure 5.21 – Evaluation of Proposed Plastic Force Equation

5.3.2.1 Summary of Approximated Idealized Pushover Curve

Table 5.4 presents a summary of equations that can be used to approximate an idealized pushover curve for an RC bridge column. **Figure 5.13** schematically shows the two key points of the idealized pushover curve including some statistical parameters. Note that the approximated idealized curve should not replace a finite element pushover analysis. It is provided as an additional tool for quick assessment.

Table 5.4 – Summary of Proposed Equations for Estimation of Idealized Pushover Curve

Key Points	Proposed Equation
DS2	$\delta_{DS2} = \delta_y = L/4.5D_c$ for circular sections $\delta_{DS2} = \delta_y = L/5.12h_c$ for rectangular sections
Idealized Yield Drift	$\delta_{yi} = 1.2\delta_{DS2}$
Plastic Shear Force	$V_p = 0.35f_{yl}\frac{D_c^3}{L}\left(\frac{A_{sl}}{A_g}\right)\left(1 + \frac{P_c}{A_g f_c'}\right)$ for circular columns $V_p = 0.45f_{yl}\frac{h_c^3}{L}\left(\frac{A_{sl}}{A_g}\right)\left(1 + \frac{P_c}{A_g f_c'}\right)$ for rectangular columns
DS6	$\delta_{DS6} = 1.3(1 + 150\rho_s)\left(1 - \frac{P_c}{A_g f_c'}\right)\left(1 + 0.3\frac{L}{D_c}\right)$ for circular sections $\delta_{DS6} = 2.2(1 + 25\rho_s)\left(1 - \frac{P_c}{A_g f_c'}\right)\left(1 + 0.3\frac{L}{h_c}\right)$ for rectangular sections

Notes: All drift ratios are in percentage (%), ρ_s is the volumetric ratio of transverse reinforcement according to AASHTO SGS, P_c is the column axial force (kips or kN), A_g is the column cross-sectional area (in^2 or mm^2), f_c' is the concrete compressive strength (ksi or MPa), L is the length of column from the point of maximum moment to the point of moment contraflexure (in. or mm), D_c is the column diameter (in. or mm), and h_c is the column side dimension in the testing (analysis) direction (in. or mm).

5.4 Validation of Proposed Drift Demand and Capacity Equations

A half-scale octagonal RC bridge column was recently tested at South Dakota State University (Sjurseth, 2021). The column was 96-in. (2438-mm) tall and had a diameter of 24 in. (610 mm). The column was longitudinally reinforced (with a circular pattern) with 10-No. 8 (Ø25-mm) bars and was transversely reinforced with No. 4 (Ø13-mm) hoops at 2 in. (51 mm). The concrete strength at the test day was 4.92 ksi (33.9 MPa) and the yield strength of the longitudinal bars was 69.3 ksi (477.8 MPa). The clear cover was 1 in. (25.4 mm). The column axial load was 155 kips (689.5 kN). Note this column was not included in the RC bridge column database thus it may be used as an additional verification of the proposed equations above and beyond the statistical validation discussed in the previous sections. **Table 5.5** presents a summary of the calculations using the proposed equations, and **Fig. 5.22** schematically shows the calculated and measured responses. The proposed method estimates that this column will have a few flexural cracks at 0.53% drift, which agrees with the observed damage at this drift. The proposed method estimates that the column will yield at 0.89% drift. In fact, the column yielded in the testing during the first cycle of 0.75% drift. The drifts at DS3 and DS5 were overestimated, which is safe since the column will be assessed for larger demands. The estimated drifts at DS4 and DS6 were very close to those seen in the test. The column failed by the bar fracture during the first cycle of 10% drift. The proposed DS6 equation accurately estimates this drift level. Overall, a good agreement was observed.

Table 5.5 – Validation of Proposed Drift Demand and Capacity Equations for a Half-Scale Octagonal Column

Key Parameters	Column Length, L = 96 in. (2438 mm); Column Diameter (Octagonal), D_c = 24 in. (610 mm); Number of Long. Bars = 10; Area of Each Long. Bar, A_{sl} = 0.76 in^2 (509 mm^2); Spacing b/w Transverse Bars, s = 2 in. (51 mm); Area of Each Transverse Bar, A_{sp} = 0.2 in^2 (129 mm^2); Concrete Strength, f_c' = 4.92 ksi (33.9 MPa); Column Axial Load, P_c = 155 kips (689.5 kN)
Intermediate Parameters	A_g (octagonal) = 476.9 in^2 (307676.8 mm^2); Clear cover = $0.045 D_c = 0.045 \times 24 = 1.08\ in.\ (27.4\ mm)$, only 8% error compared with the actual cover of 1 in.; $\rho_s = \frac{4A_{sp}}{sD'_c} = \frac{4 \times 0.2}{2 \times (24 - 2 \times 1.08 - 0.5)} = 0.01874$; f_{yl} = 68 ksi (468.8 MPa) according to AASHTO SGS not test data; $\frac{P_c}{A_g f_c'} = \frac{155}{476.9 \times 4.92} = 0.066$;
Critical Points	**Proposed Equations**
DS6	$\delta_{DS6} = 1.3(1 + 150\rho_s)\left(1 - \frac{P_c}{A_g f_c'}\right)\left(1 + 0.3\frac{L}{D_c}\right) = 1.3(1 + 150 \times 0.01874)(1 - 0.066)(1 + 0.3 \times 4) = 10.18\%$
DS5	$\delta_{DS5} = 0.8\delta_{DS6} = 0.8 \times 10.18 = 8.14\%$
DS4	$\delta_{DS4} = 0.5\delta_{DS6} = 0.5 \times 10.18 = 5.09\%$
DS3	$\delta_{DS3} = 0.3\delta_{DS6} = 0.3 \times 10.18 = 3.05\%$
DS2	$\delta_{DS2} = \delta_y = \frac{L}{4.5D_c} = \frac{96}{4.5 \times 24} = 0.89\%$
DS1	$\delta_{DS1} = 0.6\delta_{DS2} = 0.6 \times 0.89 = 0.53\%$
Idealized Yield Drift	$\delta_{yi} = 1.2\delta_{DS2} = 1.07\%$
Plastic Shear Force	$V_p = 0.35 f_{yl}\frac{D_c^3}{L}\left(\frac{A_{sl}}{A_g}\right)\left(1 + \frac{P_c}{A_g f_c'}\right) = 0.35 \times 68 \times \frac{24^3}{96} \times \frac{10 \times 0.79}{476.9} \times (1 + 0.066) = 60.5$ kips (or 269 kN)

Figure 5.22 – Validation of Proposed Damage State Based Drift Equations for Octagonal Bridge Column Tested by Sjurseth (2021)

In the figure:

Damage State 2
$\delta_{DS2}^{Obs.} = 0.75\%$
$\delta_{DS2}^{Cal.} = 0.89\%$

Damage State 6
$\delta_{DS6}^{Obs.} = 10.0\%$
$\delta_{DS6}^{Cal.} = 10.18\%$

Damage State 5
$\delta_{DS5}^{Obs.} = 7.0\%$
$\delta_{DS5}^{Cal.} = 8.14\%$

$V_p^{Obs.} = 275\ kN$
$V_p^{Cal.} = 269\ kN$

Damage State 1
$\delta_{DS1}^{Obs.} = 0.5\%$
$\delta_{DS1}^{Cal.} = 0.53\%$

$\delta_{yi}^{Obs.} = 0.72\%$
$\delta_{yi}^{Cal.} = 1.07\%$

Damage State 3
$\delta_{DS3}^{Obs.} = 2.0\%$
$\delta_{DS3}^{Cal.} = 3.05\%$

Damage State 4
$\delta_{DS4}^{Obs.} = 5.0\%$
$\delta_{DS4}^{Cal.} = 5.09\%$
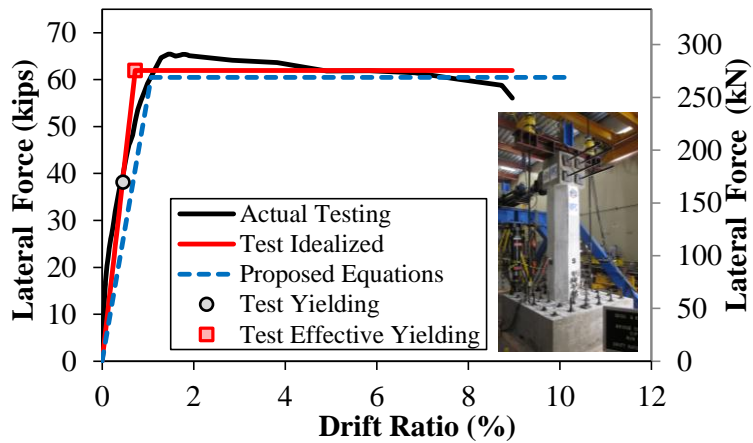
Figure 5.23 – Estimated versus Measured Idealized Pushover Curves for Octagonal Bridge Column Tested by Sjurseth (2021)

Figure 5.23 shows the measured and estimated idealized pushover curves for the half-scale octagonal RC bridge column. It can be seen that the proposed method results in an overall good agreement with the measured data, thus may be used for a quick assessment of RC bridge columns after an earthquake.

5.5 Summary

Estimation of displacement demands and capacities for RC bridge columns are required for a detailed damage assessment. This chapter reviewed past studies on the topic and proposed new techniques to estimate RC bridge column demands and capacities at different damage states. Empirical damage state based drift equations were proposed through statistical analysis of the RC bridge column experimental database. The proposed equations reproduced the test data with a reasonable accuracy. Furthermore, flowcharts were proposed to develop cloud-based analytical tools to perform dynamic and pushover analyses of affected bridges quickly after an earthquake. To showcase the feasibility of the cloud-based analytical tools, a website was designed which can perform pushover analysis of any circular RC bridge column using only eight parameters.

CHAPTER 6. RC COLUMN DAMAGE DETECTION SOFTWARE

6.1 Introduction

In the early works on computer-vision-based damage detection, heuristic filters designed by human experts have been used to detect target damages. Image processing methods such as edge detection (Jahanshahi et al., 2013; Kim et al., 2020), threshold-based clustering (Otsu et al., 1979), and hand-crafted filter-based object detection methods (Dalal et al., 2005; Ge et al., 2014) have been used. Nishikawa et al. (2012) applied multiple sequential image filters for detecting damages and estimating their properties. Paal et al (2015) presented a computer vision-based method to determine damage states of RC building columns by localizing each component (crack, spalling, and exposed steel bar) and quantifying the properties of distinct textures of regions using the Canny operator. Yeum et al. (2015) used object detection approaches to detect and localize fatigue cracks in steel bars. These rule-based approaches with hand-crafted feature extraction techniques worked well in many Civil Engineering applications. However, they are sensitive to the properties of input images, such as noise level and exposure. Therefore, using the abovementioned approaches, it is hard to develop a generalized model that works well with new input data.

The deep learning technique differs from the traditional computer-vision-based approaches in that deep learning learns important features and representations from the data and objectives. For instance, in the case of object detection problem, it learns the hierarchy of image filters critical to improving the detection accuracy from the data. The loss or error metric is defined as a form of a mathematical equation, and the backpropagation method updates contributions of internal components to the computation of output of the model. There have been studies that utilized deep neural networks in damage detection. Kim et al. (2019) formulated a damage detection program as an image classification problem. Convolutional neural networks (CNNs) and speeded-up robust features (SURF) were used. AlexNet (Krizhevsky et al., 2012) and GoogleNet (Szegedy et al., 2015) were tested in the classification of cracking and spalling. Yeum et al. (2018) and Cha et al. (2018) modeled damage detection as a detection problem. Compared to the patch-classification-based approaches, detection-based methods can provide more accurate location information of the damage instances. Yeum et al. (2018) used region responses from the R-CNN model for detecting objects with bounding boxes. Cha et al. (2018) used the Faster R-CNN, which can detect different shapes and sizes of delamination.

In this project, a deep learning technique was used to detect damages and quantify their properties for RC bridge column damage assessments. An instance segmentation technique (e.g., Mask R-CNN [He et al., 2017]) was used to detect damages and find the exact areas of them in the input image. The segmented areas were used to extract useful properties, such as length, orientation, and the number of instances within a specific region (Yein et al., 2018). A cascade approach has been developed by using deep neural networks (DNNs) designed for classification (e.g., MobileNet [Sandler et al., 2018]) and instance segmentation (e.g., Mask R-CNN) tasks. The MobileNet V2, a CNN architecture for classification, was used for detecting cracks by classifying small image patches. The Mask R-CNN was used to detect and segment the target column, spalling, and exposed vertical/horizontal bars in the image. The output of the DNNs was processed to extract the parameters used in defining damage states.
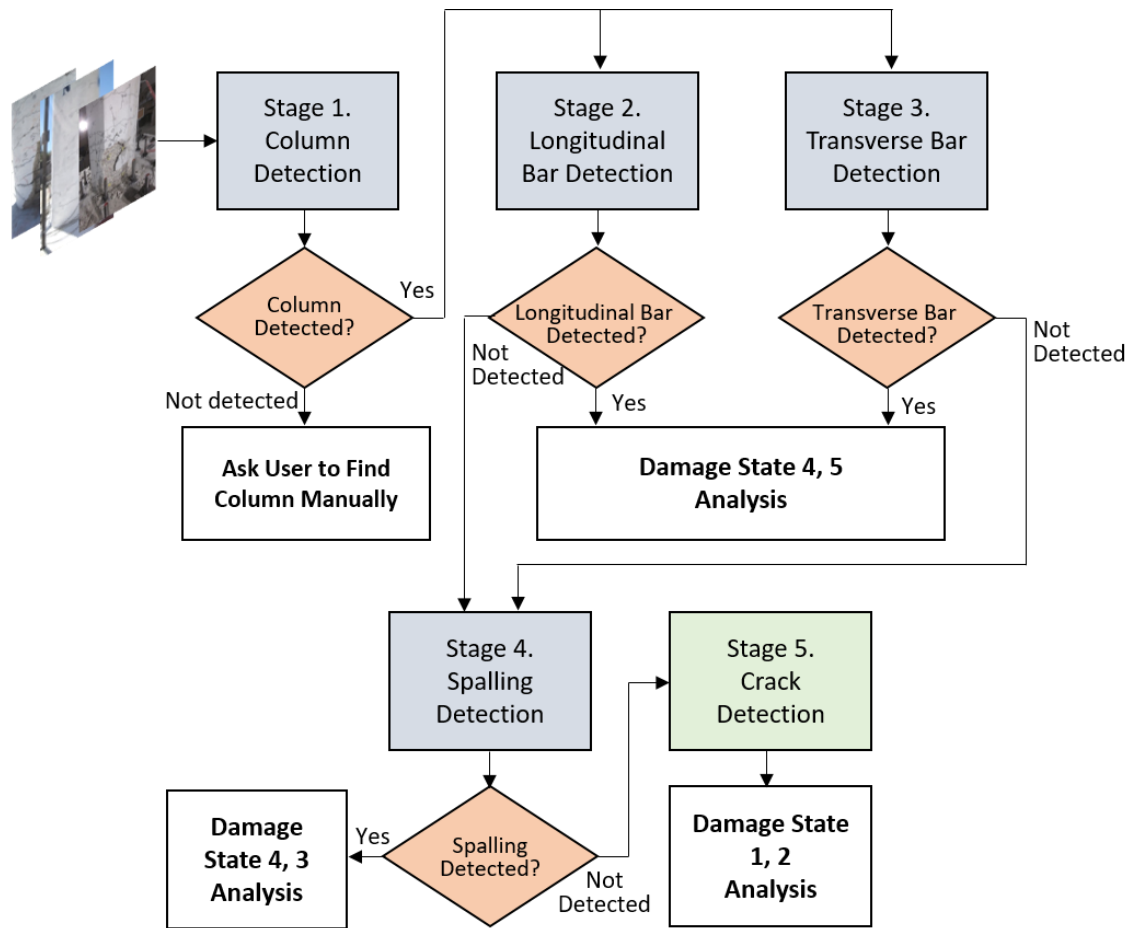
Figure 6.1 – AI-based Damage State Decision Flowchart

Figure 6.1 shows the flowchart of the cascade damage detection and damage state analysis. The proposed Computer Vision Tool (CVT) starts the analysis first with the column detection, then looks for rebars. If no rebar is detected, it searches for spalling. If there is no spalling, the cracks are detected. This order of damage detection was selected because more server damages such as exposed rebar are more critical for damage assessment than cracking. For a successful damage state identification, cracking is evaluated with the number of horizontal and vertical cracks and their angles. For the spalling, the ratio of the longest width within the spalled region to the column width is estimated, and the number of vertical and horizontal exposed steel bars is counted. Based on these results, the proposed CVT determines the damage state following the proposed definition (**Table 3.2**).

The workflow was implemented using DNNs and additional computer codes that process the outcomes of DNNs and extract properties. For efficient computation, the DNN models for the detection tasks of Stages 1 to 4 were combined into a single DNN module, but the crack detection in Stage 5 was implemented as an independent module due to the different characteristics of the component. The flowchart contains potential interactions with the user for the case that the DNNs fail to identify components in the image. Each of these modules is further discussed in the following sections.

6.1.1 Deep Convolutional Neural Network (DCNN)

Deep Convolutional Neural Network (DCNN), which consists of convolution layers and fully connected layers, has revolutionized high-level recognition tasks such as image classification, object detection, and image segmentation tasks (Krizhevsky et al., 2015; He et al., 2017; Szegedy et al., 2018). The basic building block of a DCNN is a convolution layer that consists of convolution kernels (i.e., filters). Each kernel consists of a 2-dimensional array of neurons. The main idea of having kernels and multiple layers of them is to share the artificial neurons for all areas of an input image and aggregate low-level features (responses of early-stage kernels) into high-level spatial features (kernels closer to the output layer). In addition, nonlinear activation functions and pooling layers are used after each convolution layer to summarize the responses from the previous layers. These properties enable the DCNNs to approximate very complex functions.

LeCun et al. (1989) explored the performance of a CNN in classifying hand-writing digit datasets and the term "convolutional neural network" was first introduced. LeNet-5 (LeCun et al., 1998) is one of the earliest CNNs with shallow architecture, which only has 1 or 2 hidden layers. After the advent of LeNet-5, many state-of-the-art networks have been inspired and created to solve complex classification and object detection tasks. **Figures 6.2** and **6.3** illustrate the convolution operation of a CNN. In **Fig. 6.2**, a 3-by-3 convolution kernel and a 5-by-5 input image are illustrated. Convolution is the element-wise multiplication of the kernel and input, followed by summation. During the convolution, important components of an image will contribute more to the feature map, and the rest will be suppressed.

Input   Conv. Kernel   Feature Map
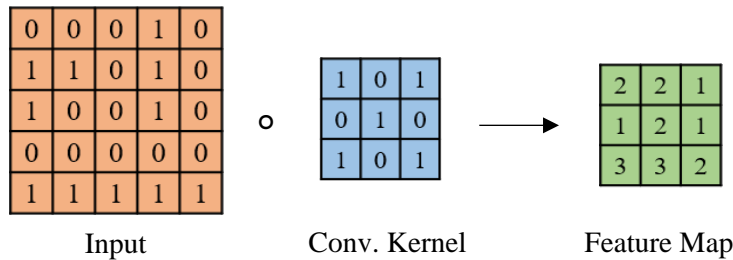
Figure 6.2 – Concept of a Convolution Kernel and Convolution Layer
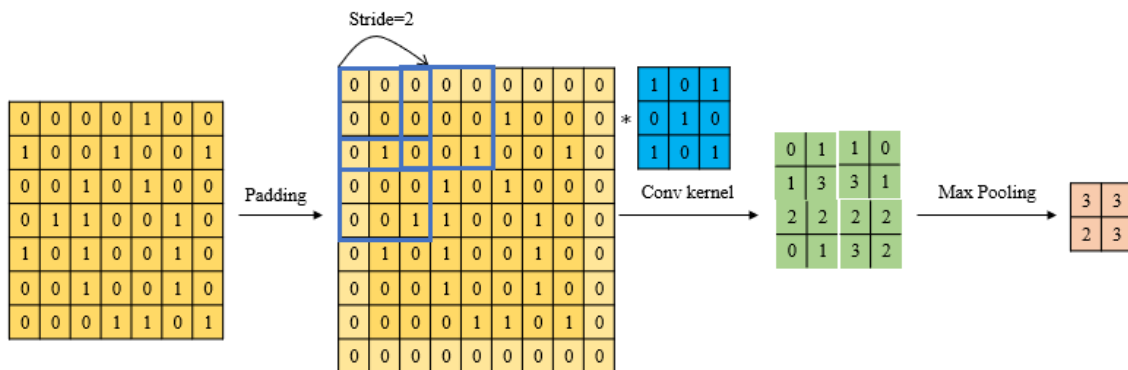
Figure 6.3 – Convolution and Pooling Operation

Li et al. (2021) emphasized the advantages of using CNN. First, there are local connections that are different from previous multi-layer perceptrons, and these connections are cost- and time-efficient by reducing the number of parameters. The perceptron is an algorithm for supervised learning of binary classifiers. Second, a group of local connections shares the same weights, which accelerates the training

process. Lastly, the pooling layer after the feature map can reduce the dimension of a feature map. The pooling layer down samples the previous feature map and summarizes useful information. **Figure 6.3** shows convolution and pooling operations on a convolution layer (Li et al., 2021). An optional process, padding, is to handle the convolution operation on the boundaries of an image by adding more columns and rows to the boundaries. The pooling operation helps to reduce redundant information to the next stage and prevents overfitting of the model.

6.2 Detection of RC Bridge Columns and Damages

In general, the development of a deep learning-based method consists of data preparation, training, and performance evaluation. In the early stages of training, DNN produces erroneous output. Backpropagation method, which is a supervised learning using gradient descent, adjusts internal weight matrices (internal parameters) of the DNN architecture for minimized errors.

The first task of the proposed CVT is to detect columns. Subsequently, the exposed steel bars and concrete spalling are detected. The cracking is detected last. Finally, the column damage state is determined following the proposed damage state definitions (**Table 3.2**). A Mask-R-CNN model for the initial detection of each type of damage was utilized. The input of the DNN architecture is the image of the column (which is damaged). The output of DNN is a series of binary masks that represent the location and categories of objects (in the proposed CVT, the objects to look for are the column boundaries, steel bars, and concrete spalling). For each category, unity (1) represents the object, and zero (0) represents the background. To obtain a DNN that produces high-quality detection results, DNN must be trained with many annotated data in a supervised manner.

6.2.1 Data Preparation

As discussed in the previous section, in AI-based computer vision tasks, a large amount of labeled high-quality images are essential to achieve reasonable performance. Insufficient data or low-quality images may lead to poor performance in terms of detection accuracy and generalization capacity.

In the present project, the research team had access to 1692 photographs of multiple RC bridge columns tested under slow-cyclic loading. More than 1340 additional photos (totaling 3036) were provided by other researchers (Amiri et al., 2021; Ameli et al., 2016; Ameli and Pantelides, 2017; Haber et al., 2013; Marshall et al., 2020; Mashal et al., 2021; Nikoukalam and Sideris, 2017) and also Puerto Rico DOT (Dr. Manuel Coll). Of which, 216 images were selected and used for training and evaluation of the DNN model. The dataset was divided into 80% for training and 20% for testing, which corresponds to 170 training and 46 testing images, respectively. The images contained different components (column, spalling, rebar, and cracking) and were in various sizes with the minimum spatial resolution of 2000 by 1980 pixels. The images were annotated manually for each category of components. The labels were polygons aligned to the column boundaries, spalling, horizontal and vertical steel bars, and cracking in the image coordinate. **Figure 6.4** shows examples of polygons superimposed on the column areas, and **Fig. 6.5** shows labeled damages (cracking not shown). Labelbox, an online labeling software, was used for image labelling. The annotation results were saved in a "JSON" file and imported to the DNN training modules.

A data-augmentation technique was used to populate more data for the development of a generalized model on possible transformations. Horizontal flip and Gaussian blur operation with a standard deviation of 0.5 were used. The annotated polygons were also flipped horizontally. **Figure 6.6** shows samples of data augmentation operations.

The images were converted to the same resolution. In the conversion process, additional columns or rows of images were padded to the input to maintain the aspect ratio and then scaled to the target resolution because the aspect ratio is one of the important factors that characterizes columns in images.
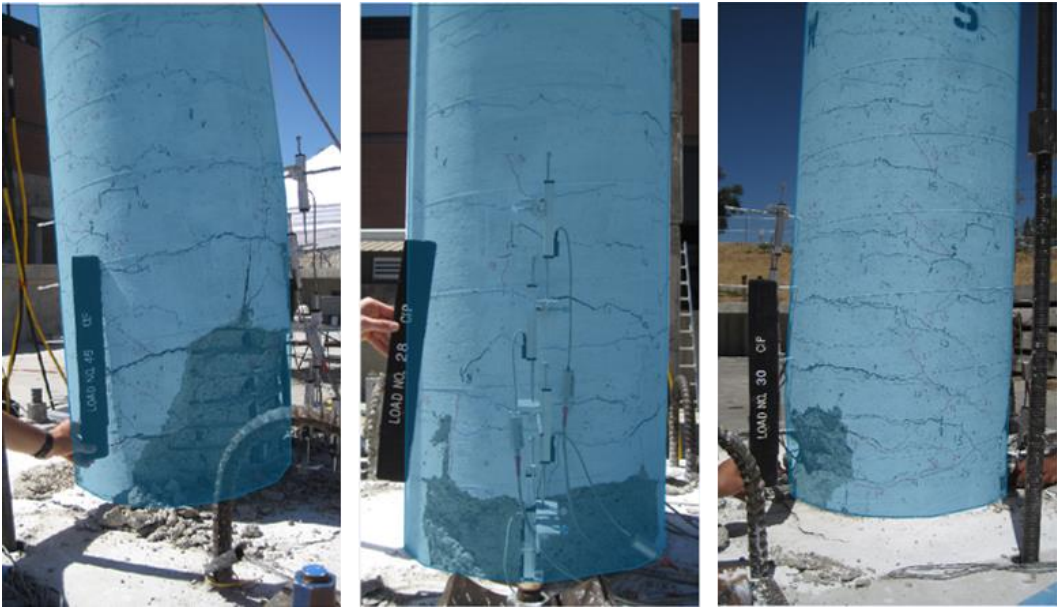
Figure 6.4 – Samples of Labeled Columns
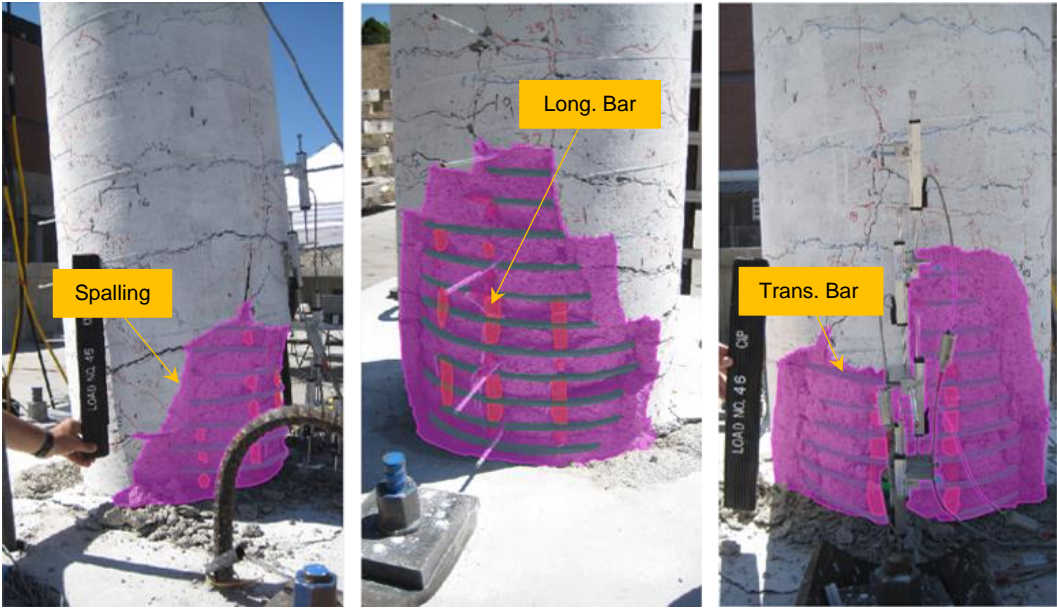
Figure 6.5 – Samples of Damage Annotation

| (a) Original Image | (b) Horizontal Flip | (c) Gaussian Blur (σ = 0.5) |
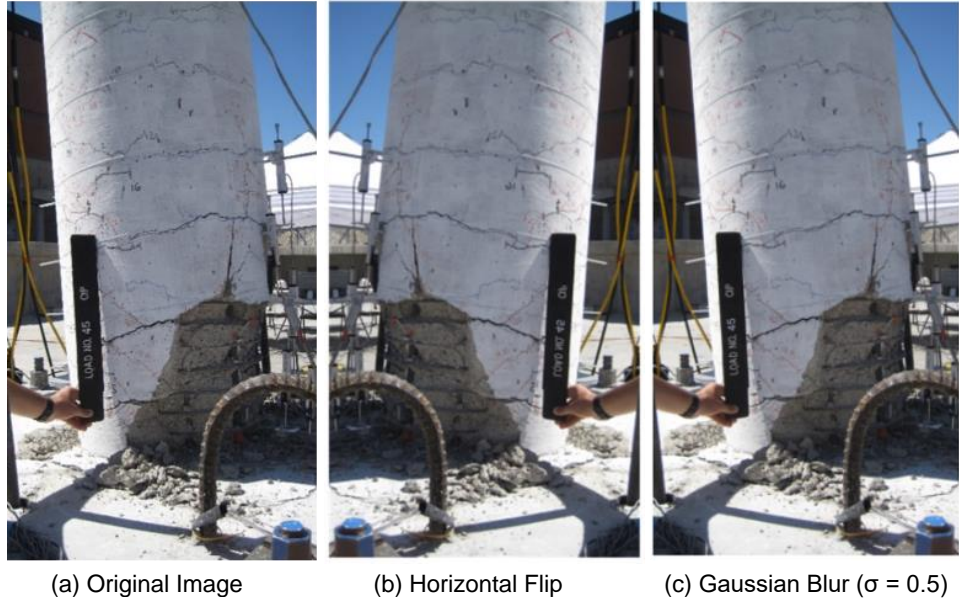
Figure 6.6 – Samples of Data Augmentation

6.2.2 Training Mask R-CNN Model on Damage Dataset

Mask R-CNN (He et al., 2017) was used for the initial detection of different damages (**Fig. 6.7**). ResNet101 (He et al., 2016) architecture was used as the backbone network, which is responsible for the hierarchical spatial feature extraction. The Region Proposal Network (RPN) in the Mask R-CNN architecture generates anchors (rectangular areas of various scales and aspect ratios) over the image and scores the probability of the existence of objects at each location and bounding box. Bounding boxes with high probability were selected and downsized to a unit scale for the subsequent classification layers and mask generation layers. The classification subnetwork was fully connected layers with categorical output. The mask generation was done by predicting the binary value of each pixel in the mask. The size and location of the results of these subnetworks were recovered with respect to the input image. The backbone network is typically trained on a very large image dataset, such as ImageNet (Krizhevsky et al., 2012). However, other components of Mask R-CNN must be retrained on the target problem and dataset.
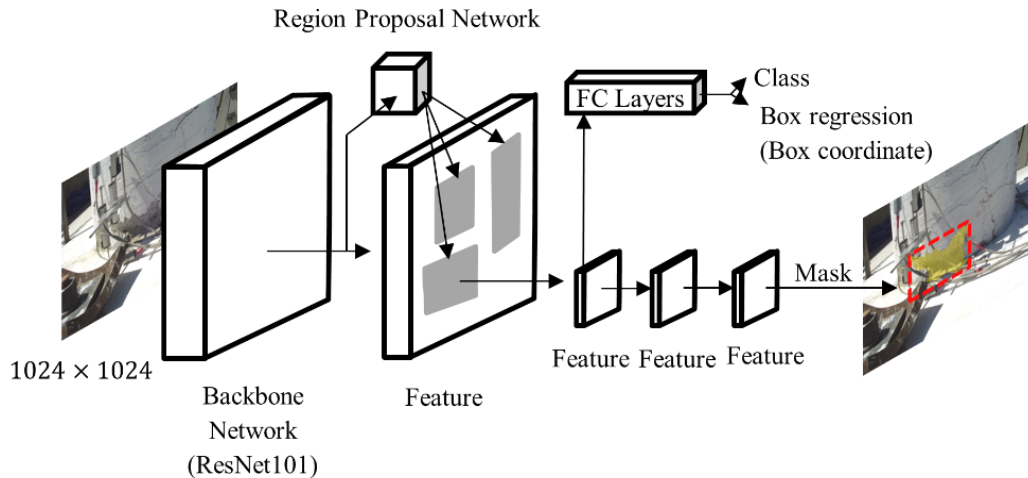
Figure 6.7 – Overall Mask R-CNN Architecture

6.2.3 Analysis of Damage State

The Mask R-CNN trained (fine-tuned) with the column damage dataset should detect the RC column, steel bars, and the concrete spalled region from an image. The column diameter may or may not be known to the user in a preliminary analysis. However, the proposed damage state definition (DS3 & DS4 in **Table 3.2**) requires obtaining the ratio of the maximum length of the spalled region to the column diameter. Since the column diameter will be known in pixel unit, the proposed CVT calculates this ratio (max spalled length to the column diameter) based on pixels. **Figure 6.8** shows the flowchart of the implemented analysis approach in the proposed CVT.
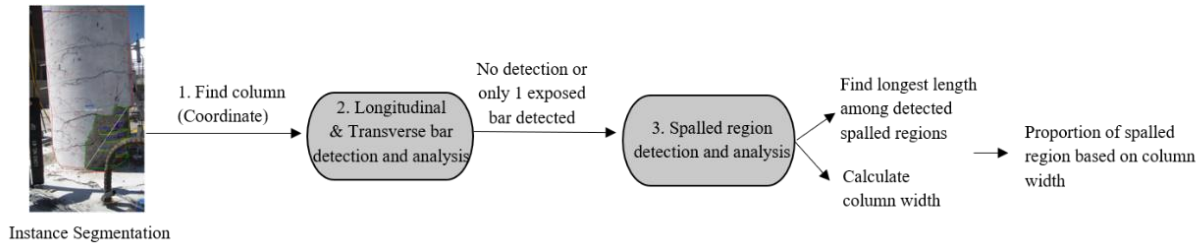
Figure 6.8 – Target Object Analysis

First, the column instances are analyzed. The column area identified by the initial detection is used to set a region of interest (ROI) for the subsequent analysis. In other words, any damage assessment is done within the column boundaries as detected by CVT. From the column's location, which includes the coordinate of its left-top and right-bottom corners, the area that is needed for a close inspection is highlighted by a colored box. All detections outside of ROI are considered false and are discarded.

Second, the module for the transverse and longitudinal bar analysis is performed, followed by the column detection phase discussed above. The proposed module counts the number of detected bars and determines whether the observed damage is Damage State 5 or 4. A detected longitudinal bar may consist of several separate instances (segments) due to the overlap by transverse bars (as shown in **Fig. 6.9**). The instances that have a similar x-coordinate (horizontal position) are merged into one instance. The centroid of pixels of each initial detection was used as the horizontal position.
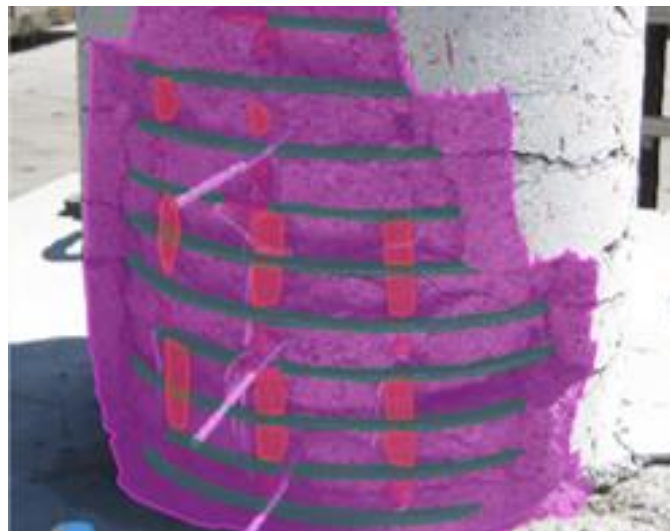
Figure 6.9 – Detection of Longitudinal and Transverse Bars

The spalled region analysis is performed if the above-discussed steps do not detect any components related to DS5 and/or DS4. The maximum length of the spalled region in any direction is needed in DS4 and DS3. The initial detection of spalling was in the form of polygons (a sequence of points at the boundary). To measure the longest length of the spalled region, the following algorithm was developed and implemented:

Table 6.1 – Algorithm to Determine Maximum Length of Spelled Region

Input: Points: a polygon represented as a sequence of N 2D-points
Output: max_dist: maximum width of the spalled area

```
max_dist = 0
for i in range (1 to N-1):
     for j in range (i+1 to N):
          dx = Points(i).x - Points(j).x
          dy = Points(i).y - Points(j).y
          cur_dist = sqrt(dx*dx + dy*dy)
          if max_dist < cur_dist
               max_dist = cur_dist
          end
     end
end
```

In addition to the maximum length, column diameter (in pixel unit) is also required to determine different damage states. The initial detection of the column boundaries was used to obtain the diameter. Due to the low-resolution region proposals in the Mask R-CNN architecture, the detected mask is not perfectly aligned to the boundary of a column. RANSAC algorithm (Fischler et al., 1981) was used to obtain two vertical lines of each column. RANSAC takes random samples from the contour of the mask and fits two vertical lines by excluding outlier points. Each line is represented as a linear equation. Since the column diameter (or side dimension) may be different along the y-axis of a 2D photograph due to the camera angle, the column diameter is calculated at the smallest y-coordinate of the bounding box of the spalled area. Finally, the maximum length of the spalled area was normalized to the column diameter by dividing the maximum spalled length to the column diameter, both in pixel units.

6.3 Crack Detection and Crack Angle

The DNN architectures designed for the instance segmentation task are not favorable to detect cracks because they are thin and irregular shapes. Furthermore, the number of cracks and their angles are needed in the present study. In this project, the crack detection task has been modeled as a patch classification problem, and the properties were extracted by processing the output of DNN. The input image was divided into image patches of 64 by 64 pixels based on a regular grid. MobileNet (Ver. 2) was used to classify patches into cracked and uncracked patches. A total of 20,458 image patches were extracted from the image dataset. Of which, 11,458 had cracking and 9,000 patches did not have any concrete cracking. **Figure 6.10** shows samples of cracked/uncracked concrete image patches.

(a) Uncracked (Two on Left)   (b) Cracked (Two on Right)

Figure 6.10 – Sample Image Patches

MobileNet (Ver. 2) is a lightweight model with less computation than other existing networks. **Figure 6.11** shows the flowchart of the implemented crack detection procedure, and **Fig. 6.12** shows the results of a sample analysis. The model takes image patches and classifies them into cracked or uncracked classes. Each image patch is cropped from a regular grid of the input image (damaged column). Subsequently, the classification of each patch results in a map of cracked and uncrack patches. Then, the connected crack patches were merged into a single object. Two conditions were used in the merging process: (1) the pixel distance between two patches should be less than the size of the patch, which is 64 pixels, and (2) the orientation difference between cracks of the adjacent patches should be less than 45 degrees. After merging the crack patches along the direction of cracks, each crack instance is represented as a bounding box containing the merged crack.
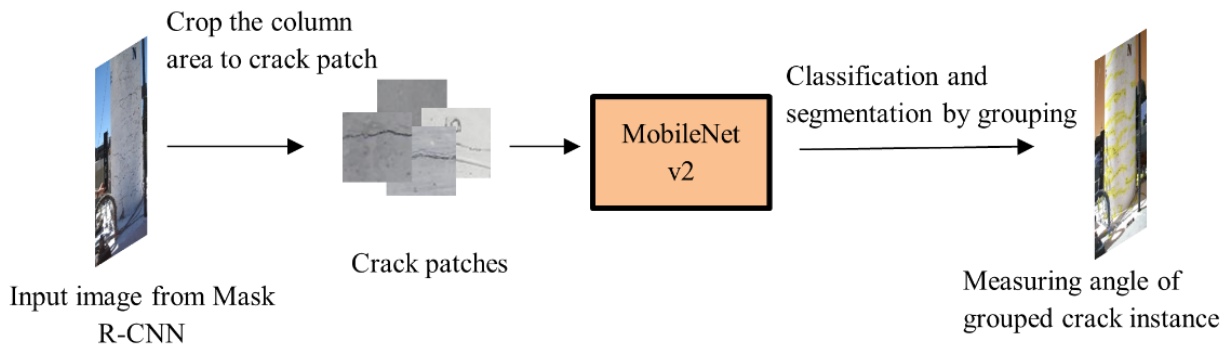
Figure 6.11 – Crack Detection and Analysis
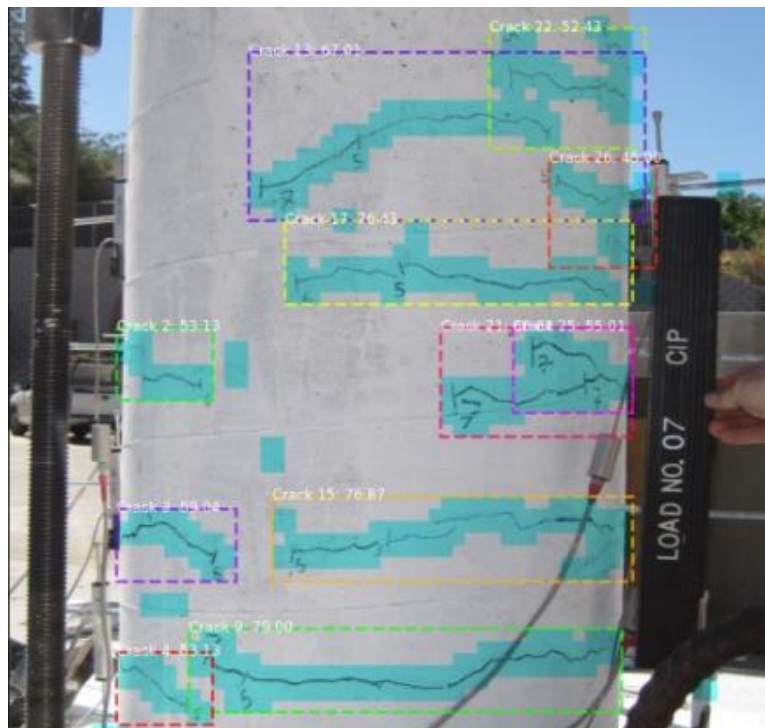
Figure 6.12 – Sample Crack Detection Analysis Using Patch-Based Method

A histogram was proposed in the present study to estimate the major angle of each crack. Since the crack path is locally noisy (cracks usually go around large aggregates) but generally follows a line from the start to the end, the histogram reveals the major angle along the path. Histogram of oriented gradient (HOG) (Dalal et al., 2005) was used to represent each crack instance and to determine the dominant orientation of the crack. Horizontal and vertical intensity gradients were calculated, and the magnitude and angle were used to form a histogram. **Figure 6.13** shows examples of the histogram of oriented gradient for three cases. In the figure, each bar represents 5 degrees. The maximum bar and the corresponding angle are selected as the representative orientation of the crack. Note that per proposed damage state definitions (**Table 3.2**), zero degree for a crack means it is a vertical crack, and 90 degree means the crack is horizontal, or perpendicular to the longitudinal axis of the column.

(a) 45 Degree (b) 80 Degree (c) 25 Degree
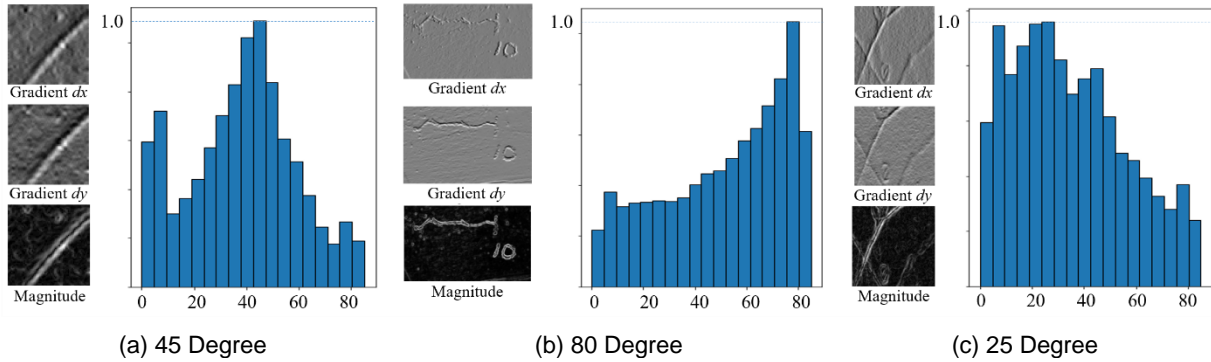
Figure 6.13 – Histograms of Oriented Gradient of Crack Instances

6.4 Damage Detection Results

For training the Mask R-CNN module, each image was labeled with four classes (column, spalling, transverse bar, and longitudinal bar) and one background class. The weight was initialized by pre-trained weights of the COCO dataset (Lin et al., 2014) with a batch size of 2 to fine-tune the network using the dataset collected in the present study. The model was trained with NVIDIA GeForce GTX 1080 Ti, which is equipped with 12GB GPU RAM. The backbone architecture was ResNet101 and trained for 70 epochs with a learning rate of 0.02. During the training, Mask R-CNN weights were updated using a multi-task loss function (**Eq. 6.1**), where $\mathcal{L}_{cls}$ is the log loss function over two classes (classification loss), $\mathcal{L}_{box}$ is the difference between the localization of ground truth and output result, and $\mathcal{L}_{mask}$ is defined as the average binary cross-entropy loss associated with the ground truth classes.

$$\mathcal{L} = \mathcal{L}_{cls} + \mathcal{L}_{box} + \mathcal{L}_{mask} \tag{6.1}$$

The MobileNet v2 for crack detection was trained with the dataset collected in this study, and this module takes an input size of 224×224. MobileNet v2 rescaled the crack patches, and the same GPU was used. The batch size was 96. Further, a batch normalization was used between layers, and the ReLU activation function was used. The loss function of this network was a categorical cross-entropy loss, and the learning rate was empirically chosen as 0.0001.

In the testing step, three shapes of RC columns (circular, octagonal, and rectangular) were evaluated. Note that the current rectangular column dataset does not include images for DS-1 to DS-3; thus, only DS-4 and DS-5 results were presented herein. **Figures 6.14** to **6.24** show sample computer vision analysis results, and **Tables 6.2** to **6.12** present a summary of each analysis. DS was also determined following the proposed definitions. In DS3 to DS5, each detected component was color-coded (red for columns, green for spalled region, blue for transverse bars, and purple for longitudinal bars).

Figure 6.14 – Sample Computer Vision Results for a Circular RC Column at DS1

Column Photo from Haber et al. (2013) with Author's Permission

Table 6.2 – Computer Vision Analysis Results for Circular RC Column in Fig. 6.14

Analysis Component	Computer Vision Analysis Results	Ground Truth (Actual)
Number of Horizontal Cracks	11	12
Number of Vertical Cracks	2	1
Maximum Length of Spalled Region (px)	N/A	N/A
Column Width (px)	N/A	N/A
Number of Transverse (Horizontal) Bars	N/A	N/A
Number of Longitudinal (Vertical) Bars	N/A	N/A
Damage State (DS)	**1**	**1**
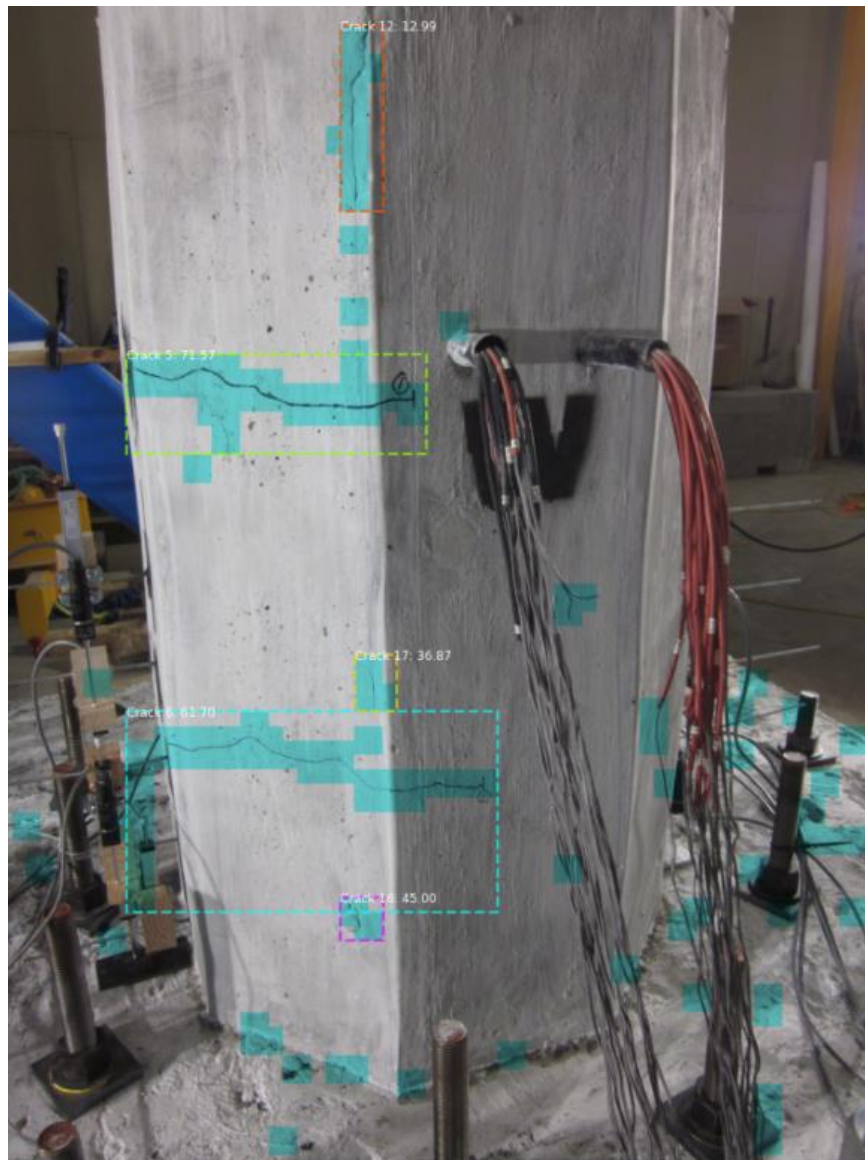
Figure 6.15 – Sample Computer Vision Results for an Octagonal RC Column at DS1

Table 6.3 – Computer Vision Analysis Results for Octagonal RC Column in Fig. 6.15

Analysis Component	Computer Vision Analysis Results	Ground Truth (Actual)
Number of Horizontal Cracks	5	2
Number of Vertical Cracks	2	0
Maximum Length of Spalled Region (px)	N/A	N/A
Column Width (px)	N/A	N/A
Number of Transverse (Horizontal) Bars	N/A	N/A
Number of Longitudinal (Vertical) Bars	N/A	N/A
Damage State (DS)	**1**	**1**
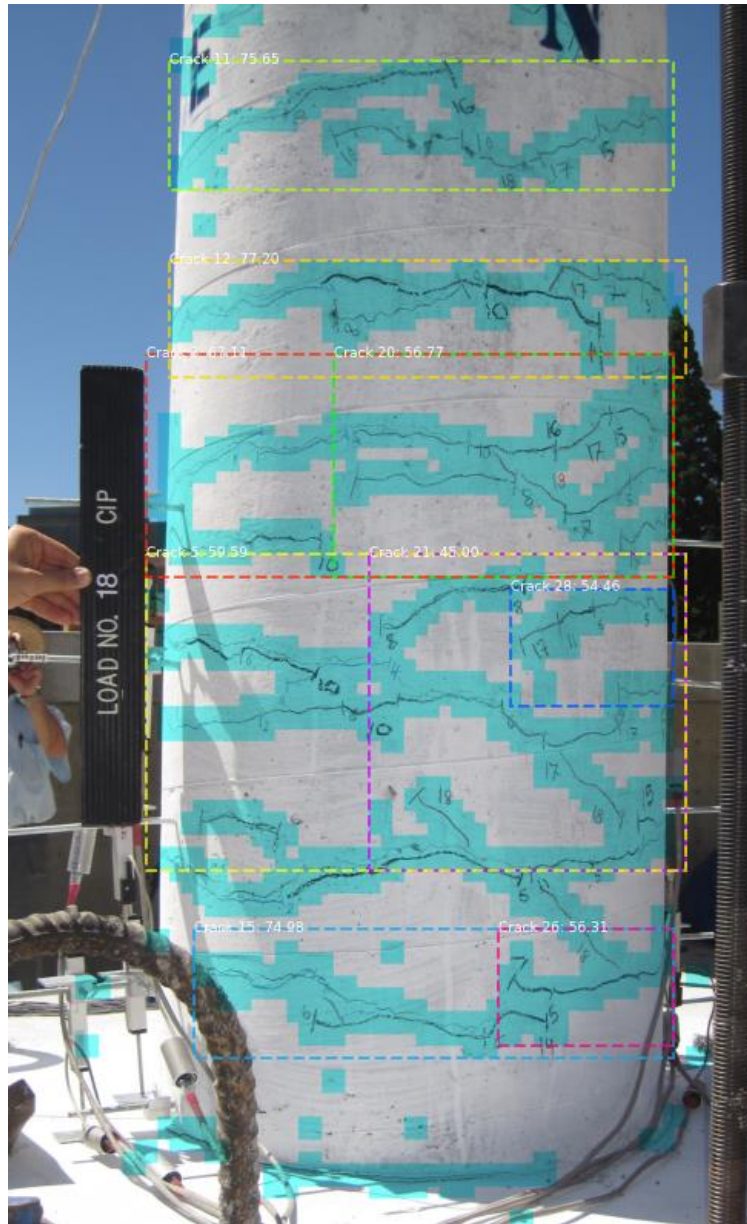
Figure 6.16 – Sample Computer Vision Results for a Circular RC Column at DS2

Column Photo from Haber et al. (2013) with Author's Permission

Table 6.4 – Computer Vision Analysis Results for Circular RC Column in Fig. 6.16

Analysis Component	Computer Vision Analysis Results	Ground Truth (Actual)
Number of Horizontal Cracks	9	10
Number of Vertical Cracks	4	3
Maximum Length of Spalled Region (px)	N/A	N/A
Column Width (px)	N/A	N/A
Number of Transverse (Horizontal) Bars	N/A	N/A
Number of Longitudinal (Vertical) Bars	N/A	N/A
Damage State (DS)	**2**	**2**
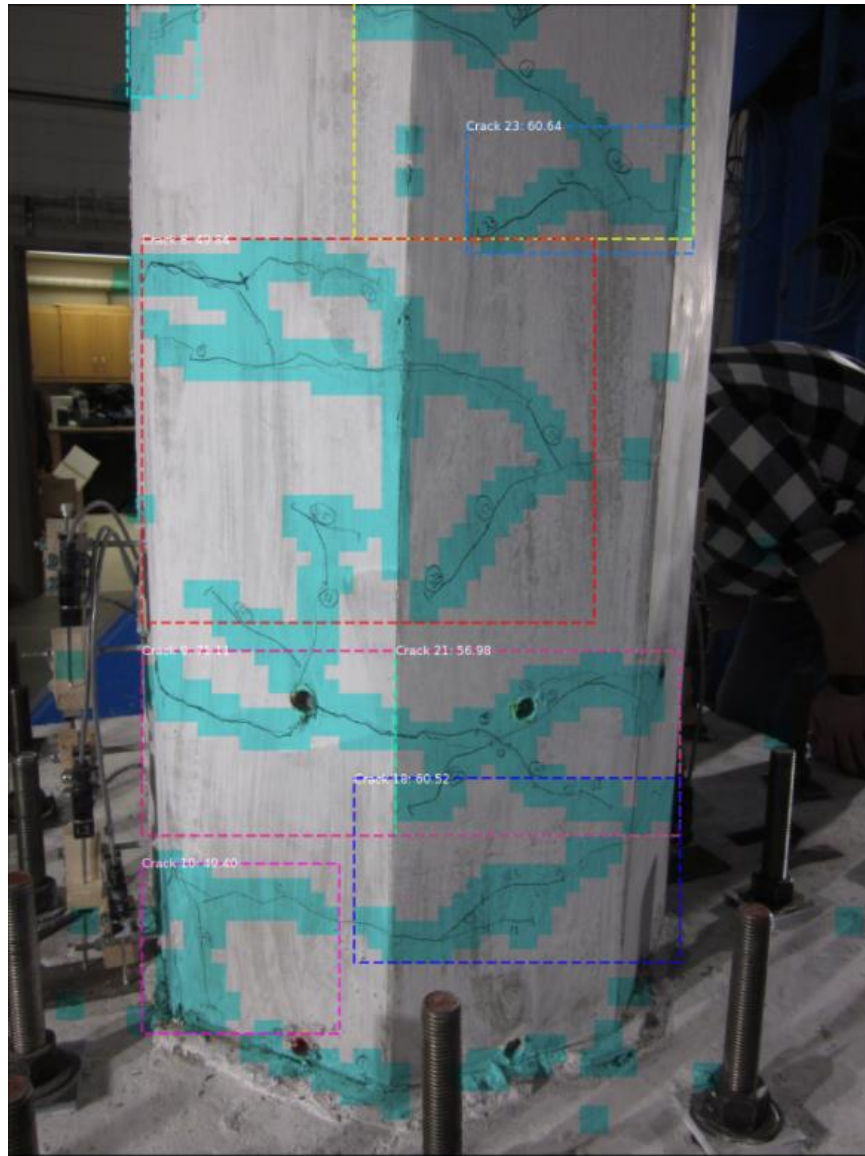
Figure 6.17 – Sample Computer Vision Results for an Octagonal RC Column at DS2

Table 6.5 – Computer Vision Analysis Results for Octagonal RC Column in Fig. 6.17

Analysis Component	Computer Vision Analysis Results	Ground Truth (Actual)
Number of Horizontal Cracks	2	3
Number of Vertical Cracks	5	5
Maximum Length of Spalled Region (px)	N/A	N/A
Column Width (px)	N/A	N/A
Number of Transverse (Horizontal) Bars	N/A	N/A
Number of Longitudinal (Vertical) Bars	N/A	N/A
Damage State (DS)	**2**	**2**
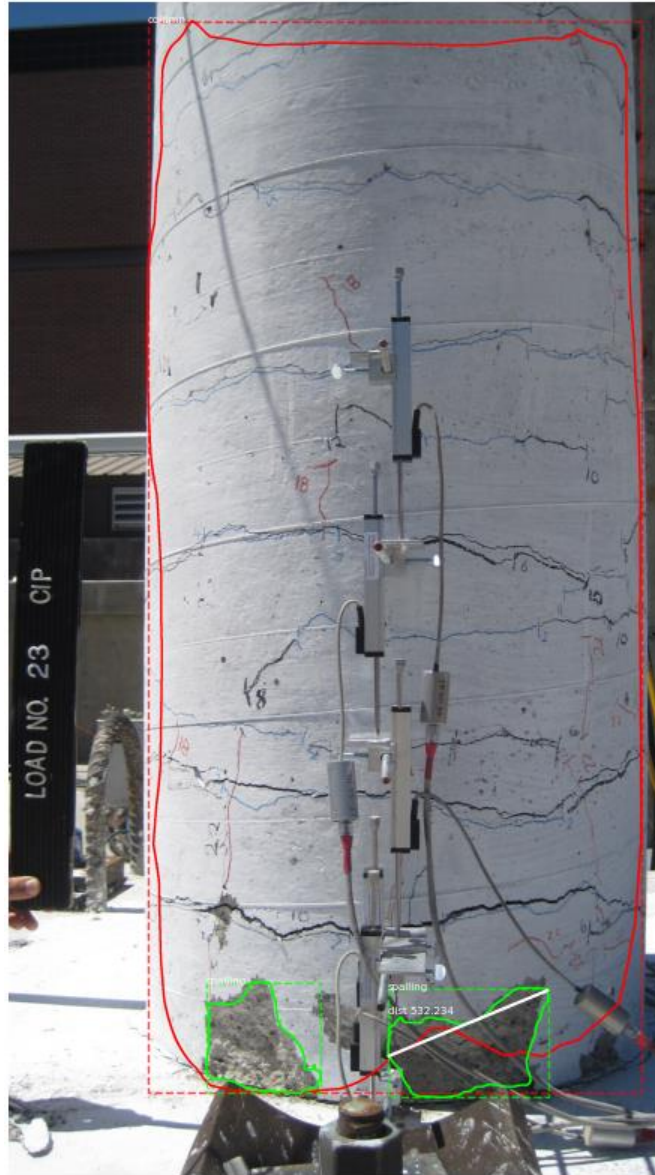
Figure 6.18 – Sample Computer Vision Results for a Circular RC Column at DS3

Column Photo from Haber et al. (2013) with Author's Permission

Table 6.6 – Computer Vision Analysis Results for Circular RC Column in Fig. 6.18

Analysis Component	Computer Vision Analysis Results	Ground Truth (Actual)
Number of Horizontal Cracks	N/A	N/A
Number of Vertical Cracks	N/A	N/A
Maximum Length of Spalled Region (px)	532	731
Column Width (px)	1610	1552
Number of Transverse (Horizontal) Bars	N/A	N/A
Number of Longitudinal (Vertical) Bars	N/A	N/A
Damage State (DS)	**3**	**3**
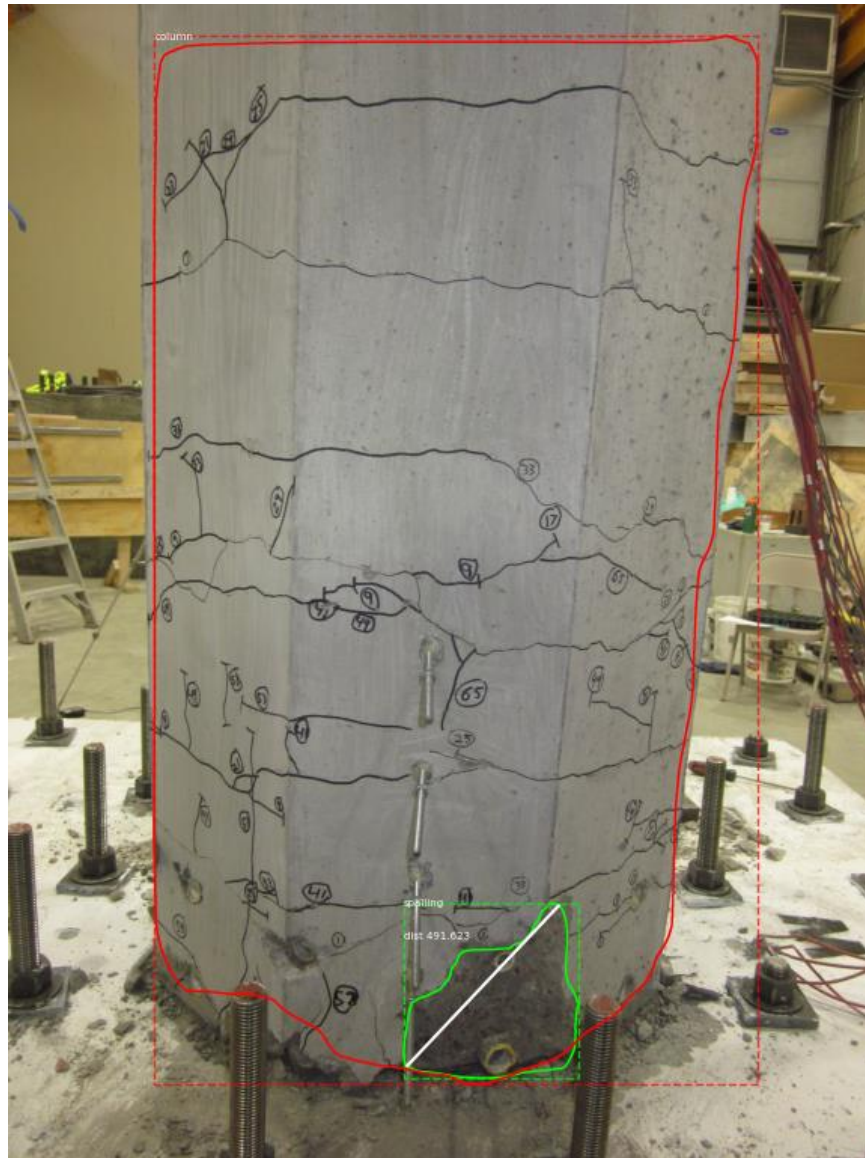
Figure 6.19 – Sample Computer Vision Results for an Octagonal RC Column at DS3

Table 6.7 – Computer Vision Analysis Results for Octagonal RC Column in Fig. 6.19

Analysis Component	Computer Vision Analysis Results	Ground Truth (Actual)
Number of Horizontal Cracks	N/A	N/A
Number of Vertical Cracks	N/A	N/A
Maximum Length of Spalled Region (px)	492	530
Column Width (px)	1610	1154
Number of Transverse (Horizontal) Bars	N/A	N/A
Number of Longitudinal (Vertical) Bars	N/A	N/A
Damage State (DS)	**3**	**3**
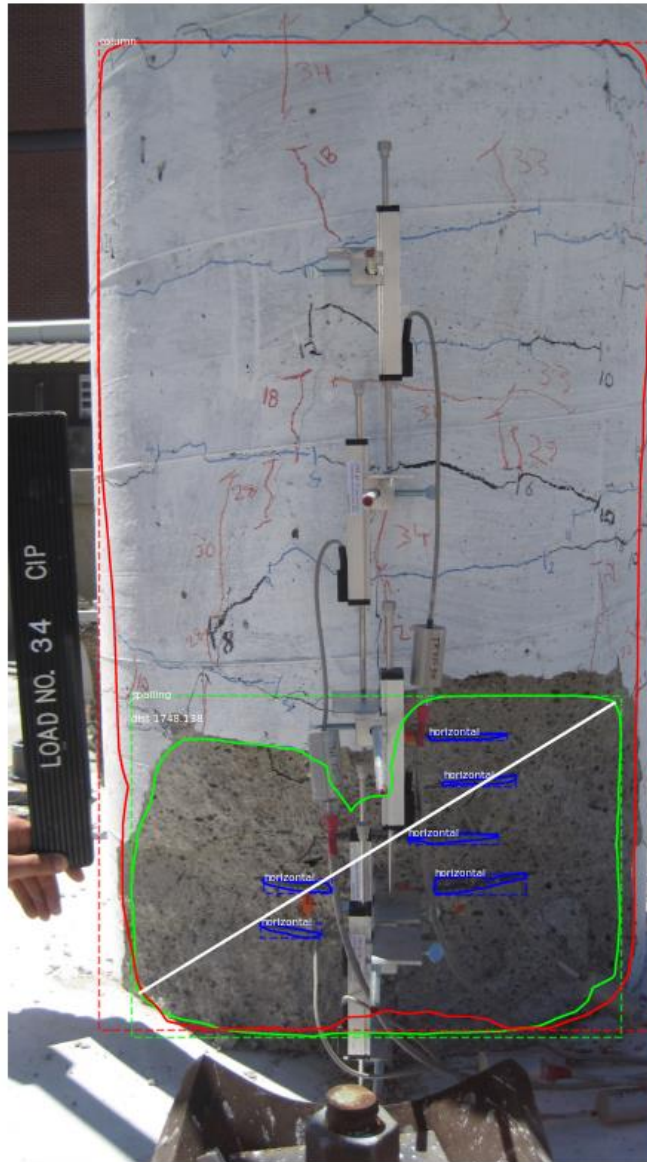
Figure 6.20 – Sample Computer Vision Results for a Circular RC Column at DS4

Column Photo from Haber et al. (2013) with Author's Permission

Table 6.8 – Computer Vision Analysis Results for Circular RC Column in Fig. 6.20

Analysis Component	Computer Vision Analysis Results	Ground Truth (Actual)
Number of Horizontal Cracks	N/A	N/A
Number of Vertical Cracks	N/A	N/A
Maximum Length of Spalled Region (px)	1748	1867
Column Width (px)	1810	1747
Number of Transverse (Horizontal) Bars	6	5
Number of Longitudinal (Vertical) Bars	N/A	N/A
Damage State (DS)	**4**	**4**
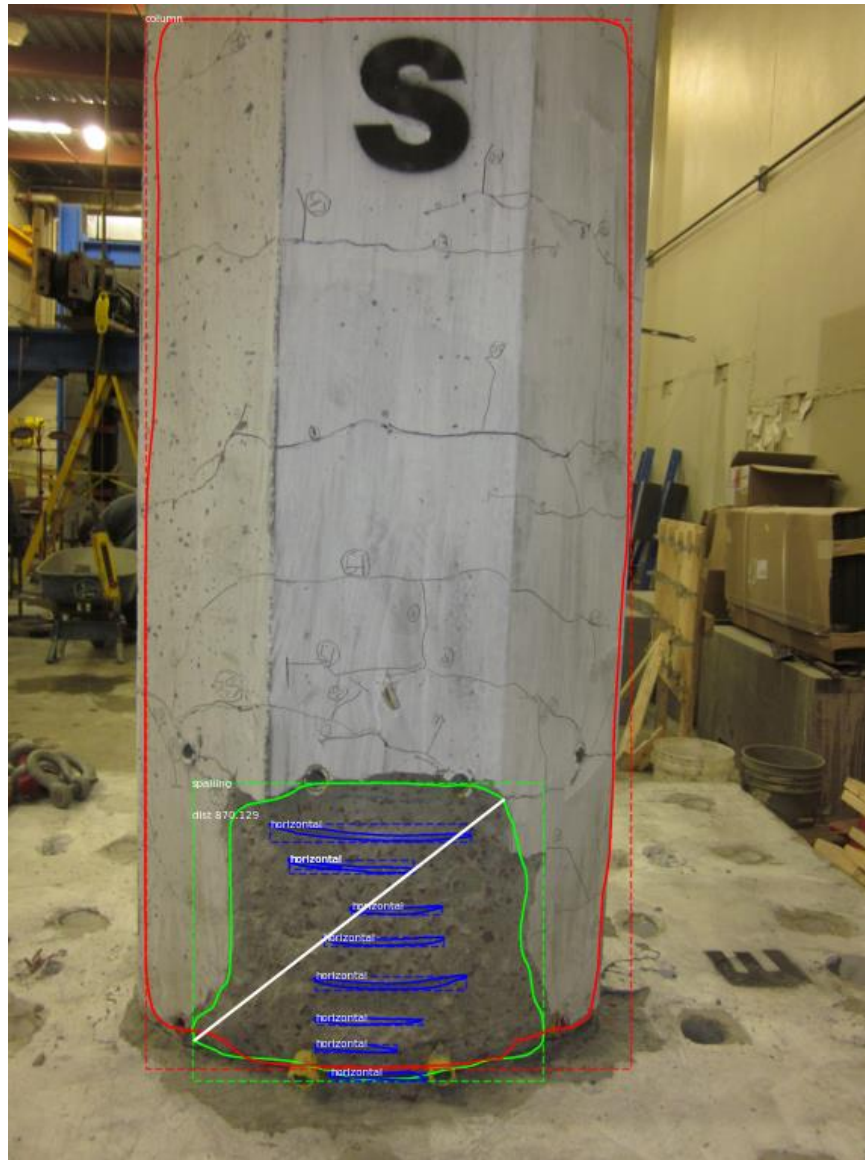
Figure 6.21 – Sample Computer Vision Results for an Octagonal RC Column at DS4

Table 6.9 – Computer Vision Analysis Results for Octagonal RC Column in Fig. 6.21

Analysis Component	Computer Vision Analysis Results	Ground Truth (Actual)
Number of Horizontal Cracks	N/A	N/A
Number of Vertical Cracks	N/A	N/A
Maximum Length of Spalled Region (px)	870	906
Column Width (px)	N/A	1058
Number of Transverse (Horizontal) Bars	8	8
Number of Longitudinal (Vertical) Bars	0	0
Damage State (DS)	**4**	**4**
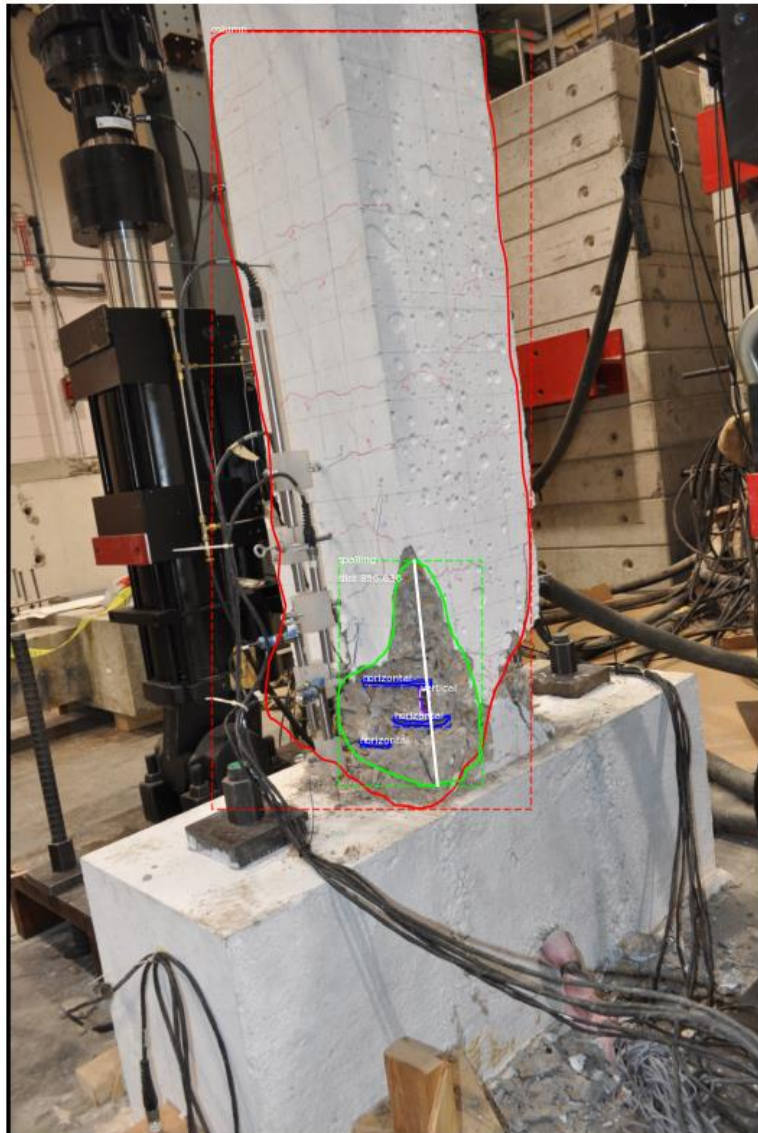
Figure 6.22 – Sample Computer Vision Results for a Rectangular RC Column at DS4

Column Photo from Nikoukalam and Sideris (2017) with Author's Permission

Table 6.10 – Computer Vision Analysis Results for Rectangular RC Column in Fig. 6.22

Analysis Component	Computer Vision Analysis Results	Ground Truth (Actual)
Number of Horizontal Cracks	N/A	N/A
Number of Vertical Cracks	N/A	N/A
Maximum Length of Spalled Region (px)	857	956
Column Width (px)	1021	1040
Number of Transverse (Horizontal) Bars	3	4
Number of Longitudinal (Vertical) Bars	1	1
Damage State (DS)	**4**	**4**
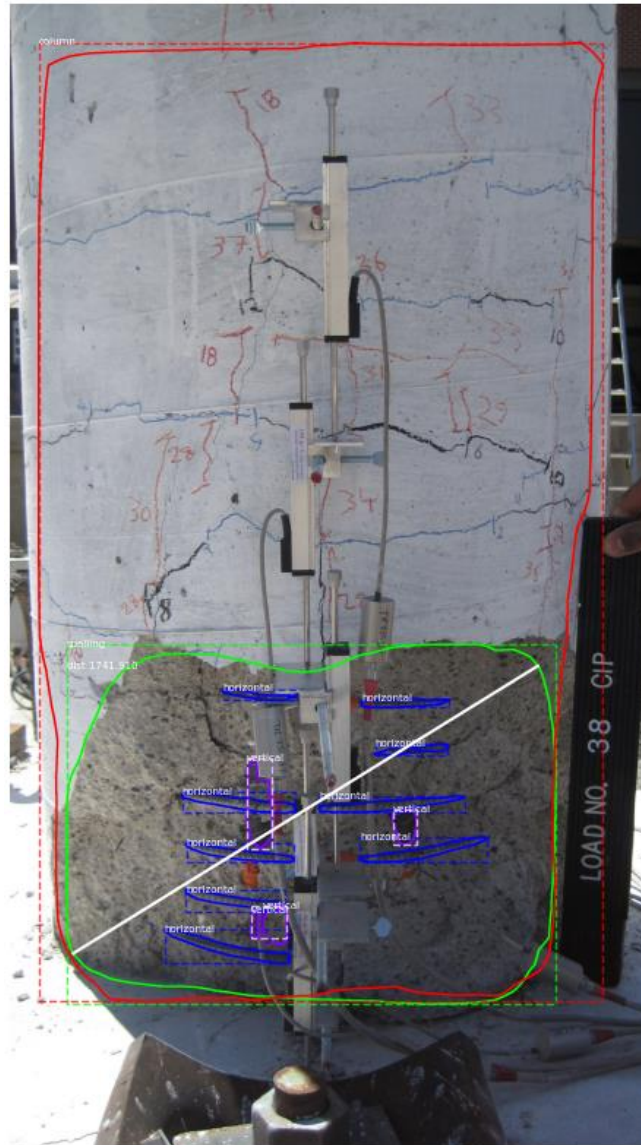
Figure 6.23 – Sample Computer Vision Results for a Circular RC Column at DS5

Column Photo from Haber et al. (2013) with Author's Permission

Table 6.11 – Computer Vision Analysis Results for Circular RC Column in Fig. 6.23

Analysis Component	Computer Vision Analysis Results	Ground Truth (Actual)
Number of Horizontal Cracks	N/A	N/A
Number of Vertical Cracks	N/A	N/A
Maximum Length of Spalled Region (px)	1742	1904
Column Width (px)	N/A	1847
Number of Transverse (Horizontal) Bars	6	6
Number of Longitudinal (Vertical) Bars	2	2
Damage State (DS)	**5**	**5**
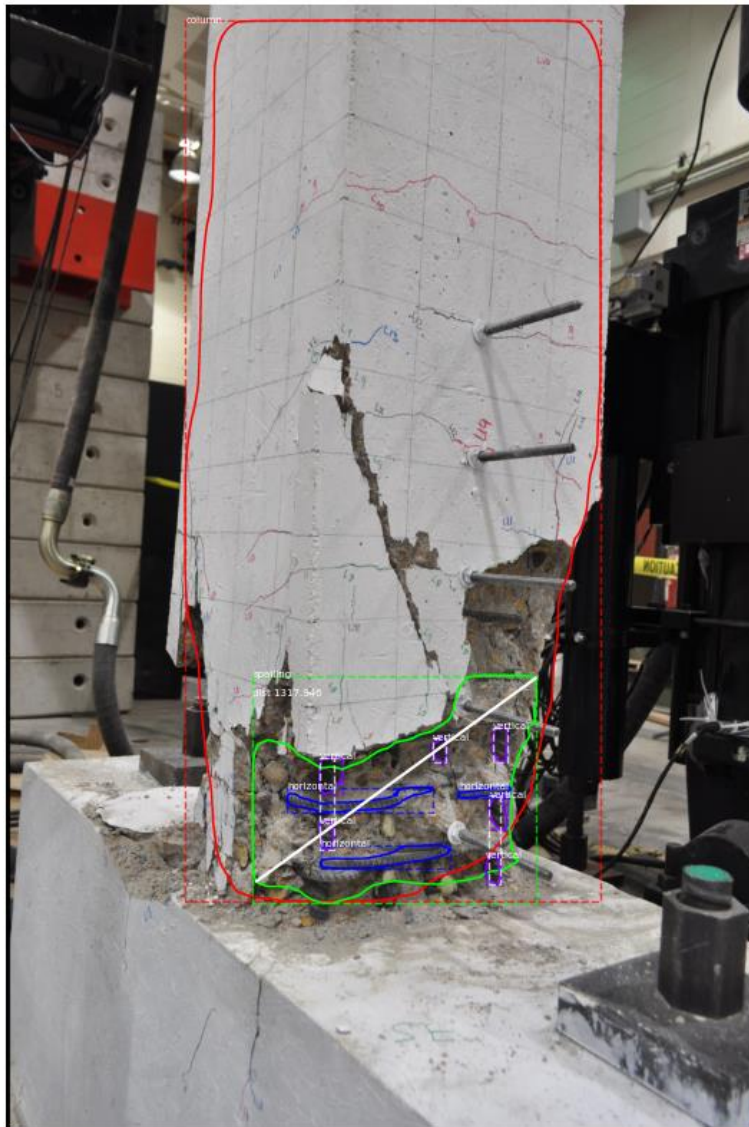
Figure 6.24 – Sample Computer Vision Results for a Rectangular RC Column at DS5

Column Photo from Nikoukalam and Sideris (2017) with Author's Permission

Table 6.12 – Computer Vision Analysis Results for Rectangular RC Column in Fig. 6.24

Analysis Component	Computer Vision Analysis Results	Ground Truth (Actual)
Number of Horizontal Cracks	N/A	N/A
Number of Vertical Cracks	N/A	N/A
Maximum Length of Spalled Region (px)	1317	1887
Column Width (px)	N/A	1538
Number of Transverse (Horizontal) Bars	3	5
Number of Longitudinal (Vertical) Bars	2	4
Damage State (DS)	**5**	**5**

6.4 Performance Evaluation

The performance of the trained Mask R-CNN was evaluated in terms of "precision" and "recall", which are calculated by the instances of true positives (TPs), true negatives (TNs), false positives (FPs), and false negatives (FNs). The precision is the ratio of the true positives to the overall positive responses (TPs+FPs), and the recall is the ratio of the true positive to the sum of the true positives and false negatives. Each number is determined from the overlapping areas between resulted detection (masks) and the ground truth (actual). The evaluation was performed on 20% of the dataset (equivalent to 46 images) which was set aside for testing. **Figure 6.25** illustrates the concept of Intersection over Union (IoU), in which the red box is the ground truth, and the blue box is the predicted output of each object. Each object is classified as TP if the IoU is over 0.5, and is classified as FP if IoU is less than 0.5. FN is the case when the neural network fails to detect an object stated in the ground truth image.

Intersection over Union =
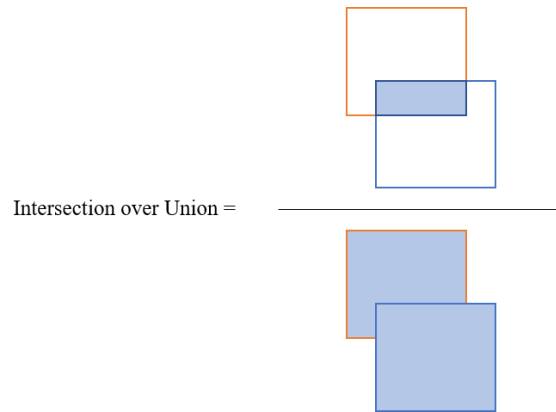
Figure 6.25 – Intersection over Union (IoU)

$$Precision = \frac{\#\,TPs}{\#TPs + \#FPs} \tag{6.2}$$

$$Recall = \frac{\#\,TPs}{\#TPs + \#FNs} \tag{6.3}$$

The performance of the trained Mask R-CNN module was measured in terms of the precision and recall for localization and segmentation. The localization performance was measured based on the bounding boxes, and the segmentation performance was measured based on pixel-level detection results. **Table 6.13** presents the average precision/recall for each category (column, spalling, and exposed bars). There were 41 columns, 72 spalled areas, 56 transverse bars and 31 longitudinal bars in the 42 testing images. The result shows that the performance of localization is above 90 percent and, similarly, the segmentation performance is over 88.9 percent.

Table 6.13 – Evaluation of Target Deficiency Detection for Each Component

Components	Number of Instances	Localization Precision (%)	Localization Recall (%)	Segmentation Precision (%)	Segmentation Recall (%)
Column	41	90.13	90.91	88.90	89.23
Spalled area	72	95.28	95.88	93.97	88.71
Transverse bar	56	95.27	95.82	92.71	93.14
Longitudinal bar	31	92.31	92.79	91.83	92.17
	Average	93.24	93.85	91.10	90.81

Furthermore, the crack classification network was evaluated using precision and recall. A total of 4,842 images (2,320 images with cracks and 2,522 images without cracks) were tested, and the precision and recall scores were measured for each class (cracked, uncracked, **Table 6.14**). Overall, the trained model showed over 95% precision and recall. The classifier showed slightly better performance on uncracked images. On average, the developed model showed 97.4% and 96.1% precision and recall, respectively.

Table 6.14 – Evaluation of Crack Classification

Component	Number of Images	Precision (%)	Recall (%)
Cracked	2,320	96.32	95.28
Uncracked	2,522	98.45	96.94
	Average	97.38	96.11

Figures 6.26 and **6.27** show sample results of the proposed approach on RC bridge columns damaged under actual earthquakes. CVT determined the damage state of the column in **Fig. 6.26** as DS2 due to the number of detected vertical crack segments, which matches if the damage assessment is done by an inspector following the proposed damage state definitions (**Table 3.2**). However, CVT did not report damage state for columns in **Fig. 2.27** mainly because the column bounding box could not be detected. As discussed before, the column detection is an essential step in the proposed computer vision analysis. However, if the input images are taken too close or too far from the column, the neural network model is not able to detect columns and therefore the subsequent steps, which uses the column information, are not performed. As a result, in **Fig. 6.27**, the tool was not able to determine the damage states even though the spalled areas are detected. This issue can be resolved by engaging the user in the process. For example, when the tool cannot see the columns, the user can draw the column boundaries for the software to proceed.

Another limitation of the developed approach could be when parts of the columns are not visible or covered by other objects (steel jacket, FRP jacket, etc.). **Figure 2.28** shows sample cases where the proposed CVT was not able to detect column and then damages. By nature, a deep neural network-based approach requires a huge annotated dataset. Even though mitigation techniques, such as transfer learning and data augmentation, have been used in developing the tool, the dataset is much smaller than that of typical image classification datasets (e.g., 14 million images). The use of deep generative models (Goodfellow et al., 2020) can be a solution to the domain shift problem and data insufficiency problem.

Figure 6.26 – Computer Vision Analysis Results for Real Earthquake Caused Damaged RC Bridge Column

Computer Vision Tool Estimated DS-2

Photo Courtesy: Dr. Manuel Coll (Puerto Rico DOT)
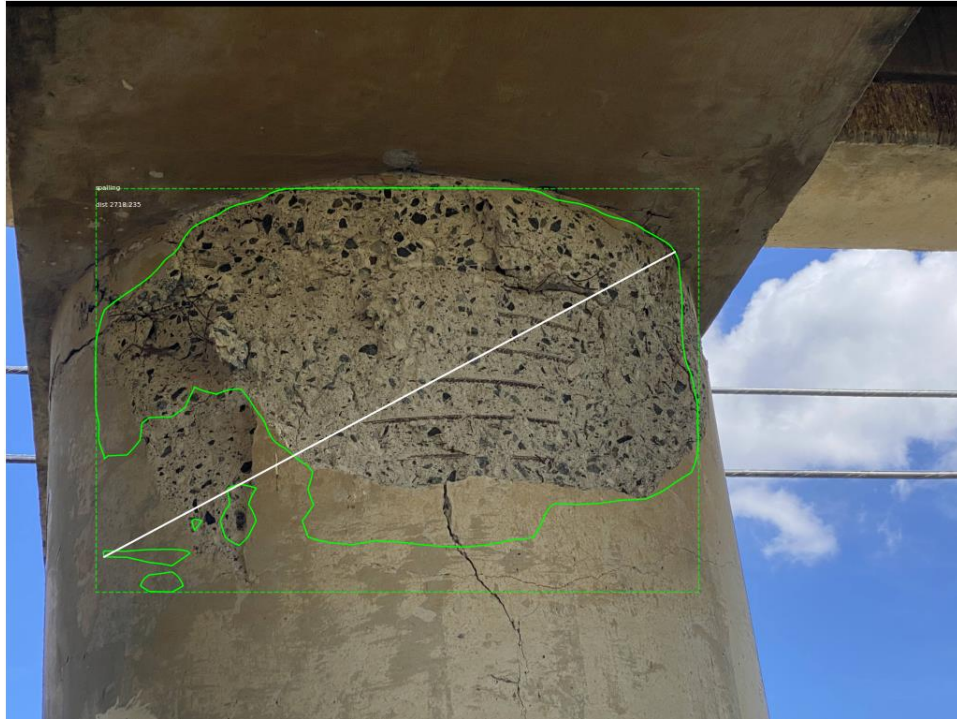
Figure 6.27 – Computer Vision Analysis Results for Real Earthquake Caused Damaged RC Bridge Column

Computer Vision Tool could not estimate Damage State

Photo Courtesy: Dr. Manuel Coll (Puerto Rico DOT)

Figure 6.28 – Samples of Detection Failure Cases

6.5 Summary

This chapter presented a cascade deep neural network for analyzing post-earthquake bridge serviceability. The proposed approach consists of Mask R-CNN and MobileNet deep learning architectures, and additional analysis modules. Mask R-CNN consists of region proposal network, classification, and mask segmentation network. It was used in the present project to detect and segment columns, spalling, and rebars. MobileNet used in the present project classifies image patches into cracked and uncracked ones. With the initial detection and segmentation of the components, damage state is determined by subsequent analysis of the numbers of vertical and/or horizontal cracks, the maximum length of the spalled region with respect to the column width, and the number of exposed vertical and/or horizontal bars. The deep learning models were trained with 216 images for 100 epochs. The performance was measured for 42 testing images containing 41 columns, 72 spalled areas, 56 transverse bars, and 31 longitudinal bars. Precision and Recall were used as the performance measure. On average, the trained model showed 93% of localization performance and 91% of segmentation performance. In crack detection, a total of 4,842 image patches were evaluated and the tool showed 97% precision and 96% recall, on average.

As future study, the deep neural network architectures for detecting buckling of bars and total collapse of structures, which has been described in Damage State 6, need to be developed. In addition, to achieve real-time performance, the computation cost for Mask R-CNN will be optimized by modifying the underlaying backbone architecture and region proposal networks for the objects of interests.

CHAPTER 7. PROPOSED POST-EARTHQUAKE BRIDGE COLUMN EVALUATION METHODOLOGY

7.1 Introduction

Quick and safe assessment of bridges, specifically RC bridge columns, are needed after an earthquake to maximize serviceability and access to the affected sites. Quantitative definitions for RC bridge column damage states were proposed in Chapter 3, which is suited for computer programing. Empirical equations were developed in Chapter 5 to estimate drift demands of RC bridge columns at different damage states. Furthermore, a computer vision software equipped with artificial intelligence (AI) was developed in Chapter 6 to determine the RC bridge column damage states using photographs. A methodology is proposed herein to perform different levels of post-earthquake assessments for RC bridge columns using the tools and techniques developed in the present project.

7.2 Proposed Post-Earthquake Bridge Column Serviceability Assessment

NCHRP 833 (Olsen et al., 2016) proposed a four-stage post-event assessment for transportation infrastructure (**Table 2.3 & Fig. 2.4**): (1) Fast Reconnaissance (FR), (2) Preliminary Damage Assessment (PDA), (3) Detailed Damage Assessment (DDA), and (4) Extended Investigation (EI). Furthermore, the NCHRP report marks and tags each affected structure using three levels:

- Inspected: Green tagged, meaning no damaged was observed,
- Limited Use: Yellow tagged, limiting the access to light traffics and first responders, and
- Unsafe: Red tagged, the structure must be closed to all traffics.

Due to a lack of national and unified specifications for bridges, the four-level assessment and the three-level coding proposed in the NCHRP 833 report were adopted in the present project to assess bridges after earthquakes. Of the four assessment levels, a relatively quick post-earthquake evaluation of RC bridge columns at PDA and DDA levels is feasible due to the incorporation of computer tools. **Figure 7.1** shows a flowchart on how to carry out PDA and DDA using the tools and methods developed in the present project. PDA is done using photographs of columns and DDA requires the column detailing in addition to the photos. The steps to perform PDA and DDA are further discussed herein.

7.3 Preliminary Damage Assessment (PDA)

In PDA, the user (who may not necessarily be a trained inspector or bridge engineer, but an authorized local personnel) will upload the bridge column damage photograph(s) to the computer vision tool (CVT). The photographs can be taken by a cellphone, tablet, or drone. Per each photo of the column, this tool counts the exposed longitudinal and transverse bars, if any, measures the maximum spalled region length, if any, and counts the number of horizontal and vertical cracks. Subsequently, the column damage state (DS) is determined, and its serviceability is evaluated based on the proposed DS definitions (**Table 7.1**). For example, if DS4 is reported by CVT, the bridge is "yellow" tagged meaning that it should be open only to light traffics and first responders.
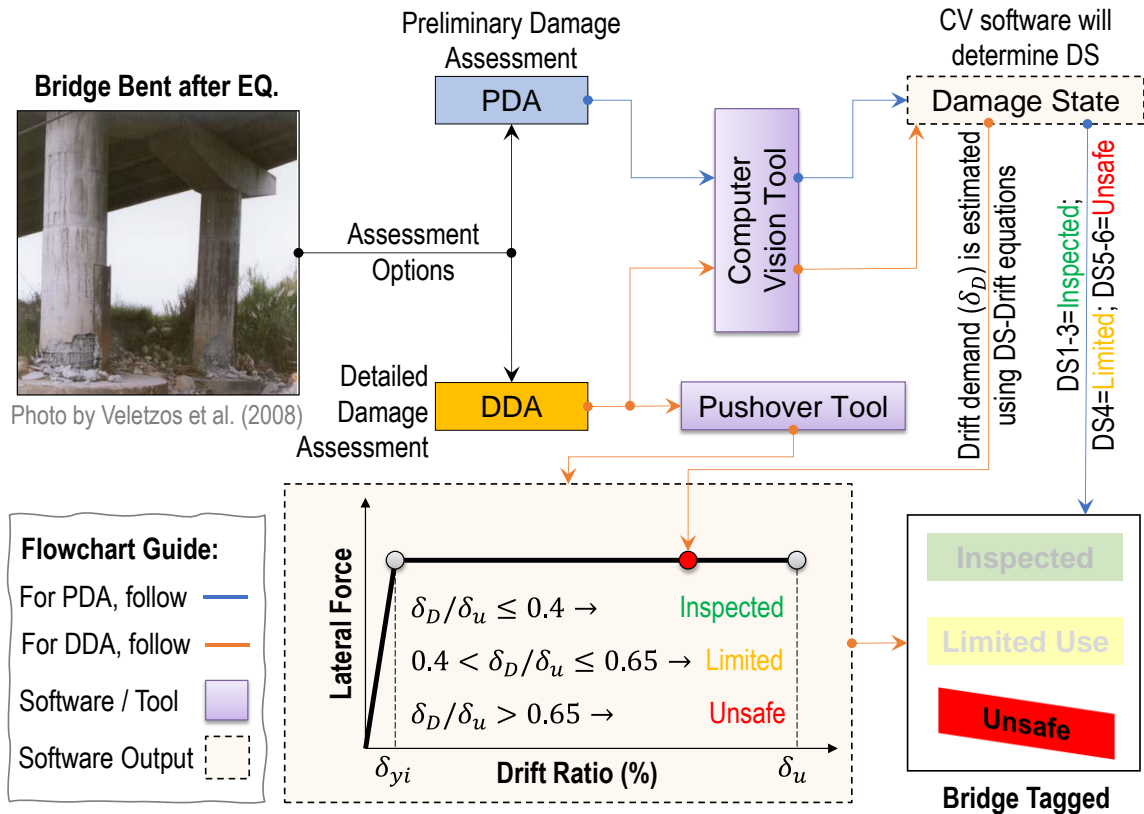
Figure 7.1 – Proposed Post-Earthquake RC Bridge Column Evaluation Using Computer Vision

Table 7.1 – Preliminary Damage Assessment (PDA) of RC Bridge Columns Using Damage States

Damage State	Qualitative Damage Description	Quantitative Damage Description for Computer Vision	Equivalent Drift Demand	Tag as
1	Hairline cracks	Horizontal cracks each with an angle of $|\theta| > 80°$ (**Fig. 3.1**)	$\delta_{DS1} \approx 0.09\delta_{DS6}$	Inspected
2	Theoretical first yielding of longitudinal bars	At least three diagonal cracks each with an angle of $|\theta| < 70°$ (**Fig. 3.2**)	$\delta_{DS2} \approx 0.15\delta_{DS6}$	Inspected
3	Extensive cracks and spalling	Length of spalled region in any direction at any column face is greater than $0.1D_c$ but smaller than $0.3D_c$ (**Fig. 3.3**)	$\delta_{DS3} = 0.3\delta_{DS6}$	Inspected
4	Visible transverse and/or longitudinal reinforcement	Length of spalled region in any direction at any column face is greater than $0.5D_c$ and detect one transverse bar and/or one longitudinal bar (**Fig. 3.4**)	$\delta_{DS4} = 0.5\delta_{DS6}$	Limited Use
5	First buckling and/or rupture of longitudinal bar(s), crushing of core concrete	Detect the first buckling and/or rupture of longitudinal bar(s), and/or detect at least two longitudinal bars and three transverse bars (**Fig. 3.5**)	$\delta_{DS5} = 0.8\delta_{DS6}$	Unsafe
6	Total collapse in which the permanent drift ratio exceeds 10%	The angular change of the line connecting the column ends with respect to the column initial position exceeds 10° ($|\alpha| > 10°$) (**Fig. 3.6**)	$\delta_{DS6} \approx \delta_u$	Unsafe

Notes: α is the angle between the column axial direction before and after the deformation; θ is the angle between the crack and the undeformed column axial direction; and D_c is the undamaged column diameter or largest side dimension.

In PDA, the tagging is done using images, and a pushover analysis of the column is not directly required as part of the evaluation. The pushover analysis is somewhat embedded in the process since each DS is equivalent to a drift ratio as discussed in Chapter 5 and summarized in **Table 7.1**. DS1 and DS2 fall

within the linear-elastic range of the column pushover curve (e.g., the approximated pushover discussed in **Sec. 5.3.2**) thus a column with DS1 or DS2 will have a large, reserved displacement capacity before failure. Furthermore, columns at DS3 will have 70% reserved displacement capacity. Therefore, columns rated with DS1 through DS3 in PDA are safe to be open to any traffic and can be tagged "green". Columns with DS4 have a displacement demand to capacity ratio of 50%, and may be tagged "yellow" with a limited serviceability. Nevertheless, the safety margin before the failure for columns with DS5 and DS6 is very narrow to none, and the failure is imminent. Such columns must be tagged "red", and the bridge must be closed immediately.

7.4 Detailed Damage Assessment (DDA)

In DDA, DS of the affected column should be determined, and the column pushover curve should be generated for the complete analysis. DS is determined using CVT (**Ch. 6**). Subsequently, the column drift demand is determined using the proposed DS based drift equations (**Table 5.2**). OpenSees or any other structural analysis software may be used to carry out a pushover analysis. Note that if the approximated idealized pushover curve (**Table 5.4**) is used in lieu of an actual pushover analysis, the results of DDA and PDA are the same thus the benefits of DDA may not be realized. Then, the estimated drift demand should be mapped on the pushover curve. Based on the drift demand to the drift capacity ratio (δ_D/δ_u), the bridge column serviceability can be assessed (**Table 7.2**).

Nevertheless, DS-based drift demand equations only estimate six drifts while a range of drifts per serviceability is needed in DDA (**Fig. 7.2**). It is proposed to use the average of DS3 and DS4 drifts as the end limit for the "inspected" serviceability range and to use the average of DS4 and DS5 drifts as the start point of the "unsafe" region. For example, the DS4 drift is 50% of that for DS6, and the DS5 drift is 80% of the DS6 drift. Thus, the unsafe serviceability range starts at 65% of the failure drift.

Table 7.2 – Drift Demand to Capacity Ratio in Detailed Damage Assessment (DDA) of RC Bridge Columns

Damage State	Drift Demand (δ_D)	Drift Capacity (δ_u)	Drift Demand to Capacity Ratio	Tag as
Determine DS1-6 using the computer vision tool (Sec. 5.2)	Estimate drift demand using the proposed damage state based drift equations (Table 5.2)	Obtain the drift capacity through a pushover analysis (e.g., generic OpenSees models for RC bridge columns, Sec. 5.3)	$\delta_D/\delta_u \leq 0.4$	Inspected
			$0.4 < \delta_D/\delta_u \leq 0.65$	Limited Use
			$\delta_D/\delta_u > 0.65$	Unsafe

Figure 7.2 – Serviceability Range for RC Bridge Columns in Detailed Damage Assessment (DDA)

7.5 Cloud-Based RC Bridge Column Post-Earthquake Assessment Tools

To facilitate the implementation of the proposed PDA and DDA, a website was developed to perform these analyses for RC bridge columns. When a damage photo of an RC bridge column is uploaded, the website runs the AI computer vision tool (**Ch. 6**) for PDA and DDA, and also OpenSees (**Ch. 5**) for DDA on a server and reports back to the user a summary result for PDA and DDA. Sample results for PDA and DDA using the cloud-based tools are shown in **Fig. 7.3-7.4**. **Appendix B** of the present report includes the details of the bridge assessment website.

Preliminary Damage Assessment - Results

Level 2
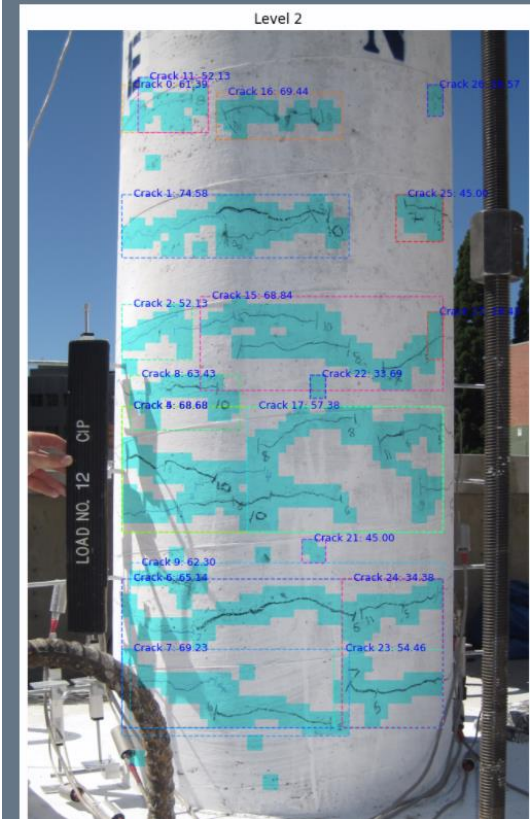
Number of Horizontal Cracks:

14

Number of Vertical Cracks:

6

Maximum Length of Spalled Region(% of column diameter of side dimension):

N/A

Number of exposed Transverse (Horizontal) Bars:

N/A

Number of exposed Logitudinal (Vertical) Bars:

N/A

Damage State:

Level 2

Bridge Evaluation:

Safe - Bridge can be opened

Get a copy of the report

Figure 7.3 – Sample Results of Cloud-Based Tools for Bridge Column Preliminary Damage Assessment

Detailed Damage Assessment - Results
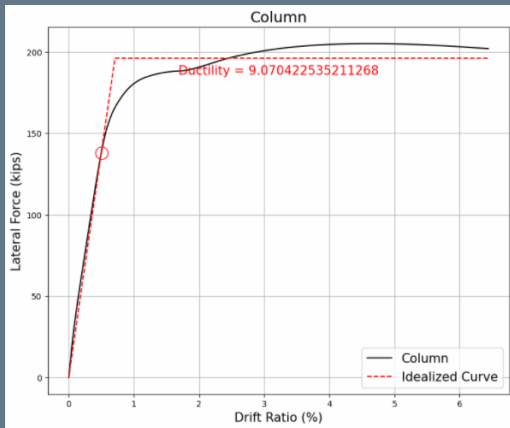
Summary of Pushover Analysis

Pushover analysis by OpenSees

Idealized Yield Drift: 0.71%

Drift Capacity: 6.44%

Demand

Demand analysis using estimated damage state

Damage State: Level 2

Drift Demand: 0.89%

Bridge Assessment:

Drift Demand to Capacity Ratio: 0.14

Inspected - Bridge can be opened

Figure 7.4 – Sample Results of Cloud-Based Tools for Bridge Column Detailed Damage Assessment

116

CHAPTER 8. SUMMARY AND CONCLUSIONS

8.1 Summary

Even though bridges are designed for the "collapse prevention" performance level, they may damage under large earthquakes. For reinforced concrete (RC) bridges, the columns are usually the main source of ductility during an earthquake in which concrete cover, core, and reinforcement may damage, and the column may experience a large permanent lateral deformation. A quick assessment of bridges immediately after severe events is needed to maximize serviceability and access to the affected sites, and to minimize casualties and costs.

The main goal of this project was to accelerate post-earthquake serviceability assessment of RC bridge columns using "computer vision". When sending trained personnel to the affect sites is limited or will take time, local personnel equipped with an assessment software (on various platforms such as mobile applications, cloud-based tools, or built-in with drones) can be deployed to evaluate the bridge condition. The project was focused on the damage assessment of modern RC bridge columns after earthquakes.

To achieve the project goal, several tasks were completed. First, the literature was reviewed to collect information on the visual assessment of RC bridge columns, to identify existing RC bridge column test databases, and to synthesize the latest developments on computer vision. Furthermore, resources such as Earthquake Engineering Research Institute (EERI), Federal Highway Administration, (FHWA), and Structural Extreme Events Reconnaissance (StEER) were reviewed to collect reconnaissance data for bridges.

The literature review showed that current definitions of RC bridge column damage types and/or damage states are mostly qualitative and somewhat subjective. Therefore, a new definition was proposed to quantitatively categorize RC bridge column damage states at six levels, which are suitable for a computer programming.

A few databases were identified in the literature that collected RC column experimental data. Nevertheless, they included a mix of building and bridge columns, and standard and substandard columns. In the present project, the most comprehensive test database specific to modern RC bridge columns including more than 30 parameters was compiled. The column parameters and notations included in the database were based on those defined in AASHTO SGS for consistency.

Previous studies tried to relate post-earthquake conditions of RC bridge columns to seismic demands. Nevertheless, they did not systematically quantify seismic demands for a wide range of damage. For example, Berry and Eberhard (2008) provided drift-based equations for RC bridge columns at cover spalling, bar buckling, and bar fracture. In the present project, the new RC bridge column experimental database was statistically analyzed to estimate RC bridge column drift demands at the six damage states defined in the present study.

A generic OpenSees model following the AASHTO SGS requirements was developed to obtain pushover response of any circular RC bridge column using only eight parameters. The accuracy of the generic model was evaluated by comparing the pushover results of four columns tested in past 10 years. This tool was then incorporated in a website.

Subsequently, an artificial intelligence (AI) enabled software was developed based on a photograph database of RC bridge columns to quickly detect cracking, spalling, and reinforcement, to comment on the RC column damage state, and to tag (green, yellow, or red) the column/bridge based on the extent of the damage. More than 3000 photographs of damaged RC bridge columns were compiled. Of which, 216 images with 100 epochs were used for the network training (the one for the spalling and rebar detection not cracking), and 42 images were utilized for testing the neural network. Furthermore, 20,458 photographs of concrete with (11,458) and without (9,000) cracking were used in the training and testing of the network. Approximately, 76% of the database was used for the training and 24% for the testing. An angular histogram was proposed in the present study to estimate the major angle of each crack. Since the crack path is locally noisy (cracks usually go around large aggregates) but follows a general line from the start to the end, the histogram reveals the major angle along the path.

Finally, a flowchart was proposed to perform both Preliminary Damage Assessment (PDA) and Detailed Damage Assessment (DDA) of RC bridge columns using the tools and methods developed in the project. Three serviceability levels (inspected, limited use, and unsafe) were adopted from the literature to tag bridge columns after an earthquake.

8.2 Conclusions

The following conclusions can be drawn based on the analytical, statistical, and computer vision studies:

- The literature lacks a systematic reconnaissance database for bridges especially columns after earthquakes. The damage of only a few bridges after recent earthquakes has been documented/published.
- The proposed definitions for RC bridge column damage states are quantitative and may be used in computer programs for quick identification of various damage types and levels.
- The most comprehensive RC bridge column test database collected in the present project currently includes 222 circular and 68 rectangular columns, and can be accessed through a public domain.
- The empirical equations developed in the present project to estimate RC bridge column drift demands at the six damage states showed a reasonable accuracy for a large pool of test data. The equations were further validated using a half-scale octagonal bridge column that was not in the database.
- The drifts corresponding to the proposed six-level damage states cover the full range of the column pushover response, and are proposed as a baseline for serviceability assessments.
- With a reasonable accuracy, the generic OpenSees model performs a pushover analysis of any single-column circular RC bridge bent using only eight parameters. The tool was successfully incorporated in a website to confirm the feasibility of developing online tools for quick structural analysis of damaged bridges.
- For DDA, the serviceability of any RC bridge column after an earthquake can be evaluated using the proposed drift demand to drift capacity ratio.
- The AI-based computer vision tool can detect RC bridge column cracks with a precision and recall of 97% and 96%, respectively. Furthermore, the precision and recall of this tool to detect concrete spalling was respectively more than 94% and 88%. The precision and recall for the rebar detection were more than 91%. Overall, the computer vision tool detects different damages of RC bridge columns relatively quick and with a reasonable accuracy.
- The angular histogram proposed in the present project can reveal the crack major angle with a reasonable accuracy.

A combined use of the computer vision tool, the generic pushover tool, and the empirical DS-based drift equations results in a package that can perform both PDA and DDA on RC bridge columns using a few

parameters. The proposed flowchart was found feasible and was implemented in a website. In summary, the findings of the present project can be utilized in a professional software, which can help transportation agencies with a quick, systematic, and safe serviceability assessment of RC bridge columns after earthquakes.

8.3 Future Works

Based on the findings of the present study, the following activities are recommended as future research to fill existing knowledge gaps or expand the work:

- It is recommended to establish a focused reconnaissance group, who will systematically collect and document damage of bridges under earthquakes and other natural hazards. Alternatively, each state may prepare a reconnaissance report after an event following a national standard and make such reports public.
- New RC bridge column experimental data that will be available in future may be added to the bridge column test database.
- Researchers are welcome to further investigate RC bridge column test database for different research projects such as AI-based drift prediction models, new plastic hinge length equation for AASHTO, a damage-avoidance design methodology, or the estimation of bridge demands in low- to mid-seismic regions (e.g., SDC A to C).
- Deep neural network architectures for detecting buckling of bars and total collapse of structures, which has been described in Damage State 6, can be developed. In addition, to achieve real-time performance, the computation cost for Mask R-CNN will be optimized by modifying the underlaying backbone architecture and region proposal networks for the objects of interests.
- Generic cloud-based models can be developed to perform pushover analysis of single-column rectangular and multi-column circular/rectangular RC bridge bents for a quick post-event assessment. Furthermore, such models can be expanded to carry out dynamic analysis using site spectrum or site ground motion.
- A user-friendly graphical interface can be designed to facilitate the use of the computer vision tool. Further, this interface can seek the user feedback on the detected damages for an improved accuracy.
- Similar research can be conducted for other bridge components (e.g., footings, piles, shear keys, cap beams, abutments, etc.) for full and quick evaluation of affected bridges. Furthermore, similar bridge assessment tools may be developed for other natural hazards such as flooding, tsunamis, and hurricanes.

REFERENCES

AASHTO MBEI. (2013). "Manual for Bridge Element Inspection (1st Edition) with 2015 Interim Revisions," American Association of State Highway and Transportation Officials (AASHTO), 406 pp.

AASHTO SGS. (2011). "AASHTO Guide Specifications for LRFD Seismic Bridge Design, 2nd Edition," American Association of State Highway and Transportation Officials.

ACI 341.4R. (2016). "Report on the Seismic Design of Bridge Columns Based on Drift," American Concrete Institute, Farmington Hills, MI, 76 pp.

AL-Hawarneh, M. and Alam, M.S. (2021). "Lateral Cyclic Response of RC Bridge Piers Made of Recycled Concrete: Experimental Study." Journal of Bridge Engineering, Vol. 26, No. 5, p.04021018.

Alaska DOT. (2018). "Incident Field Operation Guide," Alaska Department of Transportation and Public Facilities, 280 pp.

Alipour, A. (2016). "Post-Extreme Event Damage Assessment and Response for Highway Bridges," A Synthesis of Highway Practice, National Cooperative Highway Research Program (NCHRP) Report No. Synthesis 497, National Academies of Sciences, Engineering, and Medicine, Washington, DC, 380 pp.

Ameli, M.J., Brown, D.N., Parks, J.E., and Pantelides, C.P. (2016). "Seismic Column-to-Footing Connections Using Grouted Splice Sleeves." ACI Structural Journal, Vol. 113, No. 5, pp. 1021-1030.

Ameli, M.J., and Pantelides, C.P. (2017). "Seismic Analysis of Precast Concrete Bridge Columns Connected with Grouted Splice Sleeve Connectors." Journal Structural Engineering, ASCE, 10.1061/(ASCE)ST.1943-541X.0001678, 04016176.

Amiri, S. M. A., Moustafa, M. A., & Saunders, D. H. (2021). Seismic Design and Detailing of Bridge Columns to Account for Ground-Motion Duration (Report No. 2021/08). Pacific Earthquake Engineering Research Center. https://peer.berkeley.edu/sites/default/files/2021_08_moustafa_final.pdf.

ATC-20. (1989). "Procedures for Post-earthquake Safety Evaluations of Buildings." Applied Technology Council (ATC) Report No. ATC-20, Redwood City, CA.

Ardakani, S.S., and Saiidi, M.S. (2018). "Simple Method to Estimate Residual Displacement in Concrete Bridge Columns under Near-Fault Earthquake Motions." Engineering Structures, Vol. 176, pp. 208-219.

Azadi-Kakavand, M.R., and Allahvirdizadeh, R. (2019). "Enhanced Empirical Models for Predicting the Drift Capacity of Less Ductile RC Columns with Flexural, Shear, or Axial Failure Modes." Frontiers of Structural and Civil Engineering, 13(5), pp. 1251-1270.

Azadi-Kakavand, M.R., Sezen, H., Taciroglu, E. (2019) "Circular Column Database." DesignSafe-CI. https://doi.org/10.17603/ds2-52bz-0n63.

Azadi Kakavand, M.R., Sezen, H., Taciroglu, E. (2019) "Rectangular Column Database." DesignSafe-CI. https://doi.org/10.17603/ds2-7qg0-4303.

Bearman, C. F. (2012). "Post-earthquake Assessment of Reinforced Concrete Frames." M.S. thesis, Dept. of Civil and Environmental Engineering, Univ. of Washington, Seattle.

Basoz, N., and Mander, J. (1999). "Enhancement of the Highway Transportation Lifeline Module in HAZUS", National Institute of Building Sciences.

Berry, M.P., Parrish, M., and Eberhard, M.O. (2004). "PEER Structural Performance Database," Pacific Earthquake Engineering Research Center, University of California, Berkeley, 43 pp. Database can be found at: <https://nisee.berkeley.edu/spd/>

Berry, M.P., and Eberhard, M.O. (2008). "Performance Modeling Strategies for Modern Reinforced Concrete Bridge." Pacific Earthquake Engineering Research Center, University of California, Berkeley, 210 pp.

Buckle, I.G., Al-Ani, M. and Monzon, E. (2011). "Seismic Isolation Design Examples of Highway Bridges." National Cooperative Highway Research Program (NCHRP) Project No. 20-07, The National Academies of Sciences, Engineering, and Medicine, Washington, DC, 382 pp.

Cha, Y.J., Choi, W., Suh, G., Mahmoudkhani, S. and Büyüköztürk, O. (2018). "Autonomous Structural Visual Inspection Using Region-Based Deep Learning for Detecting Multiple Damage Types." Computer-Aided Civil Infrastructure Engineering, 33, pp. 731-747.

Chung, R. M. (1996). "The January 17, 1995 Hyogoken-Nanbu (Kobe) Earthquake: Performance of Structures, Lifelines, and Fire protection systems," National Institute of Standards and Technology Report No. NIST SP 901, 580 pp.

Dalal, N. and Triggs, B. (2005). "Histograms of Oriented Gradients for Human Detection." IEEE Computer Society Conference on Computer Vision and Pattern Recognition, pp. 1:886-893. doi: 10.1109/CVPR.2005.177.

Dung, C.V., and Anh, L.D. (2019) "Autonomous Concrete Crack Detection Using Deep Fully Convolutional Neural Network," Automation in Construction, Vol. 99, pp. 52-58.

EERI. (2011). "Observations from FHWA/UJNR/EERI Reconnaissance Team for Bridge Damage Investigation," Earthquake Engineering Research Institute, Retrieved on June 7, 2021 from: <http://learningfromearthquakes.org/2011-03-11-tohoku-japan/index.php?option=com_content&view=article&id=74>.

EERI Archive. (2020). "Learning from Earthquakes Reconnaissance Archive," Earthquake Engineering Research Institute, Retrieved on February 11, 2020 from: <https://www.eeri.org/projects/learning-from-earthquakes-lfe/lfe-reconnaissance-archive/>.

FHWA. (2020). "Bridge Condition by Functional Classification," Retrieved on June 4, 2021, 2020 from <https://www.fhwa.dot.gov/bridge/fc.cfm>.

FEMA 154. (2015). "Rapid Visual Screening of Buildings for Potential Seismic Hazards: A Handbook, Third Edition" Federal Emergency Management Agency, Washington, D.C., 388 pp.

FEMA HAZUS. (2020). "HAZUS Earthquake Model Technical Manual, HAZUS 4.2 SP3", Federal Emergency Management Agency, Washington, D.C., 436 pp.

Fischler, M. and Bolles R. (1981). "Random Sample Consensus: A Paradigm for Model Fitting with Applications to Image analysis and Automated Cartography." Communications of the ACM, 24(6), pp. 381-395. https://doi.org/10.1145/358669.358692.

Ge, S., Yang, R., Wen, H., Chen, S., and Sun, L. (2014). "Eye Localization based on Correlation Filter Bank." In 2014 IEEE International Conference on Multimedia and Expo (ICME). pp.1-5. doi: 10.1109/ICME.2014.6890249.

German, S., Brilakis, I. and DesRoches, R. (2012). "Rapid Entropy-Based Detection and Properties Measurement of Concrete Spalling with Machine Vision for Post-Earthquake Safety Assessments." Advanced Engineering Informatics, 26(4), pp. 846-858.

German, S., Jeon, J.S., Zhu, Z., Bearman, C., Brilakis, I., DesRoches, R. and Lowes, L. (2013). "Machine Vision-Enhanced Postearthquake Inspection." Journal of Computing in Civil Engineering, 27(6), pp. 622-634.

Ghannoum, W., Sivaramakrishnan, B., Pujol, S., Catlin, A.C., Fernando, S., Yoosuf, N., and Wang, Y. (2015), "NEES: ACI 369 Rectangular Column Database," https://datacenterhub.org/resources/255.

Goodfellow, I, Pouget-Abadie, J., Mirza, M., Xu, B., Warde-Farley, D., Ozair, S., Courville, A., and Bengio. Y., (2020). "Generative Adversarial networks." Communications of the ACM, 63(11), pp. 139-144, DOI: https://doi.org/10.1145/3422622.

Goodnight, J.C., Kowalsky, M.J. and Nau, J.M. (2013). "Effect of Load History on Performance Limit States of Circular Bridge Columns." Journal of Bridge Engineering, Vol. 18, No. 12, pp. 1383-1396.

Haber, Z.B., Saiidi, M.S., and Sanders, D.H. (2013). "Precast Column-Footing Connections for Accelerated Bridge Construction in Seismic Zones," Center for Civil Engineering Earthquake Research, Department of Civil and Environmental Engineering, University of Nevada, Reno, Nevada, Report No. CCEER-13-08, 612 pp.

Hart, K., Greeneway, E., and Tazarv, M. (2021). "Modern RC Bridge Column Experimental Database," in the Post-Earthquake Serviceability of RC Bridge Columns Using Visual Inspection project. DesignSafe-CI PRJ 3294, https://doi.org/10.17603/ds2-1p5e-1v55.

He, K., Gkioxari, G., Dollar, P., and Girshick, R., (2017) "Mask R-CNN," Computer Vision and Pattern Recognition, arXiv:1703.06870.

He, K., Zhang, X., Ren, S., and Sun, J. (2016). "Deep Residual Learning for Image Recognition." IEEE Conference on Computer Vision and Pattern Recognition (CVPR), pp. 770-778.

Hose Y.D. (2001). "Seismic Performance and Flexural Behavior of Plastic Hinge Regions in Flexural Bridge Columns," PhD Dissertation, University of California, San Diego, 493 pp.

Hose, Y.D. and Seible, F. (1999). "Performance Evaluation Database for Concrete Bridge Components and Systems under Simulated Seismic Loads." Pacific Earthquake Engineering Research Center (PEER) Report No. 1999/11, College of Engineering, University of California, 113 pp.

Hoskere, V., Narazaki, Y., Hoang, T. and Spencer Jr, B. (2011). "Vision-Based Structural Inspection Using Multiscale Deep Convolutional Neural Networks." The 3rd Huixian International Forum on Earthquake Engineering for Young Researchers, arXiv preprint arXiv:1805.01055, 8 pp.

Hoskere, V., Narazaki, Y., Hoang, T.A., and Spencer B.F., (2018) "Towards Automated Post-Earthquake Inspections with Deep Learning-based Condition-Aware Models," in Proc., The 7th World Conference on Structural Control and Monitoring, 7WCSCM, 10 pp.

Housner, G.W. and Thiel, C.C. (1994). "The Continuing Challenge: Report on the Northridge Earthquake of January 17, 1994," Department of Transportation, Sacramento, CA.

Hüthwohl, P., Lu, R. and Brilakis, I. (2019). "Multi-Classifier for Reinforced Concrete Bridge Defects." Automation in Construction, Vol. 105, p.102824.

Istrati, D. (2016). "Damage to Highway Bridges during the 2016 Kumamoto Earthquake in Japan," Research Gate, DOI: 10.13140/RG.2.2.33886.43849.

Jahanshahi, M.R. and Masri, S.F. (2012). "Adaptive Vision-Based Crack Detection Using 3D Scene Reconstruction for Condition Assessment of Structures." Automation in Construction, 22, pp. 567-576.

Jahanshahi, M.R., and Masri, S.F., (2013). "A New Methodology for Non-Contact Accurate Crack Width Measurement through Photogrammetry for Automated Structural Safety Evaluation." Smart Materials and Structures, 22(3), https://doi.org/10.1088/0964-1726/22/3/035019.

Kawashima, K. (2000). "Seismic Performance of RC Bridge Piers in Japan-An Evaluation after the 1995 Hyogo-ken Nanbu Earthquake," Progress in Structural Engineering Materials, pp. 82-91.

Kawashima, K. (2001). "Damage of Bridges Resulting from Fault Rupture in the 1999 Kocaeli and Duzce, Turkey Earthquakes and the 1999 Chi-Chi, Taiwan Earthquake," Seismic Fault-Induced Failures, pp. 171-190.

Kawashima, K. and Buckle, I. (2013). "Structural Performance of Bridges in the Tohoku-Oki Earthquake." Earthquake Spectra, Vol. 29, pp. 315-338.

Kim, H., Ahn, E., Shin, M., and Sim, S. (2019). "Crack and Noncrack Classification from Concrete Surface Images Using Machine Learning." Structural Health Monitoring, 18, pp. 725-738.

Kim, J., Kim, A., and Lee, S. (2020). "Artificial Neural Network-Based Automated Crack Detection and Analysis for the Inspection of Concrete Structures." Applied Sciences, 10(22), 8105. https://doi.org/10.3390/app10228105.

Krizhevsky, A., Sutskever, I., and Hinton, G.E. (2012). "ImageNet Classification with Deep Convolutional Neural Networks." Communications of the ACM, 60, pp. 84-90.

Lattanzi, D., Miller, G.R., Eberhard, M.O., and Haraldsson, O.S. (2015). "Bridge Column Maximum Drift Estimation via Computer Vision," Journal of Computing in Civil Engineering, ASCE, Vol. 30, No. 4, 04015051, 9 pp.

LeCun, Y., Boser, B., Denker, J., Henderson, D., Howard, R., Hubbard, W., and Jackel, L. (1989). "Backpropagation Applied to Handwritten Zip Code Recognition." Neural Computation, 1, pp. 541-551.

LeCun, Y., Bottou, L., Bengio, Y., and Haffner, P. (1998). "Gradient-Based Learning Applied to Document Recognition." Proceedings of the IEEE, 86(11), pp. 2278–2324.

Lee, W.K., and Billington, S.L. (2010). "Modeling Residual Displacements of Concrete Bridge Columns under Earthquake Loads Using Fiber Elements." Journal of Bridge Engineering, Vol. 15, No. 3, pp. 240-249.

Li, S., and Zhao, X. (2019) "Image-Based Concrete Crack Detection Using Convolutional Neural Network and Exhaustive Search Technique," Advances in Civil Engineering, Vol. 2019, 12 pp.

Li, Z., Yang, W., Peng, S., and Liu, F. (2021). "A Survey of Convolutional Neural Networks: Analysis, Applications, and Prospects." IEEE Transactions on Neural Networks and Learning Systems, 21 pp.

Liang X. (2019). "Image-Based Post-Disaster Inspection of Reinforced Concrete Bridge Systems Using Deep Learning with Bayesian Optimization." Computer Aided Civil and Infrastructure Engineering, 34, pp. 415-430.

Lin, T., Maire, M., Belongie, S., Hays, J., Perona, P., Ramanan, D., Dollár, P. and Zitnick, C. (2014). "Microsoft COCO: Common Objects in Context".

Lin, K.W., Wald, D.J. and Turner, L.L. (2009). "Using ShakeCast and ShakeMap for Lifeline Post-Earthquake Response and Earthquake Scenario Planning." In TCLEE 2009: Lifeline Earthquake Engineering in a Multihazard Environment, pp. 1-12.

Liu, Z., Cao, Y., Wang, Y. and Wang, W. (2019). "Computer Vision-Based Concrete Crack Detection using U-net Fully Convolutional Networks." Automation in Construction, 104, pp. 129-139.

Marsh, M.L., Buckle, I.G., and Kavazanjian, E. (2014). "LRFD Seismic Analysis and Design of Bridges: Reference Manual," National Highway Institute, Federal Highway Administration Report No. FHWA-NHI-15-004, 608.

Marshall, C., Cantrell, J., Mashal, M. and Ebrahimpour, A. (2020). "A Precast Pier system for ABC in Seismic Regions." In Structures Congress 2020, Reston, VA: American Society of Civil Engineers, pp. 183-192.

Mashal, M., Ebrahimpour, A., Acharya, M., Cantrell, J., Marshall, C., Shokrgozar, A. (2021). "A Precast Pier System for Accelerated Bridge Construction (ABC) in Idaho." Idaho Transportation Department Report 281, Boise, Idaho.

Miranda, E., Acosta Vera, A.; Aponte, L., Archbold, J., Cortes, M., Du, A., Gunay, S., Hassan, W., Heresi, P., Lamela, A., Messina, A., Miranda, S., Padgett, J., Poulos, A., Scagliotti, G., Tsai, A., Kijewski-Correa, T., Robertson, I., Mosalam, K., Prevatt, D., Roueche, D. (2020). "StEER, Reconnaissance, PVRR, Puerto Rico, Earthquakes," Preliminary Virtual Reconnaissance Report (PVRR) No. PRJ-2670, DOI: 10.17603/ds2-xfhz-fz88, 77 pp.

Moehle, J.P., Eberhard, M.O. (2000). "Earthquake Damage to Bridges." Bridge Engineering Handbook, Ed. Wai-Fah Chen and Lian Duan, Boca Raton: CRC Press.

Mohammed, M.S., Sanders, D.H. and Buckle, I.G. (2017). "Reinforced Concrete Bridge Columns Tested under Long and Short Duration Ground Motions. In 16th World Conference on Earthquake Engineering, Paper No. 2831, 12 pp.

Murphy, T.P., Marsh, L., Bennion, S., Buckle, I.G., Luco, N., Anderson, D., Kowalsky, M., and Restrepo, J. (2020). "Proposed AASHTO Guidelines for Performance-Based Seismic Bridge Design", National Cooperative Highway Research Program, NCHRP 949, National Academy of Sciences, 86 pp.

Narazaki, Y., Hoskere, V., Hoang, T.A., Fujino, Y., Sakurai, A. and Spencer Jr, B.F. (2020). "Vision-Based Automated Bridge Component Recognition with High-Level Scene Consistency." Computer-Aided Civil and Infrastructure Engineering, 35(5), pp.465-482.

Nikoukalam, M.T. and Sideris, P. (2017). "Experimental Performance Assessment of Nearly Full-Scale Reinforced Concrete Columns with Partially Debonded Longitudinal Reinforcement." Journal of Structural Engineering, 143(4), p.04016218.

Nishikawa, T., Yoshida, J., Sugiyama, T. and Fujino, Y. (2012). "Concrete Crack Detection by Multiple Sequential Image Filtering." Computer-Aided Civil and Infrastructure Engineering, 27, pp. 29-47. 10.1111/j.1467-8667.2011.00716.x.

O'Connor, J.S. (2010). "Post-Earthquake Bridge Inspection Guidelines," Multidisciplinary Center for Earthquake Engineering Research (MCEER) Report No. C-06-14, University at Buffalo, 145 pp.

Olsen, M.J., Barbosa, A., Burns, P., Kashani, A., Wang, H., Veletzos, M., Chen, Z., Roe, G., and Tabrizi, K. (2016). "Assessing, Coding, and Marking of Highway Structures in Emergency Situations," National Cooperative Highway Research Program (NCHRP) Report No. 833, The National Academies of Sciences, Engineering, and Medicine, Washington, DC, 112 pp.

Olsen, M.J., Barbosa, A., Burns, P., Kashani, A., Wang, H., Veletzos, M., Chen, Z., Roe, G., and Tabrizi, K. (2016). "Guidelines for Development of Smart Apps for Assessing, Coding, and Marking Highway Structures in Emergency Situations," National Cooperative Highway Research Program (NCHRP) Web-Only Document 223, The National Academies of Sciences, Engineering, and Medicine, Washington, DC, 47 pp.

OpenSees. (2016). "Open System for Earthquake Engineering Simulations," Version 2.4.1, Berkeley, CA, <http://opensees.berkeley.edu>.

Otsu, N. (1979). "A Threshold Selection Method from Gray-Level Histograms," IEEE Transactions on Systems, Man, and Cybernetics. 9(1), pp. 62-66. doi: 10.1109/TSNC,1979.4310076.

Paal, S.G., Jeon, J., Brilakis, I., DesRoches, R. (2015). "Automated Damage Index Estimation of Reinforced Concrete Columns for Post-Earthquake Evaluations," Journal of Structural Engineering, ASCE, Vol. 141, No. 9, 04014228, 13 pp.

Park Y.J. and Ang. A.H.S. (1985). "Mechanistic Seismic Damage Model for Reinforced Concrete," Journal of Structural Engineering, ASCE, Vol. 111, No. 4, pp. 722-739.

Peruš, I., Biskinis, D., Fajfar, P., Fardis, M.N., Grammatikou, S., Krawinkler, H. and Lignos, D. (2013). "Enrichment of the Distributed Database with Existing Data, Background Report Accompanying Deliverable D2. 7," The Seismic Engineering Research Infrastructures for European Synergies (SERIES), Seventh Framework Programme, University of Ljubljana, Faculty for Civil and Geodetic Engineering.

Prakash, S., Li, Q. and Belarbi, A. (2012). "Behavior of Circular and Square Reinforced Concrete Bridge Columns under Combined Loading Including Torsion." ACI Structural Journal, Vol. 109, No. 3, pp. 317-328.

Priestley, M.J.N., Seible, F., and Calvi, G.M. (1996). "Seismic Design and Retrofit of Bridges," John Wiley and Sons, Inc., New York, 686 pp.

Ramirez, J.A., Frosch, R.J., Sozen, M.A., and Turk, A.M. (2000). "Handbook for the Post-Earthquake Safety Evaluation of Bridges and Roads", Indiana Department of Transportation, 134 pp.

Rodriguez, M.E., and Padilla, D. (2009). "A Damage Index for the Seismic Analysis of Reinforced Concrete Members," Journal of Earthquake Engineering, Vol. 13, No. 3, pp. 364-383.

Saini, A. and Saiidi, M.S. (2014). "Probabilistic Damage Control Approach for Seismic Design of Bridge Columns." Center for Civil Engineering Earthquake Research, Department of Civil and Environmental Engineering, University of Nevada, Reno, Nevada, Report No. CCEER-14-02, 216 pp.

Schoettler, M.J., Restrepo, J.I., Guerrini, G., Duck, D.E., and Correa, F. (2015). "A Full-Scale, Single-Column Bridge Bent Tested by Shake-Table Excitation," Pacific Earthquake Engineering Research Center, PEER Report No. 2015/02, 153 pp.

ShakeMap. (2021). USGS Earthquake Hazards Program, Retrieved on June 9, 2021 from <https://earthquake.usgs.gov/data/shakemap/>.

Sjurseth, T. (2021). "Mechanically Spliced Precast Bridge Columns," MS Thesis, South Dakota State University, 197 pp., <https://openprairie.sdstate.edu/etd/5252>.

Szegedy, C., Liu, W., Jia, Y., Sermanet, P., Reed, S.E., Anguelov, D., Erhan, D., Vanhoucke, V., and Rabinovich, A. (2015). "Going Deeper with Convolutions." 2015 IEEE Conference on Computer Vision and Pattern Recognition (CVPR), pp. 1-9.

Tazarv, M. (2021). "Elastic Response Spectrum", MATLAB Central File Exchange. Retrieved August 31, 2021, <https://www.mathworks.com/matlabcentral/fileexchange/31254-elastic-response-spectrum>.

Tazarv, M., and Saiidi, M.S. (2013). "Analytical Studies of the Seismic Performance of a Full-Scale SMA-Reinforced Bridge Column." International Journal of Bridge Engineering, Vol. 1, No. 1, pp. 37-50.

Torok, M.M., Golparvar-Fard, M. and Kochersberger, K.B. (2014). Image-Based Automated 3D Crack Detection for Post-Disaster Building Assessment." Journal of Computing in Civil Engineering, 28(5), pp. A4014004.

USGS. (2018). "2018 Long-term National Seismic Hazard Map," Retrieved on February 11, 2020 from <https://www.usgs.gov/media/images/2018-long-term-national-seismic-hazard-map>.

Valença, J., Puente, I., Júlio, E., González-Jorge, H. and Arias-Sánchez, P. (2017). "Assessment of Cracks on Concrete Bridges Using Image Processing Supported by Laser Scanning Survey." Construction and Building Materials, 146, pp. 668-678.

Veletzos, M., Panagiutou, M., Restrepo, J., and Sahs, S. (2008). "Visual Inspection and Capacity Assessment of Earthquake Damaged Reinforced Concrete Bridge Elements," California Department of Transportation Report No. CA08-0284, Sacramento, CA, 392 pp.

Vosooghi, A., and Saiidi, M.S. (2010). "Seismic Damage States and Response Parameters for Bridge Columns," ACI Special Publication, Vol. 271, No. 2, pp. 29-46.

Washington Post. (2015). "A Surprisingly Accurate Map of the U.S. Made with 600,000 Bridges - and Nothing Else" Retrieved on June 4, 2021 from: <https://www.washingtonpost.com/news/wonk/wp/2015/02/03/a-surprisingly-accurate-map-of-the-u-s-made-with-600000-bridges-and-nothing-else/>.

Won, K., and Sim, C. (2020) "Automated Transverse Crack Mapping System with Optical Sensors and Big Data Analytics," Sensors, 20(7), p.1838.

Yamazaki, F., Matsuda, T., Denda, S. and Liu, W. (2015). "Construction of 3D Models of Buildings Damaged by Earthquakes Using UAV Aerial Images." In Proceedings of the Tenth Pacific Conference on Earthquake Engineering Building an Earthquake-Resilient Pacific, 8 pp.

Yamazaki, F., and Liu, W. (2016). "Remote Sensing Technologies for Post-Earthquake Damage Assessment: A Case Study on the 2016 Kumamoto Earthquake." In 6th Asia Conference on Earthquake Engineering, 13 pp.

Yashinsky, M., Oviedo, R., Ashford, S.A., Fargier-Gabaldon, L. and Hube, M. (2010). "Performance of Highway and Railway Structures during the February 27, 2010 Maule Chile Earthquake." EERI/PEER. FHWA Bridge Team Report, 46 pp.

Yein, L., Kim, B., and Cho, S. (2018). "Image-Based Spalling Detection of Concrete Structures Using Deep Learning." Journal of The Korea Concrete Institute, 30, pp. 91-99.

Yen, W.H.P., Chen, G., Buckle, I.G., Allen, T.M., Alzamora, D.E., Ger, J. and Arias, J.G. (2011). "Post-earthquake Reconnaissance Report on Transportation Infrastructure Impact of the February 27, 2010, Offshore Maule Earthquake in Chile," Federal Highway Administration Report No. FHWA-HRT-11-030, 218 pp.

Yen, W.H.P., Chen, G., Yashinski, M., Hashash, Y., Holub, C.J., Wang, K. and Guo, X. (2011). "China Earthquake Reconnaissance Report: Performance of Transportation Structures during the May 12, 2008, M7. 9 Wenchuan Earthquake." Federal Highway Administration Report No. FHWA-HRT-11-029, 54 pp.

Yeum, C., and Dyke, S. (2015). "Vision-Based Automated Crack Detection for Bridge Inspection." Computer Aided Civil Infrastructure Engineering, 30, pp. 759-770.

Yeum, C.M., Dyke, S.J., Benes, B., Hacker, T., Ramirez, J., Lund, A. and Pujol, S. (2019). "Postevent Reconnaissance Image Documentation Using Automated Classification." Journal of Performance of Constructed Facilities, 33(1), p.04018103.

Yeum, C., Dyke, S. and Ramirez, J. (2018). "Visual Data Classification in Post-Event Building Reconnaissance." Engineering Structures. 155, pp. 16-24. 10.1016/j.engstruct.2017.10.057.

Zheng, Q., Yang, C.S.W., Roblee, C., Kunnath, S., DesRoches, R., Padgett, J., Zhang, A., Mangalathu, S. (2020). "Experiment-Based Column Performance Database - RP1." DesignSafe-CI. <https://doi.org/10.17603/ds2-0nr1-8571>.

Zhu, Z., German, S. and Brilakis, I. (2010). "Detection of Large-Scale Concrete Columns for Automated Bridge Inspection." Automation in construction, 19(8), pp. 1047-1055.

Zhu, Z., German, S. and Brilakis, I. (2011). "Visual Retrieval of Concrete Crack Properties for Automated Post-Earthquake Structural Safety Evaluation." Automation in Construction, 20(7), pp. 874-883.

APPENDIX A. DAMAGE PHOTOS OF COLUMNS IN RC BRIDGE COLUMN EXPERIMENTAL DATABASE

Please see the document in PDF for this appendix, which includes 153 pages. The photographs of columns (when available) included in the RC bridge column experimental database (Chapter 4) at different damage states were compiled and reported in this section.

The database can be accessed online at <https://doi.org/10.17603/ds2-1p5e-1v55> and can be cited as:

Hart, K., Greeneway, E., and Tazarv, M. (2021). "Modern RC Bridge Column Experimental Database," in the Post-Earthquake Serviceability of RC Bridge Columns Using Visual Inspection project. DesignSafe-CI PRJ 3294, https://doi.org/10.17603/ds2-1p5e-1v55.

APPENDIX B. BRIDGE DAMAGE ASSESSMENT TOOLS

Please see the document in PDF for this appendix, which includes 18 pages. The web application to perform the bridge serviceability assessment can be accessed at:

http://brdats.sdstate.edu/

or

https://sites.google.com/people.unr.edu/mostafa-tazarv

APPENDIX A. DAMAGE PHOTOS OF COLUMNS IN RC BRIDGE COLUMN EXPERIMENTAL DATABASE

Table of Contents

A1. Introduction

Past test databases included a mix of bridge and building, standard and substandard columns, and reported parameters that might not be consistent with current codes or required in a bridge design. To achieve the current project goals, it was necessary to collect test data specific to modern RC bridge columns. A new performance database has been developed in the present work that includes all the key geometrical, material, and force-displacement properties of RC bridge columns designed with modern codes (especially those following seismic detailing). All parameters were collected following the current "AASHTO Guide Specifications for LRFD Seismic Bridge Design" definitions. Furthermore, displacements (drifts) at six different damage states as defined in this project were included when the data was available. The new database is built upon the work by Ghannoum et al. (2015), which included test data published up to 2008. Nevertheless, all substandard and/or building columns were removed, the definitions were updated to be consistent with current AASHTO SGS, and new parameters were added suited for seismic/bridge design. Furthermore, more than 100 new circular and 30 rectangular columns were added. The refined and updated RC bridge column database currently includes 222 circular and 68 rectangular columns. Two spreadsheets, one for circular and one for rectangular RC bridge columns, were developed each including more than 30 parameters per column. The definitions were also provided in the spreadsheet. The current version of the RC bridge column database in MS Excel can be found in the following reference:

Hart, K., Greeneway, E., and Tazarv, M. (2021). "Modern RC Bridge Column Experimental Database," in the Post-Earthquake Serviceability of RC Bridge Columns Using Visual Inspection project. DesignSafe-CI PRJ 3294, https://doi.org/10.17603/ds2-1p5e-1v55.

Furthermore, the photographs of the columns included in the database at different damage states are presented next.

A2. Photos of Circular RC Bridge Columns

The photographs of RC bridge columns included in the circular column database at different damage states, when available, were compiled and reported herein. The work was organized based on an alphabetical order of authors' surnames.

Note that the number in the parenthesis is the drift ratio (in %) at which the photo was taken. The drift is the ratio of the column lateral displacement to the column height.

For statistical analysis, drifts at DS2 were assumed to be at yielding not those observed in the tests. A discrepancy between the yield drift and those estimated from the photographs for DS2 exits for some test specimens. Further, sometimes the test toward the end of the experiment was strong enough to fail the column before documenting different levels of the damage. For example, DS5 and DS6 occurred in the last run of the test. If data was available, DS5 and DS6 were separately reported in this document.

Dia = 16"
Height = 72"
Force-Deformation Chart
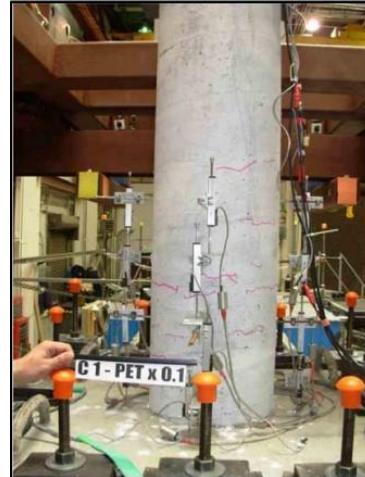
Damage State I (0.465%)

Damage State II (0.91%)
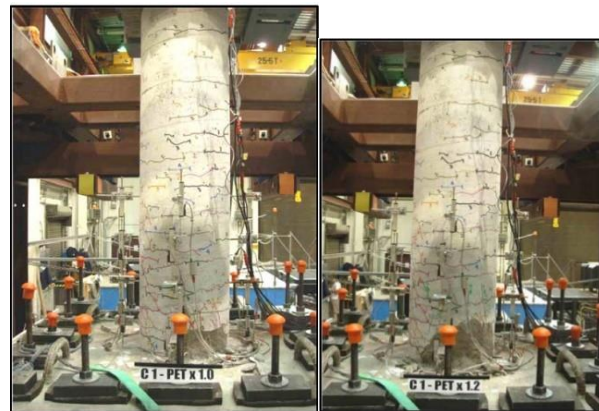
Damage State III (4.57%. 6.78%)

Damage State IV (9.15%)

Damage State V & VI (14.89%)

Damage State of Column C1 Tested by Acosta (2012)
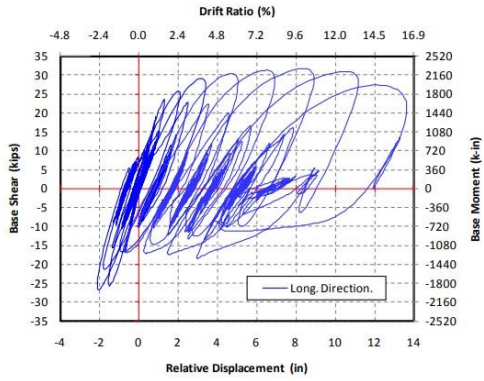
Dia = 16"
Height = 72"
Force-Deformation Chart

Damage State I (0.287%)

Damage State II (0.567%)
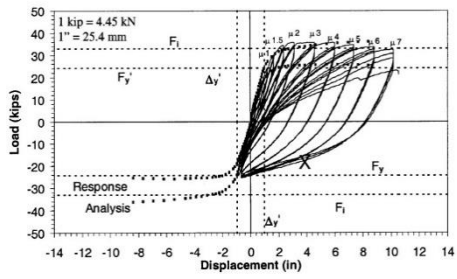

Damage State III (4.08%. 6.07%)

Damage State IV (8.33%)
Label might have been wrong, the report was double-checked for C2 Column, reported as appeared
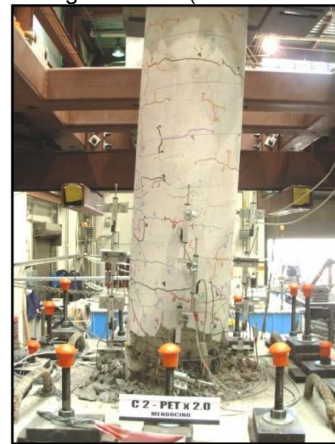
Damage State VI (16.43%)

Damage State of Column C2 Tested by Acosta (2012)
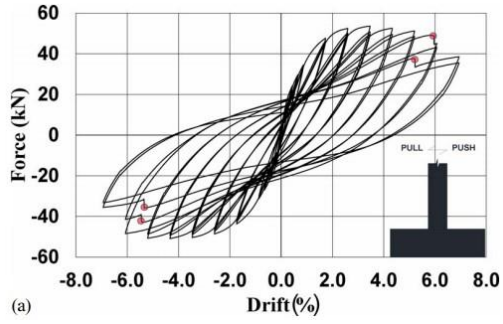
Dia= 11.81x12"
Height = 72"
Force-Deformation Chart

Damage State I

Damage State II

Damage State III

Damage State IV

Damage State VI (6.95%)

Damage State of Column RCA Tested by Al-Hawarneh and Alam (2021)
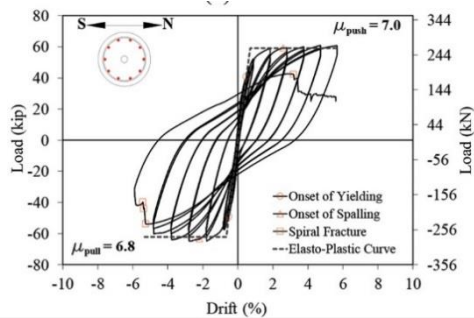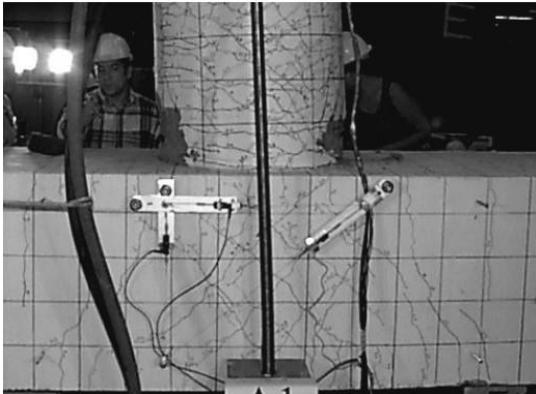
Dia = 20"
Height = 50"
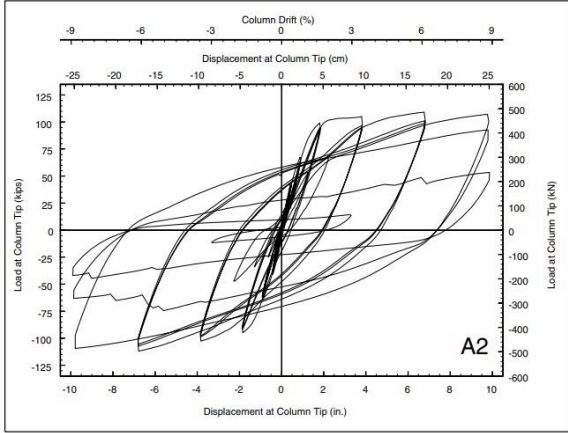Force-Deformation Chart

Damage State I

Damage State II

Damage State III

Damage State IV (4%)

Damage State VI (6%)

Damage State of Column C-25-1 Tested by Al-Jelawy et al. (2018)
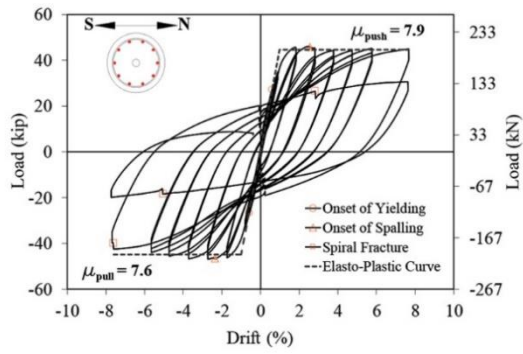
Dia = 20"
Height = 80"
Force-Deformation Chart

Damage State I

Damage State II (3%, 4%)

Damage State III (5%)
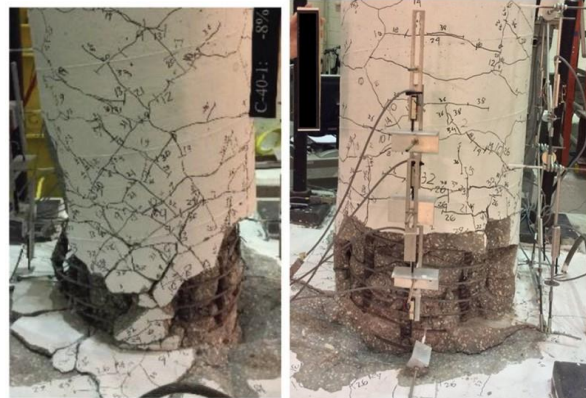
Damage State IV

Damage State VI (8%, 8%)

Damage State of Column C-40-1 Tested by Al-Jelawy et al. (2018)
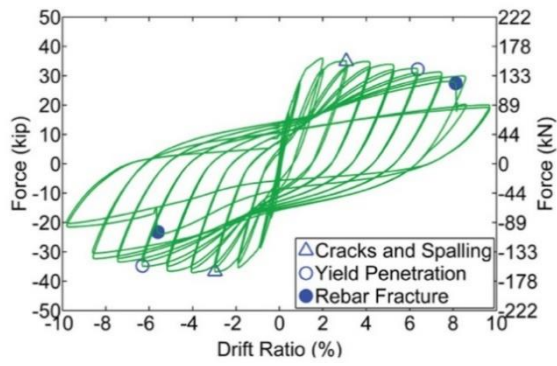
Dia = 21"
Height = 102"
Force-Deformation Chart

Damage State I
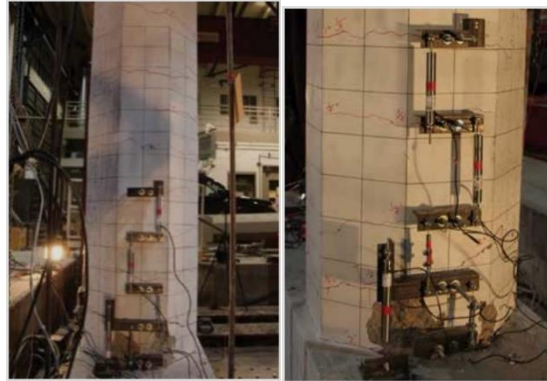
Damage State II

Damage State III (3%, 3%)
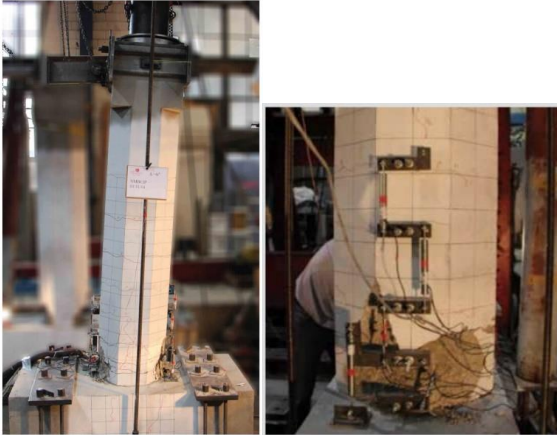
Damage State IV (6%, 6%, 6%)

Damage State VI (7.95%, 10%, 10%)

Damage State of Column CIP Tested by Amelie et al. (2016)

Dia = 16"
Height = 64"
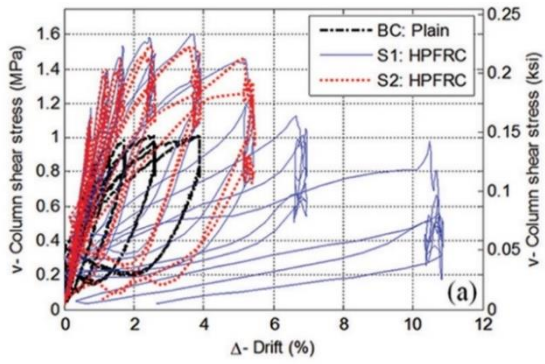
Force-Deformation Chart
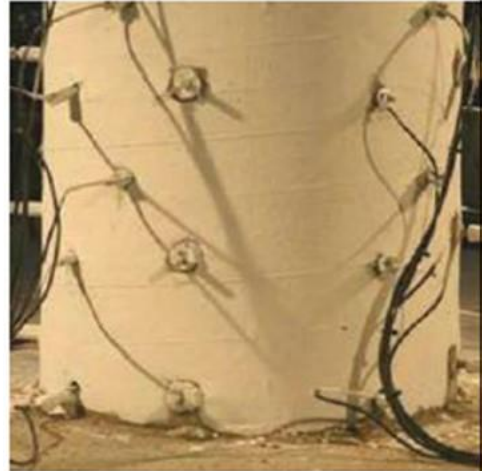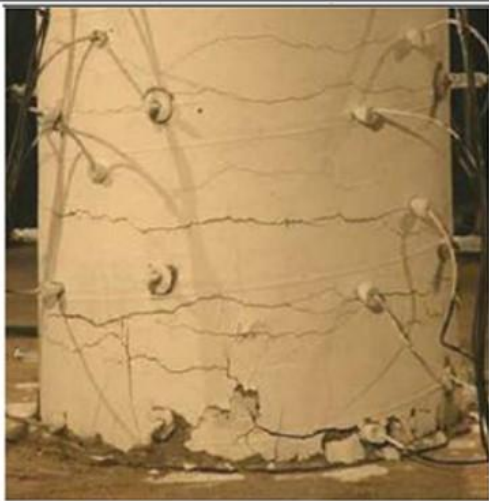
Damage State I (1.3%)

Damage State II (1.7%)
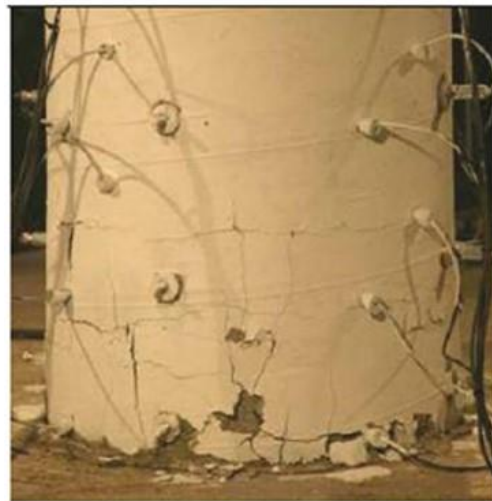
Damage State III (2.6%)

Damage State IV (3.9%)

Damage State V

Damage State of Column Plain Tested by Aviram et al. (2014)
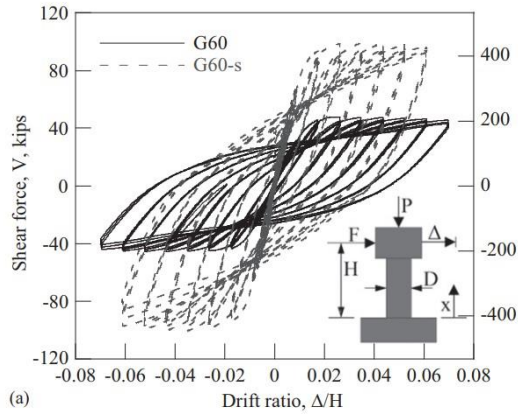
Dia = 24"
Height = 144"
Force-Deformation Chart

Damage State I

Damage State II

Damage State III

Damage State IV

Damage State V-VI (6.96%)

Damage State of Column G60 Tested by Barbosa et al. (2015)
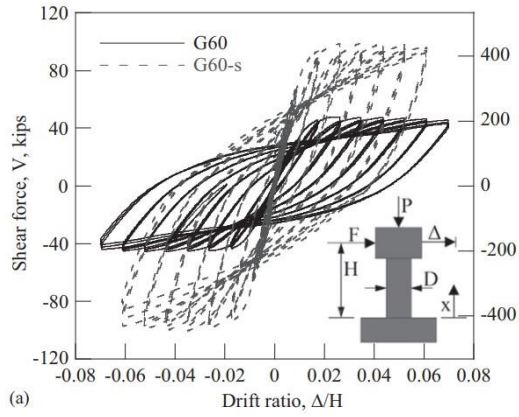
Dia = 24"
Height = 72"
Force-Deformation Chart

Damage State I

Damage State II

Damage State III

Damage State IV

Damage State V-VI (6.09%)

Damage State of Column G60-S Tested by Barbosa et al. (2015)
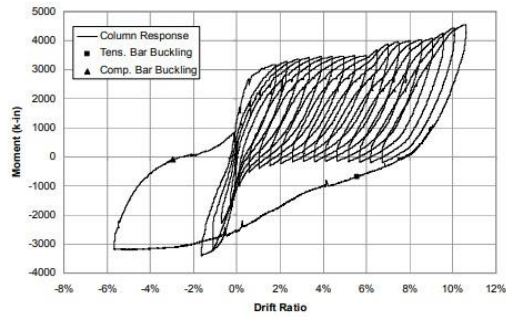
Dia = 20"
Height = 60"
Force-Deformation Chart

Damage State I

Damage State II (4.75%)

Damage State III

Damage State IV

Damage State V-VI (10.58%, 10.58%)

Damage State of Column CT6 Tested by Brown et al. (2007)

Dia = 24"
Height = 240"
Force-Deformation Chart
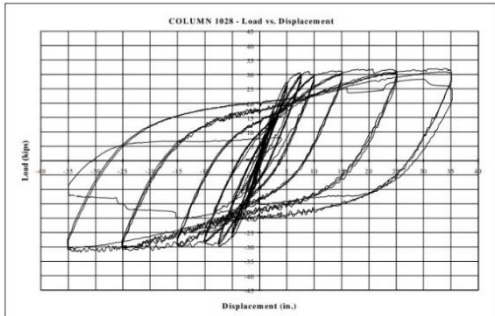
Damage State I

Damage State II
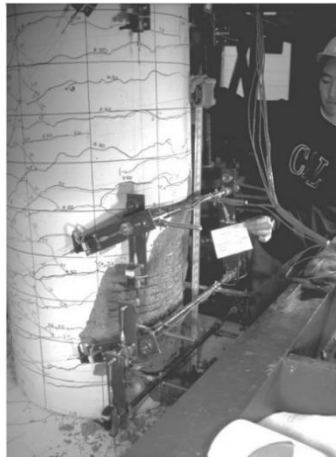
Damage State III

Damage State IV (4.17%)

Damage State V (10.42% top), VI (14.58%, 14.58%, 14.5%)

Damage State of Column 1028 Tested by Calderone (2000)
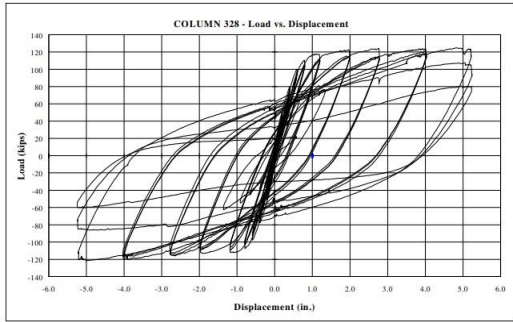
Dia = 24"
Height = 72"
Force-Deformation Chart
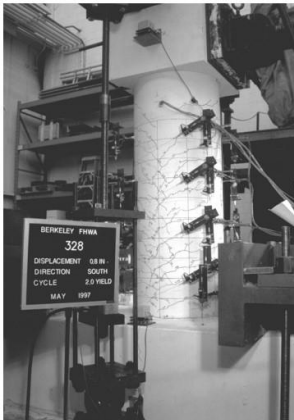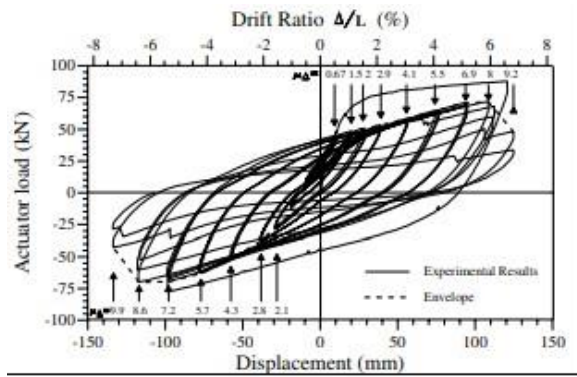
Damage State I

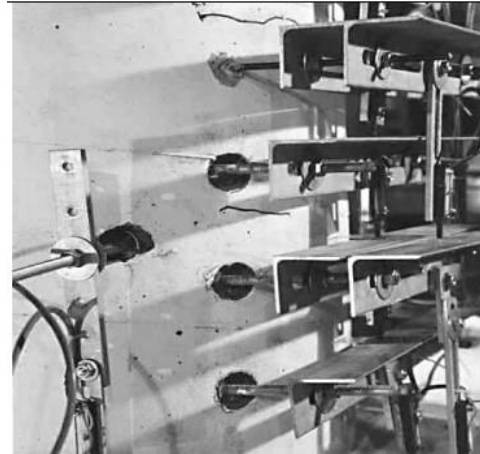Damage State II (1.11%)

Damage State III

Damage State IV (2.78%)
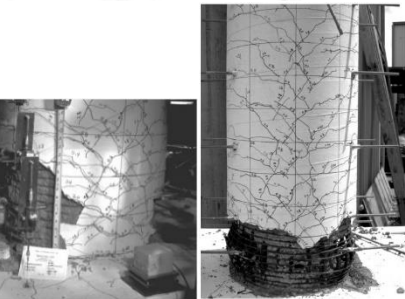
Damage State V-VI (7.22%, 7.22%, 7.27%)

Damage State of Column 328 Tested by Calderone (2000)
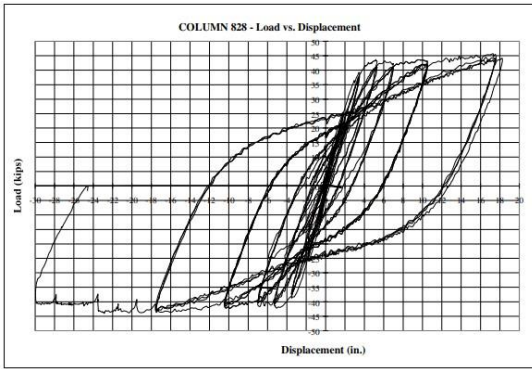
COLUMN 828 - Load vs. Displacement

Dia = 24"
Height = 192"
Force-Deformation Chart
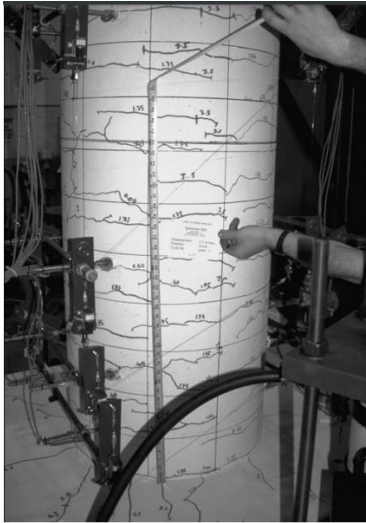
Damage State I

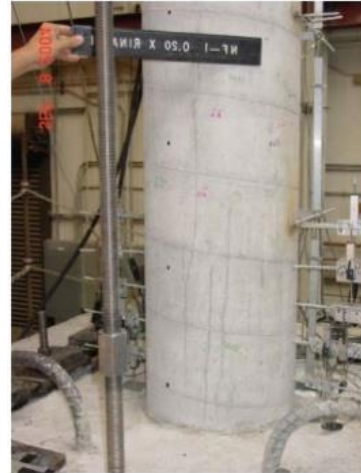Damage State II (1.82%)
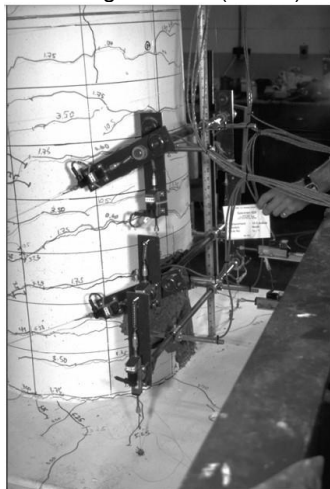
Damage State III

Damage State IV (5.47%)
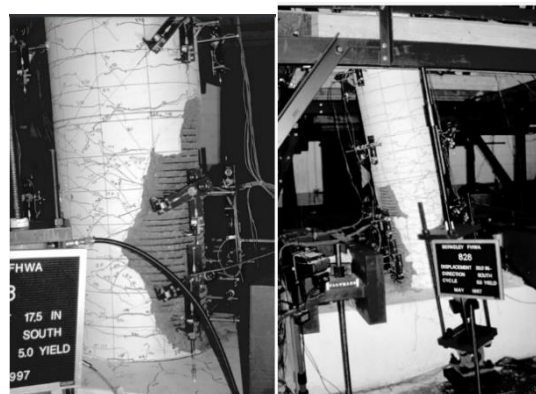
Damage State V (9.11%), VI (15.625%)

Damage State of Column 828 Tested by Calderone (2000)

Dia = 20"
Height = 50"
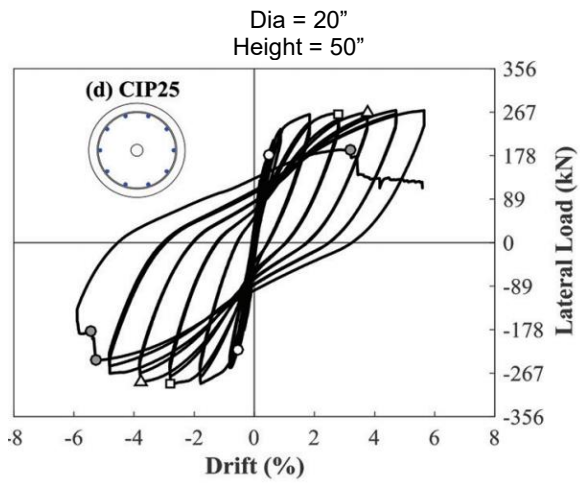
(d) CIP25

Force-Deformation Chart

Damage State I

Damage State II

Damage State III

(f) CIP25: 4% drift
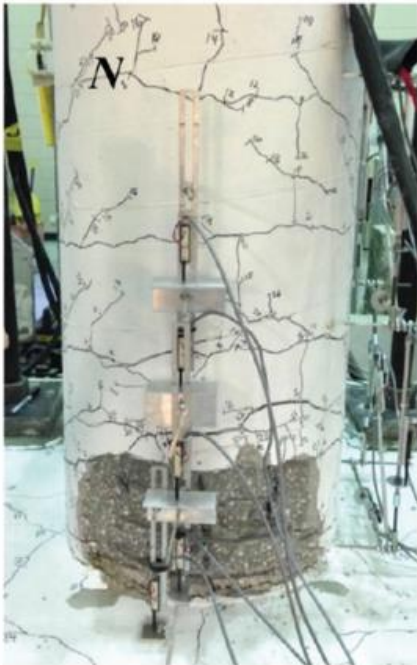
(h) CIP25: failure
(6% drift)

Damage State IV (4%)

Damage State VI (6%)

Damage State of Column CIP25 Tested by Chan et al. (2020)

Dia = 20"
Height = 80"

(b) CIP40

Force-Deformation Chart
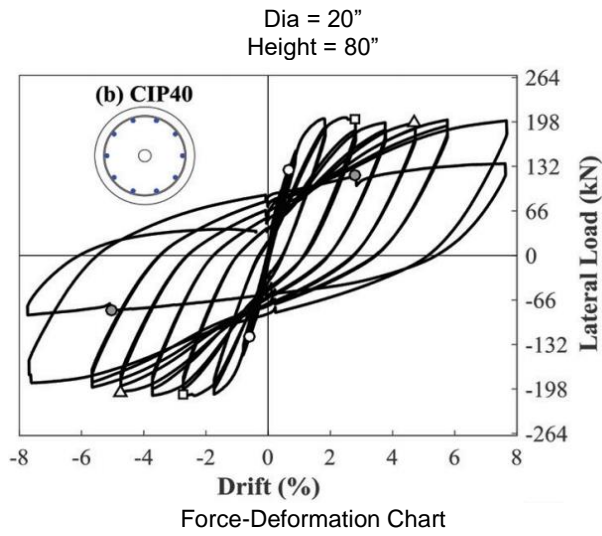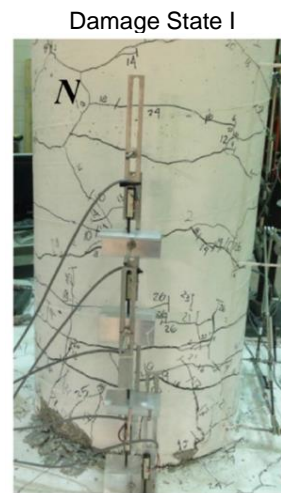
Damage State I

(b) CIP40: 4% drift

Damage State II

Damage State III (4%)

(d) CIP40: failure
(8% drift)

Damage State IV

Damage State VI (8%)

Damage State of Column CIP40 Tested by Chan et al. (2020)
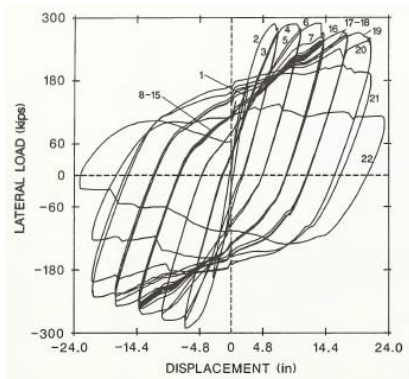
Dia = 59.84"
Height = 360"
Force-Deformation Chart

Damage State I (1.96%)
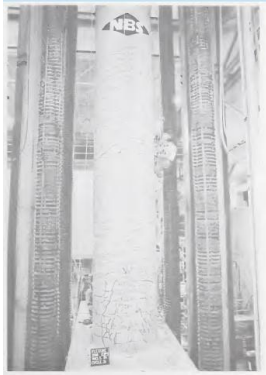
Damage State II (2.92%)

Damage State III (3.92%)
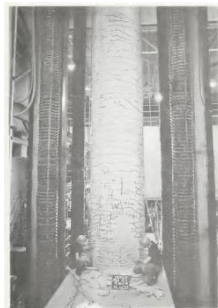
Damage State IV (4.9%)

Damage State V-VI (5.88%, 6.86%)

Damage State of Column NIST-FullScaleFlexure Tested by Cheok and Stone (1986)
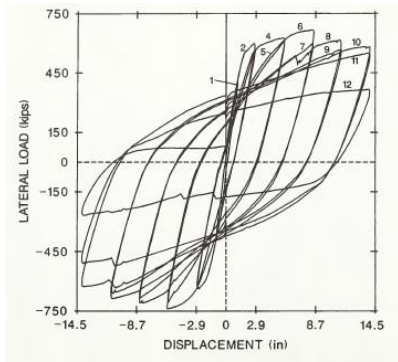
Dia = 59.84"
Height = 180"

Force-Deformation Chart
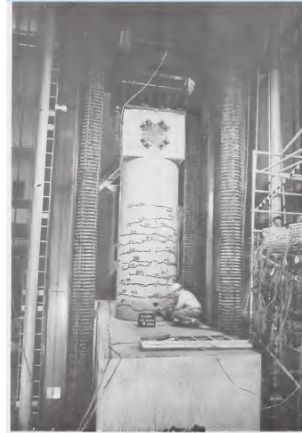
Damage State I (0.778%)

Damage State II (1.5%)
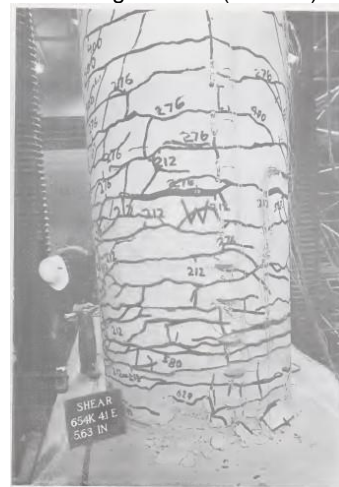
Damage State III (3.1%)
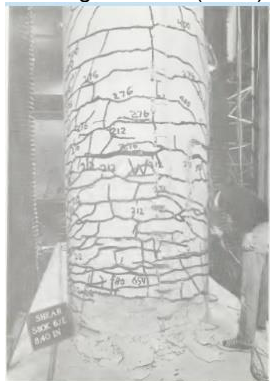
Damage State IV (4.67%)
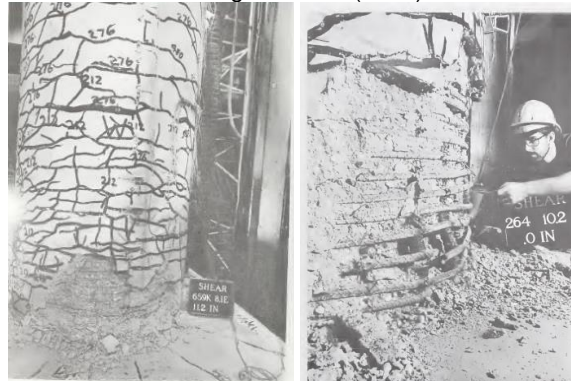
Damage State V (6.2%) & V (7.7%)

Damage State of Column NIST-FullScaleShear Tested by Cheok and Stone (1986)
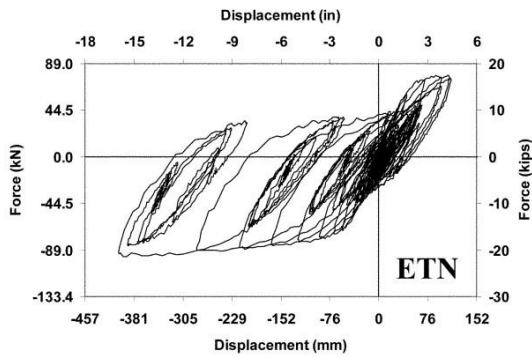
Dia = 14"
Height = 108.5"
Force-Deformation Chart
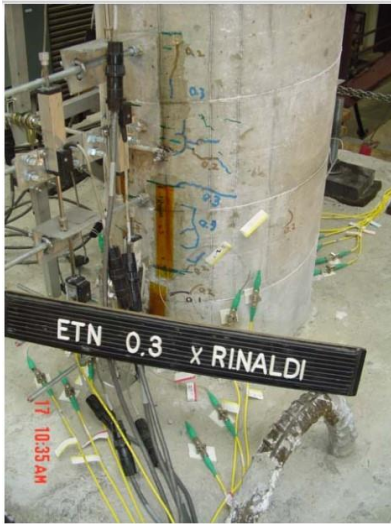
Damage State I

Damage State II (1.59%)

Damage State III

Damage State IV (7.86%)
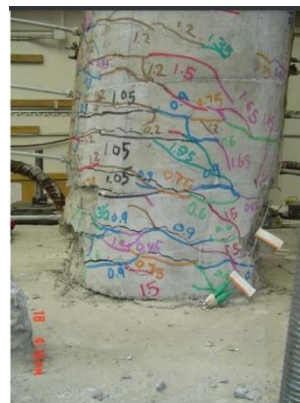
Damage State V-VI (14.69%)

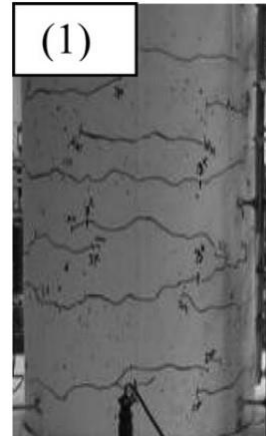**Damage State of Column ETN Tested by Choi et al. (2010)**
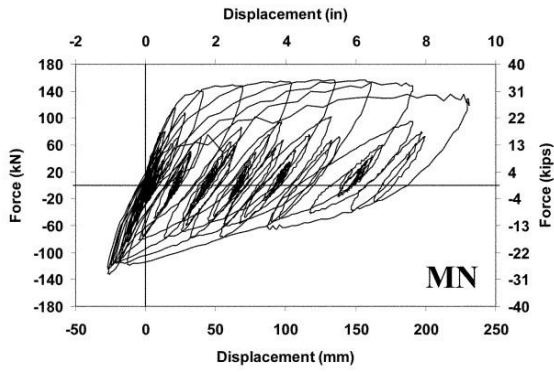
Dia = 14"
Height = 63"
Force-Deformation Chart
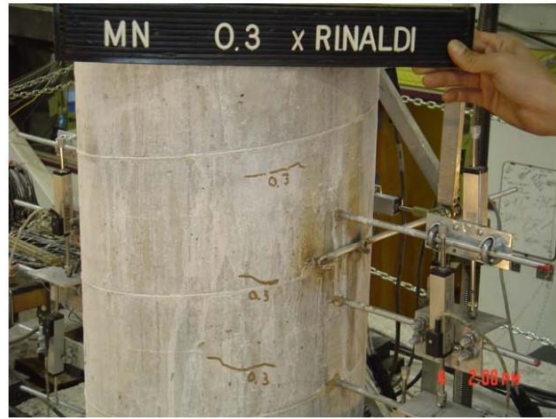
Damage State I (1.33%)

Damage State II

Damage State III (4.35%)

Damage State IV (6.52%)

Damage State V (11.92%) & VI (14.4%, 14.4%)

Damage State of Column MN Tested by Choi et al. (2010)
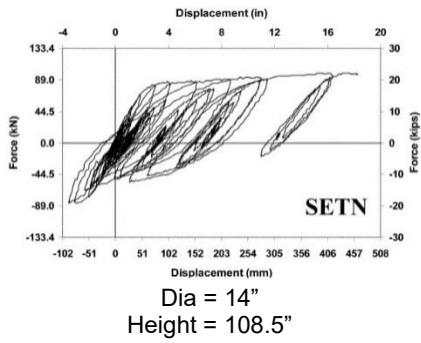
Dia = 14"
Height = 108.5"

Force-Deformation Chart
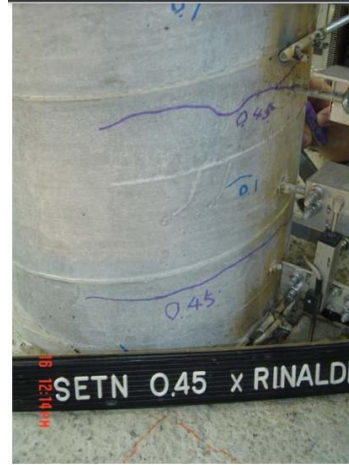
Damage State I (2.77%)

Damage State II

Damage State III

Damage State IV (5.65%, 8.02%)

Damage State V-VI (16.83%, 16.83%)

Damage State of Column SETN Tested by Choi et al. (2010)
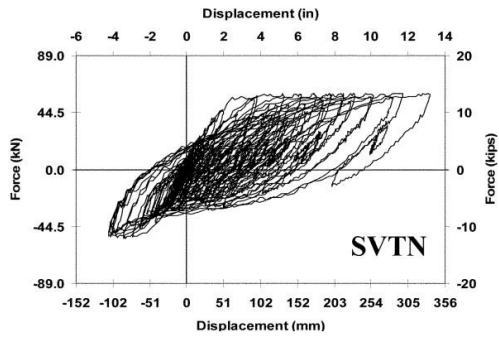
Dia = 14"
Height = 98.5"
Force-Deformation Chart

Damage State I
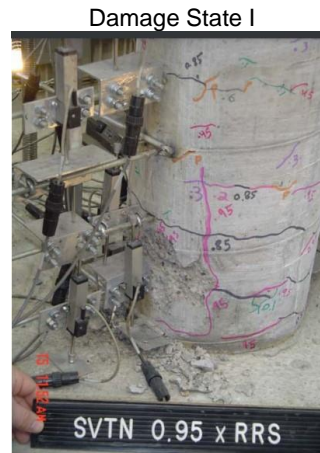
Damage State II (2%)

Damage State III (5.36%)
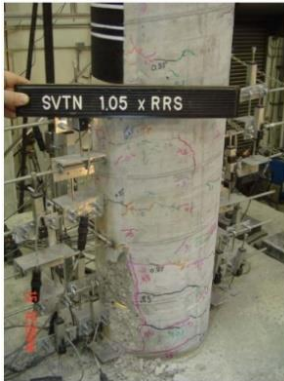
Damage State IV (6.31%, 8.65%)
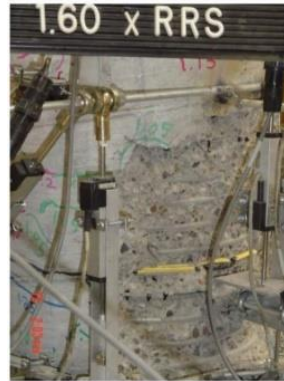
Damage State V (10.27%) & VI (13.39%)

Damage State of Column SVTN Tested by Choi et al. (2010)
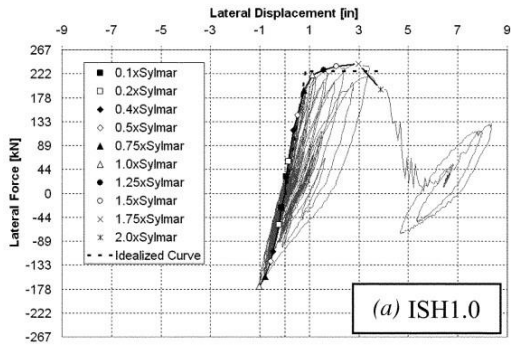
Dia = 10x14.5"
Height = 58"

Force-Deformation Chart
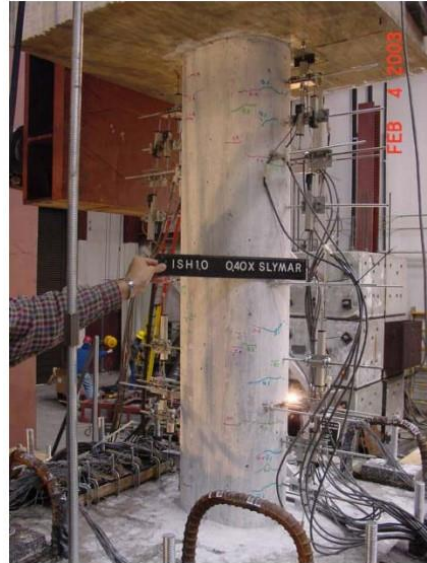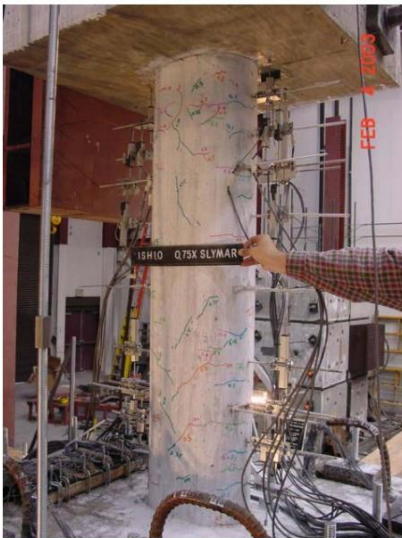
Damage State I (0.81%)

Damage State II (1.41%)
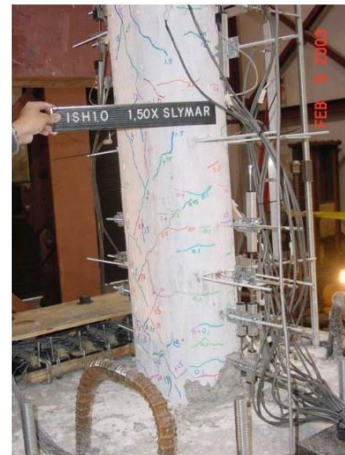
Damage State III (4.13%)
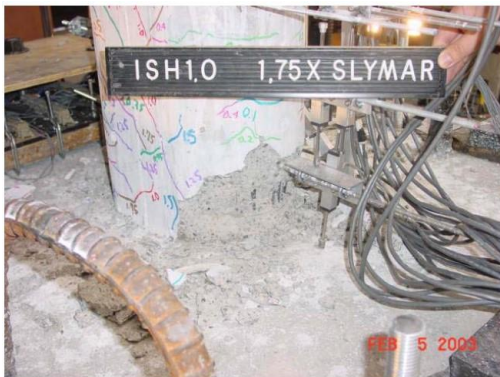
Damage State IV (5.9%)

Damage State VI (6.67%)

Damage State of Column ISH1.0 Tested by Correal et al. (2007)
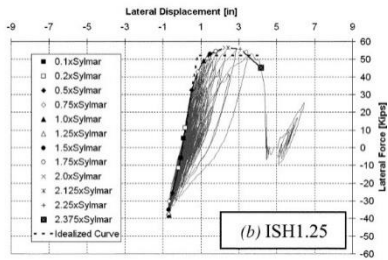
Dia = 10x15.62"
Height = 63"

Force-Deformation Chart
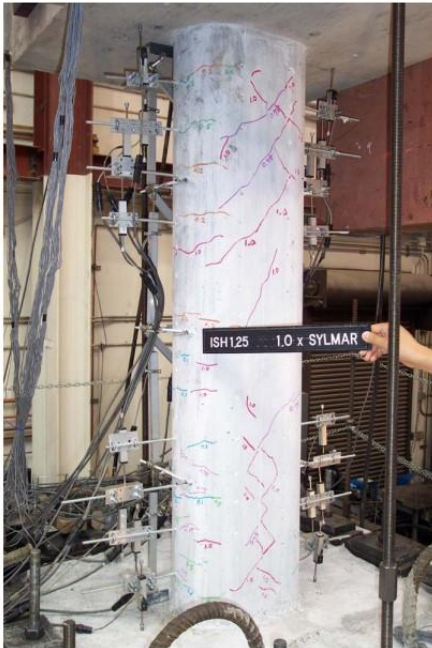
Damage State I (0.87%)

Damage State II (1.84%)

Damage State III (2.92%, 4.51%)

Damage State IV (5.52%)
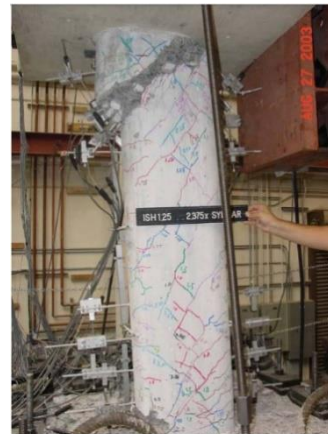
Damage State VI (6.66%)

Damage State of Column ISH1.25 Tested by Correal et al. (2007)
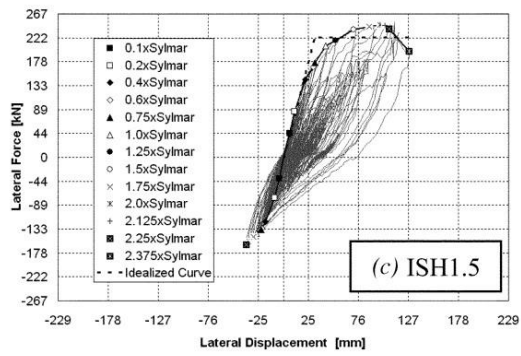
Dia = 10x16.75"
Height = 69"
Force-Deformation Chart

Damage State I

Damage State II (1.3%, 1.87%)

Damage State III (3.86%, 4.35%)

Damage State IV (6.26%, 6.45%)

Damage State V (6.67%) & VI (7.29%)

Damage State of Column ISH1.5 Tested by Correal et al. (2007)
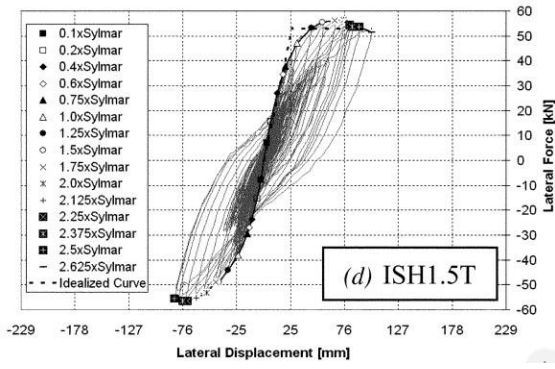
Dia = 10x16.75"
Height = 69"
Force-Deformation Chart

Damage State I (1.04%)

Damage State II (1.84%)
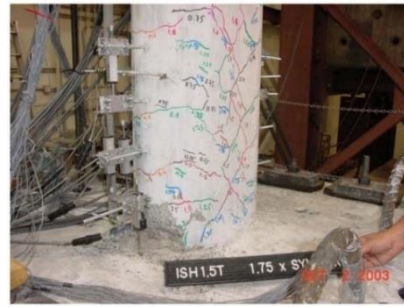
Damage State III (3.86%, 4.35%)

Damage State IV (4.64%)

Damage State V (5.16%) & VI (5.8%, 6.03%)

Damage State of Column ISH1.5T Tested by Correal et al. (2007)
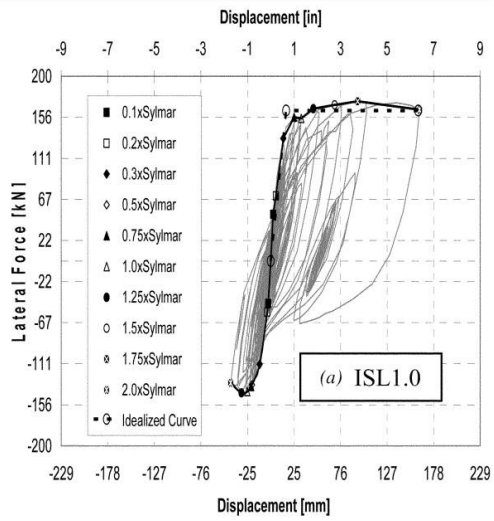
Dia = 12x17.5"
Height = 58"
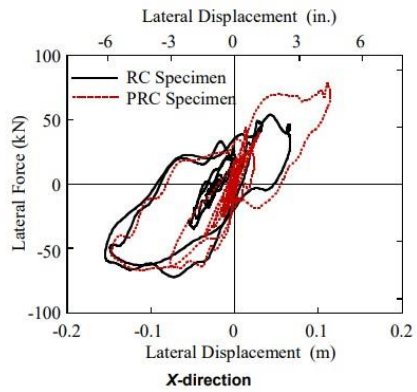Force-Deformation Chart

Damage State I

Damage State II (1.72%)
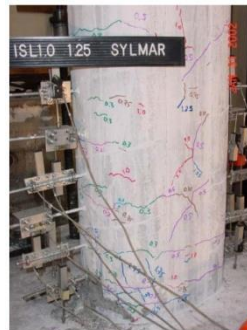
Damage State III (3.59%)

Damage State IV

Damage State VI (10.8%, 10.8%)

Damage State of Column ISL1.0 Tested by Correal et al. (2007)
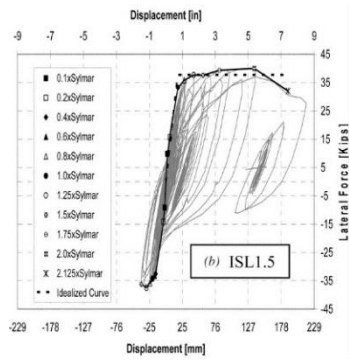
Dia = 12x20.5"
Height = 72"

Force-Deformation Chart
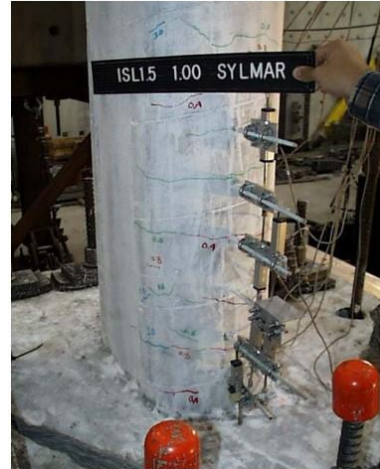
Damage State I (1.32%)
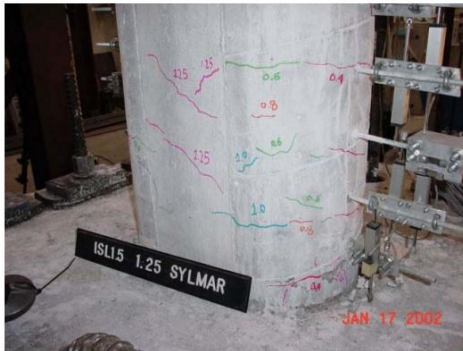
Damage State II (2.35%)

Damage State III (5.36%)

Damage State IV (7.57%)

Damage State VI (10.3%)

Damage State of Column ISL1.5 Tested by Correal et al. (2007)
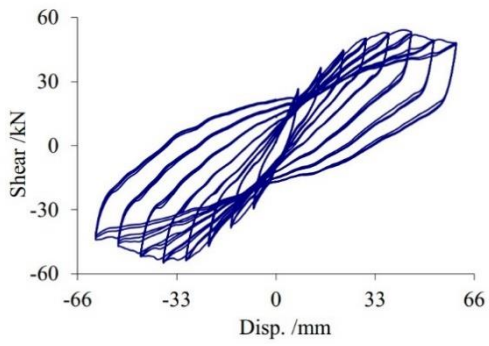
Dia = 11.81"
Height = 74.8"
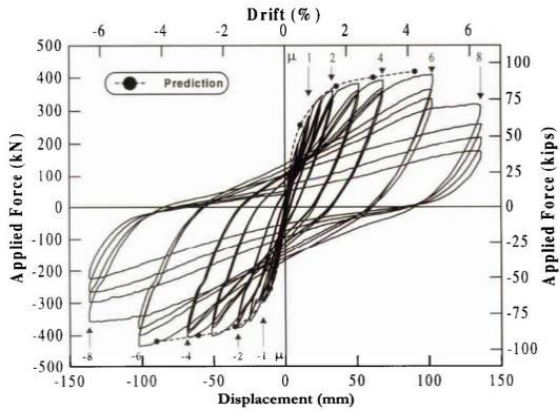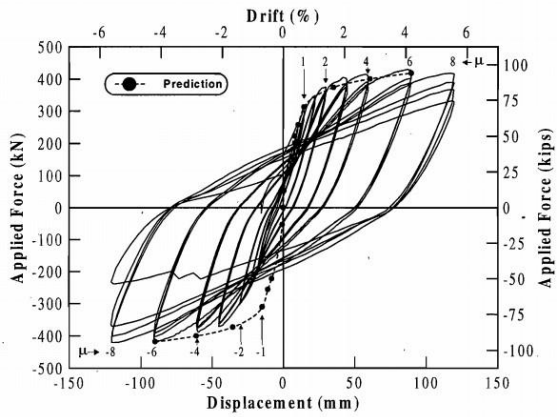Force-Deformation Chart

Damage State I
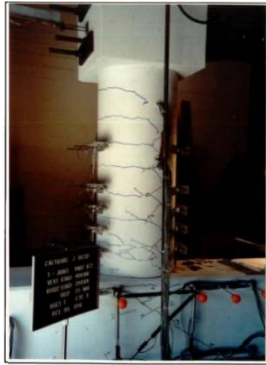
Damage State II

Damage State III

Damage State IV (2.79%)

Damage State V
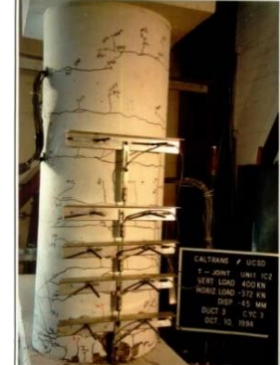
Damage State of Column A1 Tested by Deng et al. (2017)

Dia = 16"
Height = 72"
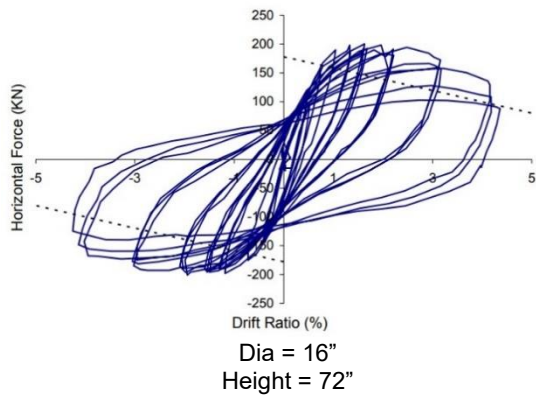
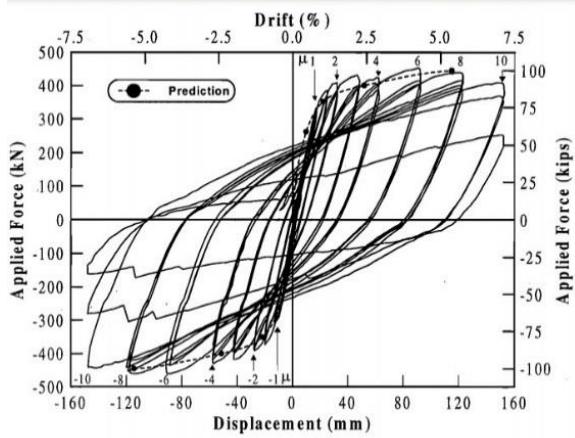Force-Deformation Chart
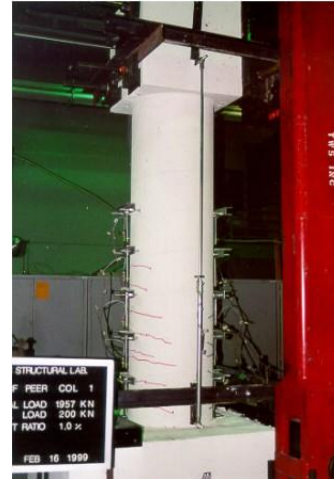
Damage State I (1%)

Damage State II
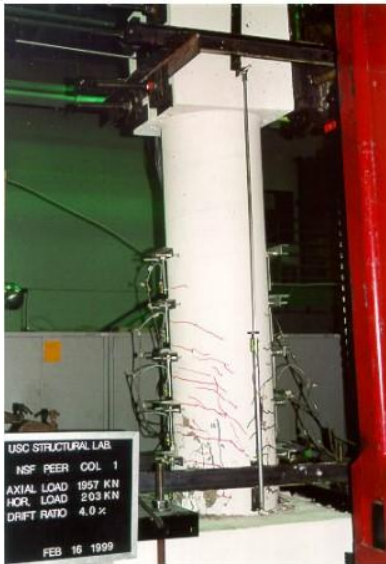
Damage State III

Damage State IV (4%, 4%, 4%)

Damage State V

Damage State of Column S1 Tested by Esmaeily (2002)

Dia = 16"
Height = 72"
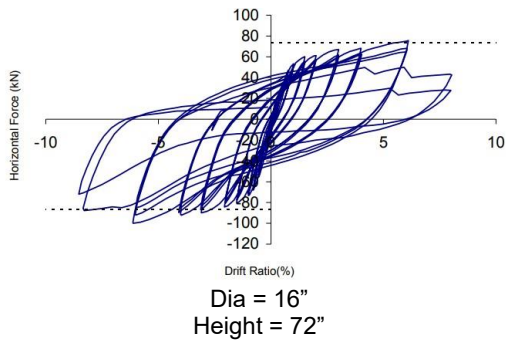
Force-Deformation Chart
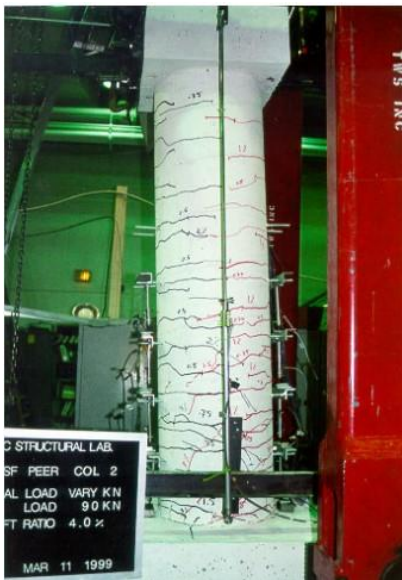
Damage State I (1%)

Damage State II (4%)

Damage State III

Damage State IV

Damage State VI (8%, 8%)

Damage State of Column S2 Tested by Esmaeily (2002)
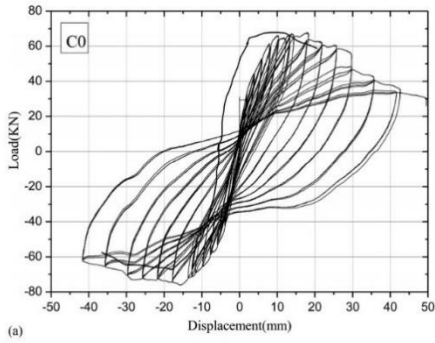
Dia = 11.81"
Height = 43.31"
Force-Deformation Chart

Damage State I

Damage State II
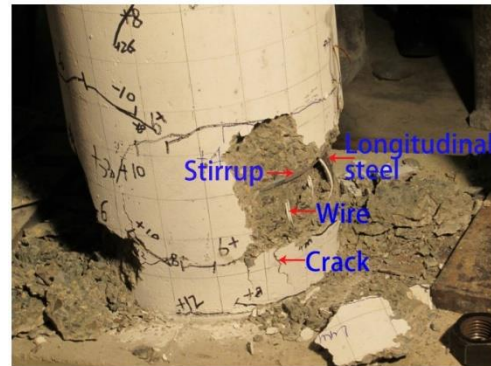
Damage State III

Damage State IV

Damage State V (2.76%)

Damage State of Column C0 Tested by Feng et al. (2007) or Yuan et al. (2017)
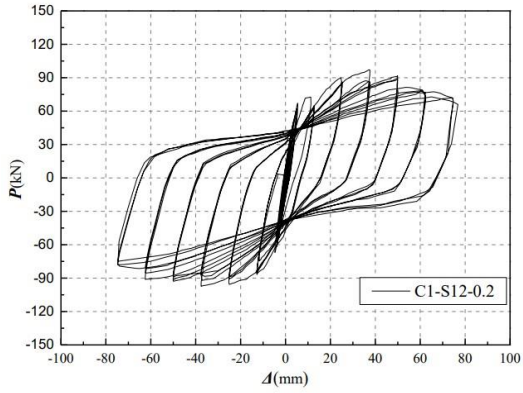
Dia = 13.78"
Height = 65"
Force-Deformation Chart

Damage State I

Damage State II

Damage State III

Damage State IV

Damage State VI (3.67%)

Damage State of Column C1-S12-0.2 Tested by Fu et al. (2019)
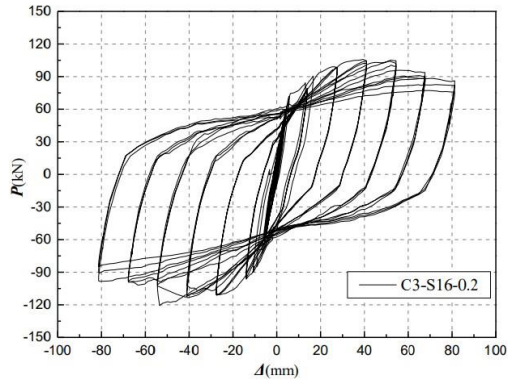
Dia = 13.78"
Height = 65"
Force-Deformation Chart

Damage State I

Damage State II

Damage State III

Damage State IV

Damage State VI (4.28%)

Damage State of Column C3-S16-0.2 Tested by Fu et al. (2019)
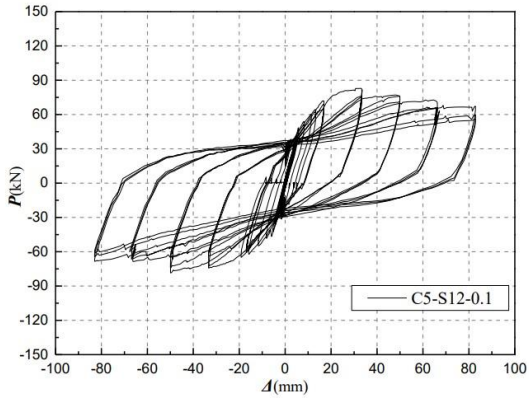
Dia = 13.78"
Height = 65"
Force-Deformation Chart

Damage State I

Damage State II

Damage State III

Damage State IV

Damage State VI (4.22%)

Damage State of Column C5-S12-0.1 Tested by Fu et al. (2019)
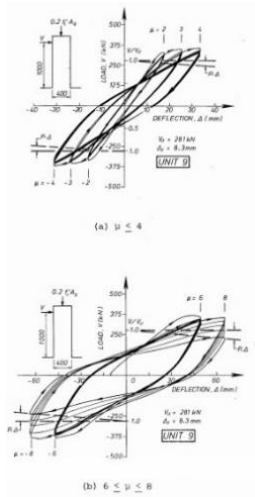
Dia = 15.75"
Height = 40"
Force-Deformation Chart

Damage State I

Damage State II

Damage State III

Damage State IV

Damage State VI (6.36%, 6.36%)

**Damage State of Column No.9 Tested by Ghee et al. (1985)**
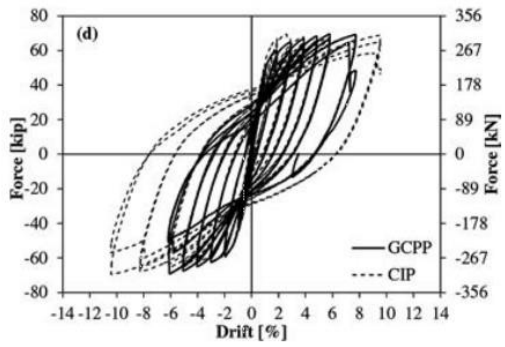
Dia = 24"
Height = 108"
Force-Deformation Chart

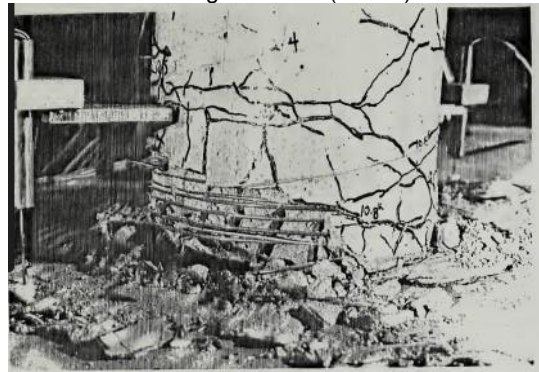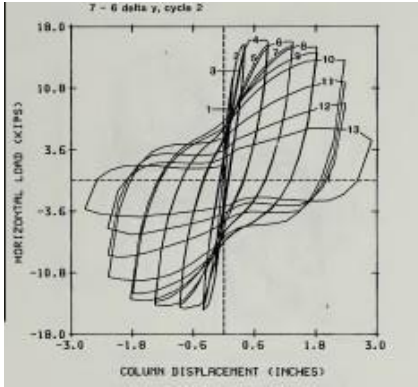Damage State I (0.5%)

Damage State II (0.75%)
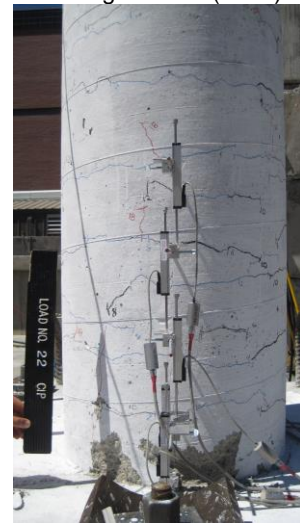
Damage State III (3%)
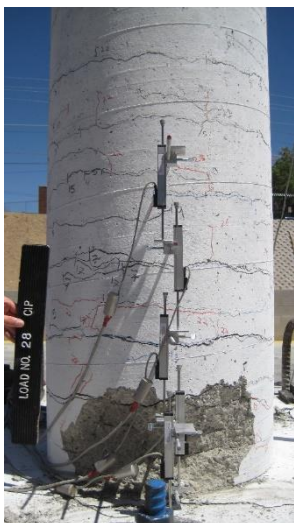
Damage State IV (4%)

Damage State V (6%)

Damage State of Column CIP Tested by Haber et al. (2014)

A-39

No hysteretic data available
Dia = 16"
Height = 96"
Force-Deformation Chart

Damage State I

Damage State II

Damage State III (5.07%)
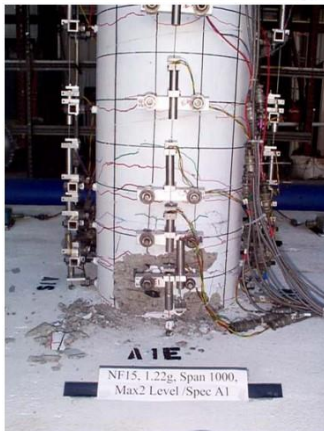
Damage State IV (5.46%, 6.95%)

Damage State V-VI (7.8%)

Damage State of Column A1 Tested by Hachem et al. (2003)

No hysteretic data available
Dia = 16"
Height = 96"
Force-Deformation Chart

Damage State I

Damage State II

Damage State III (4.96%, 5.6%)

NF15-16, (1.22g,0.99g) , Spans
(1000,277) Max2 Level/Spec A2
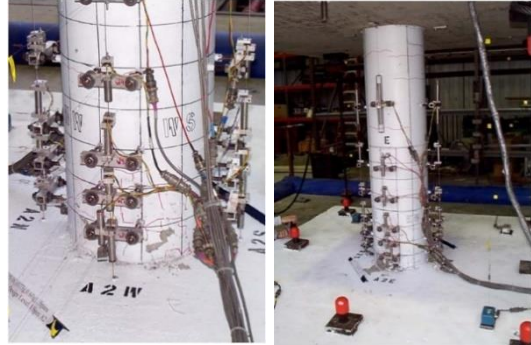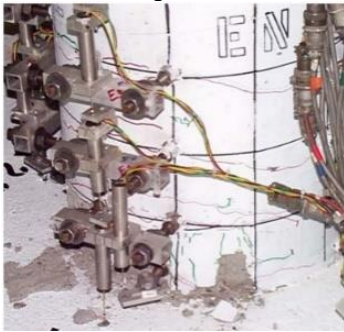
Damage State IV (Later run to 5.6%, 7.08%, 7.5%)

NF15-16, (1.22g,0.99g) , Spans
(1000,277) Max6 Level/Spec A2

Damage State V (7.65%) & VI (8.26%)

**Damage State of Column A2 Tested by Hachem et al. (2003)**

No hysteretic data available
Dia = 16"
Height = 96"
Force-Deformation Chart

Damage State I

Damage State II

Damage State III (3.56%)
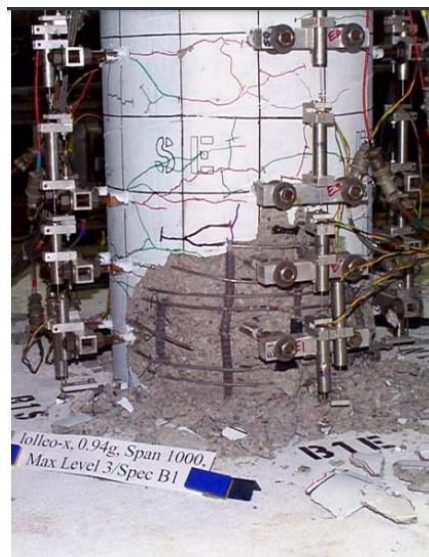
Damage State IV (6.05%)

Damage State VI (Later run to 6.05%)

Damage State of Column B1 Tested by Hachem et al. (2003)

No hysteretic data available
Dia = 16"
Height = 96"
Force-Deformation Chart

Damage State I

Damage State II
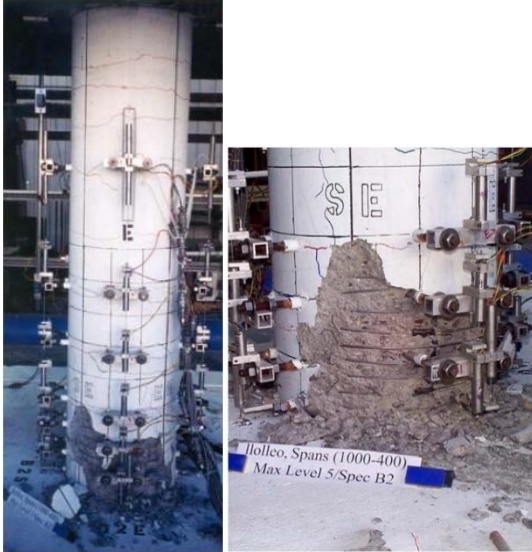
Damage State III

Damage State IV (5.82%, 5.82%)

Damage State VI (Both later runs to 5.82%)

Damage State of Column B2 Tested by Hachem et al. (2003)

Dia = 24"
Height = 144"
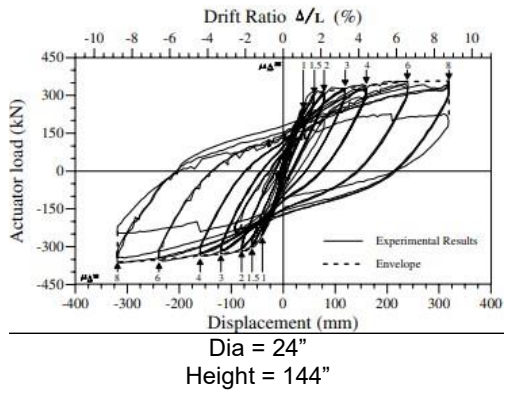
Force-Deformation Chart
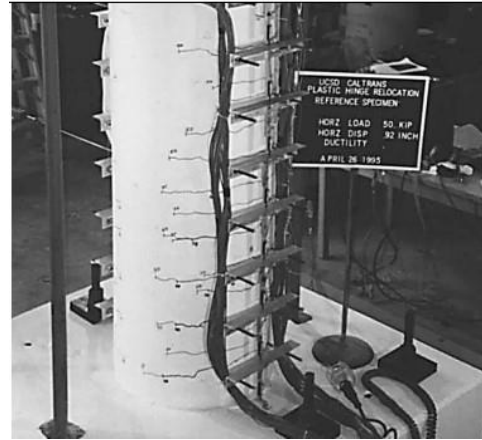
Damage State I (0.639%)
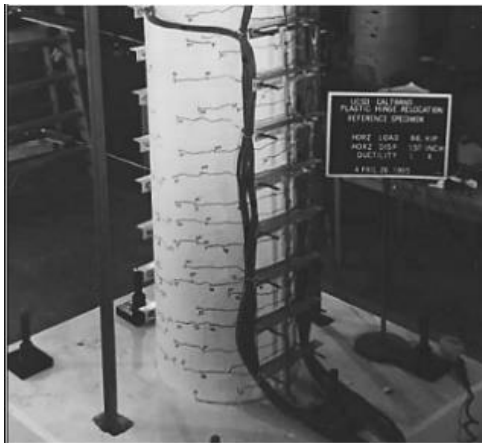
Damage State II (1.09%)
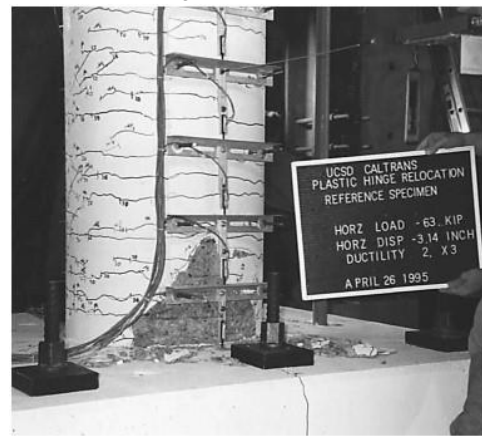
Damage State III (2.18%)

Damage State IV (6.54%)

Damage State V-VI (8.7%)

Damage State of Column Reference Tested by Hose et al. (1997)
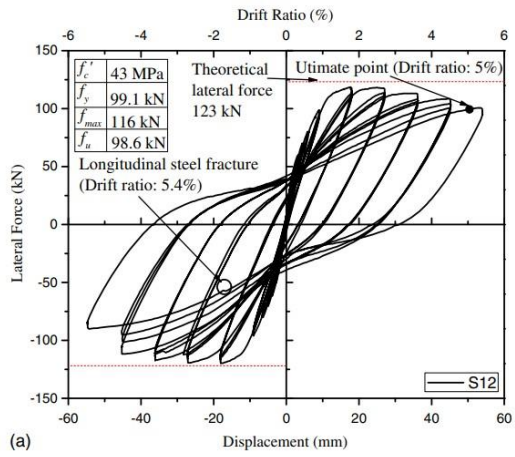
Dia = 11.81"
Height = 39.37"
Force-Deformation Chart
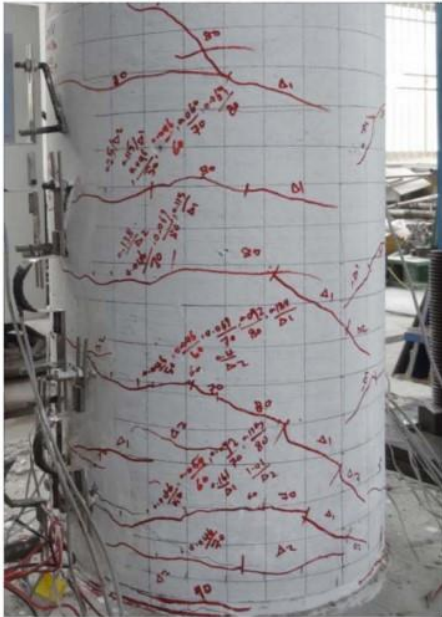
Damage State I

Damage State II (3.6%)

Damage State III

Damage State IV

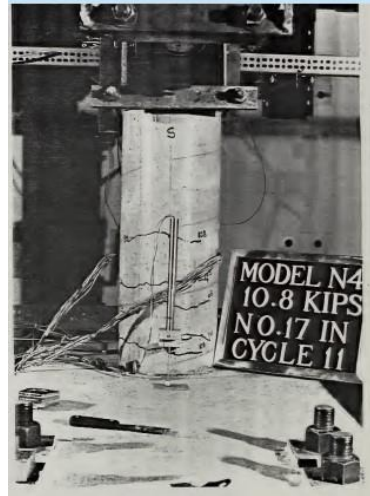Damage State V

Damage State of Column S12 Tested by Ibrahim et al. (2016)
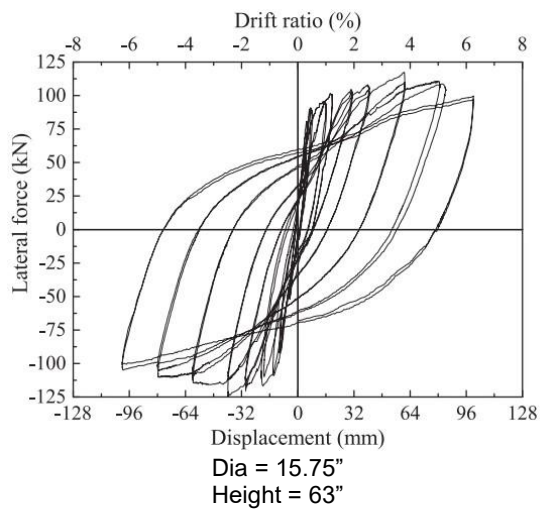
Dia = 15.75"
Height = 63"

Force-Deformation Chart
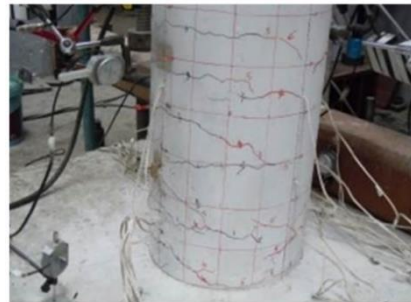
Damage State I (0.31%, 0.63%)
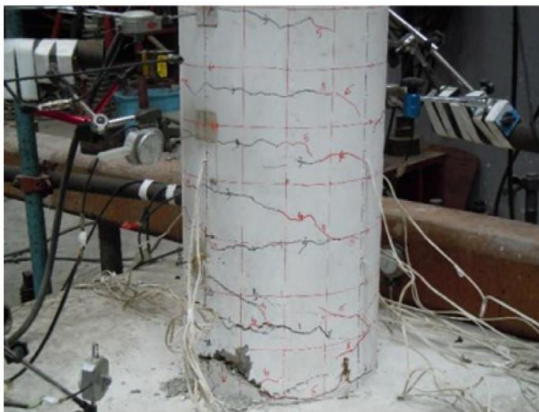
Damage State II (2.5%)

Damage State III (3.75%)

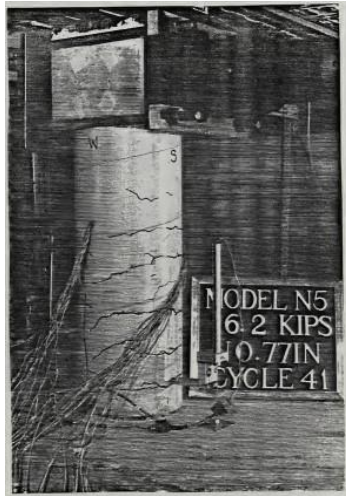Damage State IV (5%)

Damage State VI (5.9%)

Damage State of Column A1 Tested by Jia et al. (2019)
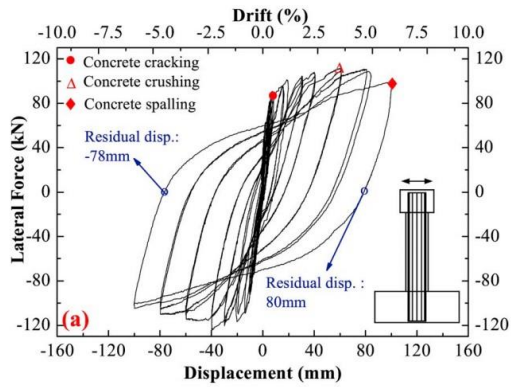
Dia = 15.75"
Height = 63"
Force-Deformation Chart

Damage State I

Damage State II

Damage State III

Damage State IV

Damage State VI (6.49%)

Damage State of Column CIP Tested by Jia et al. (2020)

Dia = 16"
Height = 72"
Force-Deformation Chart
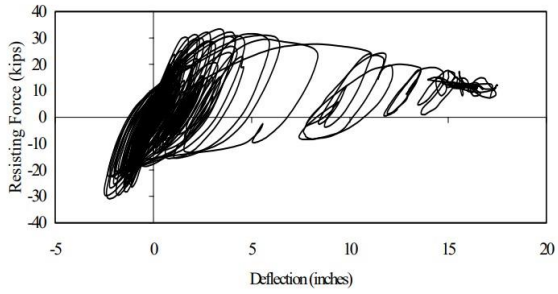
Damage State I

Damage State II

Damage State III

Damage State IV (8.89%)

Damage State VI (23.61%)

Damage State of Column 9F1 Tested by Laplace (1999)

Dia = 16"
Height = 72"
Force-Deformation Chart
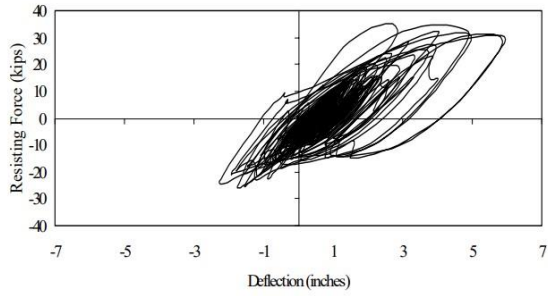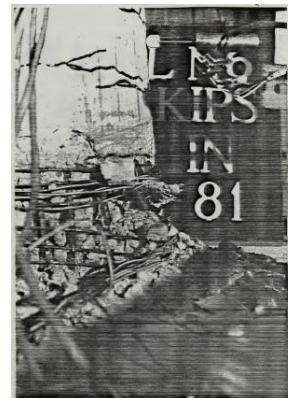
Damage State I

Damage State II

Damage State III

Damage State IV (6.94%)

Damage State V-VI (8.19%)

Damage State of Column 9F2 Tested by Laplace (1999)
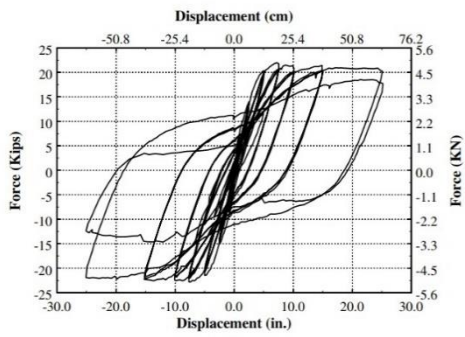
Dia = 24"
Height = 240"

Force-Deformation Chart

Damage State I

Damage State II (2.08%)
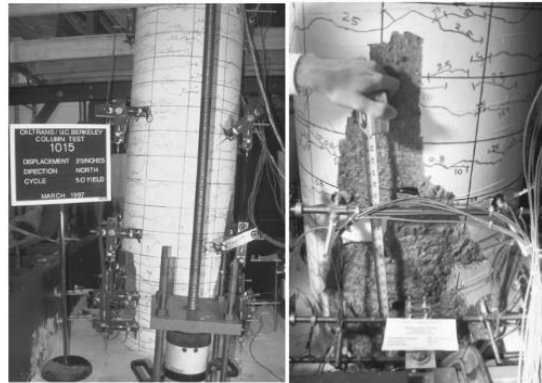
Damage State III

Damage State IV

Damage State VI (10.42%. 10.42%. 10.42%)

Damage State of Column 1015 Tested by Lehman (2000)

A-50
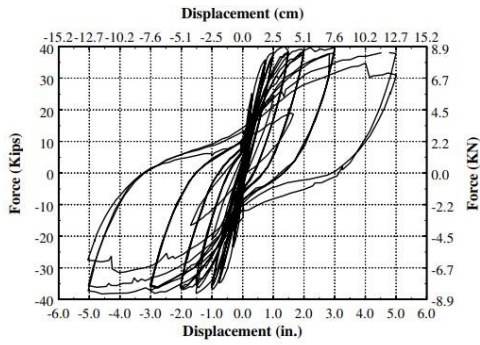
Dia = 24"
Height = 96"
Force-Deformation Chart

Damage State I
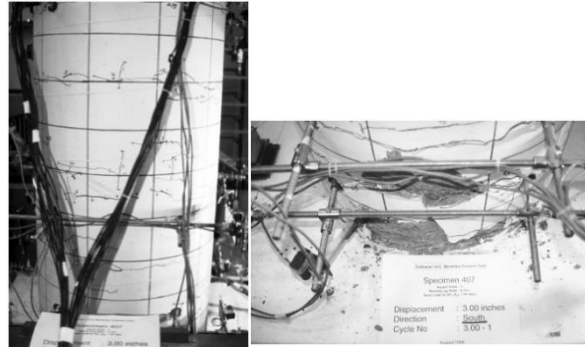
Damage State II

Damage State III (3.125%, 3.125%)
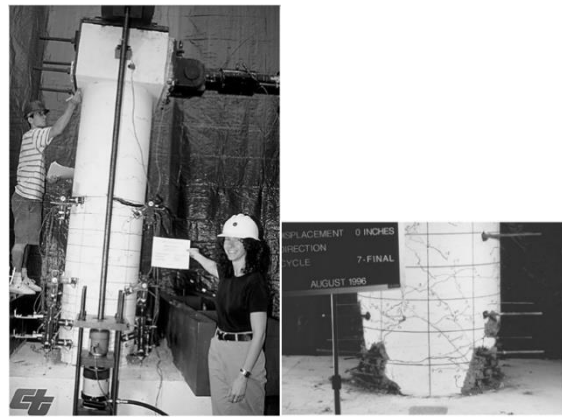
Damage State IV

Damage State V (5.21%) & VI (5.25%)

Damage State of Column 407 Tested by Lehman (2000)
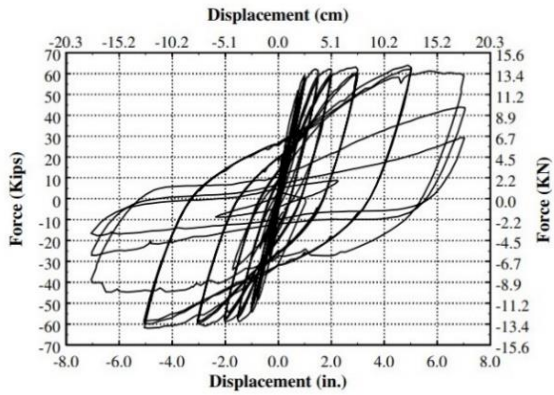
Dia = 24"
Height = 96"
Force-Deformation Chart

Damage State I

Damage State II (2.08%)
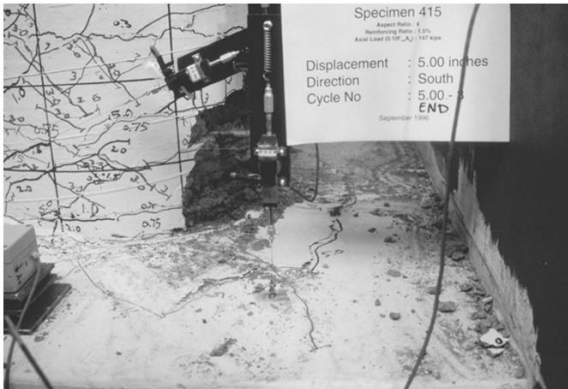
Damage State III

Damage State IV (5.21%)
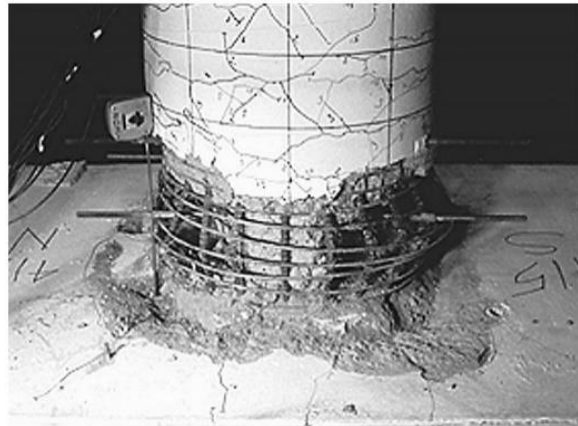
Damage State VI (7.29%)

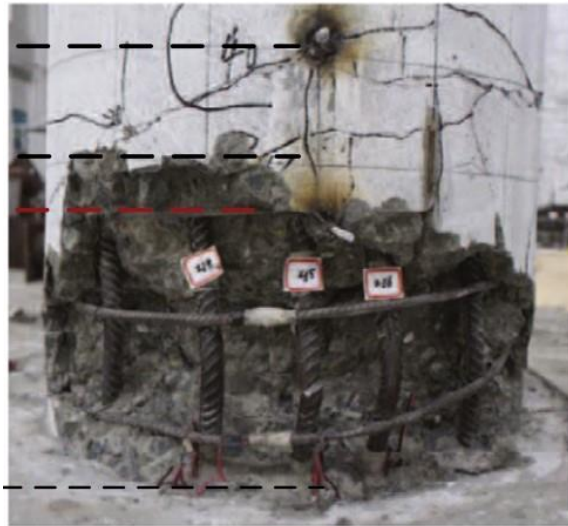**Damage State of Column 415 Tested by Lehman (2000)**
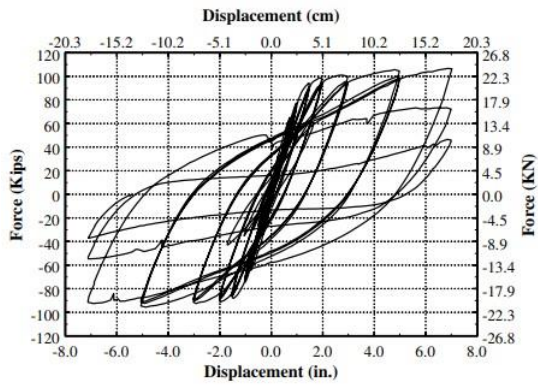
Dia = 24"
Height = 96"
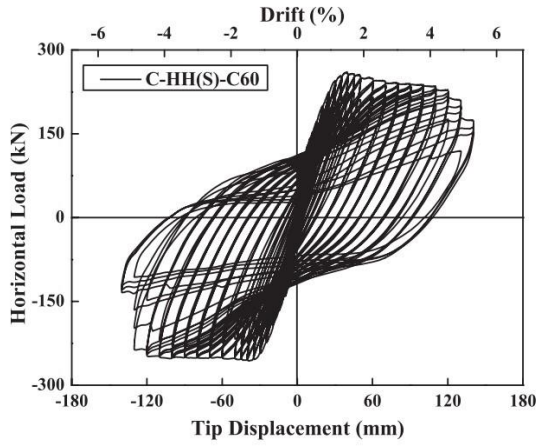Force-Deformation Chart
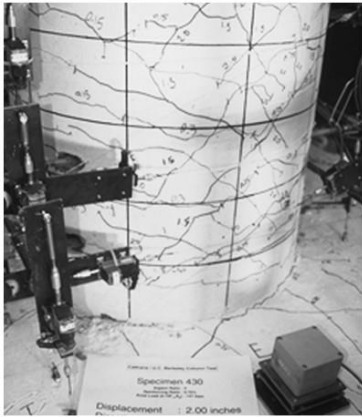
Damage State I

Damage State II (2.08%)

Damage State III

Damage State IV

Damage State VI (7.42%)

Damage State of Column 430 Tested by Lehman (2000)
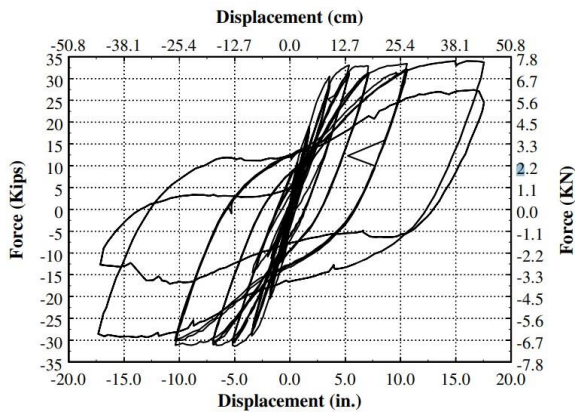
Dia = 24"
Height = 192"

Force-Deformation Chart

Damage State I

Damage State II (1.82%)

Damage State III

Damage State IV (9.11%)
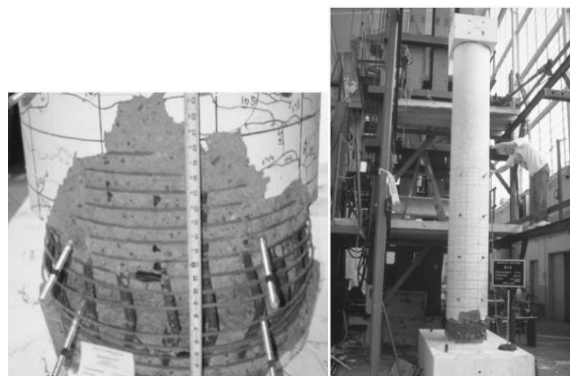
Damage State VI (9.15%, 9.15%)

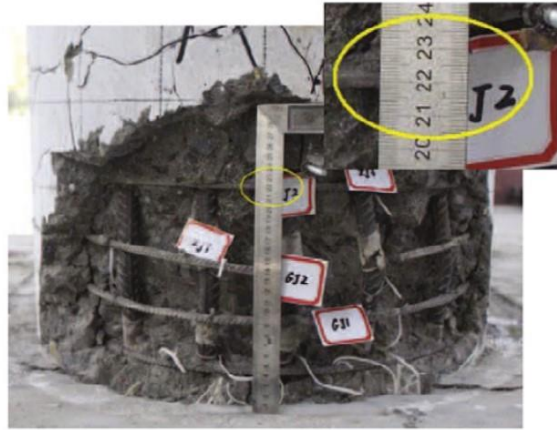**Damage State of Column 815 Tested by Lehman (2000)**
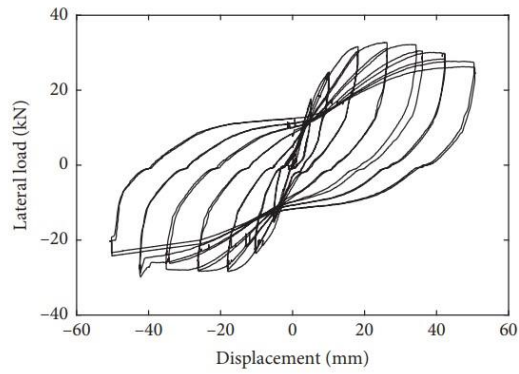
Dia = 9.45"
Height = 55.12"
Force-Deformation Chart

Damage State I

Damage State II

Damage State III

Damage State IV

Damage State VI (3.52%)

Damage State of Column NU-1 Tested by Li et al. (2019)

Octagonal
Section Diameter = 18"
Height = 78.5"
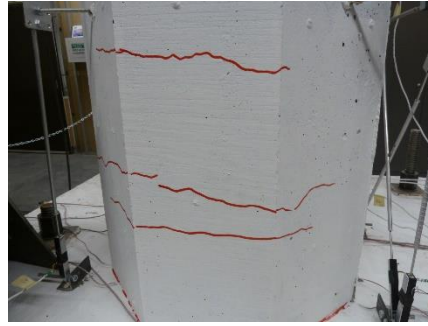
Damage State I (0.26%)

Force-Deformation Chart

Damage State II (2.65%)

Damage State III (4.42%)

Damage State IV (7.02%)

Damage State V (9.73%) & VI (10.62%)

Damage State of Column CIP Test by Marshall et al. (2020)
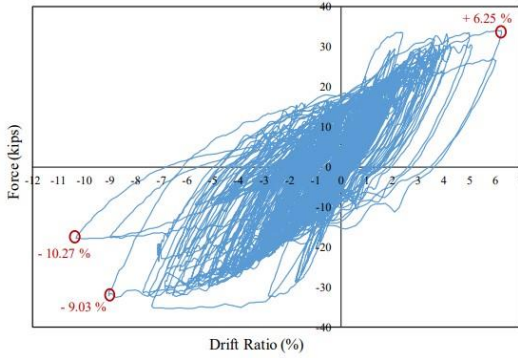
Dia = 16"
Height = 72"
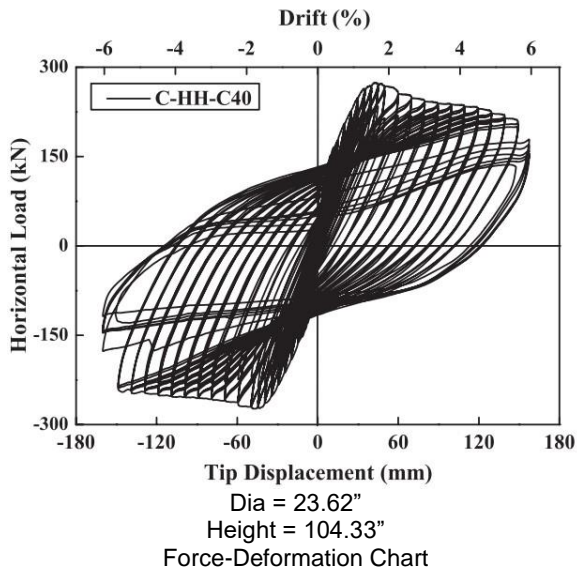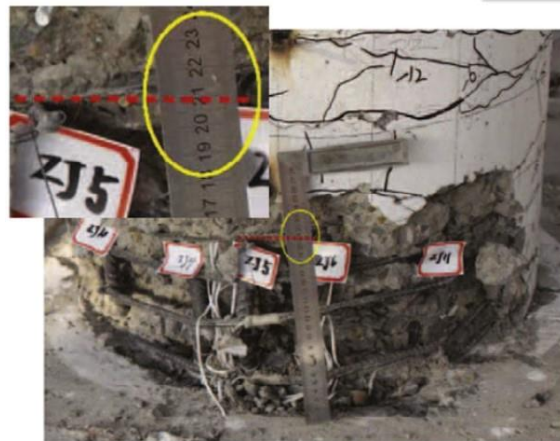Force-Deformation Chart

Damage State I

Damage State II

Damage State III

Damage State IV (7.34%, 7.7%)
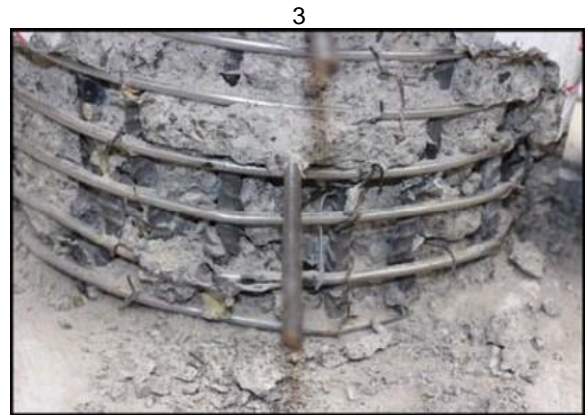
Damage State VI (9.03%)

Damage State of Column LD-C1 Tested by Mohammed et al. (2016)
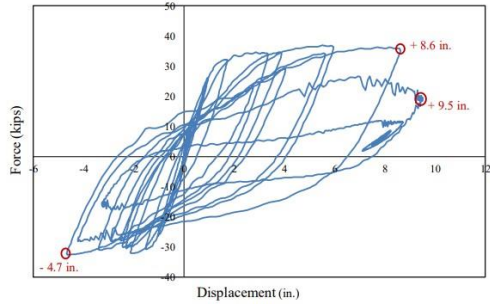
Dia = 16"
Height = 72"
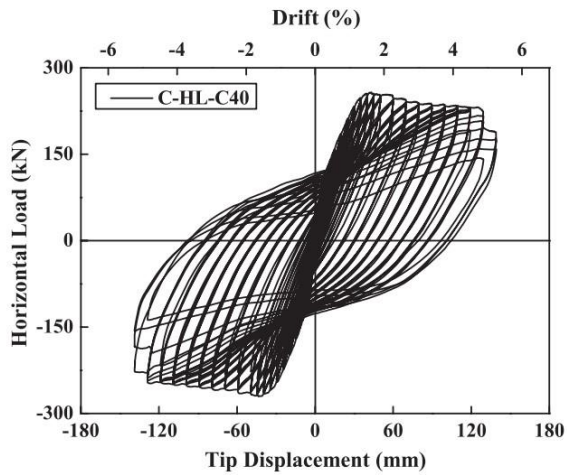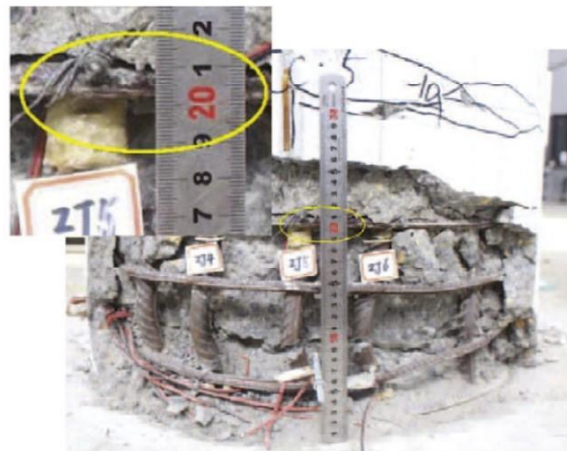Force-Deformation Chart

Damage State I

Damage State II

Damage State III

Damage State IV

Damage State VI (13.14%)

Damage State of Column LD-C2 Tested by Mohammed et al. (2016)
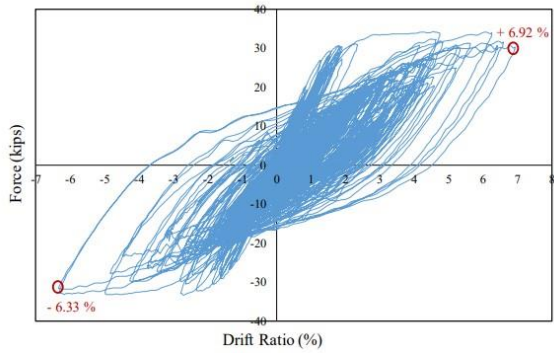
Dia = 16"
Height = 72"
Force-Deformation Chart
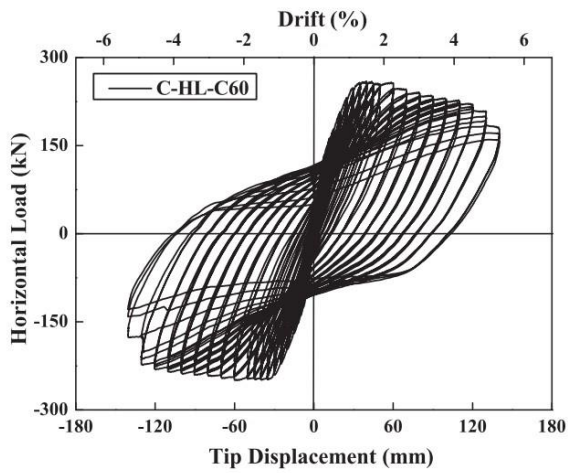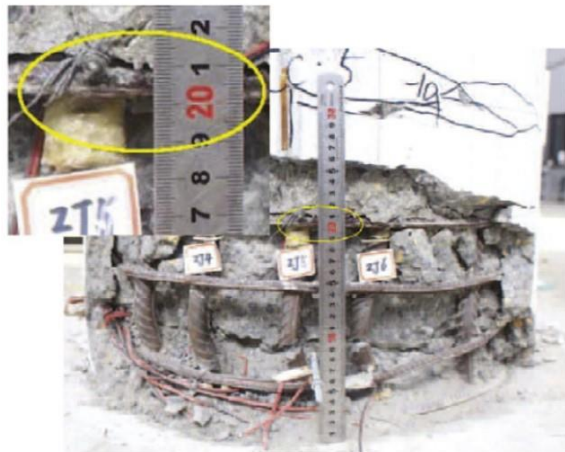
Damage State I

Damage State II

Damage State III (6.26%)

Damage State IV

Damage State VI (6.92%)

Damage State of Column LD-J1 Tested by Mohammed et al. (2016)
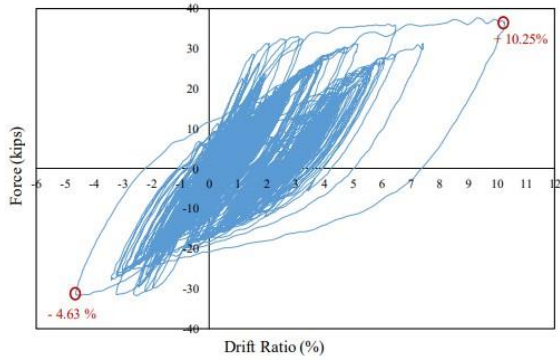
Dia = 16"
Height = 72"
Force-Deformation Chart

Damage State I

Damage State II

Damage State III (6.48%)

Damage State IV

Damage State V-VI (10.25%)

Damage State of Column LD-J2 Tested by Mohammed et al. (2016)
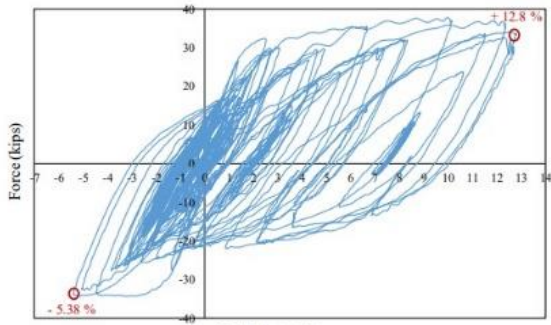
Dia = 16"
Height = 72"
Force-Deformation Chart

Damage State I

Damage State II

Damage State III (5.38%)

Damage State IV (6.67%)

Damage State VI (12.8%)

Damage State of Column SD-L Tested by Mohammed et al. (2016)
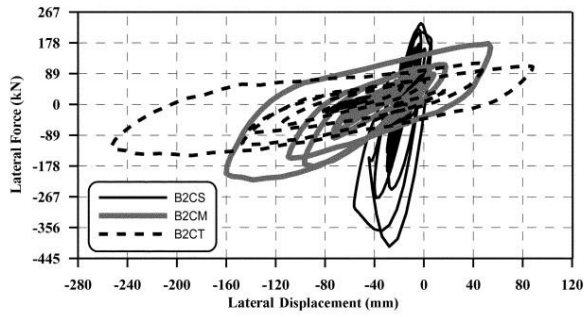
Dia = 14"
Height = 63"
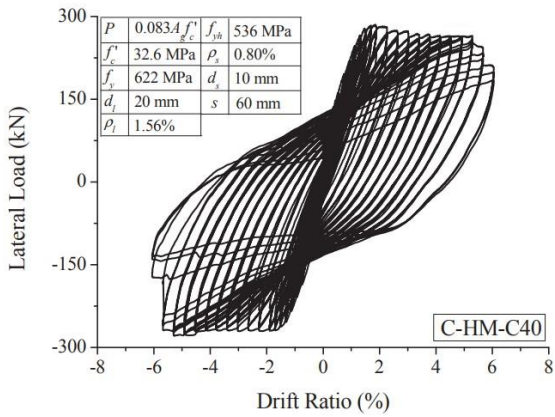Force-Deformation Chart

Damage State I

Damage State II

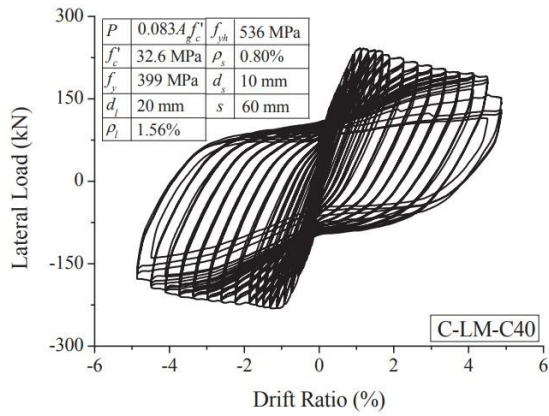Damage State III

Damage State IV

Damage State V-VI (10.02%)

Damage State of Column B2CM Tested by Moustafa et al. (2011)
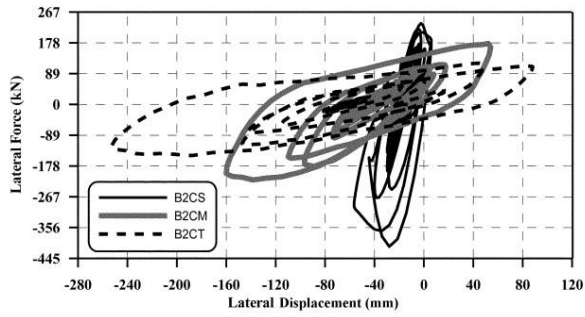
Dia = 14"
Height = 35.39"
Force-Deformation Chart

Damage State I

Damage State II
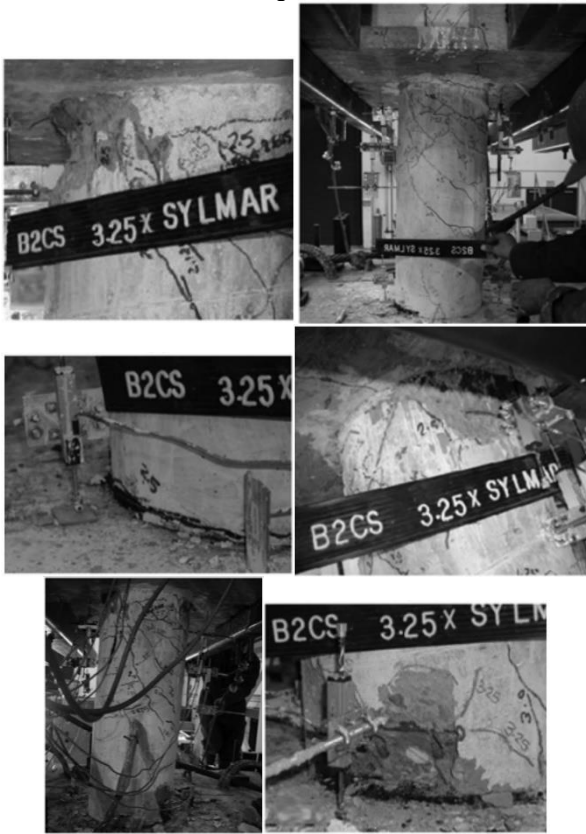
Damage State III

Damage State IV (4.84%)

Damage State V

Damage State of Column B2CS Tested by Moustafa et al. (2011)
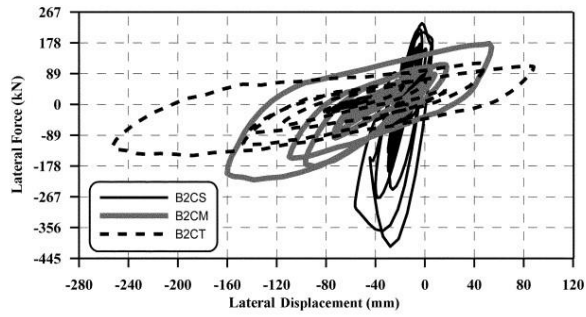
Dia = 14"
Height = 93"
Force-Deformation Chart

Damage State I

Damage State II

Damage State III

Damage State IV

Damage State V (10.66%)

Damage State of Column B2CT Tested by Moustafa et al. (2011)
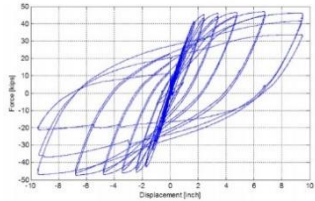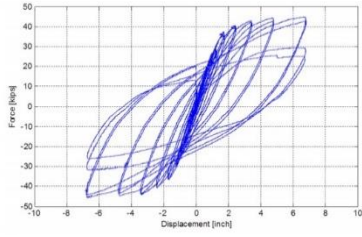
Dia = 18"
Height = 90"
Force-Deformation Chart

Damage State I

Damage State II

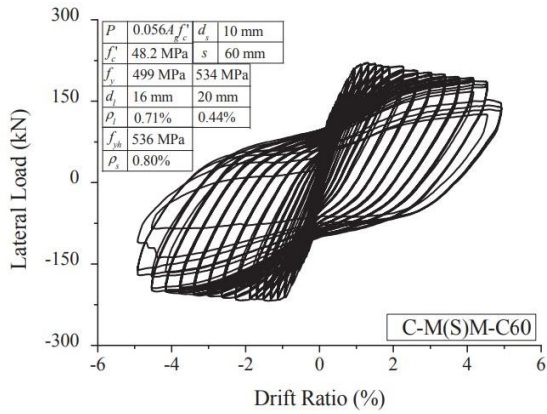Damage State III

Damage State IV

Damage State VI (10.52%. 10.52%. 10.52%, 10.52%)

Damage State of Column No1 Tested by Moustafa et al. (2015).
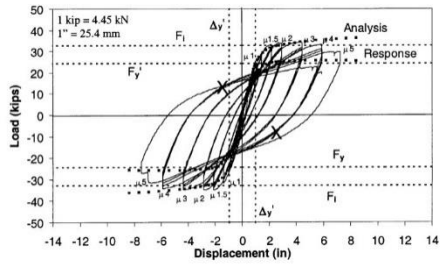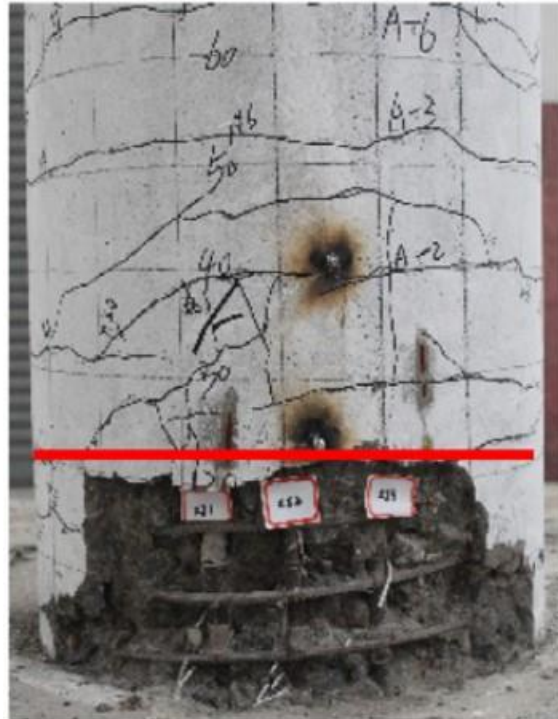
Dia = 18"
Height = 96"
Force-Deformation Chart

Damage State I

Damage State II

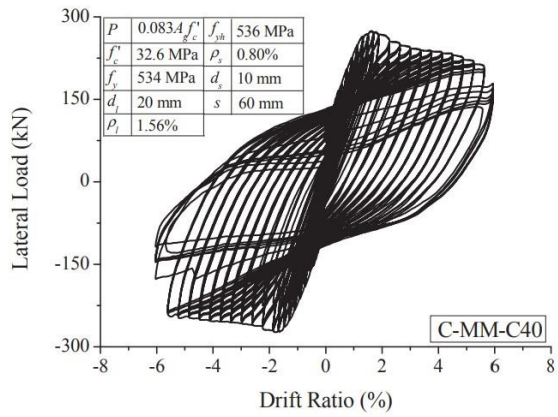Damage State III

Damage State IV

Damage State V (3.9%)

Damage State of Column Unit 1 Tested by Moyer and Kowalsky (2003)

Dia = 18"
Height = 96"
Force-Deformation Chart

Damage State I

Damage State II
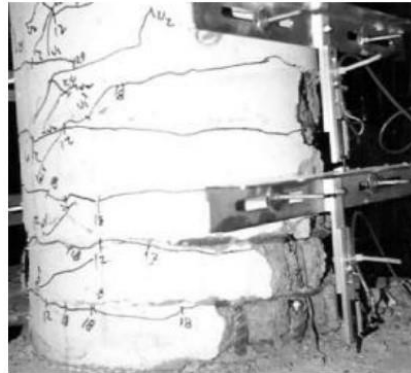
Damage State III

Damage State IV

Damage State V (6.825%)

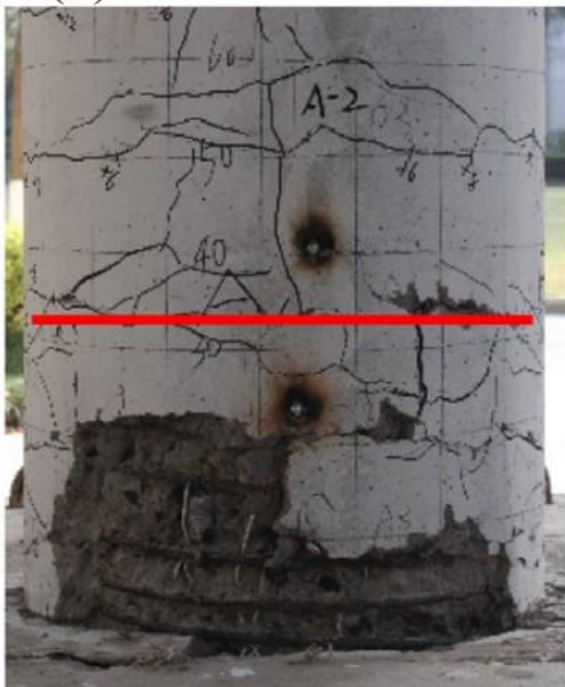**Damage State of Column Unit 2 Tested by Moyer and Kowalsky (2003)**
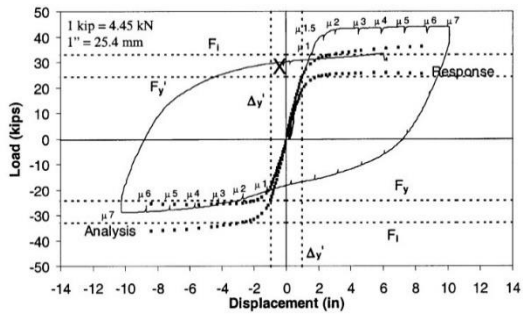
Dia = 18"
Height = 96"
Force-Deformation Chart

Damage State I

Damage State II

Damage State III

Damage State IV

Damage State V (6.825%)

Damage State of Column Unit 3 Tested by Moyer and Kowalsky (2003)
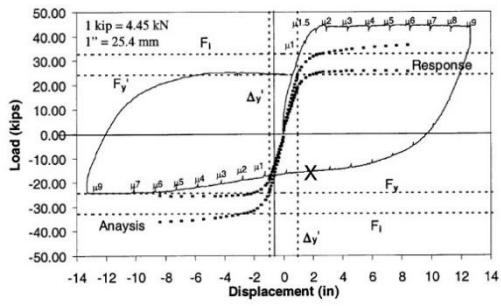
Dia = 18"
Height = 96"
Force-Deformation Chart

Damage State I

Damage State II

Damage State III

Damage State IV

Damage State V (8.775%)

Damage State of Column Unit 4 Tested by Moyer and Kowalsky (2003)
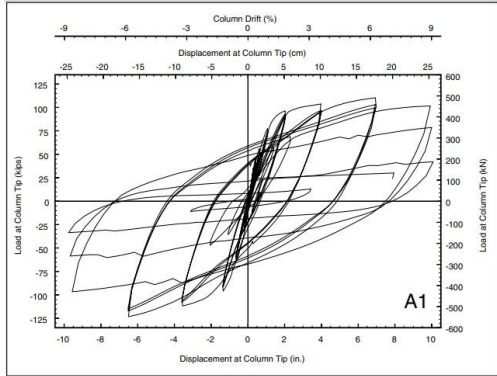
Dia = 28"
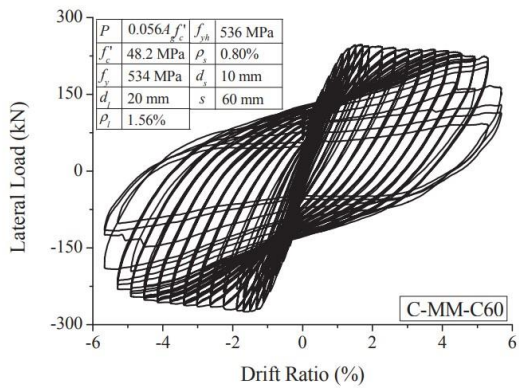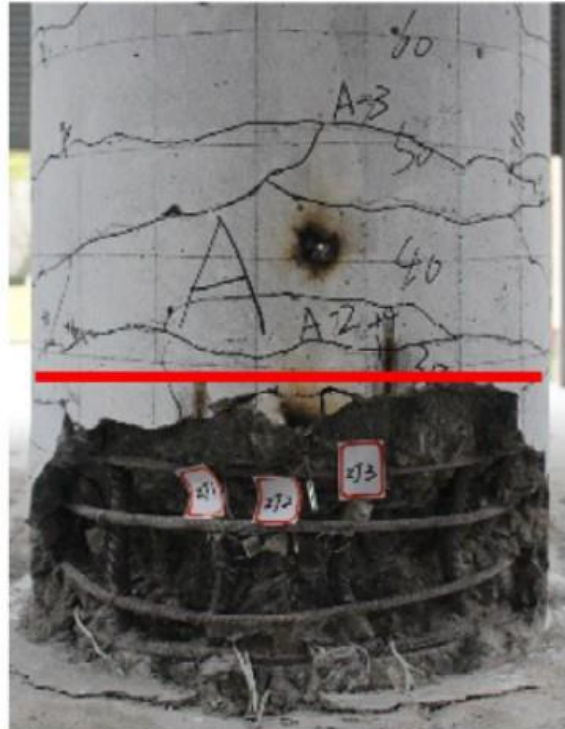Height = 111"
Force-Deformation Chart

Damage State I

Damage State II

Damage State III

Damage State IV (6.32%)

Damage State V

Damage State of Column A1 Tested by Naito (2001)

Dia = 28"
Height = 111"
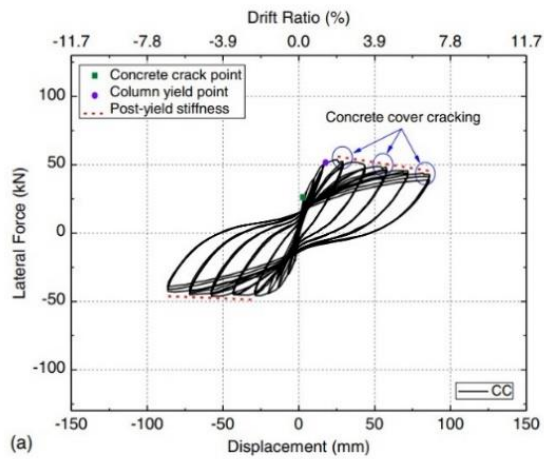Force-Deformation Chart

Damage State I

Damage State II
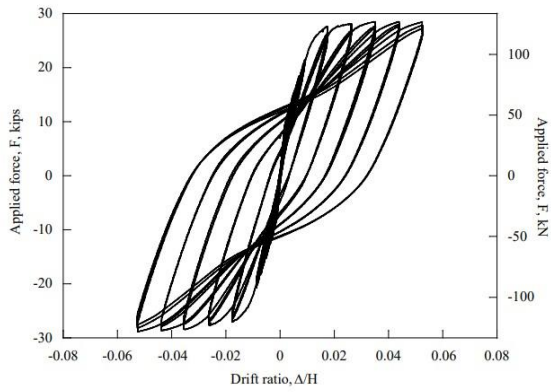
Damage State III

Damage State IV

Damage State VI (8.83%)

Damage State of Column A2 Tested by Naito (2001)
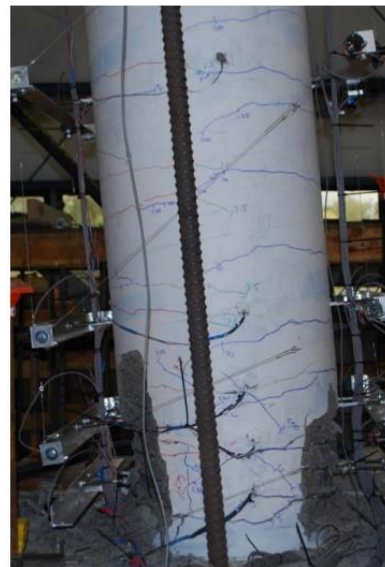
Dia = 12"
Height = 60"
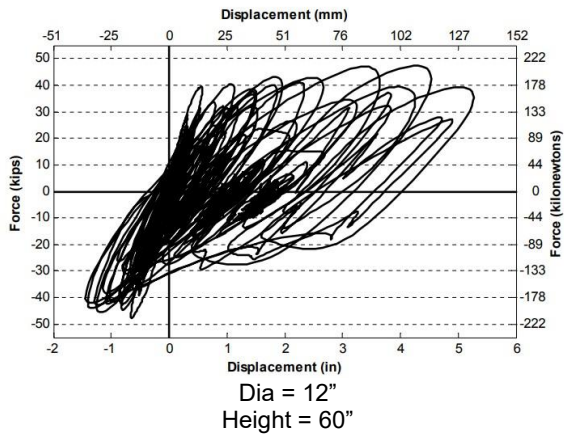
Force-Deformation Chart

Damage State I (1.13%)

Damage State II

Damage State III (2.62%)

Damage State IV

Damage State V (7.6%)

Damage State of Column Bent1 Tested by Nelson (2007)

Dia = 12"
Height = 84"
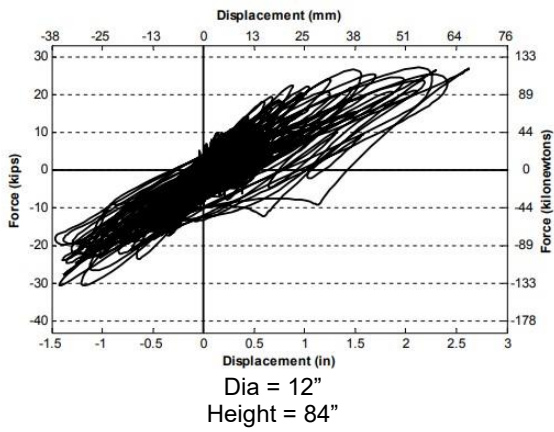
Force-Deformation Chart
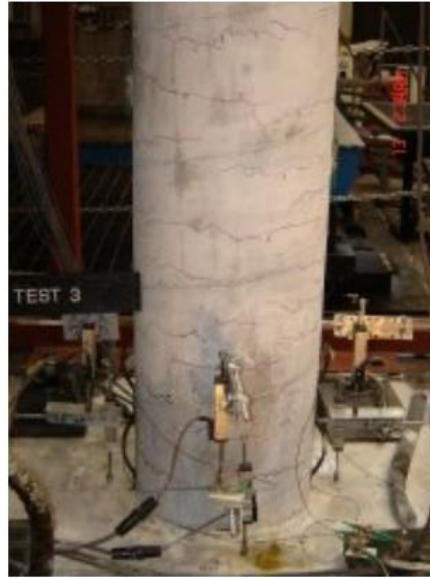
Damage State I (0.89%)
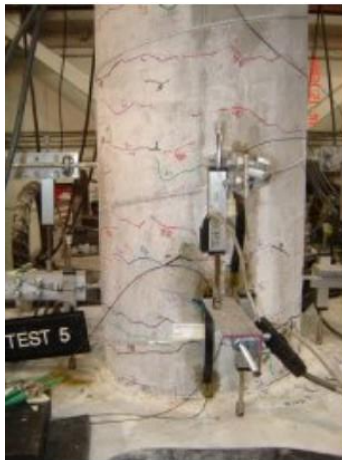
Damage State II (1.84%)

Damage State III

Damage State IV (2.82%)

Damage State V

Damage State of Column Bent2 Tested by Nelson (2007)

A-73

Dia = 12"
Height = 72"
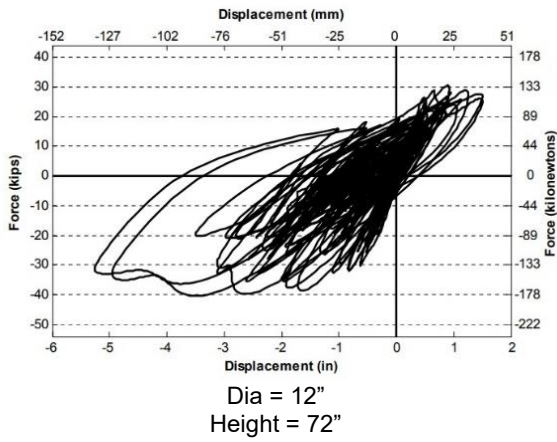
Force-Deformation Chart

Damage State I (0.76%)

Damage State II

Damage State III (2.71%)

Damage State IV (4.4%)

Damage State VI (6.97%)

Damage State of Column Bent3 Tested by Nelson (2007)

A-74
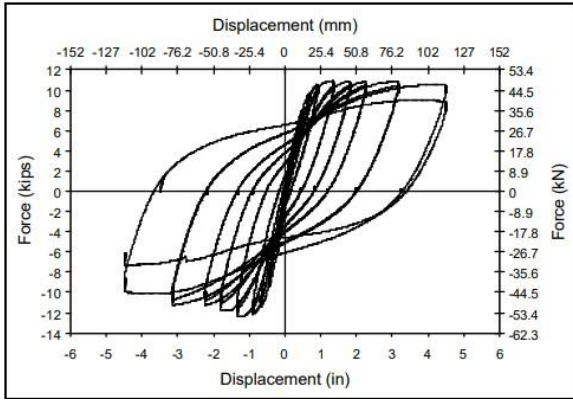
Dia = 10"
Height = 45"

Force-Deformation Chart

Damage State I (0.5%)

Damage State III (3%)

Damage State II

Damage State IV (4%)

Damage State VI (10%)

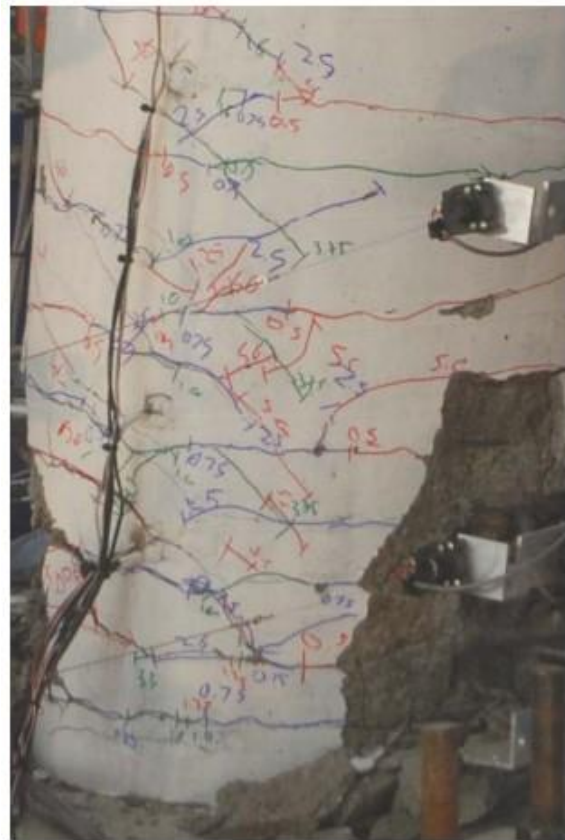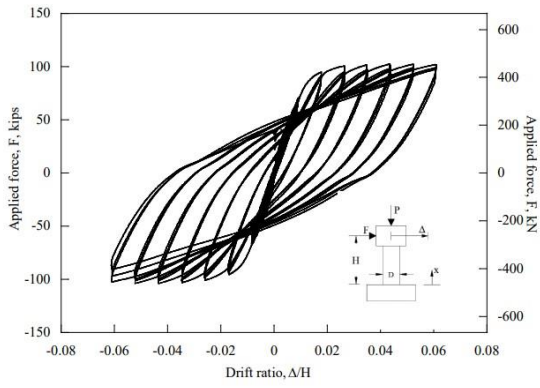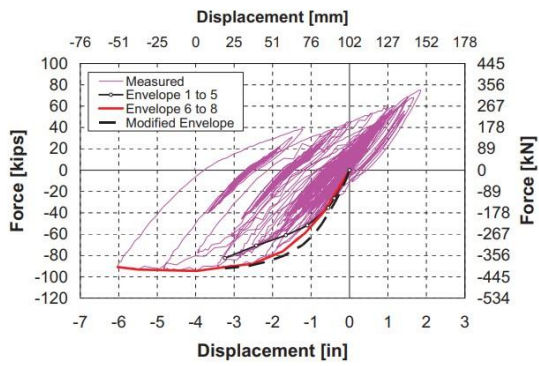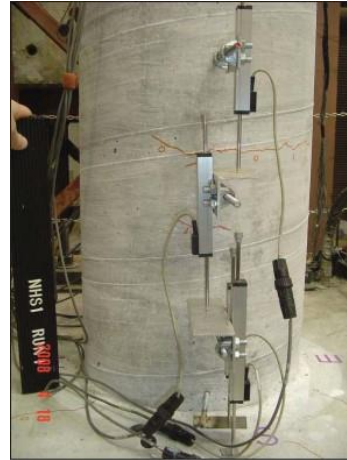**Damage State of Column RSC Tested by O'Brien et al. (2007)**

Dia = 16"
Height = 72"

Force-Deformation Chart

Damage State I (0.167%)

Damage State III (2.53%)

Damage State II

Damage State IV (5.0%)

Damage State V (6.0%)

Damage State of Column VP2 Tested by Orozco (1999)

A-76
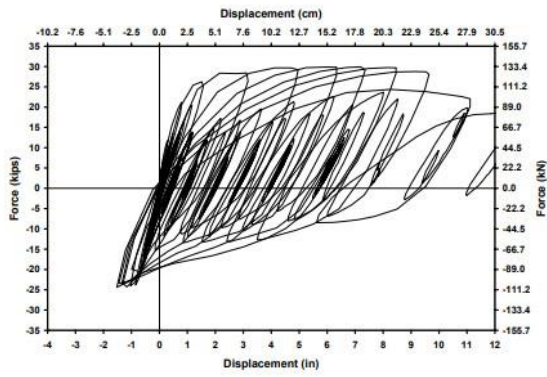
Dia = 16"
Height = 72"
Force-Deformation Chart

Damage State I (1.125%)

Damage State II (4.44%, 4.44%)

Damage State III

Damage State IV (6.92%)

Damage State V (11.82%) & VI (13.3%)

Damage State of Column NF-1 Tested by Phan et al. (2005)
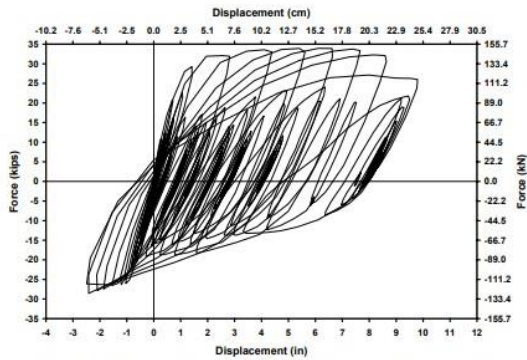
Figure 3.35 Accumulated Force Displacement Hysteresis for Specimen NF-2

Dia = 16"
Height = 72"
Force-Deformation Chart

Damage State I (0.39%)
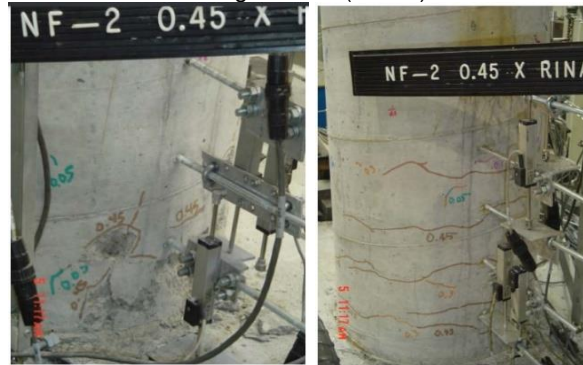
Damage State II

Damage State III (3.9%, 3.9%)

Damage State IV

Damage State VI (13.6%)

Damage State of Column NF-2 Tested by Phan et al. (2005)
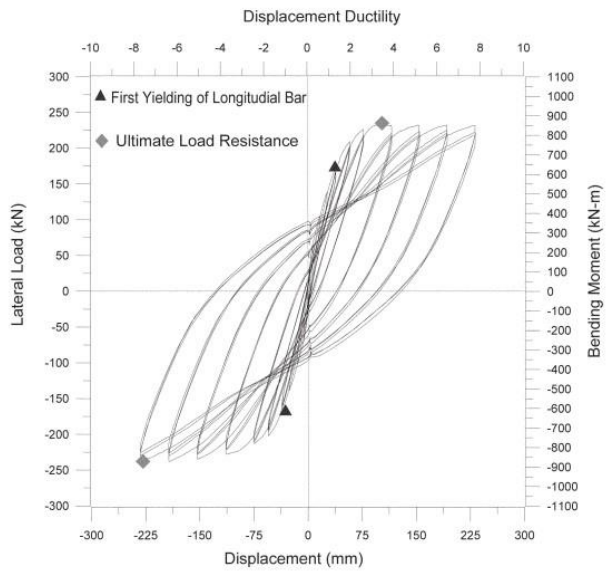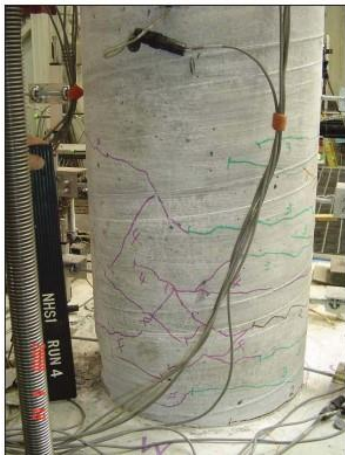
Displacement Ductility

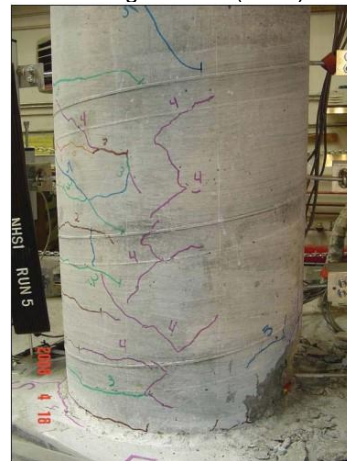Dia = 24"
Height = 144"
Force-Deformation Chart

Damage State I (0.688%)

Damage State II   Damage State III (2.08%)

Damage State IV   Damage State VI (12.7%)
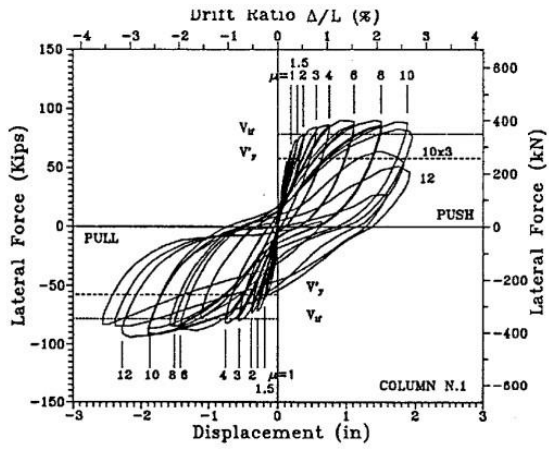
Damage State of Column HD(6)-TM(0) Tested by Prakash et al. (2012)

A-79

Dia = 24"
Height = 90"
Force-Deformation Chart

Damage State I (0.39%)

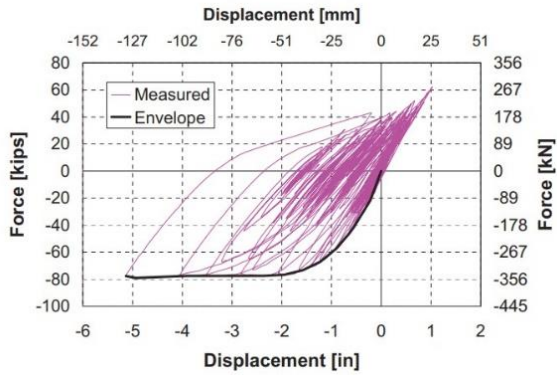Damage State II

Damage State III (1.67%)
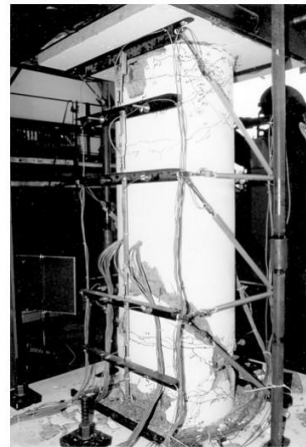
Damage State IV

Damage State V (2.04%)

**Damage State of Column NR1 Tested by Priestley and Benzoni (1996)**

A-80
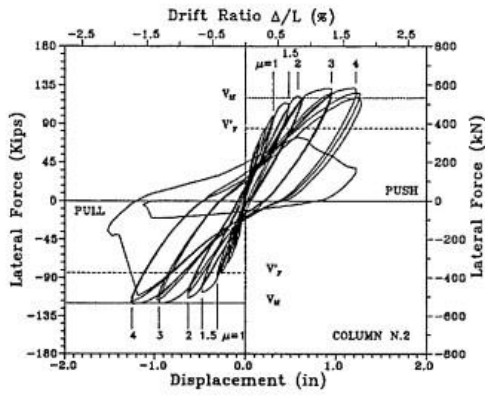
(b) Column 2

Dia = 24"
Height = 90"
Force-Deformation Chart

Damage State I

Damage State II (0.52%)

Damage State III
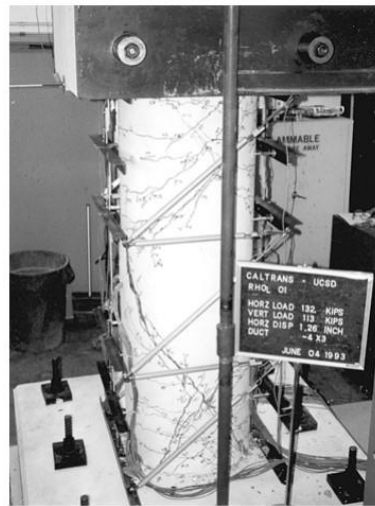
Damage State IV

Damage State V (1.4%)

Damage State of Column NR2 Tested by Priestley and Benzoni (1996)
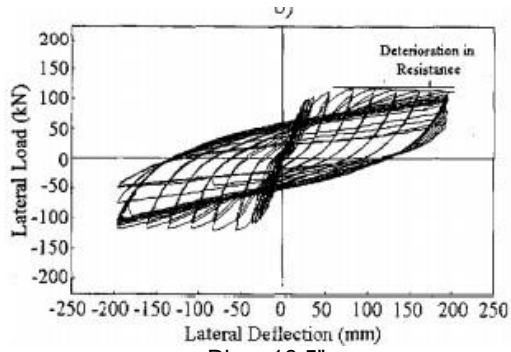
A-81

Dia = 16.5"
Height = 67.75"

| Force-Deformation Chart | Damage State I |

| Damage State II | Damage State III |

| Damage State IV (4.5%) | Damage State V |

Damage State of Column C1 Tested by Roeder et al. (2002)
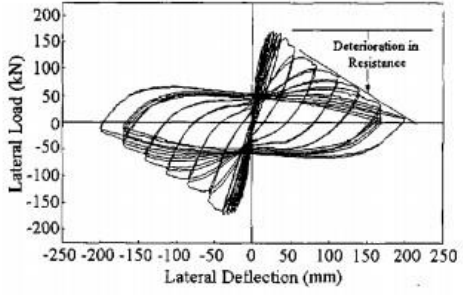
Dia = 16.5"
Height = 67.75"
Force-Deformation Chart

Damage State I

Damage State II

Damage State III

Damage State IV (4.5%)

Damage State V

Damage State of Column C4 Tested by Roeder et al. (2002)
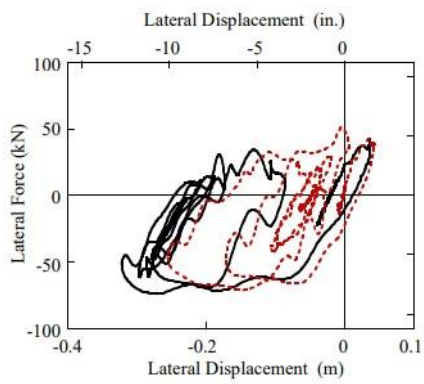
Dia = 16"
Height = 80"
Force-Deformation Chart

Damage State I

Damage State II

Damage State III (7.62%, 7.63%)

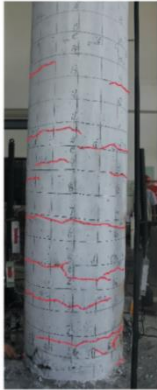Damage State IV (14.1%, 14.1%)

Damage State V

Damage State of Column RC Tested by Sakai et al. (2005)

Dia = 23.62"
Height = 72"
Force-Deformation Chart

Damage State I

Damage State II (3.74%)

Damage State III

Damage State IV

Damage State VI (7.48%)

Damage State of Column IC1 Tested by Sritharan et al. (1996)

Dia = 23.62"
Height = 72"
Force-Deformation Chart

Damage State I

Damage State II (0.819%)

Damage State III (2.46%, 2.46%)
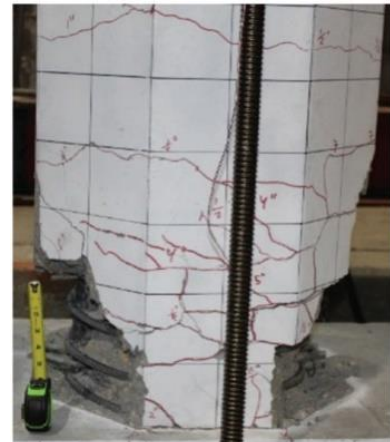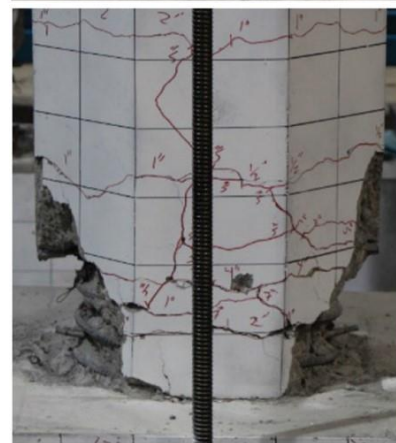

Damage State IV

Damage State VI (6.56%)

Damage State of Column IC2 Tested by Sritharan et al. (1996)

Dia = 23.62"
Height = 72"
Force-Deformation Chart
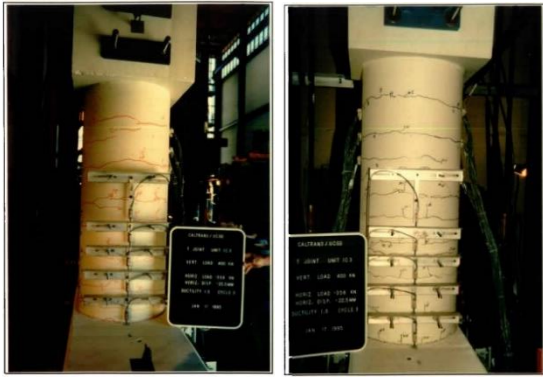
Damage State I

Damage State II (1.23%, 1.23%)
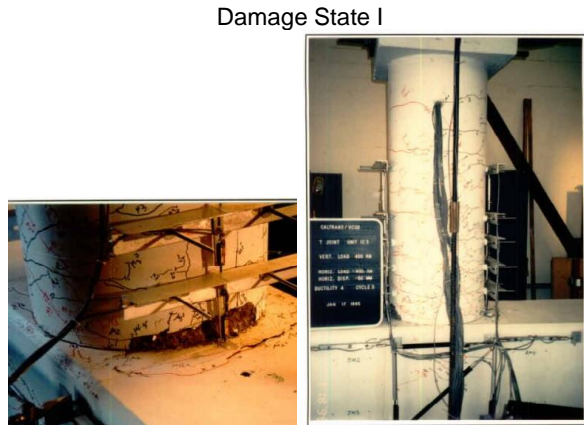
Damage State III (3.28%, 3.28%)

Damage State IV

Damage State VI (8.19%, 8.22%)

Damage State of Column IC3 Tested by Sritharan et al. (1996)
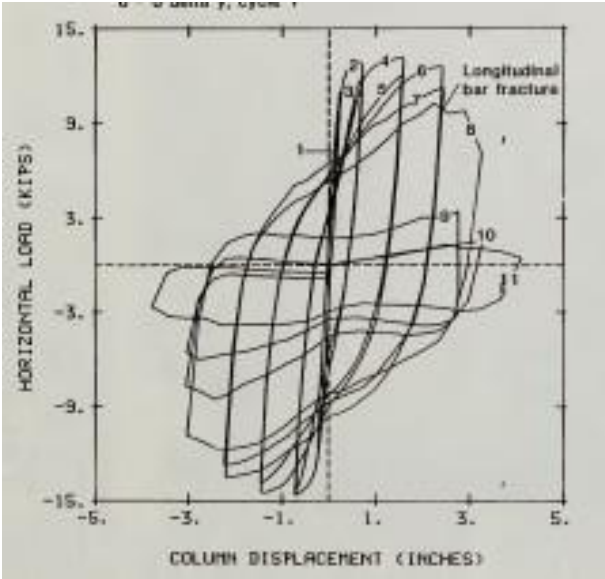
Dia = 9.84"
Height = 29.5"
Force-Deformation Chart
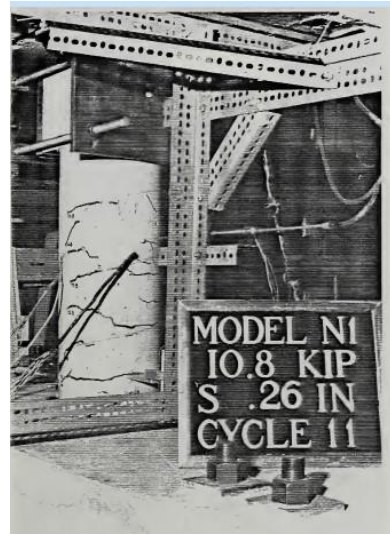
Damage State I (1.29%)

Damage State II (5.15%)
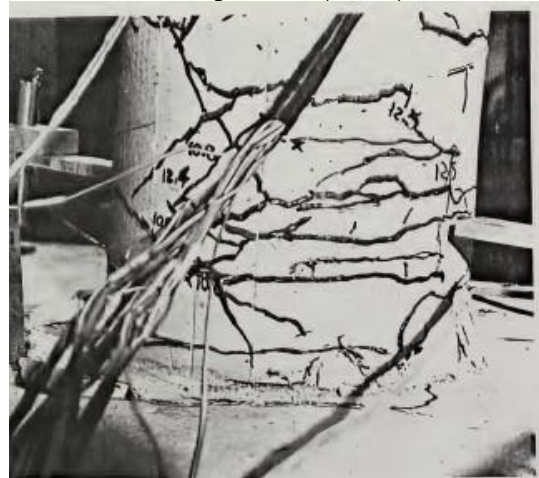
Damage State III (7.73%)

Damage State IV

Damage State VI (12.88%)

Damage State of Column N1 Tested by Stone and Cheok (1986)

Dia = 9.84"
Height = 29.5"

Force-Deformation Chart

Damage State I (0.746%)

Damage State II (1.492%)

Damage State III

Damage State IV (5.97%)

Damage State VI (8.95%)

Damage State of Column N2 Tested by Stone and Cheok (1986)
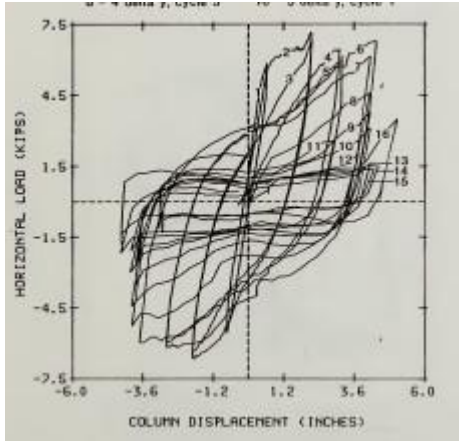
Dia = 9.84"
Height = 59"

Force-Deformation Chart
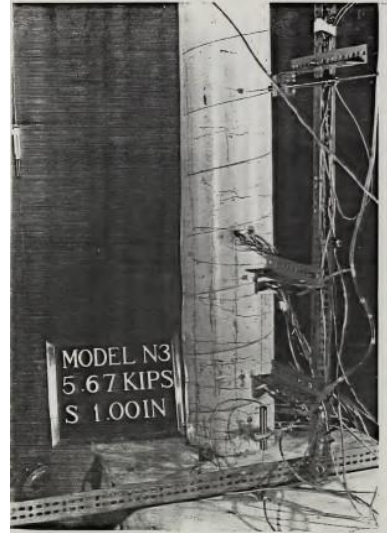
Damage State II
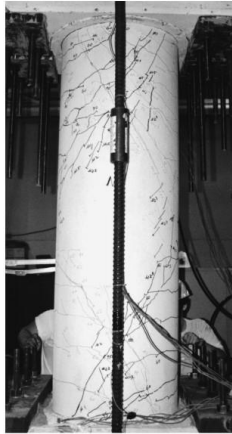

Damage State I (1.711%)

Damage State III

Damage State IV (5.14%)
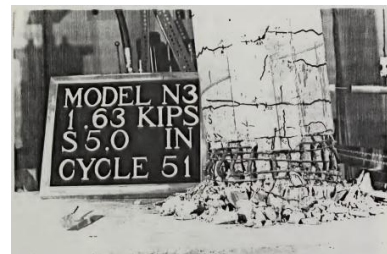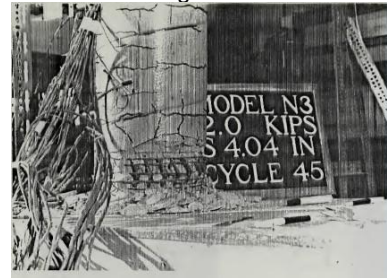
Damage State V (6.84%) & VI (8.56%)

**Damage State of Column N3 Tested by Stone and Cheok (1986)**
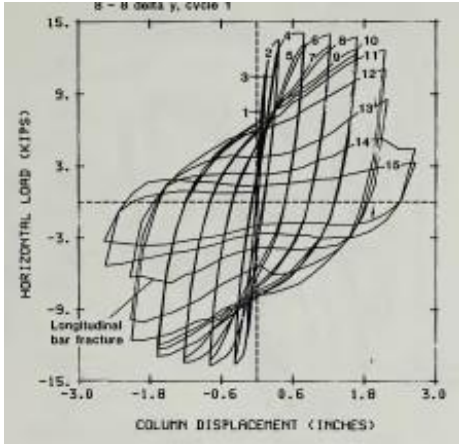
Dia = 9.84"
Height = 29.5"
Force-Deformation Chart

Damage State I (0.712%)

Damage State II (1.42%)

Damage State III

Damage State IV

Damage State V (7.12%) & VI (8.54%)

Damage State of Column N4 Tested by Stone and Cheok (1986)
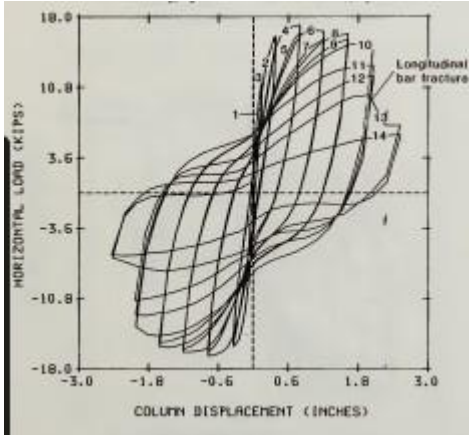
Dia = 9.84"
Height = 29.5"
Force-Deformation Chart
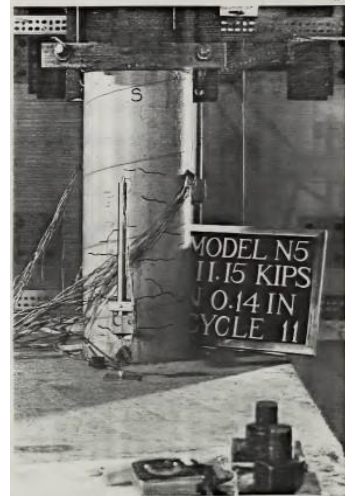
Damage State I (0.644%)

Damage State II (2.58%)

Damage State III

Damage State IV (6.44%)

Damage State VI (7.73%)

Damage State of Column N5 Tested by Stone and Cheok (1986)
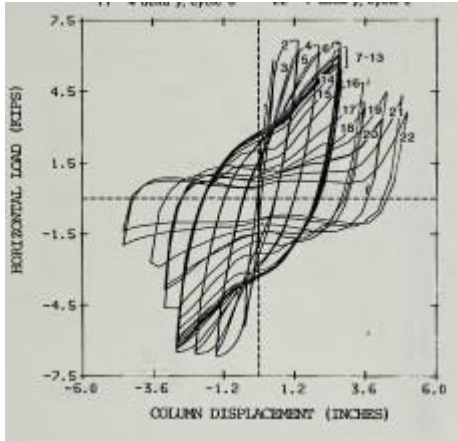
Dia = 9.84"
Height = 29.5"
Force-Deformation Chart

Damage State I (1.12%)

Damage State II (2.24%)

Damage State III
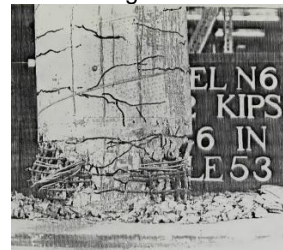
Damage State IV

Damage State VI (5.6%, 8.96%)

Damage State of Column N6 Tested by Stone and Cheok (1986)
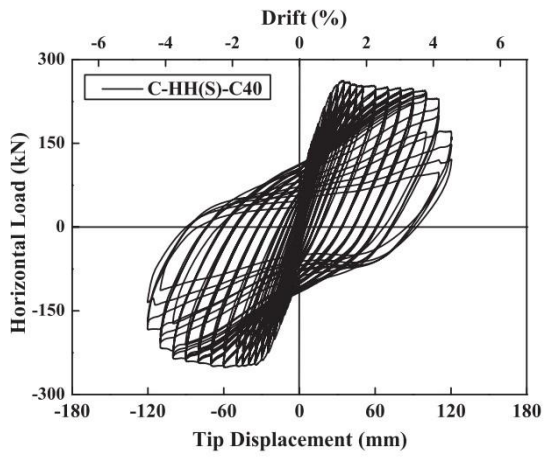
Dia = 23.62"
Height = 104.33"
Force-Deformation Chart

Damage State I

Damage State II

Damage State III

Damage State IV

Damage State VI (4.24%)

Damage State of Column C-HH(S)-C40 Tested by Su et al. (2015)

Dia = 23.62"
Height = 104.33"
Force-Deformation Chart

Damage State I

Damage State II

Damage State III

Damage State IV

Damage State VI (4.69%)

Damage State of Column C-HH(S)-C60 Tested by Su et al. (2015)

Dia = 23.62"
Height = 104.33"
Force-Deformation Chart

Damage State I

Damage State II

Damage State III

Damage State IV

Damage State VI (4.49%)

Damage State of Column C-HH-C40 Tested by Su et al. (2015)

Dia = 23.62"
Height = 104.33"
Force-Deformation Chart

Damage State I

Damage State II

Damage State III

Damage State IV

Damage State VI (4.63%)

Damage State of Column C-HL-C40 Tested by Su et al. (2015)

Dia = 23.62"
Height = 104.33"
Force-Deformation Chart

Damage State I

Damage State II

Damage State III

Damage State IV

Damage State VI (4.63%)

Damage State of Column C-HL-C60 Tested by Su et al. (2015)

(c) C-HM-C40

Dia = 23.62"
Height = 104.33"
Force-Deformation Chart

Damage State I

Damage State II

Damage State III

Damage State IV

Damage State VI (5.76%)

Damage State of Column C-HM-C40 Tested by Su et al. (2019)

P	$0.083A_gf'_c$	f_{yh}	536 MPa
f'_c	32.6 MPa	ρ_s	0.80%
f_y	399 MPa	d_s	10 mm
d_l	20 mm	s	60 mm
ρ_l	1.56%		

C-LM-C40

Dia = 23.62"
Height = 104.33"
Force-Deformation Chart

Damage State I

Damage State II

Damage State III

Damage State IV

Damage State VI (3.38%)

Damage State of Column C-LM-C40 Tested by Su et al. (2019)

A-100

Dia = 23.62"
Height = 104.33"
Force-Deformation Chart

Damage State I

Damage State II

Damage State III

Damage State IV

Damage State VI (4.55%)

Damage State of Column C-M(S)M-C60 Tested by Su et al. (2019)

P	$0.083A_g f_c'$	f_{yh}	536 MPa
f_c'	32.6 MPa	ρ_s	0.80%
f_y	534 MPa	d_s	10 mm
d_l	20 mm	s	60 mm
ρ_l	1.56%		

C-MM-C40

Dia = 23.62"
Height = 104.33"
Force-Deformation Chart
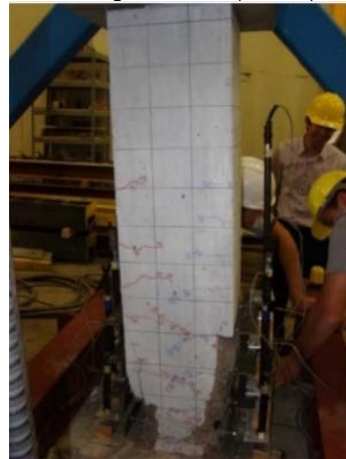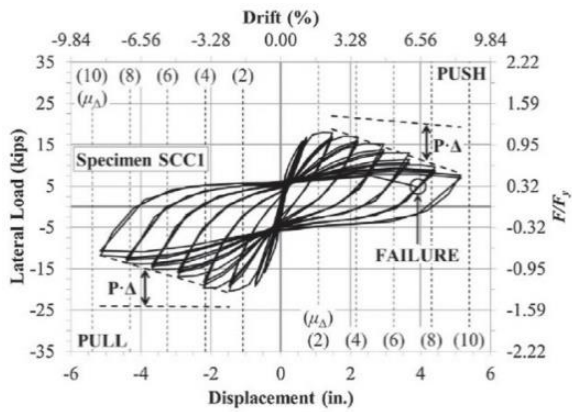
Damage State I

Damage State II

Damage State III

Damage State IV (4.51%)

Damage State V

Damage State of Column C-MM-C40 Tested by Su et al. (2019)

P	$0.056A_gf_c'$	f_{yh}	536 MPa
f_c'	48.2 MPa	ρ_s	0.80%
f_y	534 MPa	d_s	10 mm
d_l	20 mm	s	60 mm
ρ_l	1.56%		

C-MM-C60

Dia = 23.62"
Height = 104.33"
Force-Deformation Chart

Damage State I

Damage State II

Damage State III

Damage State IV

Damage State VI (5.3%)

Damage State of Column C-MM-C60 Tested by Su et al. (2019)

A-103

Dia = 11.81"
Height = 58"
Force-Deformation Chart

Damage State I

Damage State II

Damage State III

Damage State IV

Damage State VI (5.61%)

Damage State of Column CC Tested by Tang et al. (2019)

A-104

Dia = 24"
Height = 144"
Force-Deformation Chart

Damage State I

Damage State II

Damage State III

Damage State IV (4.3%)

Damage State V-VI (5.22%)

Damage State of Column C1 Tested by Trejo et al. (2014)
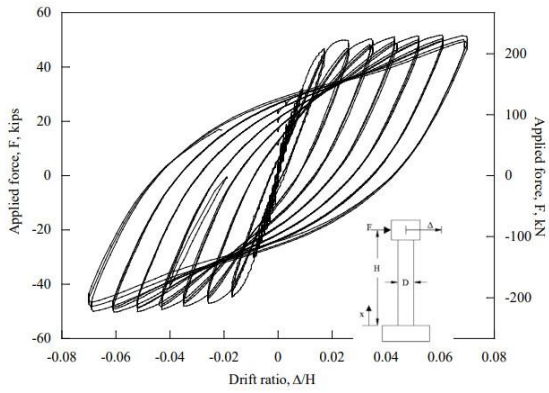
Dia = 24"
Height = 144"
Force-Deformation Chart

Damage State I

Damage State II

Damage State III

Damage State IV

Damage State V-VI (6.95%)

Damage State of Column C3 Tested by Trejo et al. (2014)

A-106

Dia = 24"
Height = 72"
Force-Deformation Chart

Damage State I

Damage State II

Damage State III

Damage State IV

Damage State VI (6.14%)

Damage State of Column C5 Tested by Trejo et al. (2014)

Dia = 16"
Height = 80"
Force-Deformation Chart

Damage State I (0.5%)

Damage State II (3.03%)

Damage State III (4.05%)

Damage State IV (4.20%)

Damage State V (6.87%)

Damage State of Column NSH1 Tested by Vosooghi (2010)

A-108

Dia = 16"
Height = 80"
Force-Deformation Chart

Damage State I (0.81%)

Damage State II (1.53%)
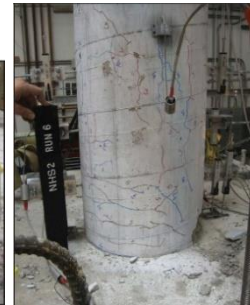
Damage State III (2.95%, 4.28%)
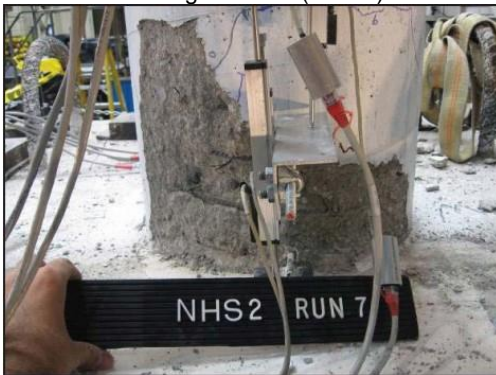
Damage State IV (4.87%)

Damage State V (6.17%)

Damage State of Column NSH2 Tested by Vosooghi (2010)
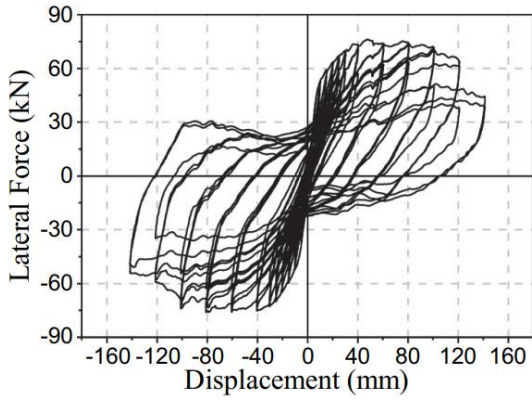
(a) CIP column

Dia = 19.67"
Height = 114.17"
Force-Deformation Chart

(a) Stage 1

Damage State I (0.35%, 0.86%)

(b) Stage 2

Damage State II (0.86%)

(d) Stage 4

Damage State III (2.76%)

Damage State IV

Damage State VI (4.155%, 4.155%)

Damage State of Column CIP Tested by Wang et al. (2020)
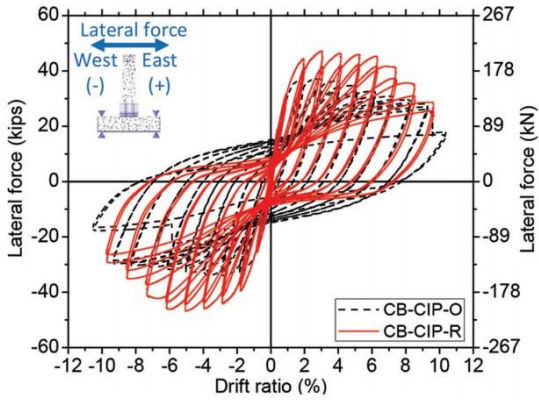
Dia = 21"
Height = 96"
Force-Deformation Chart
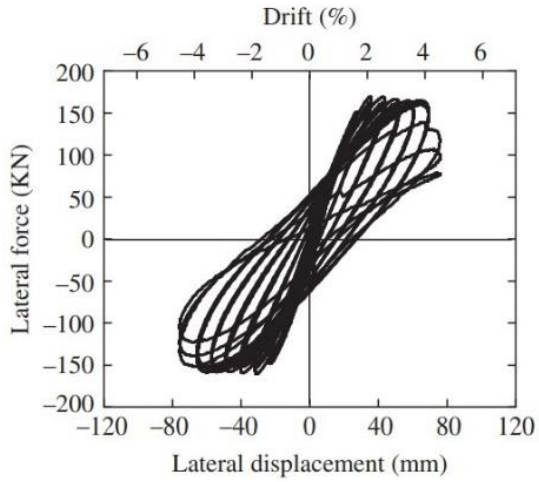
Damage State II

Damage State I

Damage State III

Damage State IV

Damage State VI (7.36%)

Damage State of Column CB-CIP-O Tested by Wu and Pantelides (2017)
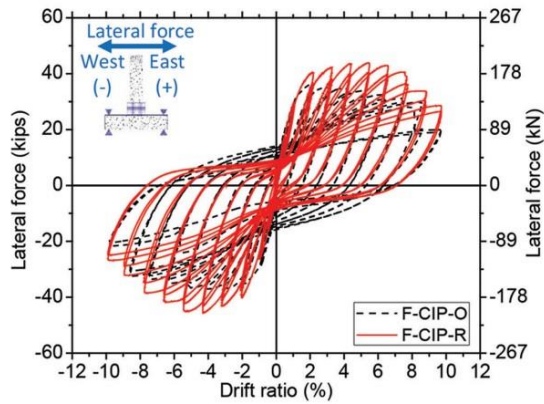
Dia = 21"
Height = 96"
Force-Deformation Chart

Damage State I

Damage State II
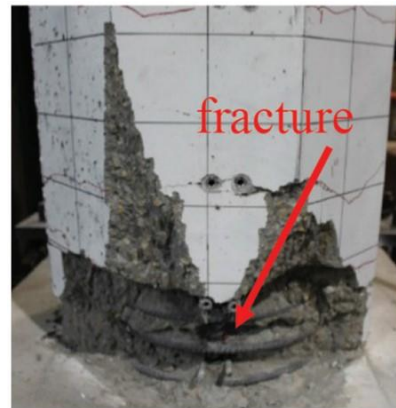
Damage State III

Damage State IV

Damage State VI (8.02%)

Damage State of Column F-CIP-O Tested by Wu and Pantelides (2017)
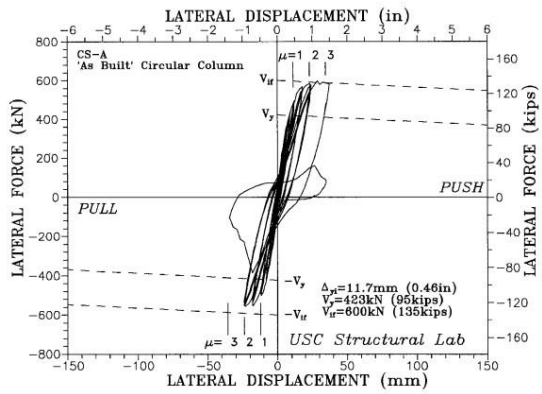
Dia = 24"
Height = 80"
Force-Deformation Chart

Damage State I

Damage State II (1.14%)
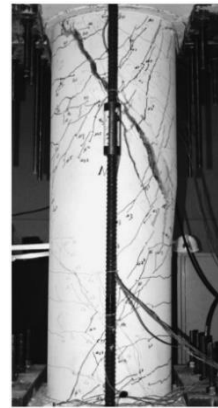
Damage State III (1.71%)
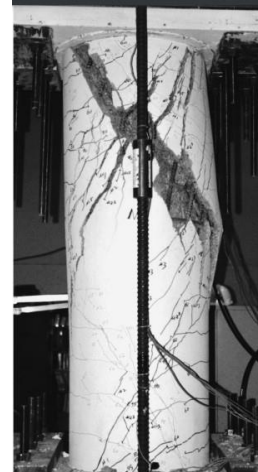
Damage State IV

Damage State VI (5.93%)

Damage State of Column CS-A Tested by Xiao et al. (1999)
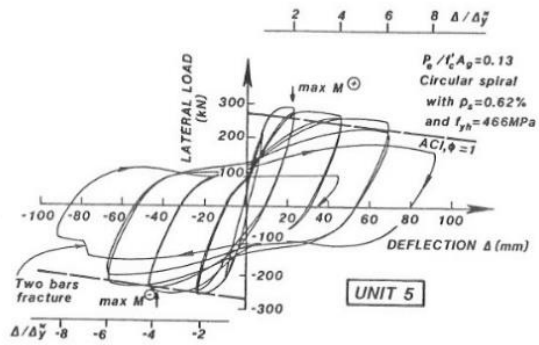
Fig. 3.57 : Measured Horizontal Load-Horizontal Deflection Hysteresis Loops - UNIT 5

Dia = 15.75"
Height = 63"
Force-Deformation Chart

Damage State I

Damage State II
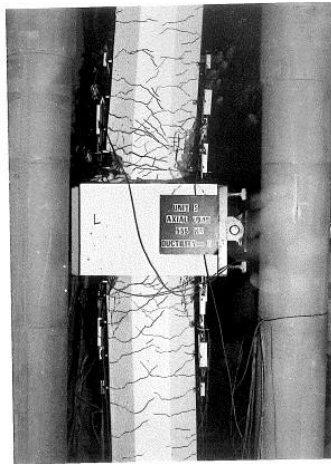
Damage State III

Damage State IV (4.255%)
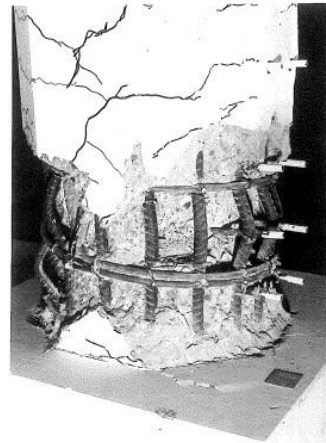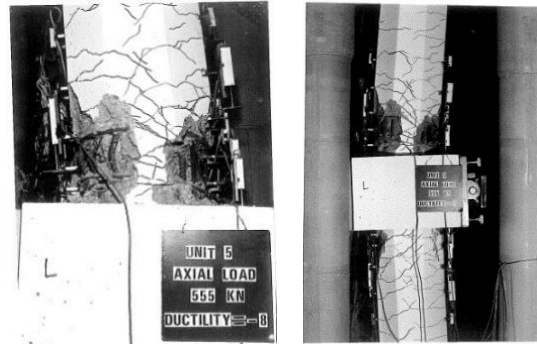
Damage State VI (5.8%, 5.8%, 5.8%)

Damage State of Column Unit5 Tested by Zahn (1985)

End of Circular Column Section

A-114

THIS PAGE LEFT INTENTIONALLY BLANK

A3. Photos of Rectangular RC Bridge Columns

The photographs of RC bridge columns included in the rectangular column database at different damage states, when available, were compiled and reported herein. The work was organized based on an alphabetical order of authors' surnames.

Note that the number in the parenthesis is the drift ratio (in %) at which the photo was taken. The drift is the ratio of the column lateral displacement to the column height.

For statistical analysis, drifts at DS2 were assumed to be at yielding not those observed in the tests. A discrepancy between the yield drift and those estimated from the photographs for DS2 exits for some test specimens. Further, sometimes the test toward the end of the experiment was strong enough to fail the column before documenting different levels of the damage. For example, DS5 and DS6 occurred in the last run of the test. If data was available, DS5 and DS6 were separately reported in this document.

Cross Section = 12x12"
Height = 61"

Force-Deformation Chart
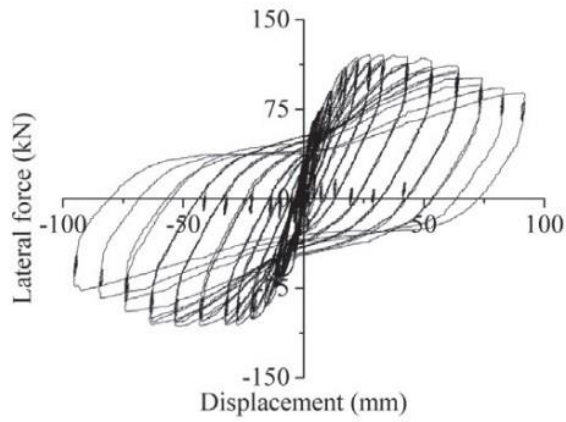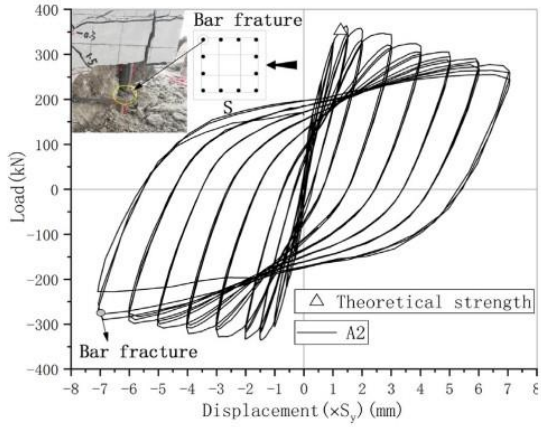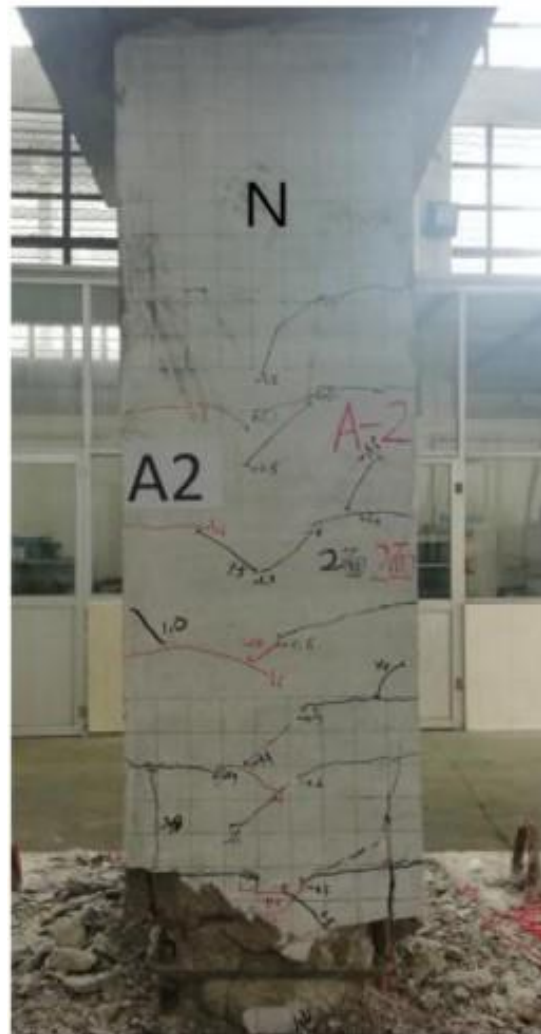

Damage State I (0.774%)
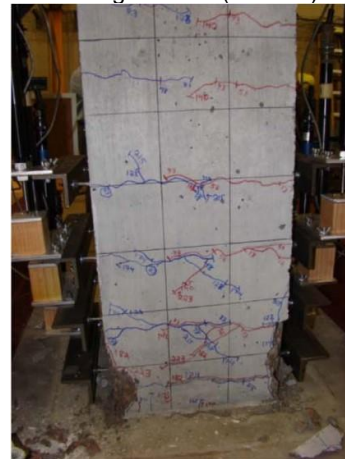
Damage State II

Damage State III (3.87%)
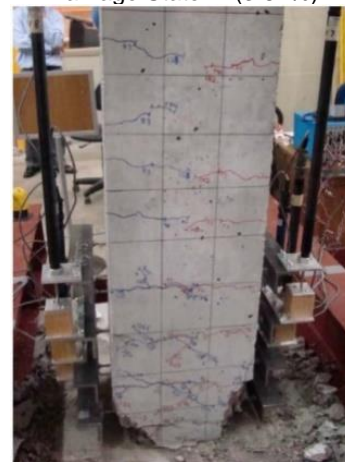
Damage State IV

Damage State VI (6.966%)

Damage State of Column CC1 Tested by Ghadban et al. (2019)

Cross Section = 12x12"
Height = 61"
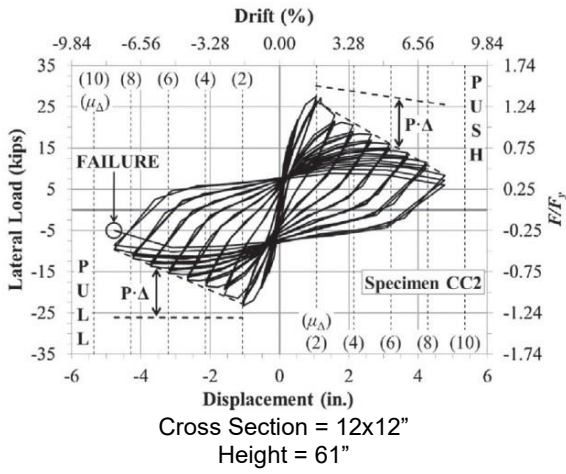
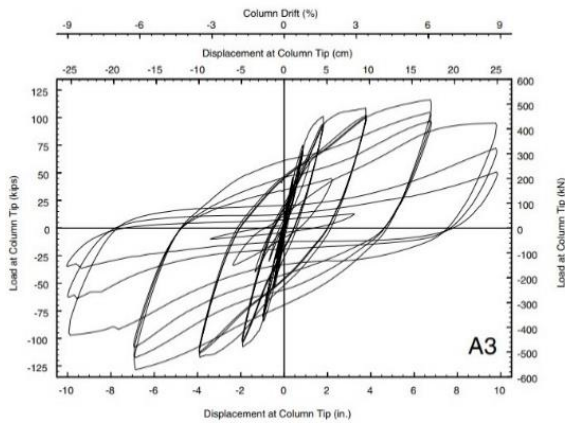Force-Deformation Chart
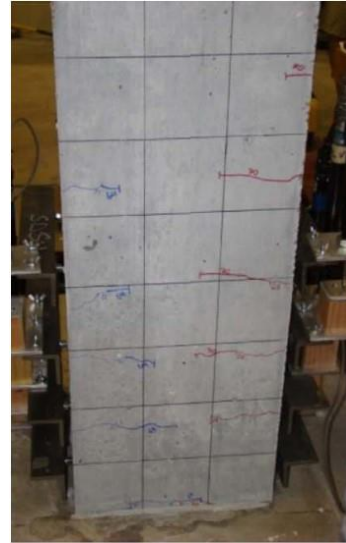
Damage State I (0.877%)
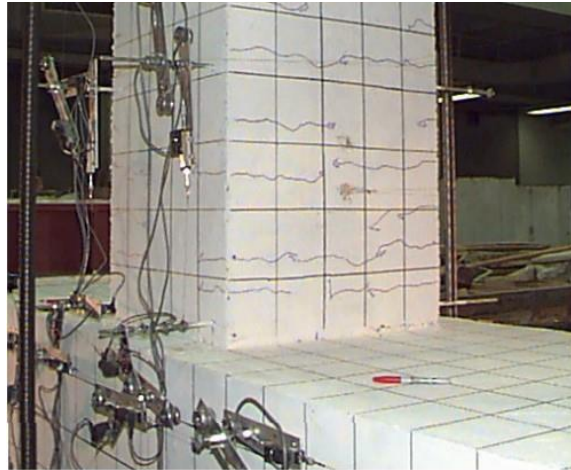
Damage State II

Damage State III (3.51%)

Damage State IV

Damage State VI (7.02%)

Damage State of Column CC2 Tested by Ghadban et al. (2019)

A-118

Cross Section = 12x12"
Height = 61"
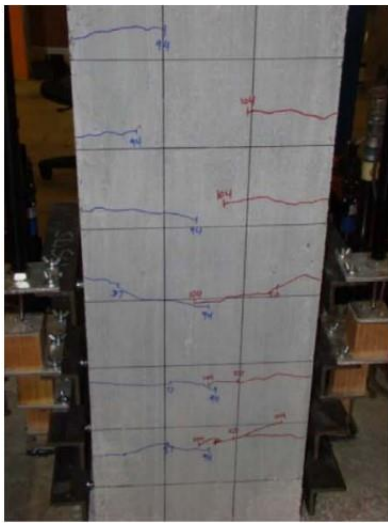
| Force-Deformation Chart | Damage State I |

| Damage State II (1.24%) | Damage State III (4.86%) |

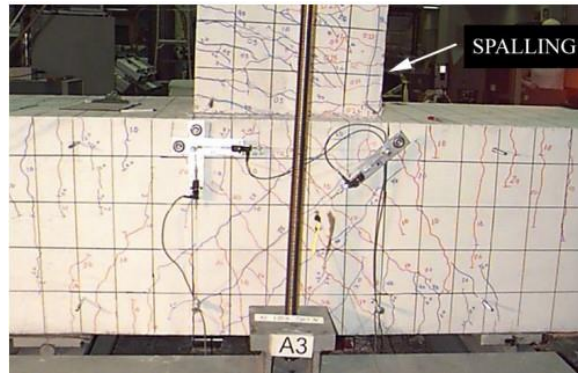| Damage State IV | Damage State VI (8.45%) |
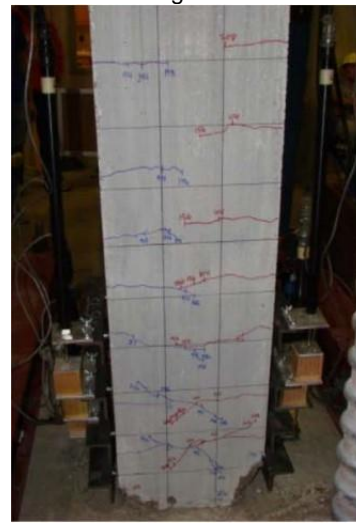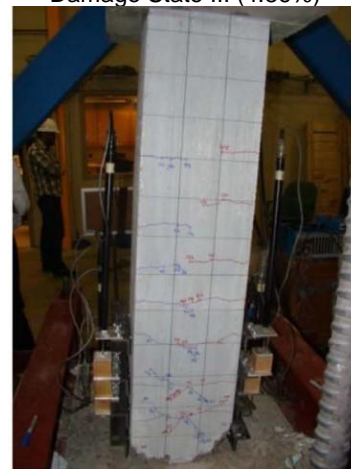
Damage State of Column SCC1 Tested by Ghadban et al. (2019)
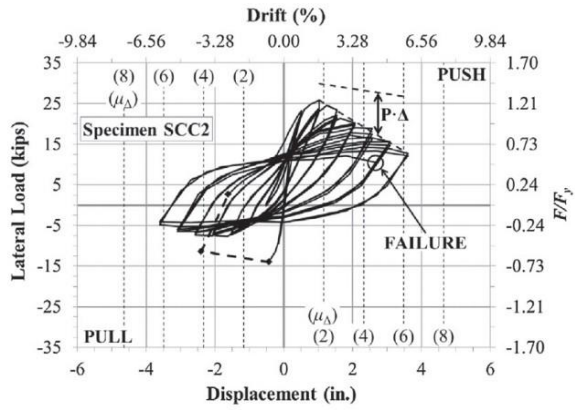
Cross Section = 12x12"
Height = 61"
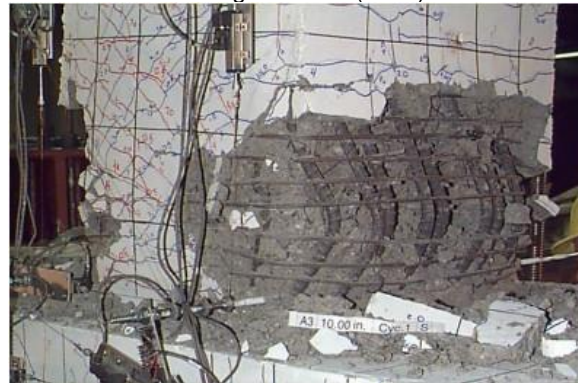Force-Deformation Chart
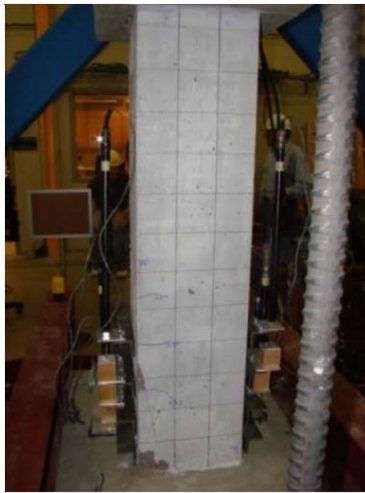
Damage State I

Damage State II (1.71%)

Damage State III

Damage State IV (3.43%)
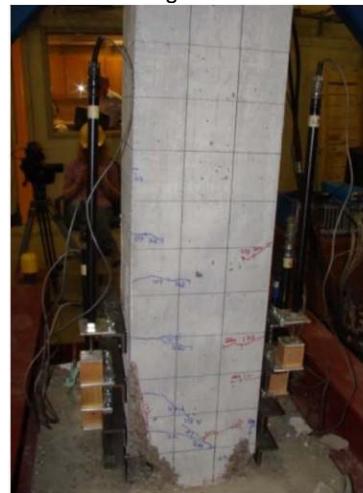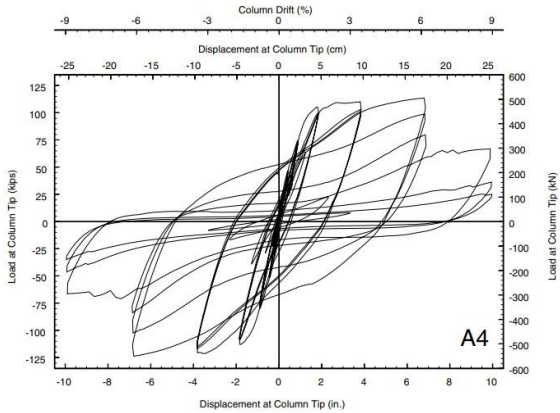
Damage State VI (5.05%)

Damage State of Column SCC2 Tested by Ghadban et al. (2019)
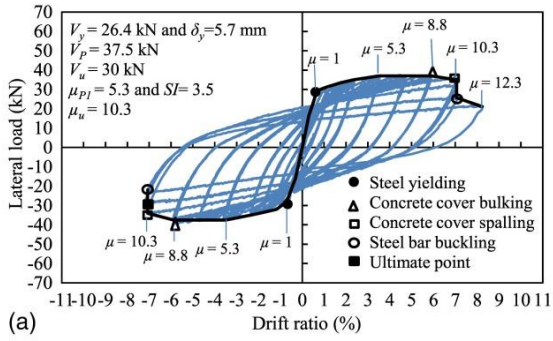
(a)

Cross Section = 7.87x7.87"
Height = 33.46"
Force-Deformation Chart

Damage State I

Damage State II

Damage State III

Damage State IV

Damage State VI (7.3%)

Damage State of Column CS-2% Tested by Ibrahim et al. (2015)
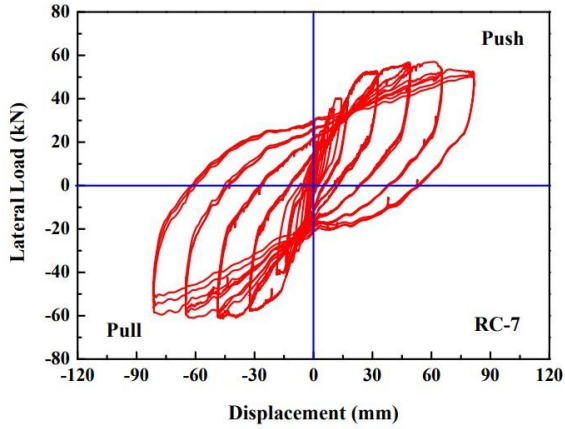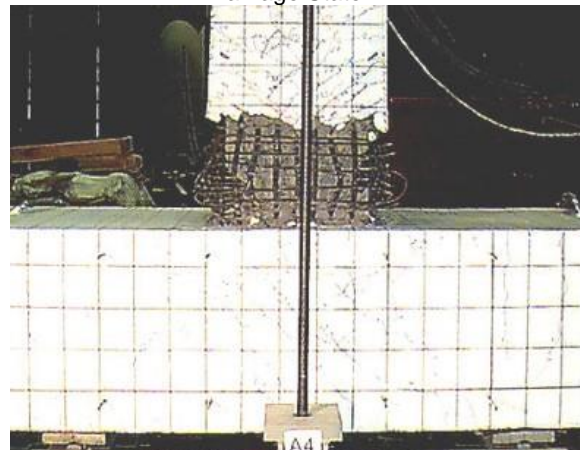
Cross Section = 11.81x11.81"
Height = 82.67"
Force-Deformation Chart

Damage State I

Damage State II

Damage State III

Damage State IV

Damage State VI (3.85%)

Damage State of Column RC-7 Tested by Jia et al. (2020)
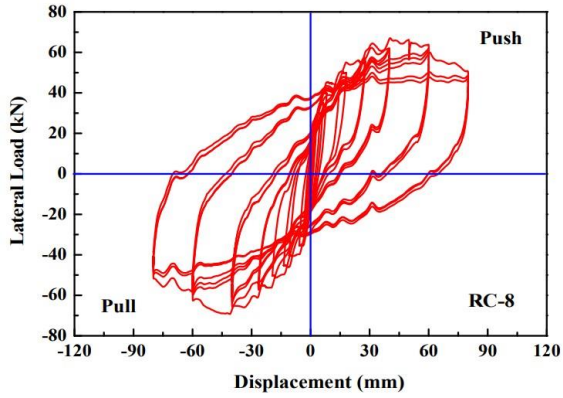
A-122

Cross Section = 11.81x11.81"
Height = 82.67"
Force-Deformation Chart

Damage State I

Damage State II

Damage State III

Damage State IV

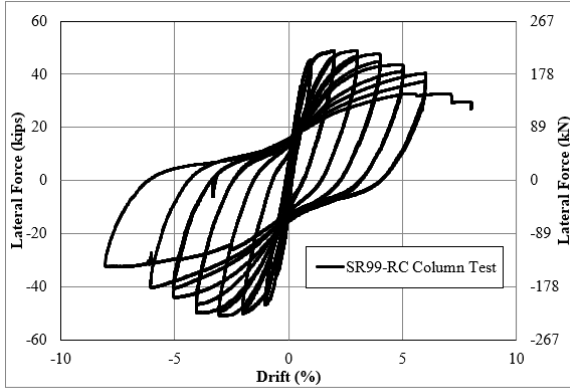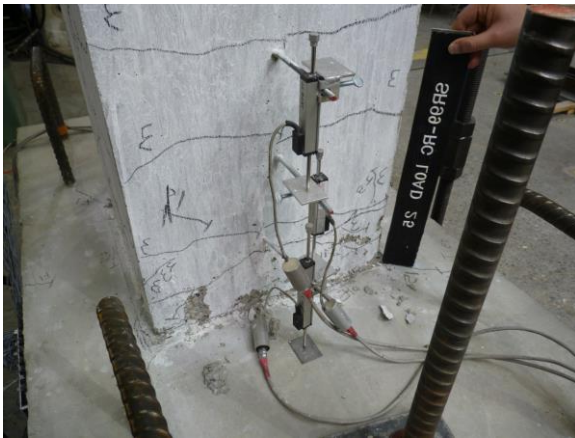Damage State VI (3.26%)

Damage State of Column RC-8 Tested by Jia et al. (2020)

Cross Section = 15.75x15.75"
Height =66.14"
Force-Deformation Chart

Damage State I

Damage State II (2.91%)

Damage State III

Damage State IV (3%)

Damage State VI (4.5%, 4.5%)

Damage State of Column RC Tested by Kawashima et al. (2011)
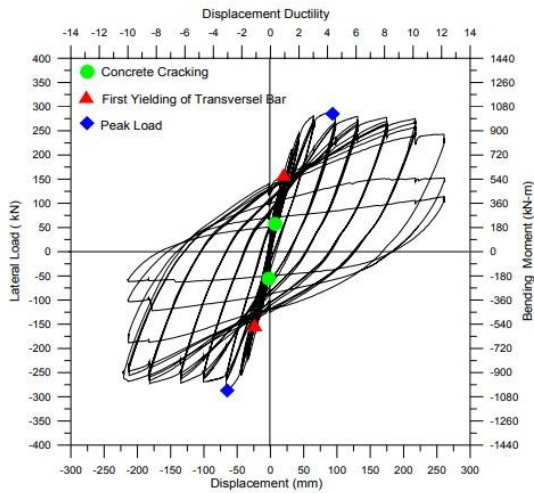
Cross Section = 21.65x21.65"
Height = 131.89"

Force-Deformation Chart

Damage State I

Damage State II (0.642%)

Damage State III

Damage State IV (2.89%)

Damage State VI (7.77%)

Damage State of Column S-HB(6)-TM(0) Tested by Li (2012)
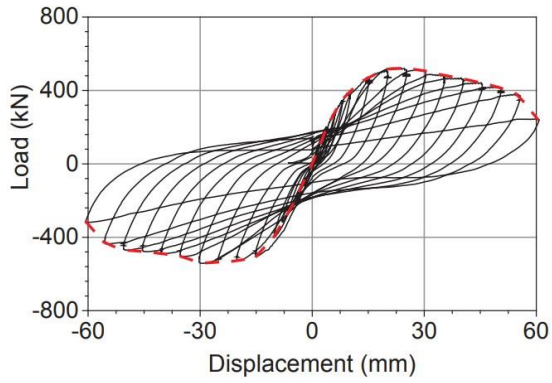
Cross Section = 20.87x19.69"
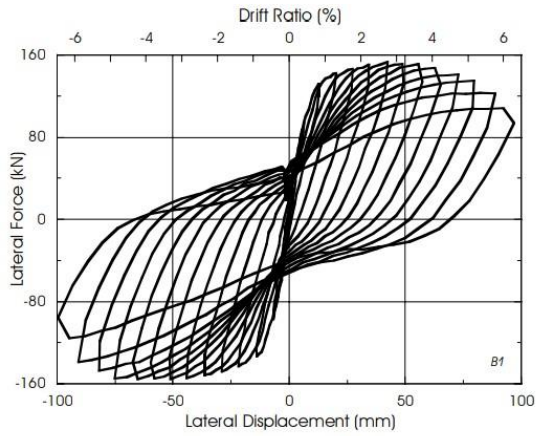Height = 35.43"
Force-Deformation Chart

Damage State I

Damage State II

Damage State III

Damage State IV

Damage State VI (6.73%)

Damage State of Column #1 Tested by Li et al. (2018)

Cross Section = 14.17x16.54"
Height = 68.9"
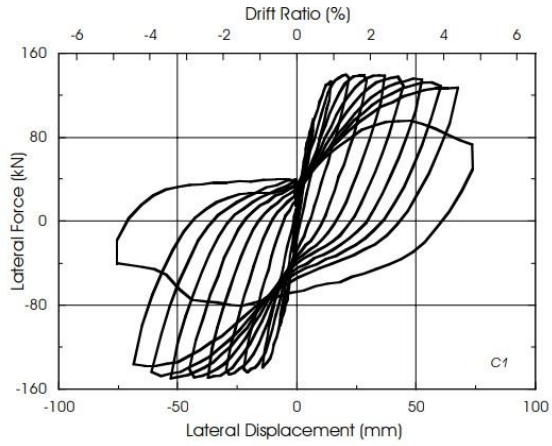Force-Deformation Chart

Damage State I

Damage State II

Damage State III

Damage State IV

Damage State VI (4.69%)

Damage State of Column RC Tested by Liu et al. (2019)

Cross Section = 17.72x17.72"
Height = 67.72"
Force-Deformation Chart

Damage State I

Damage State II
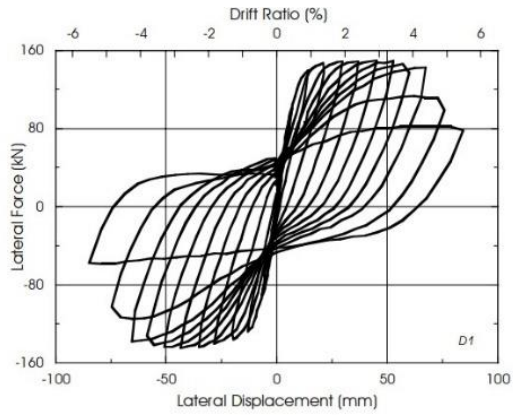
Damage State III

Damage State IV

Damage State VI (4.48%)

Damage State of Column A2 Tested by Liu et al. (2020)

A-128

Cross Section = 25x225"
Height = 111"
Force-Deformation Chart

Damage State I (0.225%)

Damage State II (0.9%)
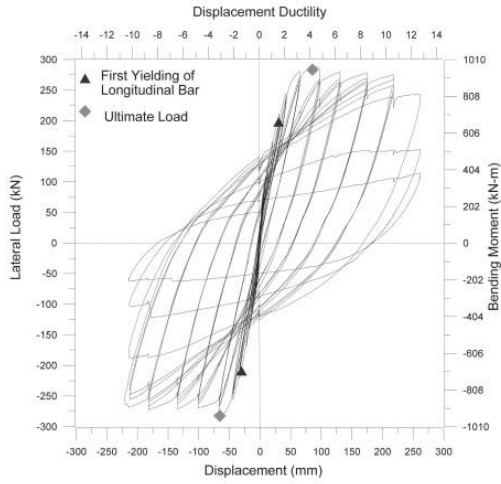

Damage State III (3.6%)

Damage State IV

Damage State VI (9.01%)

Damage State of Column A3 Tested by Naito (2001)

Cross Section = 25x25"
Height = 111"
Force-Deformation Chart

Damage State I

Damage State II

Damage State III

Damage State IV

Damage State VI (8.95%)

Damage State of Column A4 Tested by Naito (2001)

Figure 3-12: SR99-RC Force Displacement Hysteresis
Cross Section = 18"x18"
Height = 62"
Force-Deformation Chart

Damage State I (0.5% Drift)

Damage State II (3% Drift)

Damage State III (4% Drift)

Damage State IV (5% Drift)

Damage State VI (6%, 8%)

Damage State of Column SR99-RC Tested by Nakashoji (2014)
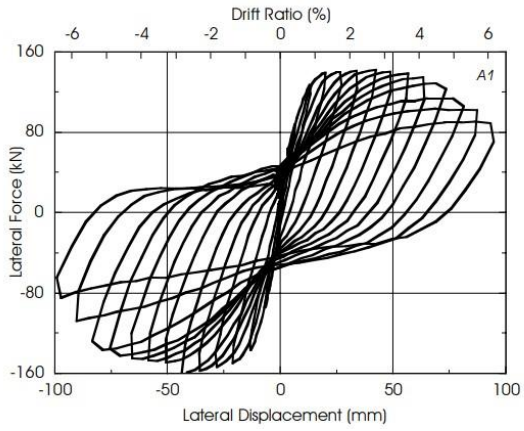
A-131

Cross Section = 15.75x15.75"
Height = 61.02"
Force-Deformation Chart
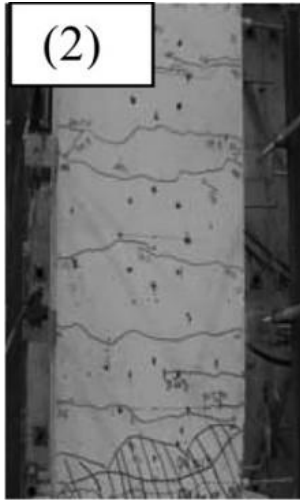
Damage State I

Damage State II

Damage State III

Damage State IV

Damage State VI (6.5%)

Damage State of Column A1 Tested by Ongsupankul et al. (2007)

c) specimen B1

Cross Section = 15.75x15.75"
Height = 61.02"

| Force-Deformation Chart | Damage State I |

| Damage State II | Damage State III |

| Damage State IV | Damage State VI (6.5%) |

Damage State of Column B1 Tested by Ongsupankul et al. (2007)

A-133

Drift Ratio (%)

Lateral Force (kN)

Lateral Displacement (mm)

C1

Cross Section = 15.75x15.75"
Height = 61.02"
Force-Deformation Chart

Damage State I

Damage State II

Damage State III

Damage State IV
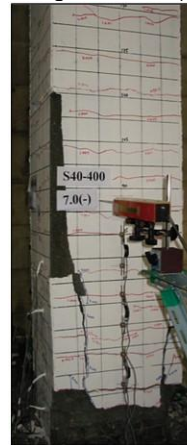
Damage State VI (5%)

Damage State of Column C1 Tested by Ongsupankul et al. (2007)

A-134

Cross Section = 15.75x15.75"
Height = 61.02"
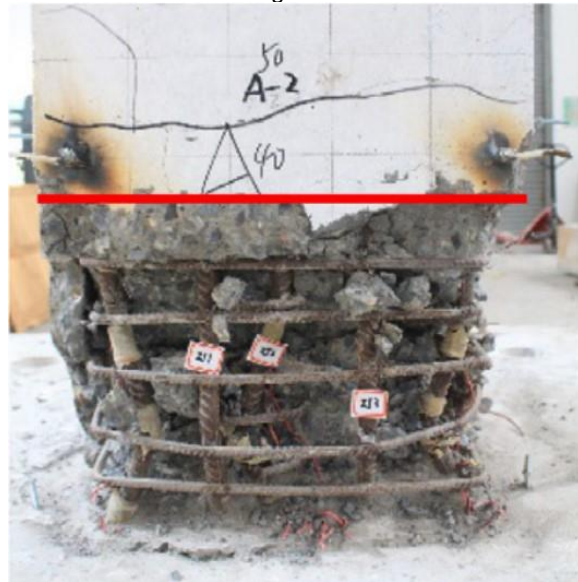Force-Deformation Chart

Damage State I

Damage State II

Damage State III

Damage State IV

Damage State VI (5.5%)

Damage State of Column D1 Tested by Ongsupankul et al. (2007)

Cross Section = 22.05x22.05"
Height = 131.97"
Force-Deformation Chart

Damage State I (0.656%)

Damage State II (2.91%)

Damage State III

Damage State IV

Damage State VI (7.9%)

Damage State of Column Rectangular Tested by Prakash et al. (2012)
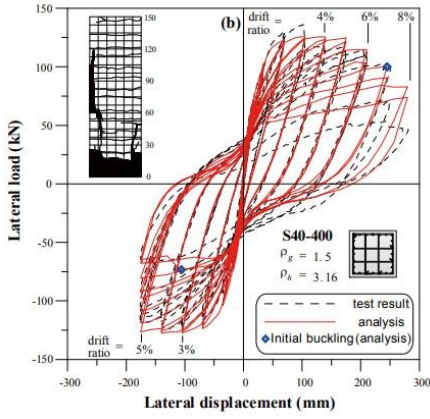
Cross Section = 17.72x17.72"
Height = 137.8"
Force-Deformation Chart

Damage State I (1%)
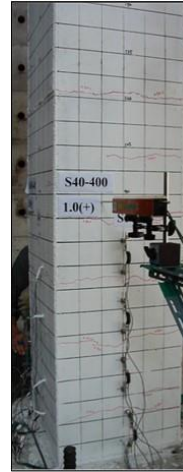
Damage State II
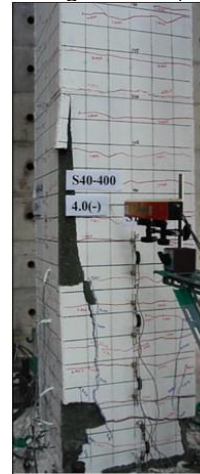
Damage State III (3%)

Damage State IV

Damage State VI (7%)

Damage State of Column S40-400 Tested by Seong et al. (2011)
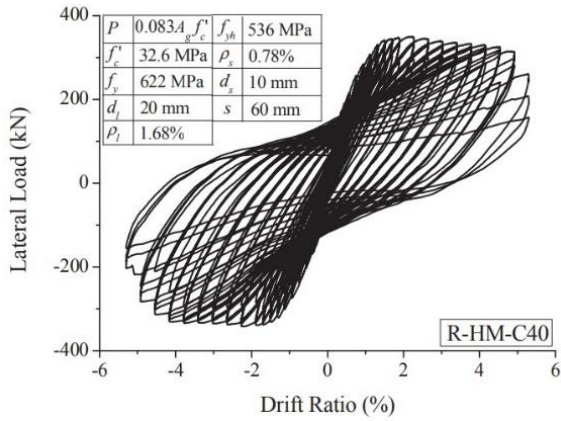
Cross Section = 23.62x19.69"
Height = 104.33"
Force-Deformation Chart
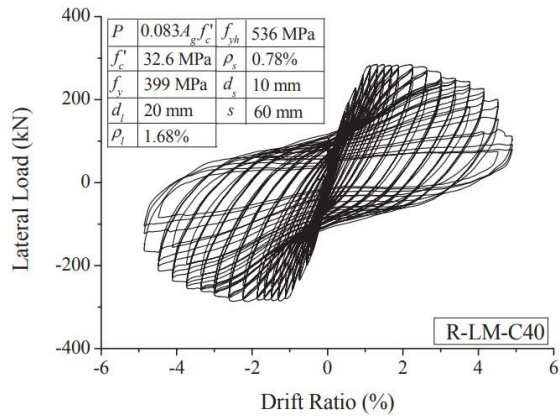
Damage State I

Damage State II

Damage State III

Damage State IV

Damage State VI (5.08%)

Damage State of Column R-HM-C40 Tested by Su et al. (2019)

Cross Section = 23.62x19.69"
Height = 104.33"
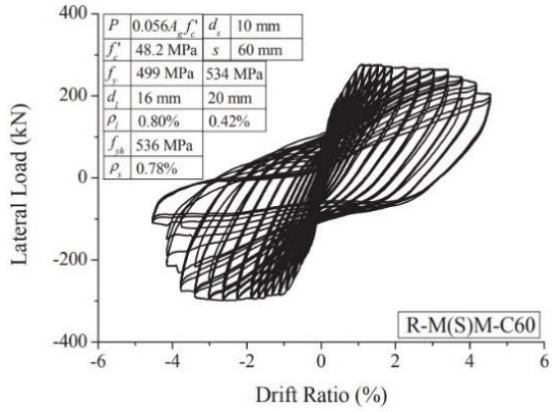Force-Deformation Chart

Damage State I

Damage State II

Damage State III

Damage State IV

Damage State VI (3.79%)

Damage State of Column R-LM-C40 Tested by Su et al. (2019)

Cross Section = 23.62x19.69"
Height = 104.33"
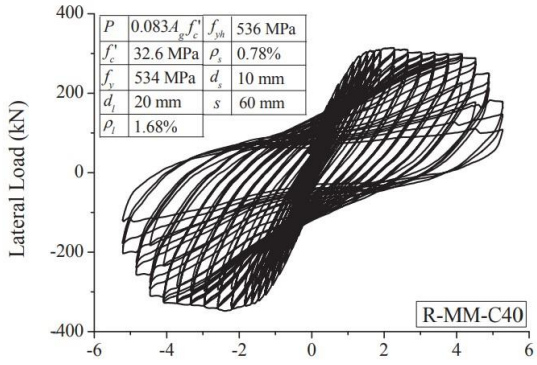Force-Deformation Chart

Damage State I

Damage State II

Damage State III

Damage State IV

Damage State VI (3.91%)

Damage State of Column R-M(S)M-C60 Tested by Su et al. (2019)
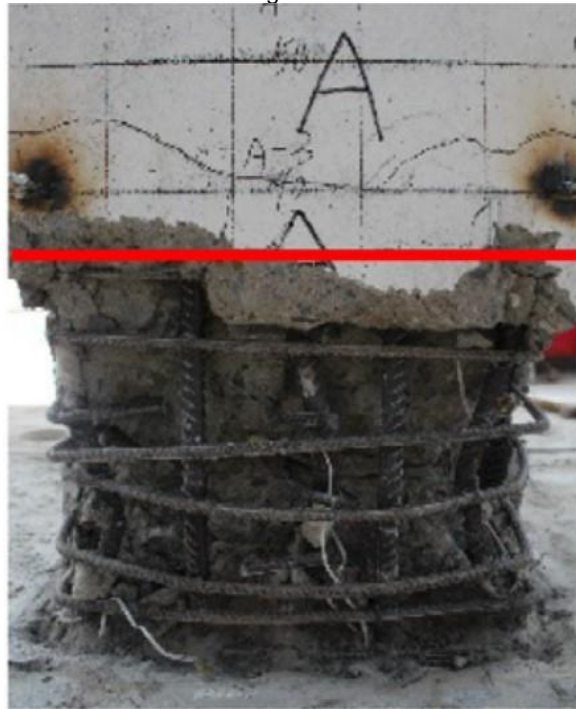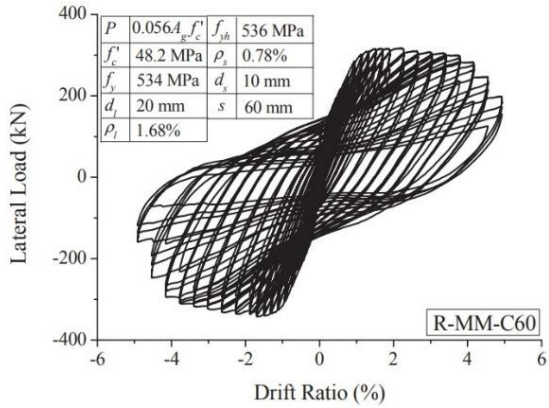
Cross Section = 23.62x19.69"
Height = 104.33"
Force-Deformation Chart

Damage State I

Damage State II

Damage State III

Damage State IV

Damage State VI (4.57%)

Damage State of Column R-MM-C40 Tested by Su et al. (2019)

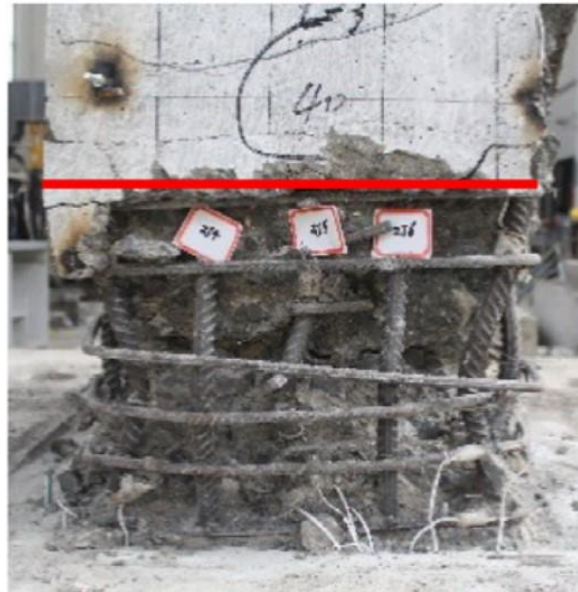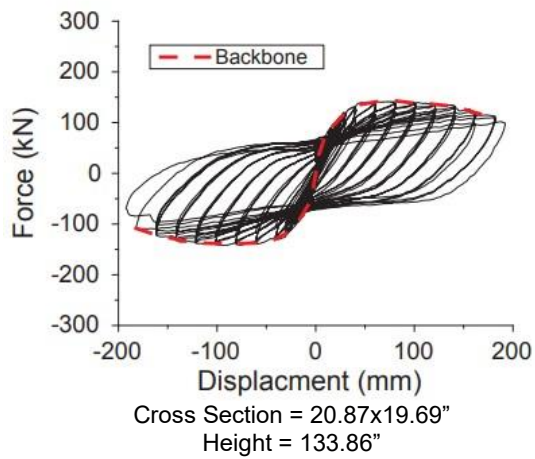| P	$0.056A_g f_c'$	f_{yh}	536 MPa
f_c'	48.2 MPa	ρ_t	0.78%
f_y	534 MPa	d_s	10 mm
d_l	20 mm	s	60 mm
ρ_l	1.68%		

R-MM-C60

Cross Section = 23.62x19.69"
Height = 104.33"
Force-Deformation Chart

Damage State I

Damage State II

Damage State III

Damage State IV

Damage State VI (4.18%)

Damage State of Column R-MM-C60 Tested by Su et al. (2019)

A-142

Cross Section = 20.87x19.69"
Height = 133.86"

Force-Deformation Chart

Damage State I (0.441%)

Damage State II (1.76%)

Damage State III (3.53%)

Damage State IV

Damage State VI (5.36%)

Damage State of Column #1 Tested by Wang et al. (2018)

Cross Section = 15.75x15.75"
Height = 87.4"
Force-Deformation Chart
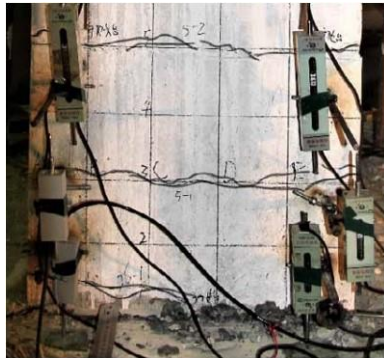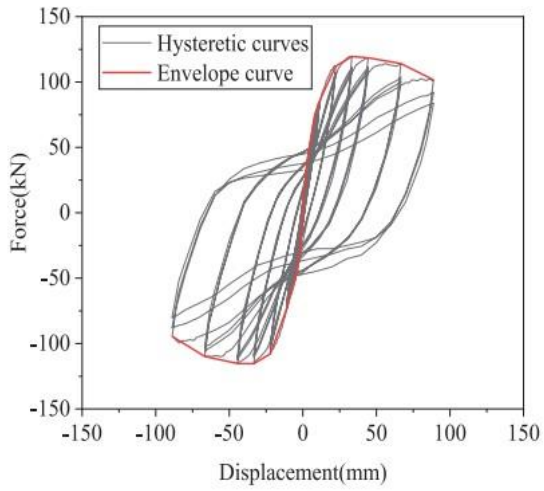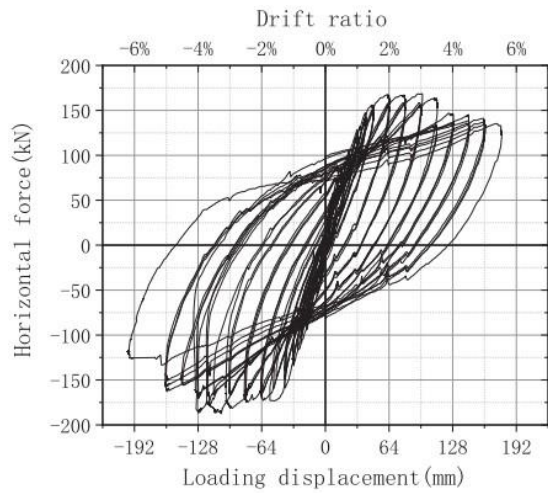
Damage State I

Damage State II

Damage State III

Damage State IV

Damage State VI (4%)

Damage State of Column CIP Tested by Xie et al. (2020)

Cross section= 20.866x20.866"
Height = 125.98"
Force-Deformation Chart

Damage State I
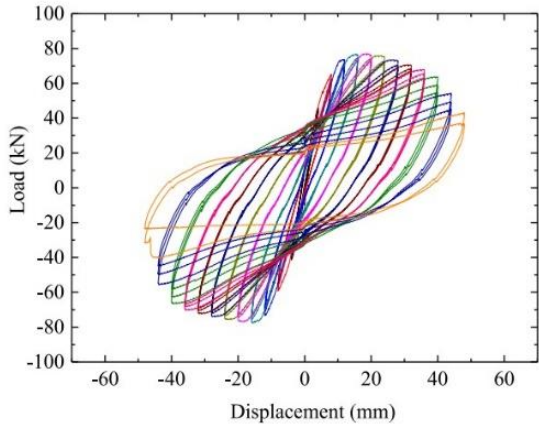
Damage State II

Damage State III

Damage State IV

Damage State VI (5.34%)

Damage State of Column RCP Tested by Xin et al. (2021)

Cross Section = 11.81x11.81"
Height = 47.24"
Force-Deformation Chart

Damage State I

Damage State II

Damage State III

Damage State IV

Damage State VI (3.67%)

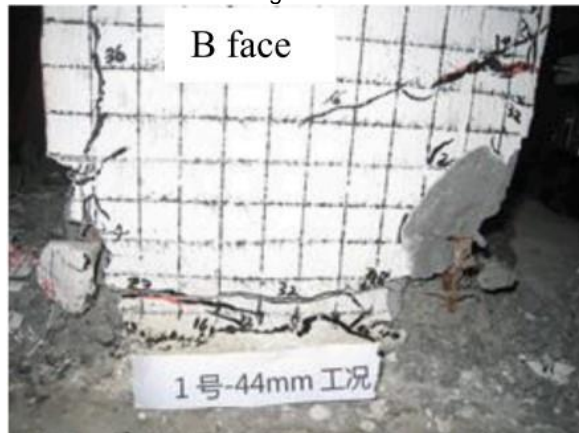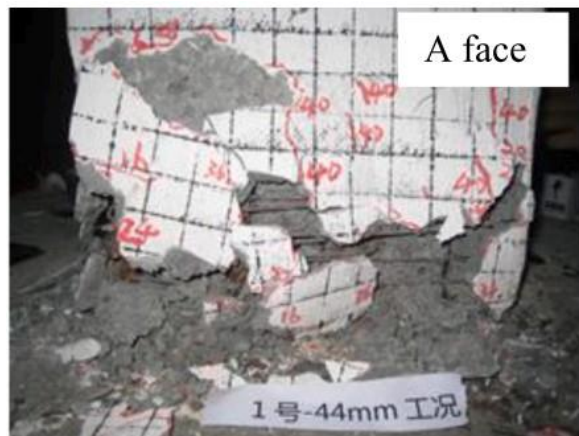**Damage State of Column RCC Tested by Zhang et al. (2019)**

A4. References for RC Bridge Column Database

The references used in development of the RC bridge column database are as follows:

A4.1 References used in RC Circular Column Database

Acosta, J.G.A., 2011. Seismic Performance of Circular and Interlocking Spirals RC Bridge Columns under Bidirectional Shake Table Loading. University of Nevada, Reno.

Al-Hawarneh, M. and Alam, M.S., 2021. Lateral Cyclic Response of RC Bridge Piers Made of Recycled Concrete: Experimental Study. Journal of Bridge Engineering, 26(5), p.04021018.

Al-Jelawy, H.M., Mackie, K.R. and Haber, Z.B., 2018. Shifted plastic hinging for grouted sleeve column connections. ACI Structural Journal, 115(4), pp.1101-1114.

Alian Amiri, S., 2020. Performance of Reinforced Concrete Bridge Columns with Various Reinforcement Details Subject to Long-Duration Earthquakes (Doctoral dissertation).

Ameli, M.J. and Pantelides, C.P., 2017. Seismic analysis of precast concrete bridge columns connected with grouted splice sleeve connectors. Journal of Structural Engineering, 143(2), p.04016176.

Ameli, M. J., Brown, D. N., Parks, J. E., Pantelides, C. P., 2016. Seismic Column-to-footing Connections Using Grouted Splice Sleeves. ACI Structural Journal, 113 (5), pp. 1021-1030.

Ang, B.G., 1981. Ductility of reinforced concrete bridge piers under seismic loading.

Aviram, A., Stojadinovic, B. and Parra-Montesinos, G.J., 2014. High-performance fiber-reinforced concrete bridge columns under bidirectional cyclic loading. ACI Structural Journal, 111(2), p.303.

Barbosa, A.R., Link, T. and Trejo, D., 2016. Seismic performance of high-strength steel RC bridge columns. Journal of Bridge Engineering, 21(2), p.04015044.

Barcley, L. and Kowalsky, M., 2020. Seismic performance of circular concrete columns reinforced with high-strength steel. Journal of Structural Engineering, 146(2), p.04019198.

Brown, W.A., Lehman, D.E. and Stanton, J.F., 2008. Bar buckling in reinforced concrete bridge columns. Pacific Earthquake Engineering Research Center.

Calderone, A.J., 2001. Behavior of reinforced concrete bridge columns having varying aspect ratios and varying lengths of confinement. Pacific Earthquake Engineering Research Center.

ChaiI, Y.H., Priestley, M.N. and Seible, F., 1991. Seismic retrofit of circular bridge columns for enhanced flexural performance. Structural Journal, 88(5), pp.572-584.

Chan, T., Mackie, K.R. and Haber, Z.B., 2020. Precast Seismic Bridge Column Connection Using Ultra-High-Performance Concrete Lap Splice. ACI Structural Journal, 117(1).

Cheok, G.S. and Stone, W.C., 1986. Behavior of 1/6-scale model bridge columns subjected to cycle inelastic loading, NBSIR 86-3494. Center for Building Technology, National Engineering Laboratory, National Institute of Standards and Technology.

Choi, H., Saiidi, M.S., Somerville, P. and El-Azazy, S., 2010. Experimental Study of Reinforced Concrete Bridge Columns Subjected to Near-Fault Ground Motions. ACI Structural Journal, 107(1).

Chung, Y.S., Lee, D.H., Park, C.K. and Park, J.Y., 2002. Seismic enhancement of circular RC bridge piers with fiber composites. KSCE Journal of Civil Engineering, 6(4), pp.485-493.

Correal, J.F., Saiidi, M.S., Sanders, D. and El-Azazy, S., 2007. Analytical evaluation of bridge columns with double interlocking spirals. ACI structural journal, 104(3), p.314.

Deng, J., John Ma, Z., Liu, A., Cao, S. and Zhang, B., 2017. Seismic performance of reinforced concrete bridge columns subjected to combined stresses of compression, bending, shear, and torsion. Journal of Bridge Engineering, 22(11), p.04017099.

Elsanadedy, H.M., 2002. Seismic performance and analysis of ductile composite-jacketed reinforced concrete bridge columns. University of California, Irvine.

Esmaeily-Ghasemabadi, A., 2003. Seismic behavior of bridge columns subjected to various loading patterns.

Fang, C., Yuan, Z., Yang, S. and Zhang, J., 2017, December. Performance of corroded bridge piers under cyclic loading. In Proceedings of the Institution of Civil Engineers-Bridge Engineering (Vol. 170, No. 4, pp. 255-270). Thomas Telford Ltd.

Fu, Q., Wang, X. and Liang, S., 2019, September. Accumulated Damage-based Experimental Study on Seismic Performance of HRBF500 Rebar Reinforced RC Bridge Columns. In IOP Conference Series: Materials Science and Engineering (Vol. 603, No. 3, p. 032025). IOP Publishing.

Ghee, A.B., Priestley, M.N. and Paulay, T., 1989. Seismic shear strength of circular reinforced concrete columns. Structural Journal, 86(1), pp.45-59.

Goodnight, J.C., 2015. The effects of load history and design variables on performance limit states of circular bridge columns. North Carolina State University.

Haber, Z.B., Saiidi, M.S. and Sanders, D.H., 2014. Seismic performance of precast columns with mechanically spliced column-footing connections. ACI Structural Journal, 111(3), pp.639-650.

Hachem, M.M., Moehle, J.P. and Mahin, S.A., 2003. Performance of circular reinforced concrete bridge columns under bidirectional earthquake loading. Berkeley, CA: Pacific Earthquake Engineering Research Center.

Hamilton, C.H., Pardoen, G.C. and Kazanjy, R.P., 2002. Experimental testing of bridge columns subjected to reversed-cyclic and pulse-type loading histories. Report 2001-03. Civil Engineering Technical Report Series, University of California, Irvine.

Hamilton, C.H., Pardoen, G.C. and Kazanjy, R.P., 2001. Experimental testing of bridge columns subjected to reversed-cyclic and pulse-type loading histories. Rep. No, 3.

Hose, Y.D., Priestley, M.J.N. and Seible, F., 1997. Strategic relocation of plastic hinges in bridge columns (No. SSRP-97/05).

Ibrahim, A.I., Wu, G., Sun, Z. and Cui, H., 2017. Cyclic behavior of concrete columns reinforced with partially unbonded hybrid. Engineering Structures, 131, pp.311-323.

Jaradat, O.A., 1996. Seismic evaluation of existing bridge columns. Washington State University.

Jia, J., Zhang, K., Wu, S., Guo, Y., Du, X. and Wang, X., 2020. Seismic performance of self-centering precast segmental bridge columns under different lateral loading directions. Engineering Structures, 221, p.111037.

Jia, J., Zhao, L., Wu, S., Wang, X., Bai, Y. and Wei, Y., 2020. Experimental investigation on the seismic performance of low-level corroded and retrofitted reinforced concrete bridge columns with CFRP fabric. Engineering Structures, 209, p.110225.

Kowalsky, M.J., Priestly, M.N. and Seible, F., 1999. Shear and flexural behavior of lightweight concrete bridge columns in seismic regions. ACI structural journal, 96, pp.136-148.

Kunnath, S.K., El-Bahy, A., Taylor, A.W. and Stone, W.C., 1997. Cumulative seismic damage of reinforced concrete bridge piers. In Cumulative seismic damage of reinforced concrete bridge piers (pp. 120-120).

Laplace, P.N., 1999. Shake table testing of flexure-dominated reinforced concrete bridge columns. University of Nevada, Reno.

Lehman, D.E., 1998. Seismic performance of well-confined concrete bridge columns. University of California, Berkeley.

Li, Y., Xie, M.F. and Liu, J.B., 2019. Experimental study on the seismic behaviour of reinforced concrete bridge piers strengthened by BFRP sheets. Advances in Civil Engineering, 2019.

Lim, K.Y. and Mclean, D.I., 1991. Scale model studies of moment-reducing hinge details in bridge columns. Structural Journal, 88(4), pp.465-474.

Lopez, A., Dusicka, P. and Bazaez, R., 2020. Performance of seismically substandard bridge reinforced concrete columns subjected to subduction and crustal earthquakes. Engineering Structures, 207, p.110216.

Marshall, C., Cantrell, J., Mashal, M. and Ebrahimpour, A., 2020, April. A precast pier system for ABC in seismic regions. In Structures Congress 2020 (pp. 183-192). Reston, VA: American Society of Civil Engineers.

Mohammed, M.S., 2016. Effect of earthquake duration on reinforced concrete bridge columns. University of Nevada, Reno.

Moustafa, K.F., Sanders, D., Saiidi, M.S. and El-Azazy, S., 2011. Seismic Performance of Reinforced Concrete Bridge Bents. ACI Structural Journal, 108(1).

Moustafa, M.A. and Mosalam, K.M., 2015. Structural Behavior of Column-Bent Cap Beam-Box Girder Systems in Reinforced Concrete Bridges Subjected to Gravity and Seismic Loads Part II: Hybrid Simulation and Post-Test Analysis (No. CA16-2171B).

Moyer, M.J. and Kowalsky, M.J., 2003. Influence of tension strain on buckling of reinforcement in concrete columns. ACI Structural Journal, 100(1), pp.75-85.

Munro, I.R.M., 1976. Seismic behaviour of reinforced concrete bridge piers.

Naito, C.J., 2001. Experimental and computational evaluation of reinforced concrete bridge beam-column connections for seismic performance.

Nelson, R.B., 2007. Experimental evaluation of performance of conventional bridge systems. University of Nevada, Reno.

O'Brien, M., Saiidi, M.S. and Sadrossadat-Zadeh, M., 2007. A study of concrete bridge columns using innovative materials subjected to cyclic loading.

Orozco, G.L., 2001. The effects of a large velocity pulse on reinforced concrete bridge columns. Department of Structural Engineering, University of California, San Diego.

Orozco, G.L. and Ashford, S.A., 2002. Effects of large velocity pulses on reinforced concrete bridge columns, PEER Report 2002/23. University of California, Berkeley.

Phan, V., Saiidi, M.S., Anderson, J. and Ghasemi, H., 2007. Near-fault ground motion effects on reinforced concrete bridge columns. Journal of structural engineering, 133(7), pp.982-989.

Prakash, S., Li, Q. and Belarbi, A., 2012. Behavior of circular and square reinforced concrete bridge columns under combined loading including torsion. ACI Structural Journal, 109(3), pp.317-328.

Priestley, M.N. and Benzoni, G., 1996. Seismic performance of circular columns with low longitudinal reinforcement ratios. Structural Journal, 93(4), pp.474-485.

Ranf, R.T., Eberhard, M.O. and Stanton, J.F., 2006. Effects of displacement history on failure of lightly confined bridge columns. ACI SPECIAL PUBLICATIONS, 236, p.23.

Roeder, C.W., Graff, R., Soderstrom, J. and Yoo, J.H., 2005. Seismic performance of pile-wharf connections. Journal of Structural Engineering, 131(3), pp.428-437.

Sakai, J., Mahin, A.S. and Espinoza, A., 2006. Earthquake Simulation Tests on Reducing Residual Displacements of Reinforced Concrete Bridge Columns, PEER Report. University of California, Berkeley.

Sritharan, S., Priestley, M.N. and Seible, F., 2000. Nonlinear finite element analyses of concrete bridge joint systems subjected to seismic actions. Finite elements in analysis and design, 36(3-4), pp.215-233.

Stone, W.C. and Cheok, G.S., 1989. Inelastic behavior of full-scale bridge columns subjected to cyclic loading (No. NIST BSS 166).

Su, J., Li, Z., Wang, J. and Dhakal, R.P., 2020. Numerical simulation and damage analysis of RC bridge piers reinforced with varying yield strength steel reinforcement. Soil Dynamics and Earthquake Engineering, 130, p.106007.

Su, J., Wang, J., Bai, Z., Wang, W. and Zhao, D., 2015. Influence of reinforcement buckling on the seismic performance of reinforced concrete columns. Engineering Structures, 103, pp.174-188.

Tang, Y., Wu, G., Sun, Z. and Zhang, Y., 2019. Seismic performance of underwater bridge columns strengthened with prestressed-concrete panels and FRP reinforcement. Journal of Composites for Construction, 23(3), p.04019019.

Trejo, D., Barbosa, A.R. and Link, T., 2014. Seismic performance of circular reinforced concrete bridge columns constructed with grade 80 reinforcement (No. FHWA-OR-RD-15-02). Pacific Northwest Transportation Consortium.

Trono, W., Jen, G., Panagiotou, M., Schoettler, M. and Ostertag, C.P., 2015. Seismic response of a damage-resistant recentering posttensioned-HYFRC bridge column. Journal of Bridge Engineering, 20(7), p.04014096.

Vosooghi, A., 2010. Post-earthquake evaluation and emergency repair of damaged RC bridge columns using CFRP materials. University of Nevada, Reno.

Wang, Z., Wu, C., Li, T., Xiao, W., Wei, H. and Qu, H., 2020. Experimental Study on the Seismic Performance of Improved Grouted Corrugated Duct Connection (GCDC) Design for Precast Concrete Bridge Column. Journal of Earthquake Engineering, pp.1-22.

Wong, Y.L., Paulay, T. and Priestley, M.N., 1993. Response of circular reinforced concrete columns to multi-directional seismic attack. Structural Journal, 90(2), pp.180-191.

Wu, R.Y. and Pantelides, C.P., 2017. Rapid Seismic Repair of Reinforced Concrete Bridge Columns. ACI Structural Journal, 114(5).

Xiao, Y., Wu, H., and Martin, G.R., 1999. Prefabricated composite jacketing of RC columns for enhanced shear strength. Journal of structural engineering, 125(3), pp.255-264.

Yalcin, C., 1998. Seismic evaluation and retrofit of existing reinforced concrete bridge columns. University of Ottawa, Canada.

Yarandi, M.S., 2007. Seismic retrofit and repair of existing reinforced concrete bridge columns by transverse prestressing, Doctoral dissertation, University of Ottawa, Canada.

Yuan, Z., Fang, C., Parsaeimaram, M. and Yang, S., 2017. Cyclic behavior of corroded reinforced concrete bridge piers. Journal of Bridge Engineering, 22(7), p.04017020.

Zahn, F.A., 1985. Design of reinforced concrete bridge columns for strength and ductility. Dissertation, University of Canterbury, 405 pp.
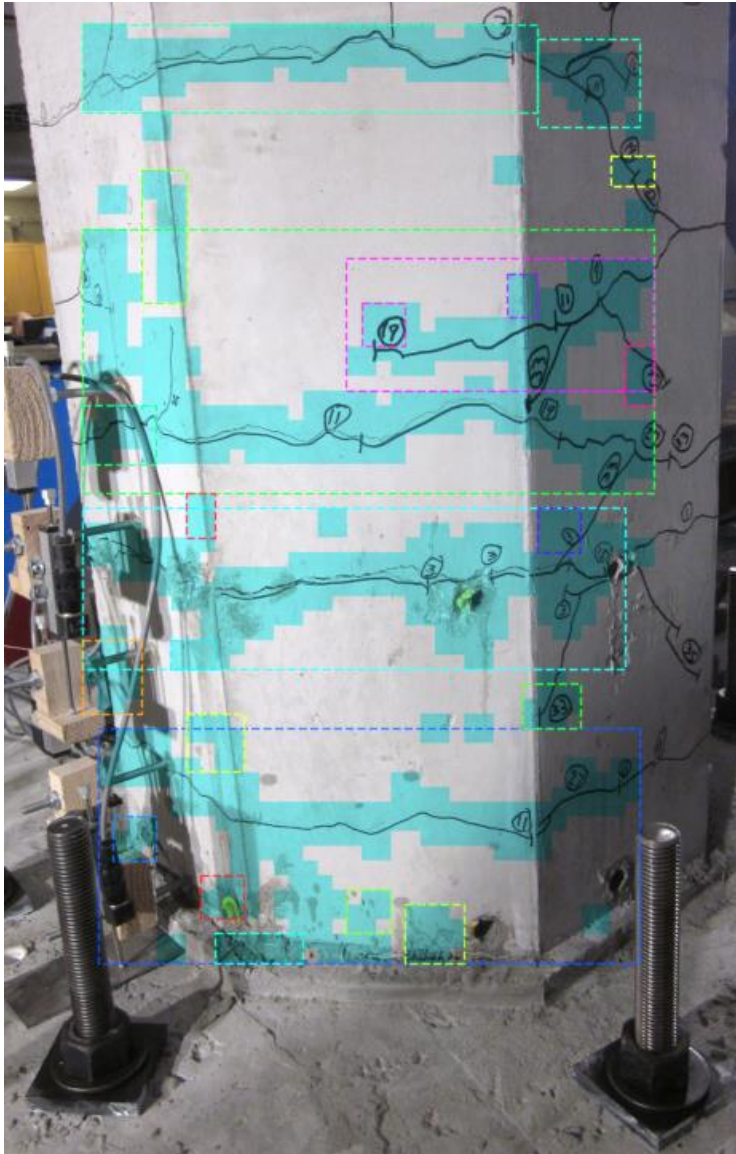
A4.2 References used in RC Rectangular Column Database

Ang, B.G., 1981. Ductility of reinforced concrete bridge piers under seismic loading.

Bechtoula, F., Mehani, Y. And Kibboua, A., 2014. Effect Of Loading History on Fragility Curves of Reinforced Concrete Bridge Piers Under Multidirectional Loading. In Second European Conference on Earthquake Engineering and Seismology, Istanbul Aug, pp. 25-29.

Ghadban, A.A., Wehbe, N.I. and Pauly, T., 2018. Seismic performance of self-consolidating concrete bridge columns. Engineering Structures, 160, pp.461-472.

Ibrahim, A.M., Wu, Z., Fahmy, M.F. and Kamal, D., 2016. Experimental study on cyclic response of concrete bridge columns reinforced by steel and basalt FRP reinforcements. Journal of Composites for Construction, 20(3), p.04015062.

Jia, Y., Zhao, R., Li, F., Zhou, Z., Wang, Y., Zhan, Y. and Shi, X., 2020. Seismic performance of bridge piers constructed with PP-ECC at potential plastic hinge regions. Materials, 13(8), p.1865.

Kawashima, K. and Koyama, T., 1988. Effect of cyclic loading hysteresis on dynamic behavior of reinforced concrete bridge piers. Proc. JSCE, Structural Eng./Earthquake Eng, 5(2).

Kawashima, K., Zafra, R., Sasaki, T., Kajiwara, K. and Nakayama, M., 2011. Effect of polypropylene fiber reinforced cement composite and steel fiber reinforced concrete for enhancing the seismic performance of bridge columns. Journal of Earthquake Engineering, 15(8), pp.1194-1211.

Legeron, F. and Paultre, P., 2000. Behavior of high-strength concrete columns under cyclic flexure and constant axial load. Structural Journal, 97(4), pp.591-601.

Li, Q., 2012. Performance of RC bridge columns under cyclic combined loading including torsion (Doctoral dissertation).

Li, T., Qu, H., Wang, Z., Wei, H. and Jiang, S., 2018. Seismic performance of precast concrete bridge columns with quasi-static cyclic shear test for high seismic zones. Engineering Structures, 166, pp.441-453.

Liu, X., Li, J., Tsang, H.H., Wang, J. and Zhong, J., 2020. Experimental evaluation of seismic performance of unbonded prestressed reinforced concrete column. Engineering Structures, 208, p.109913.

Liu, Y., Li, X., Zheng, X. and Song, Z., 2020. Experimental study on seismic response of precast bridge piers with double-grouted sleeve connections. Engineering Structures, 221, p.111023.

Mo, Y.L. and Wang, S.J., 2000. Seismic behavior of RC columns with various tie configurations. Journal of Structural Engineering, 126(10), pp.1122-1130.

Naito, C.J., 2001. Experimental and computational evaluation of reinforced concrete bridge beam-column connections for seismic performance.

Nakashoji, B.A., 2014. Seismic performance of square nickel-titanium reinforced ECC columns with headed couplers. University of Nevada, Reno.

Ohno, T. and Nishioka, T., 1984. An experimental study on energy absorption capacity of columns in reinforced concrete structures. Doboku Gakkai Ronbunshu, 1984(350), pp.23-33.

Ongsupankul, S., Kanchanalai, T. and Kawashima, K., 2007. Behavior of reinforced concrete bridge pier columns subjected to moderate seismic load. ScienceAsia, 33, pp.175-185.

Pandey, G.R. and Mutsuyoshi, H., 2005. Seismic performance of reinforced concrete piers with bond-controlled reinforcements. ACI structural journal, 102(2), p.295.

Popa, V., Papurcu, A., Cotofana, D. and Pascu, R., 2015. Experimental testing on emulative connections for precast columns using grouted corrugated steel sleeves. Bulletin of Earthquake Engineering, 13(8), pp.2429-2447.

Prakash, S., Li, Q. and Belarbi, A., 2012. Behavior of circular and square reinforced concrete bridge columns under combined loading including torsion. ACI Structural Journal, 109(3), pp.317-328.

Priestley, M.N., Seible, F., Xiao, Y. and Verma, R., 1994. Steel jacket retrofitting of reinforced concrete bridge columns for enhanced shear strength-part 1: Theoretical considerations and test design. Structural Journal, 91(4), pp.394-405.

Seong, D., Kim, T., Oh, M. and Shin, H., 2011. Inelastic performance of high-strength concrete bridge columns under earthquake loads. Journal of Advanced Concrete Technology, 9(2), pp.205-220.

Su, J., Wang, J., Li, Z. and Liang, X., 2019. Effect of reinforcement grade and concrete strength on seismic performance of reinforced concrete bridge piers. Engineering Structures, 198, p.109512.

Tanaka, H., 1990. Effect of lateral confining reinforcement on the ductile behaviour of reinforced concrete columns.

Wang, Z., Qu, H., Li, T., Wei, H., Wang, H., Duan, H. and Jiang, H., 2018. Quasi-static cyclic tests of precast bridge columns with different connection details for high seismic zones. Engineering Structures, 158, pp.13-27.

Wehbe, N., 1998. EERI Annual Student Paper Award Confinement of Rectangular Bridge Columns in Moderate Seismic Areas. Earthquake spectra, 14(2), pp.397-406.

Xie, Q., Zhao, X., Yao, X., Hao, W. and Hu, F., 2020. Seismic behaviors of precast assembled bridge columns connected with prestressed threaded steel bar: Experimental test and hysteretic model. Advances in Structural Engineering, 23(9), pp.1975-1988.

Xin, G., Xu, W., Wang, J., Yan, X., Chen, Y., Yan, W. and Li, J., 2021, October. Seismic performance of fabricated concrete piers with grouted sleeve joints and bearing-capacity estimation method. In Structures (Vol. 33, pp. 169-186). Elsevier.

Yalcin, C., 1998. Seismic evaluation and retrofit of existing reinforced concrete bridge columns. University of Ottawa (Canada).

Yarandi, M.S., 2007. Seismic retrofit and repair of existing reinforced concrete bridge columns by transverse prestressing (Doctoral dissertation, University of Ottawa (Canada)).

Zhang, R., Meng, Q., Shui, Q., He, W., Chen, K., Liang, M. and Sun, Z., 2019. Cyclic response of RC composite bridge columns with precast PP-ECC jackets in the region of plastic hinges. Composite Structures, 221, p.110844.

South Dakota State University

APPENDIX B. BRIDGE DAMAGE ASSESSMENT TOOLS

Aditya Harshvardhan, Kwanghee Won, Mostafa Tazarv
South Dakota State University
2021

Table of Contents

B1. Introduction

Bridge Damage Assessment Tools (BrDATs) are a collection of tools for damage assessment of bridges after an event. The tools are accessible via a web app using any of the popular web browsers like Google Chrome, Mozilla Firefox or Microsoft Edge.

Note: The application only supports Windows 10 as of now due to certain scripts. MacOS and Linux support will be added in the future.

B2. Web App Setup (for Internal Use)

B2.1 Prerequisites:

1. Install Node,js (latest version) - https://nodejs.org/en/
    a. Check if npm is installed using npm install command in the Command Prompt

2. Install Vue3 (https://v3.vuejs.org/guide/installation.html#npm) from the command line using npm install vue@next

3. Install Vue.js Command Line Interface using npm install -g @vue/cli

4. Install Bootstrap CSS Framework using npm install bootstrap - https://getbootstrap.com/docs/5.1/getting-started/download/

5. Install Python 3 - https://www.python.org/downloads/

6. Install Flask- https://flask.palletsprojects.com/en/2.0.x/installation/

7. Install Visual Studio Code (If editing the code)- https://code.visualstudio.com/

B2.2 Starting the services:

1. Open Visual Studio Code
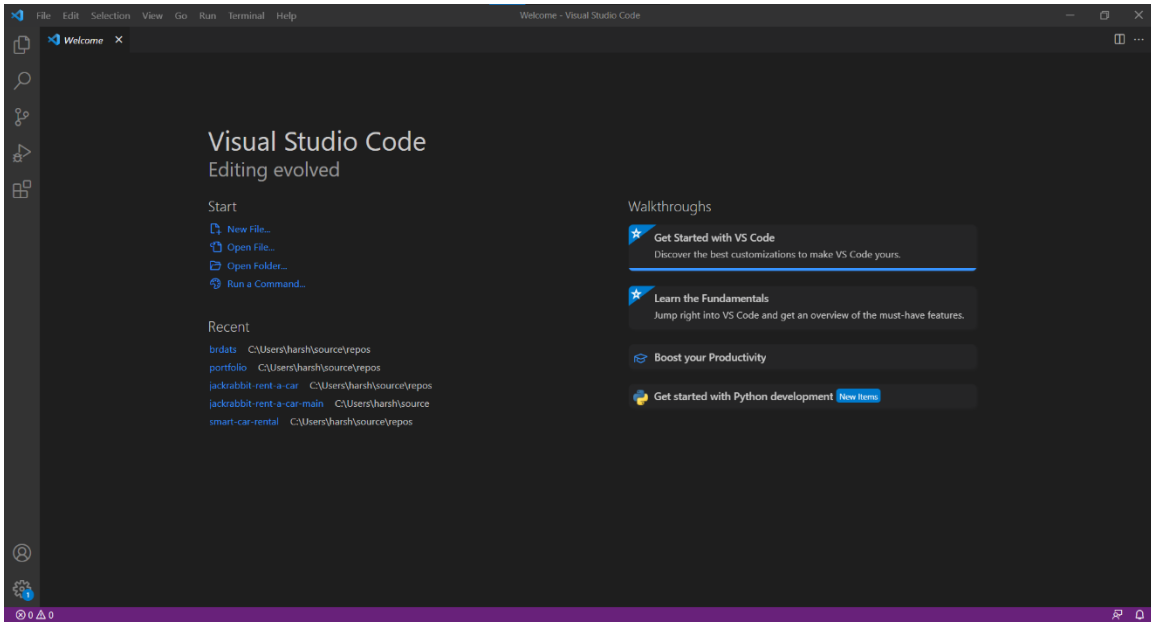
2. Go to File -> Open Folder… It will then open a dialog box. Browse to the location where "brdats" folder is, the click "Select Folder".
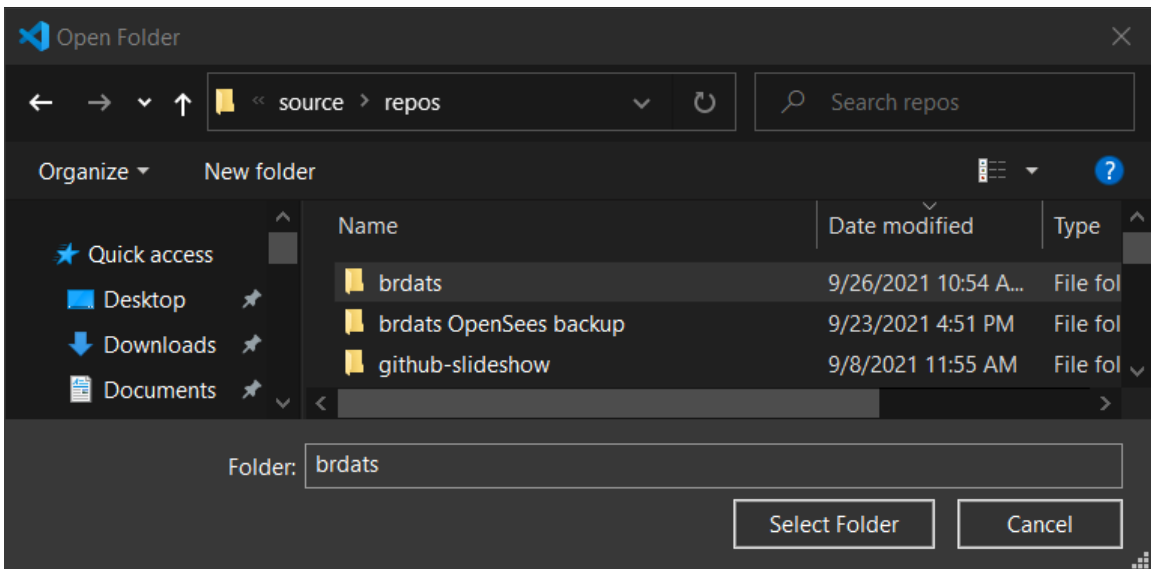
3. The "brdats" folder opens and editor should look something like this:
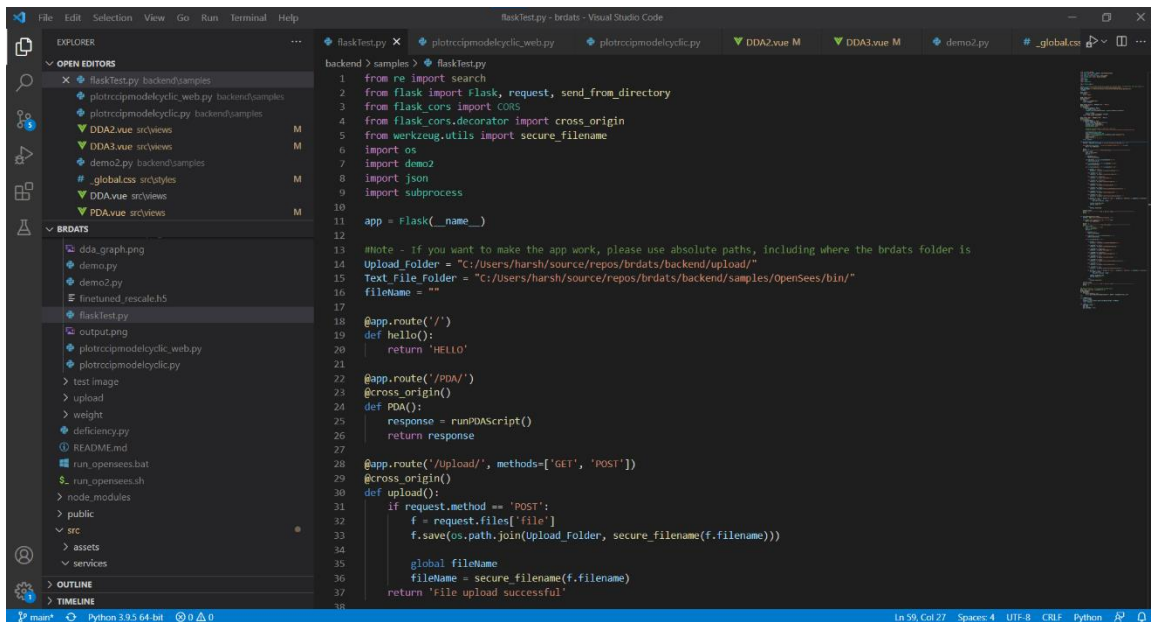
4. Go to "Terminal" -> "New Terminal"
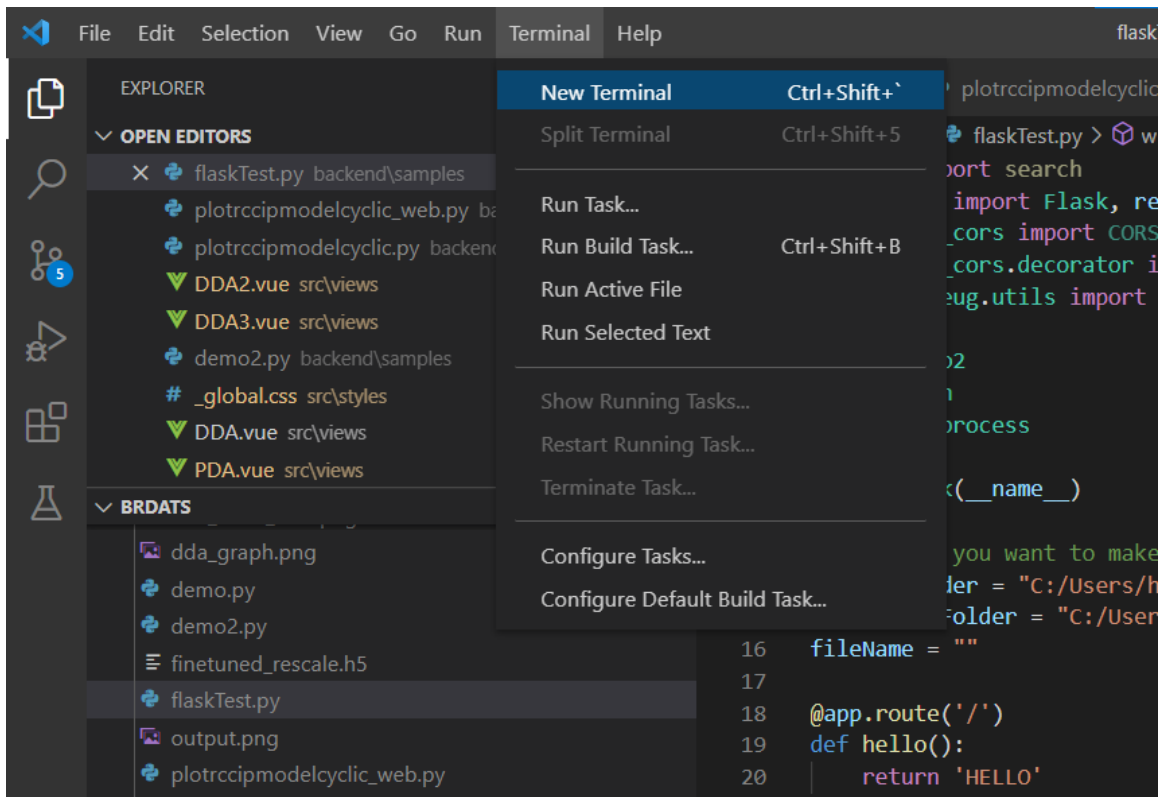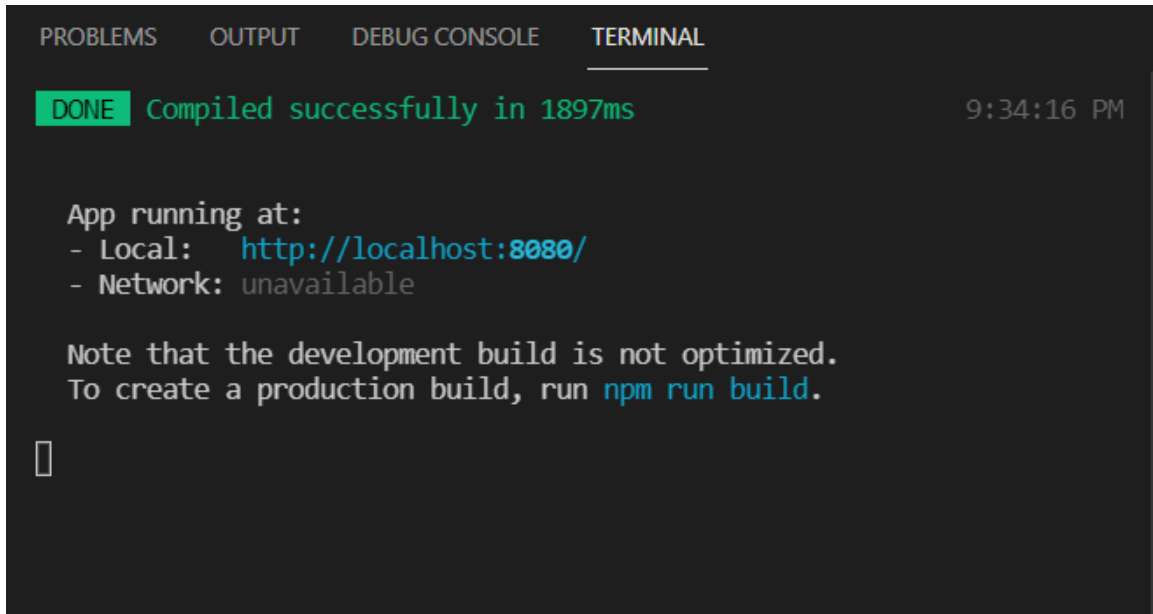
5. Visual Studio window looks like this:
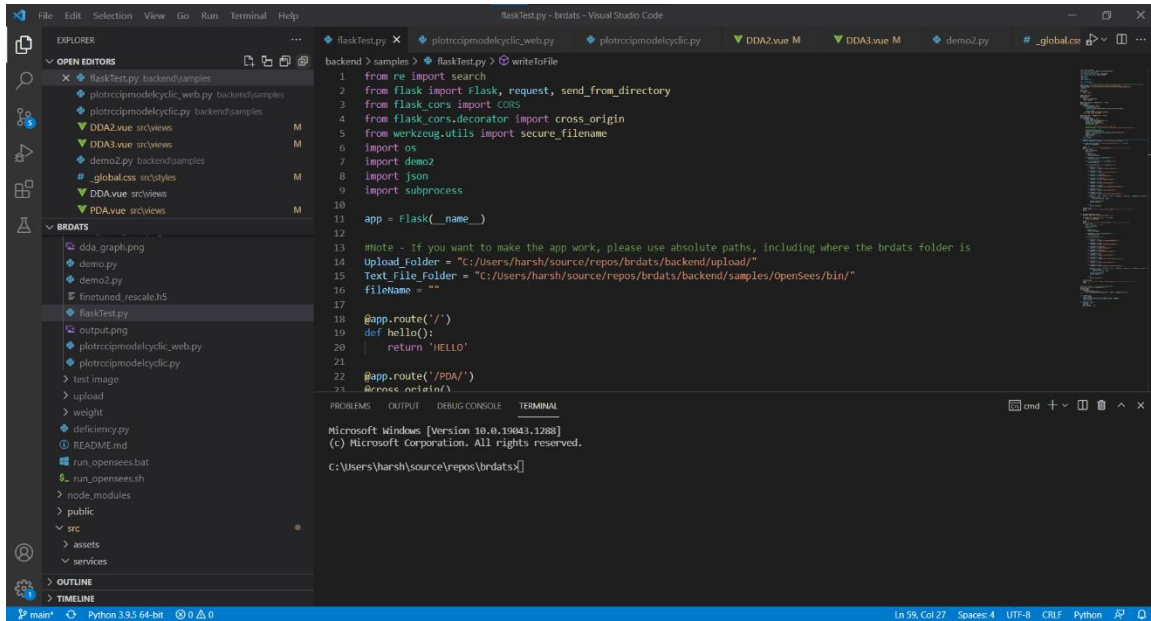
6. Click "Split Terminal" to Open a new terminal
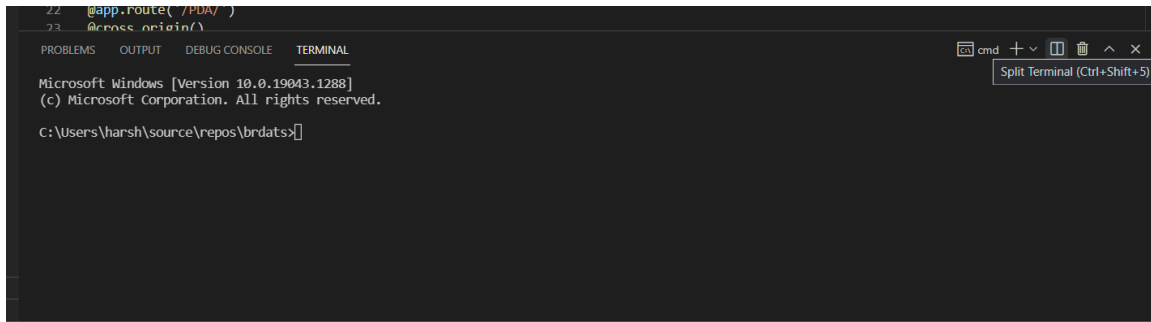
7. Now the Terminal looks like this:
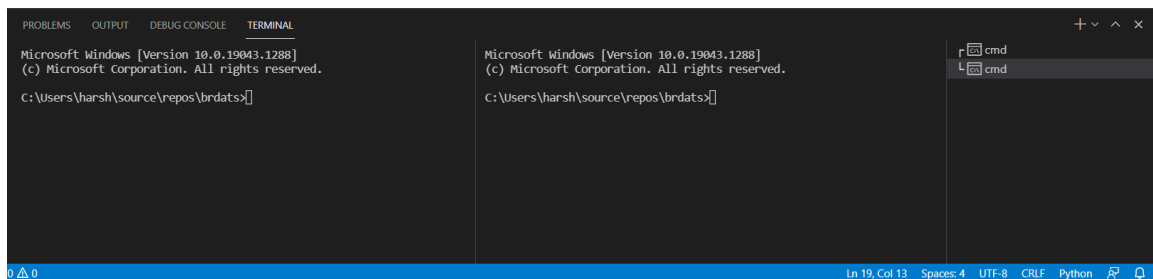
8. Now on first window type npm run serve (Compiles the User Interface service and should return the below message saying that App is running).

```
PROBLEMS    OUTPUT    DEBUG CONSOLE    TERMINAL

 DONE  Compiled successfully in 1897ms                    9:34:16 PM


  App running at:
  - Local:   http://localhost:8080/
  - Network: unavailable

  Note that the development build is not optimized.
  To create a production build, run npm run build.

 []
```

9. Then follow the below commands in the second window (with output)

```
Microsoft Windows [Version 10.0.19043.1288]
(c) Microsoft Corporation. All rights reserved.

C:\Users\harsh\source\repos\brdats>cd backend/brdatsflask/Scripts

C:\Users\harsh\source\repos\brdats\backend\brdatsflask\Scripts>Activate

(brdatsflask) C:\Users\harsh\source\repos\brdats\backend\brdatsflask\Scripts>cd ..

(brdatsflask) C:\Users\harsh\source\repos\brdats\backend\brdatsflask>cd ..

(brdatsflask) C:\Users\harsh\source\repos\brdats\backend>cd samples

(brdatsflask) C:\Users\harsh\source\repos\brdats\backend\samples>py flaskTest.py
2021-10-20 21:37:14.071018: W tensorflow/stream_executor/platform/default/dso_loader.c
c:64] Could not load dynamic library 'cudart64_110.dll'; dlerror: cudart64_110.dll not
 found
2021-10-20 21:37:14.071139: I tensorflow/stream_executor/cuda/cudart_stub.cc:29] Ignor
e above cudart dlerror if you do not have a GPU set up on your machine.
 * Serving Flask app 'flaskTest' (lazy loading)
 * Environment: production
   WARNING: This is a development server. Do not use it in a production deployment.
   Use a production WSGI server instead.
 * Debug mode: on
 * Restarting with stat
2021-10-20 21:37:17.682075: W tensorflow/stream_executor/platform/default/dso_loader.c
c:64] Could not load dynamic library 'cudart64_110.dll'; dlerror: cudart64_110.dll not
 found
2021-10-20 21:37:17.682609: I tensorflow/stream_executor/cuda/cudart_stub.cc:29] Ignor
e above cudart dlerror if you do not have a GPU set up on your machine.
 * Debugger is active!
 * Debugger PIN: 596-028-823
 * Running on http://127.0.0.1:5000/ (Press CTRL+C to quit)
▯
```

10. Now service is running.

B2.3 Opening BrDATs web application:

1. Open a web browser (ex. Chrome) and type "localhost:8080" in the address bar.

2. Now the web page should look like this:

B3. Application Features:

The web application has three main features:
  1. User account (Sign In and Create Account)
  2. Preliminary Damage Assessment
  3. Detailed Damage Assessment

B3.1 User Account:

B3.1.1 Sign In:
This allows users to Sign In to their respective accounts before they can access the Preliminary Damage Assessment and Detailed Damage Assessment features.

Sign In requires Email ID and a Password to log into the system. This screen also has an option to create a new account in case the user is new to the application.

B3.1.2 Create Account:
This an extension of the Sign In functionality to create a new account which also automatically signs in to the application and gives access to the Preliminary Damage Assessment and Detailed Damage Assessment.

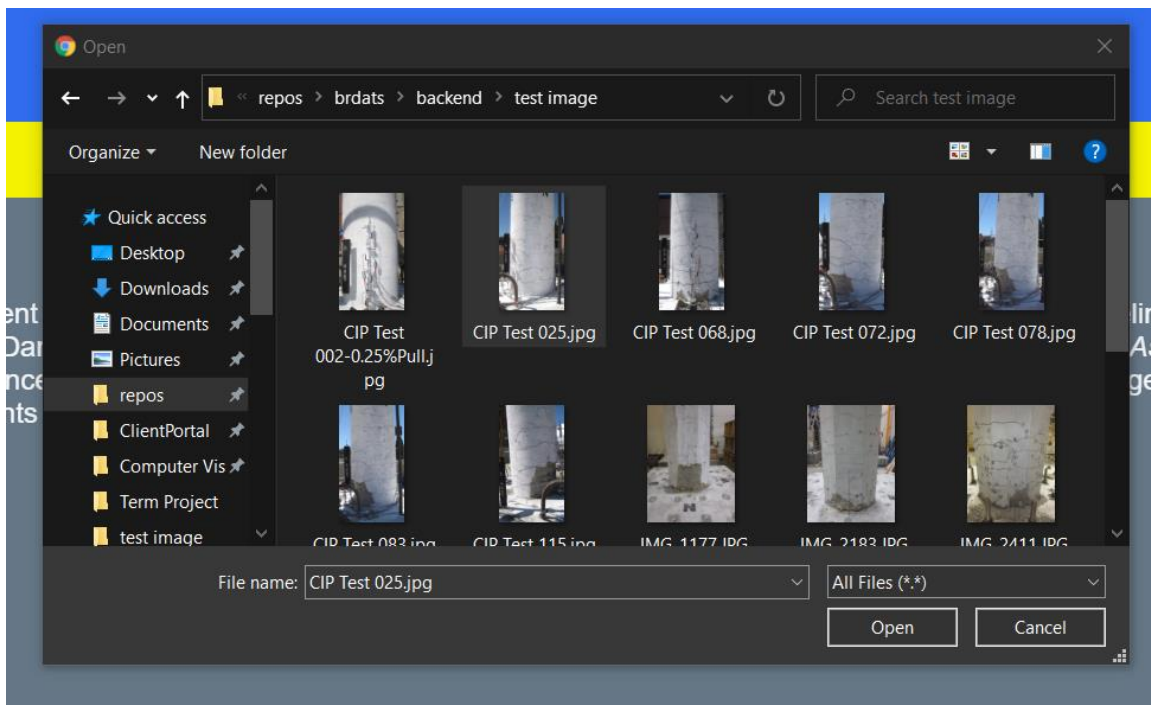This requires a First Name, Last Name, Email ID and Password to complete the registration process.

B3.2 Preliminary Damage Assessment:

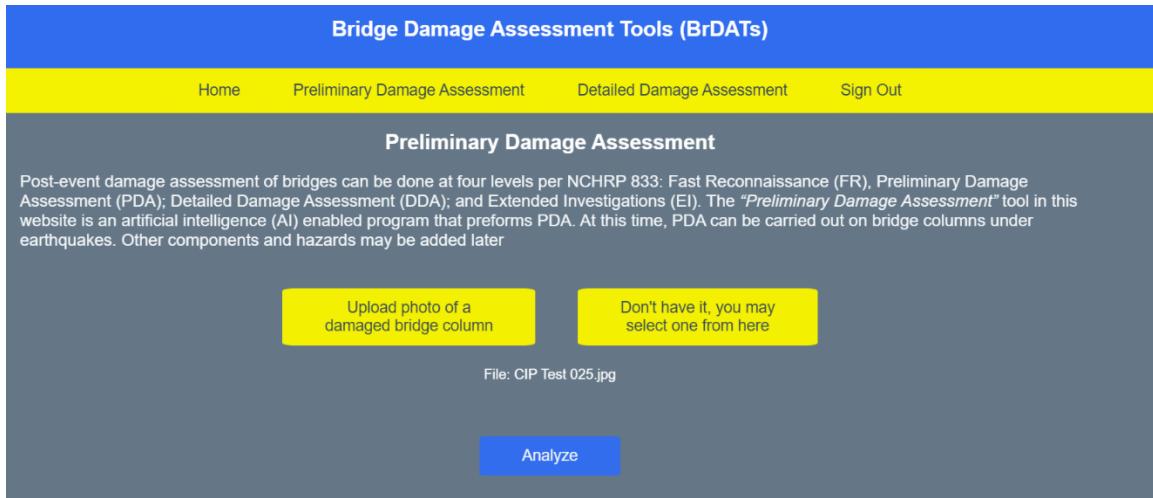After logging in the application when user clicks "Preliminary Damage Assessment", the following page is shown:
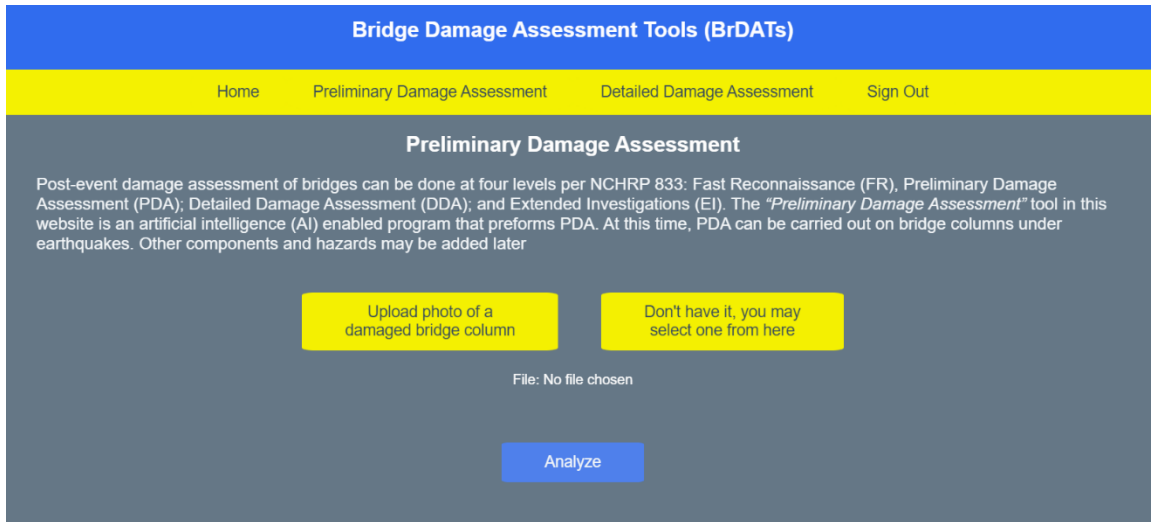
To perform preliminary analysis:
- Click on 'Upload photo of a damaged bridge column' button and select a photo of bridge column (Note- the button on the right is a work in progress).

- Then click Analyze

- The preliminary analysis starts and is shown like below. The process takes about 0.5 to 1 minute.

- Once the PDA analysis is done, the output is shown as below (Screenshot taken after scaling down to fit the page)
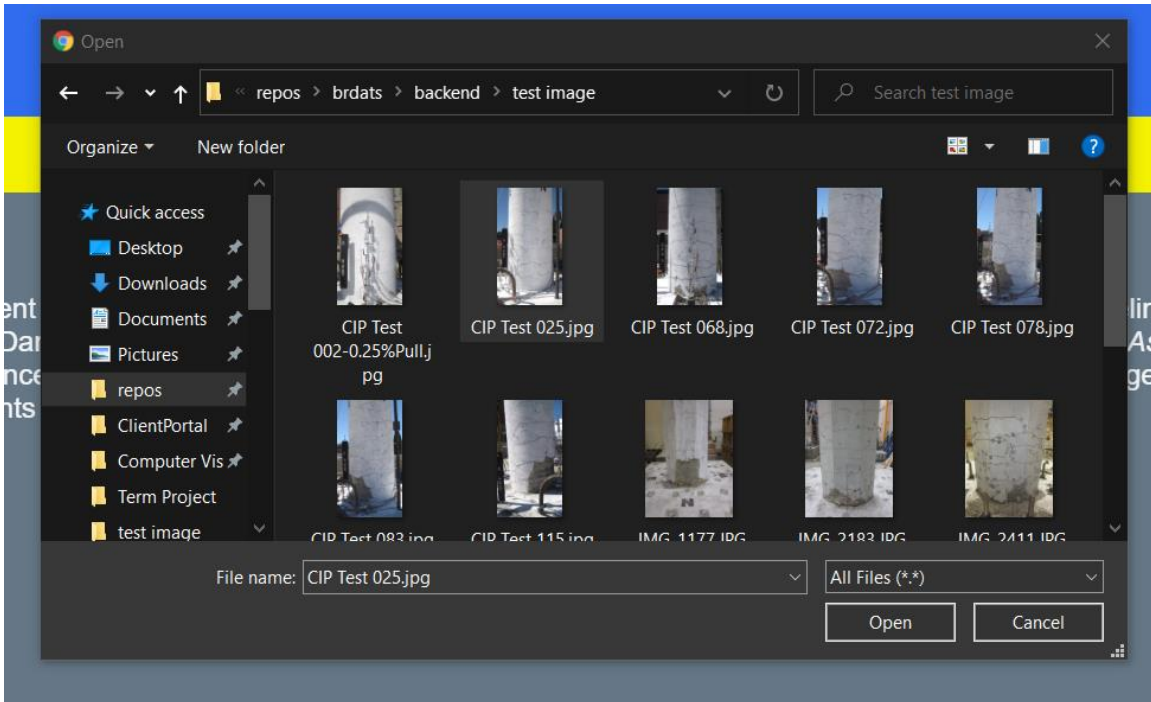
B3.3 Detailed Damage Assessment:

After logging in the application when user clicks "Detailed Damage Assessment", the following page is shown:

To perform preliminary analysis:
- Click on 'Upload photo of a damaged bridge column' button and select a photo of bridge column (Note- the button on the right is a work in progress).

- Then click "Next"

- The following page is shown. This page is more geared towards engineers or who has technical knowledge of bridge column details:

- Once the above-mentioned field are correctly filled to the real metrics for bridges, click "Analyze". The screen should look like:

Bridge Damage Assessment Tools (BrDATs)

| Home | Preliminary Damage Assessment | Detailed Damage Assessment | Sign Out |

Number of Columns per Bent: `1`

Column Length per AASHTO SGS: `192.0` in.

Column Diameter or Side Dimension: `48.0` in.

Column Section Shape: ● Circular Or ● Square

No. of Longitudinal Reinforcing Bar: `22`

Area of Each Longitudinal Reinforcing Bar: `1.00` in.^{2}

Transverse Reinforcement Spacing: `4.0` in.

Area of Transverse Reinforcement: `0.44` in.^{2}

Concrete Strength: `5.0` ksi

Column Axial Load from Superstructure: `400` kips

Analyze

Please Wait...

- This will trigger the backend services to perform PDA first to estimate the Damage State. The drift demand is calculated using the damage state from PDA following the empirical equations developed in the present study (Tazarv et al., 2021). The input from user is then passed to OpenSees, which performs a pushover analysis of the column using a generic model discussed in the present report. The analysis results are post-processed using a Python code to calculate the key points of the pushover curve and to calculate the column failure. The failure was defined as the minimum displacement in which the core crushes, the steel bar ruptures, and the column lateral load carrying capacity is reduced by 15% compared with the peak lateral load capacity. An idealized pushover curve based on AASHTO SGS (2011) is also generated. Using the ratio of the drift demand to the drift capacity and following the limits proposed in this project, the bride column serviceability is assessed. Finally, the results of PDA and OpenSees are summarized and on the website as shown in the next page.

Note: This process (PDA and Pushover) takes anywhere from 3 – 5 minutes, depending upon the CPU load and other background tasks. When it runs on a professional server, this time will be significantly reduced.

Detailed Damage Assessment - Results
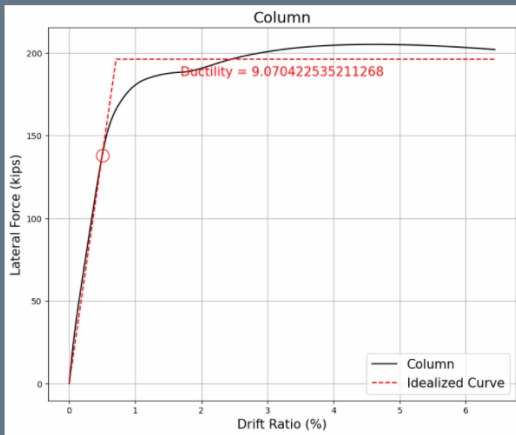
Summary of Pushover Analysis

Pushover analysis by OpenSees

Idealized Yield Drift: 0.71%

Drift Capacity: 6.44%

Demand

Demand analysis using estimated damage state

Damage State: Level 2

Drift Demand: 0.89%

Bridge Assessment:

Drift Demand to Capacity Ratio: 0.14

Inspected - Bridge can be opened

References:

AASHTO SGS. (2011). "AASHTO Guide Specifications for LRFD Seismic Bridge Design, 2nd Edition," American Association of State Highway and Transportation Officials.

OpenSees. (2016). "Open System for Earthquake Engineering Simulations," Version 2.4.1, Berkeley, CA, <http://opensees.berkeley.edu>.

This appendix is part of a research performed at South Dakota State University, and can be cited as:

Tazarv, M., Won, K., Jang, Y., Hart, K., Greeneway, E., and Harshvardhan, A. (2021). "Post-Earthquake Serviceability Assessment of RC Bridge Columns Using Computer Vision," National Center for Transportation Infrastructure Durability and Life Extension (TriDurLE) Report No: 2020-SDSU-01, Washington State University, Pullman, WA, 338 pp.